

- I. RELAXATION TIME OF ONE-DIMENSIONAL, LAMINAR
DEFLAGRATION FOR FIRST ORDER REACTIONS
- II. REFLECTION AND TRANSMISSION OF ELECTROMAGNETIC
WAVES AT ELECTRON DENSITY GRADIENTS

Thesis by
Frank A. Albini

In Partial Fulfillment of the Requirements
For the Degree of
Doctor of Philosophy

California Institute of Technology
Pasadena, California

1962

This thesis is composed of two separate parts; pagination and chapter enumeration, however, are continuous.

Part I. RELAXATION TIME OF ONE-DIMENSIONAL, LAMINAR
DEFLAGRATION FOR FIRST ORDER REACTIONS page 1

Part II. REFLECTION AND TRANSMISSION OF ELECTRO-
MAGNETIC WAVES AT ELECTRON DENSITY GRADIENTS
page 74

I. RELAXATION TIME OF ONE-DIMENSIONAL, LAMINAR
DEFLAGRATION FOR FIRST ORDER REACTIONS

ACKNOWLEDGMENT

The author wishes to express his deep appreciation to Professor Frank E. Marble for stimulating discussions and patient guidance in this effort, and to the Hughes Aircraft Company, Culver City, California, under whose sponsorship this work was carried out.

ABSTRACT

The one-dimensional, time-dependent equations describing laminar deflagration are solved by an integral method, under the assumption of a physical model for the flame structure and behavior, with restrictions on the type of deviation from steady-state behavior. By virtue of application of a hot-boundary approximation of the von Kármán type, certain sensitive integrals are expressed in a form independent of the temperature profile assumed. Two cases are considered: the "thermal theory" neglecting diffusion, and the case of unity Lewis number (temperature/concentration similarity). Only first order reactions are considered. Arguments supporting the generality of the results are included, along with a discussion of accuracy, and some comparison with experimental work. Graphical display of the results anticipates the utility of the theory for correlating and cross-checking experimental data.

It is concluded that the relaxation time is closely related to the time required for the gas undergoing rapid chemical reaction to pass through the flame.

TABLE OF CONTENTS

<u>Section</u>	<u>Title</u>	<u>Page</u>
	Acknowledgment	
	Abstract	
	Table of Contents	
	Terminology	
I.	INTRODUCTION	1
II.	A SIMPLIFIED MODEL OF THE NONSTEADY FLAME	7
III.	DEVELOPMENT OF INTEGRAL RELATIONS	11
IV.	THE HOT BOUNDARY APPROXIMATIONS	23
V.	SOLUTION FOR RELAXATION TIME	31
VI.	NUMERICAL RESULTS	41
	<u>Index to Figures</u>	55
	<u>Figures</u>	56
VII.	CONCLUDING REMARKS	63
VIII.	ANNOTATED BIBLIOGRAPHY	66

TERMINOLOGY

ρ	density (gm/cc)
U	velocity (cm/sec)
T	temperature ($^{\circ}\text{K}$)
k	thermal conductivity ($\text{cal}/\text{cm}^2 - \text{sec} - ^{\circ}\text{K}$)
C_p	specific heat capacity ($\text{cal}/\text{gm} - ^{\circ}\text{K}$)
Y	fuel mass fraction (dimensionless)
n	normalized fuel mass fraction (Y/Y_0)
$W(T)$	reaction rate (sec^{-1})
H_f	fuel heating value (cal/gm)
D	diffusion coefficient (cm^2/sec)
θ	dimensionless temperature (T/T_f)
L_T	characteristic length associated with T
L_n	characteristic length associated with n (or Y)
t	time (sec)
x	distance (cm)
y	dummy variable
\bar{A}	average value of A

Subscripts

o	original, unburnt gas -- upstream conditions
f	final, burnt gas -- downstream conditions

I. INTRODUCTION

Consider a steady, laminar deflagration standing in a stream of premixed, combustible gas. The gas approaches the flame from the left at temperature T_0 , density ρ_0 , and velocity U_0 , with a fuel mass fraction Y_0 (see fig. 1.1). The gas is heated on approaching the zone of chemical reactions, begins to burn, and finally passes out the hot end of the flame with temperature T_f , density ρ_f , and velocity U_f . Assume all the fuel is consumed in the reaction. For simplicity, further assume that the reaction is first order so that the rate of consumption of the fuel is proportional to the fuel concentration -- the "constant" of proportionality is the temperature-dependent reaction rate $W(T)$. The flow is along the x axis, positively directed, and can be considered uniform over any y - z plane. Assume that everywhere the gas velocity is very much smaller than the local speed of sound, so the change in pressure is everywhere negligible, and the kinetic energy of the gas is small compared to thermal enthalpy. The perfect gas law may be used in the form $\rho T = \text{constant}$, assuming small change in mean molecular weight due to reaction.

The analysis of the situation described has been effected in various approximate forms^(1, 2). Special cases frequently treated are that in which the diffusion of chemical species is neglected (the so-called "thermal theory"),⁽³⁾ and that in which there is a strict relationship between temperature and chemical composition by virtue of mathematical analogy (the case of unity Lewis number).⁽⁴⁾ The results of such calculations are in adequate agreement with experiment.

Now consider the problem of this same flame, perturbed slightly

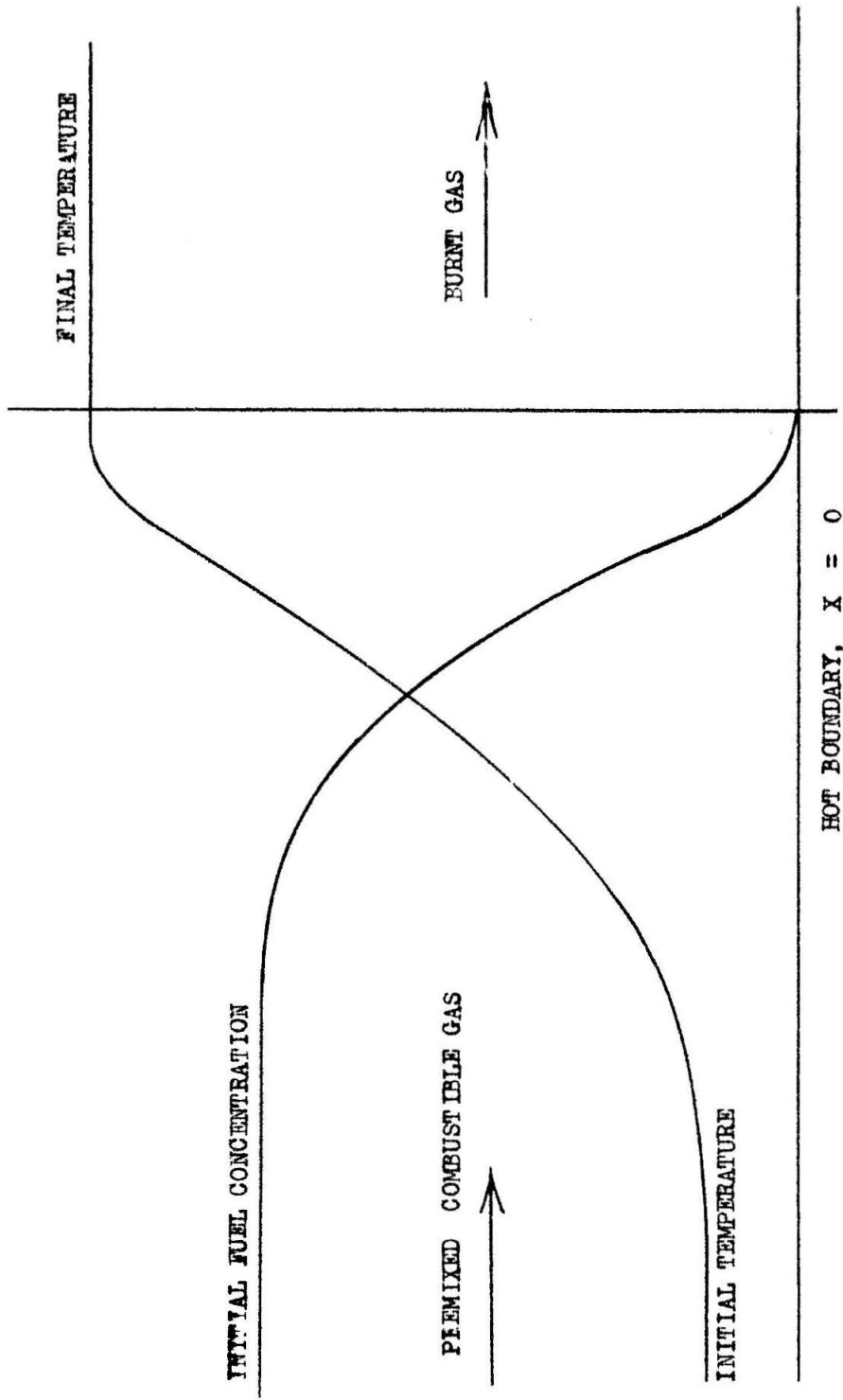


Figure 1.1 Schematic sketch of temperature and fuel concentration profiles in laminar flame.

from the steady-state structure in some manner. It is desired to compute the "relaxation time" -- i. e., the characteristic time it takes for the flame to restore itself to steady state behavior. This problem has not been so successfully attacked. The problem as stated is of limited practical importance*, but the determination of the parametric dependence of the relaxation time and an order-of-magnitude estimate for it would be of considerable interest to designers and analysts of combustion-operated machines. To this end, the following effort is directed.

Writing the governing equations for the simplified flame model outlined above reveals immediately the difficulty of obtaining an "exact" solution:

Conservation of mass

$$\frac{\partial \rho}{\partial t} + \frac{\partial}{\partial x} (\rho U) = 0 \quad (1.1)$$

Conservation of energy

$$\frac{\partial}{\partial t} (\rho C_p T) + \frac{\partial}{\partial x} (\rho U C_p T) = \frac{\partial}{\partial x} (k \frac{\partial T}{\partial x}) + \rho n \bar{C}_p (T_f - T_o) W(T) \quad (1.2)$$

Conservation of fuel species

a) Diffusion-free (thermal theory)

$$\frac{\partial}{\partial t} (\rho n) + \frac{\partial}{\partial x} (\rho U n) = - \rho n W(T) \quad (1.3)$$

b) Diffusion included

$$\frac{\partial}{\partial t} (\rho n) + \frac{\partial}{\partial x} (\rho U n) = \frac{\partial}{\partial x} (\rho D \frac{\partial n}{\partial x}) - \rho n W(T) \quad (1.4)$$

In (1.2) use has been made of the gross thermodynamic relationship:

* It is of importance in establishing the stability of the deflagration, but theoreticians as yet have not agreed among themselves on the approach or interpretation of such calculations. The mathematical subtleties are numerous, and many arguments have existed. See references 5 to 15.

$$Y_0 H_f = \bar{C}_p (T_f - T_0), \quad (1.5)$$

and the fuel fraction has been normalized everywhere by the initial fuel fraction Y_0 .

The momentum equation is conspicuous by its absence from the above system. As mentioned above, this is a result of the low Mach number condition prevalent in laminar deflagration waves. To be explicit, the pressure change across a one-dimensional steady velocity change in frictionless flow is of the form $\Delta P/P_1 = \gamma M_1^2 (\Delta U/U_1)$, so the constant of proportionality between dimensionless pressure change and dimensionless velocity change is γM_1^2 , where γ is the ratio of specific heats and M_1 is the initial Mach number. For a plane deflagration, a high speed would be ~ 3.0 meters/sec, and assuming an initial temperature of 0°C , the speed of sound is ~ 300 meters/sec, so $M_1^2 \sim 10^{-4}$. Thus for all intents and purposes, the pressure may be assumed constant, and the equation of state simplified to $\rho T = \text{constant}$. This fundamental observation removes completely all dynamical effects from the problem, an important point in the assignment of coordinates later.

An "exact" solution to the problem, then, would consist of the solution of the three equations (1.1), (1.2), and (1.4), with an initial distribution $\rho(x)$, $U(x)$, $T(x)$, and $n(x)$ at time zero. These distributions will vary with the passage of time and, if they reach stable conditions, eventually describe the steady-state flame. Although such a description is desirable and, in theory possible, the practical difficulty of obtaining such a general solution is prohibitive.

In many cases a set of equations such as those above is rendered tractable by the approximate method of perturbation analysis. (7-13) In such an analysis, each dependent variable is described by the sum of two terms, the steady-state function of x plus a (very small) non-steady "perturbation quantity." The substitution of such forms into the set of equations and subsequent dismissal of products of the small quantities results in a system of linear, coupled, partial differential equations with spatially-dependent coefficients. The reader can easily verify that this procedure applied to the present problem results in a very complicated system of equations, which does not permit simple solutions -- in fact, there is little other than linearity to recommend this approach to the present problem. The fundamental assumption of perturbation analysis is that conditions are not far removed from steady state, so the ratio of the perturbation correction term to the steady state term is much less than unity. In the present problem, the controlling factor which limits the size of the perturbations permitted is the reaction rate $W(T)$. Because of its extreme sensitivity to temperature, temperature perturbations must be severely restricted, a fact apparently overlooked by some investigators in this area. (8, 9)

Another method of solution has enjoyed certain popularity. Spalding, (16) following the example of Marble and Adamson, (17) employed an integral technique to solve several interesting initial-value problems in flame propagation. His method and the techniques of application are remarkably similar to the calculations displayed later here, but his work was not consulted until well after the effort was essentially complete. His remarks concerning the validity and accuracy of the technique are encouraging but felt to be slightly optimistic.

Apparently some such method is required if tractable analytical procedure is to be effected. The method employed in this work consists basically of three steps:

- 1) The assumption of a simplified physical model for the flame in non-steady behavior, with simplifying restrictions placed on the permitted perturbations;
- 2) The application of an integral formulation to this simple, restricted model;
- 3) The employment of an approximation developed for steady-state analysis which relates temperature and fuel concentration behavior at the hot edge of the flame.

With the aid of these three steps, a generalized analysis of the transient behavior of a laminar flame driven by a first-order reaction is effected for the two special cases mentioned above -- the thermal theory, and the case of unity Lewis number. No rigorous estimate of error is generated, and little justification of the physical model is attempted. ⁽¹⁴⁾ The procedure is remote from exactness and limited in scope, but physical insight coupled with the (generally accepted but seldom proven) notion that the relaxation time is only weakly dependent on the nature of the restrictions on and the form of the perturbation provide a feeling of credibility for the attack. Each of the steps listed above will be discussed under separate headings below.

II. A SIMPLIFIED MODEL OF THE NONSTEADY FLAME

First assume that an adequate simplified model of the flame is to be given by a finite length in which all processes occur. (7, 14, 16) In other words, let us attach a coordinate system to the hot end of the flame. For all positive x , all observables are constant, and for all $x < -L_T$ all observables are again constant. Physically this cannot be a bad approximation, for flames are generally observed to be of millimeter measurable thickness. (18, 19, 20) Mathematically, it is permissible to attach the coordinate system to the (possibly) accelerating hot end of the flame because all inertial effects have been disregarded in formulating the problem. This assumption may seem trivial, but is of fundamental importance to the application of the integral method. Emmons, et al. (21) have demonstrated by numerical calculation the insensitivity of flame speed to the initial temperature derivative assumed, thus fortifying the physical-reasoning conclusion that the mathematically troublesome cold boundary has little to do with determining the observable characteristics of the steady flame. This conclusion is carried over into the transient calculation here, and T is assumed to go to T_0 with zero slope. This might be viewed as a finite-distance "heat front" approximation to the conduction-heating portion of the flame upstream. The same applies as a "diffusion front" approximation in the unity Lewis number case.

The arbitrary forcing of the hot end temperature profile to a limit with zero slope must be treated much more gingerly. Von Kármán early recognized and often emphasized the dominant importance of the hot end of the flame zone. (1-3) Thus although an arbitrary, zero end

slope approximate profile will be used later to evaluate certain integrals, a special treatment of the reaction-rate integral will involve the Kármán-Millan⁽³⁾ steady-state hot boundary expansion. Thus it is felt that the relevant and important physical processes are not being mistreated by this approximation -- rather it is made to strengthen as well as expedite the calculations.

The second major step in constructing a simple model is the assumption that initial and final fluid properties are unaltered under perturbation. That is, Y_0 , ρ_0 , and T_0 , as well as ρ_f and T_f do not change during the relaxation process. Thus we permit velocity perturbation and/or length-scale perturbation, but not density, temperature or fuel mixture perturbation. These restrictions are defended on the basis that any perturbation calculation assumes some restrictive form of variation, ^(7, 16) which may not even be physically realizable -- the same physical-intuitive rationalization which justifies that procedure justifies the restrictions placed on this calculation. Furthermore, the variations admitted here are certainly realizable. Again the restrictions are felt not to impair any fundamental mechanism of relaxation, but are imposed for the sake of convenience.

The third and final step in the construction of the flame model is the most tenuous and least susceptible to justification. It is assumed at this point that T is a function of $x/L_T(t)$ only, and n is a function of $x/L_n(t)$ only. As a means of rationalizing this "similarity assumption", consider the following (typical) argument. If we employ steps one and two in this model-construction and integrate the continuity equation from $-L_T(t)$ to 0 , we find:

$$\int_{-L_T}^0 \frac{\partial \rho}{\partial t} dx + \int_{-L_T}^0 \frac{\partial}{\partial x} (\rho U) dx = \frac{d}{dt} \left[\int_{-L_T}^0 \rho dx \right] - \rho_0 \frac{dL_T}{dt} + \rho_f U_f - \rho_0 U_0 = 0 . \quad (2.1)$$

Writing $\bar{\rho}$ for average density, we have:

$$\bar{\rho} \frac{dL_T}{dt} + L_T \frac{d\bar{\rho}}{dt} - \rho_0 \frac{dL_T}{dt} + \rho_f U_f - \rho_0 U_0 = 0 . \quad (2.2)$$

an elaborate expression of the conservation of mass. Note that the "similarity" assumption has not yet been imposed, for under that assumption $\bar{\rho}$ becomes a constant in time. Now let us recall the definition of L_T . It is defined as that distance which lies between the points where initial and final gas conditions are reached -- and herein we require that such conditions are met with zero slope. Therefore, the only mechanism by which $\bar{\rho}$ can change is through distortion of the profile $\rho(x)$ in time. Since we permit no changes in initial and final conditions, the only distortions which appear physically realizable are depression of the $\rho(x)$ profile near $x = -L_T$, elevation of the profile near $x = 0$, and steepening or lessening the slope near the middle of the zone. In the first case, L_T is forced to increase, encompassing more high-density cold gas; in the second, L_T must be increased at the other end, taking in more low density hot gas. Both effects tend to stabilize $\bar{\rho}$, obviously. In the other cases, the physical processes are easily duplicated by expanding or contracting the length scale, without disturbing the end conditions -- i. e., by representing ρ as $\rho(x/L_T(t))$.

The above discussion may or may not convince the reader of the soundness of the assumption of "similarity" for this restricted problem. The author feels that it is not an inherently unsound approximation, as

it leaves the basic physical processes free to operate, thus forcing L_T to describe, as best it can, what is occurring. But with or without justification, the approximation is inserted at this point into the simplified transient flame model. The dividend in ease of calculation is generous, for all average quantities are then invariant.

Under the similarity assumption, $\rho = \rho(x/L_T)$, equation (2.2) becomes simply:

$$(\bar{\rho} - \rho_0) \frac{dL_T}{dt} + \rho_f U_f - \rho_0 U_0 = 0.$$

The physical interpretation of this and other integrals will be discussed more fully in the following section.

III. DEVELOPMENT OF INTEGRAL RELATIONS

Each of the conservation equations will be integrated through the flame, using the restrictions of the simplified model outlined above. A useful integral relationship is given first:

$$\int_{-a}^0 \frac{\partial}{\partial t} (F(x/a(t))) dx = \frac{da}{dt} \left\{ \int_{-1}^0 F(y) dy - F(-1) \right\}. \quad (3.1)$$

The conservation of mass equation (2.2 above) is then:

$$\frac{dL_T}{dt} \left\{ \int_{-1}^0 \rho(y) dy - \rho_0 \right\} + \rho_f U_f - \rho_0 U_0 = 0. \quad (3.2)$$

Physically, the first term represents the rate of increase of mass confined in the flame thickness; the second term is the rate at which mass is ingested by virtue of the expansion of the flame thickness; the last two terms are the convective efflux and influx contributions to the stored mass.

The equation for the conservation of energy is simplified if C_p is replaced everywhere by \bar{C}_p , and use is made of the perfect gas relation $\rho T = \text{constant}$. Then equation (1.2) becomes:

$$\bar{C}_p \rho T \frac{\partial U}{\partial x} = \frac{\partial}{\partial x} (k \frac{\partial T}{\partial x}) + \rho n \bar{C}_p (T_f - T_0) W(T). \quad (3.3)$$

On integration through the flame there results:

$$\bar{C}_p \rho T [U_f - U_0] = \bar{C}_p (T_f - T_0) \int_{-L_T}^0 n \rho W(T) dx \quad (3.4)$$

which is a statement to the effect that the efflux of energy (first term, lhs) is greater than the influx of energy (second term, lhs) by the amount of heat liberated by chemical reaction per unit time within the

flame. Conduction of heat into or out of the zone is zero because $\frac{\partial T}{\partial x}$ has been assumed zero at the ends of the zone. The fact that there appear no storage-of-energy terms is not due to the restrictions on the problem discussed in Chapter two, but is a direct consequence of the perfect gas law/constant pressure/constant (mean) specific heat assumptions. If a rate-of-change of stored energy term were added, of the form:

$$\frac{d}{dt} \int_{-L_T}^0 \rho \bar{C}_p T dx = \text{storage rate} \quad (3.5)$$

it would be exactly balanced by the increased influx rate due to the flame zone rate of expansion:

$$\rho_o \bar{C}_p T_o \frac{dL_T}{dt} = \text{expansion-influx term} . \quad (3.6)$$

Thus the same mechanism which removes the time derivative from the differential form of the energy equation removes the length dependence from the integrated energy equation -- i. e., the assumed constancy of ρT and C_p .

The integration of the diffusion-free species conservation equation (1.3) brings to light the possibility that n could have a different characteristic length from T . Thus it is assumed that $n = n\left(\frac{x}{L_n(t)}\right)$, with $L_n < L_T$. Integrating (1.3) gives, then:

$$\int_{-L_T}^0 \frac{\partial}{\partial t} (\rho n) + \int_{-L_T}^0 \frac{\partial}{\partial x} (\rho U n) dx = - \int_{-L_T}^0 \rho n W(T) dx \quad (3.7)$$

$$\frac{d}{dt} \left[\int_{-L_T}^0 \rho n dx \right] - \rho_o \frac{dL_T}{dt} - \rho_o U_o = - \int_{-L_T}^0 \rho n W(T) dx . \quad (3.8)$$

Expanding the first integral gives:

$$\int_{-L_T}^0 \rho n dx = \int_{-L_T}^0 \rho dx - \int_{-L_n}^0 (1-n) \rho dx . \quad (3.9)$$

The last integral can be easily approximated if L_n is much smaller than L_T , for in that case

$$\int_{-L_n}^0 (1-n) \rho dx \approx \rho_f \int_{-L_n}^0 (1-n) dx . \quad (3.10)$$

It will be shown later that in the diffusion-free case, L_n is ordinarily about $(0.1)(L_T)$, thus making the lower bound estimate of (3.10) a fairly accurate approximation. For the moment, however, (3.10) must be regarded as an approximation of unassessed validity. Using the lower bound of (3.10), equation (3.8) becomes

$$\begin{aligned} \left(\int_{-1}^0 \rho(y) dy - \rho_o \right) \frac{dL_T}{dt} - \rho_f \left(\int_{-1}^0 (1-n(y)) dy \right) \frac{dL_n}{dt} - \rho_o U_o = \\ = \int_{-L_T}^0 \rho n W(T) dx , \end{aligned} \quad (3.11)$$

the physical interpretation of which should be obvious.

In order to assess, in some degree, the influence of diffusion on the properties of the transient flame, equation (1.4) could be substituted for (1.3). But, of course, if (1.4) is integrated through the

flame, the result should be identical to what was already obtained using (1.3) because D enters multiplied by $\partial n / \partial x$, vanishing at both limits. Therefore, a special case is chosen which permits an immediate similarity identification to be made. Writing the energy equation (1.2) in terms of the variable $G = (T_f - T) / (T_f - T_o)$ gives

$$\frac{\partial}{\partial t} (\rho G) + \frac{\partial}{\partial x} (\rho U G) = \frac{1}{\bar{C}_p} \frac{\partial}{\partial x} (k \frac{\partial G}{\partial x}) - \rho n W(T) \quad (3.12)$$

which is remarkably similar to the species equation (1.4):

$$\frac{\partial}{\partial t} (\rho n) + \frac{\partial}{\partial x} (\rho U n) = \frac{\partial}{\partial x} (\rho D \frac{\partial n}{\partial x}) - \rho n W(T) . \quad (3.13)$$

Now if $\rho D = k / \bar{C}_p$, n and G satisfy the same equation. It is true that for a one-component gas, simple kinetic theory predicts the dimensionless group known as the "Lewis number" to be constant:

$$Le = \frac{k}{\rho \bar{C}_p D} = \text{constant of } O(1) . \quad (3.14)$$

So it is not a highly reasonable assumption to equate the Lewis number to unity, thus making G and n satisfy the same equation. If the further restriction is imposed that

$$G(x, t = 0) = n(x, t = 0) , \quad (3.15)$$

then G and n are equal for all time. This further restriction is easily admitted to the simplified model and the other assumptions underlying the calculations up to this point. So without further elaboration, these two restrictions will be placed on the species equation with diffusion [(3.14) and (3.15)]. Therefore, in this case, the species conservation equation contributes the basic identity:

$$n = (T_f - T) / (T_f - T_o) , \quad (3.16)$$

which implies, of course, that

$$L_n \Big|_{Le = 1} = L_T . \quad (3.17)$$

At this point, "taking stock" of the set of equations generated reveals that they are insufficient in number to specify the dependent variables, L_n , L_T , U_o , and U_f . Some further approximation might be made to supplement these equations, or the differential equations might be invoked to give a relationship between variables at some point in the range of integration. (For example, one might write the continuity of mass equation in the form

$$\frac{\partial \rho}{\partial t} + \frac{\partial}{\partial x} (\rho U) = - \frac{x}{L_T^2} \frac{dL_T}{dt} \frac{d\rho}{d(x/L_T)} + \frac{1}{L_T} \frac{d}{d(x/L_T)} (\rho U) = 0,$$

then, assuming some profiles for ρ and U as functions of x/L_T , evaluate the expression at some value of x/L_T and impose this as a supplementary equation.) But to do so would be to ignore one of the powerful tools available to the integral method -- the imposition of integral conditions on the solution. Use of the integral method allows complete liberty in constructing "moments" of the equations employed.

To illustrate the principle involved, consider the following simple example:

$$\Gamma(y) = f(x, y) \quad (3.18)$$

where $\Gamma(y)$ is some non-linear operation on y . Now suppose that, as in the restricted flame problem above, variations of y occur only over a limited region $a \leq x \leq b$, with well-defined boundary conditions. If some approximate expression $y(x)$ is assumed, with some loose parameters to adjust for some degree of "fit", then the integral method permits the imposition of a number of integral conditions on

this assumed form, until the number of equations generated is sufficient to specify the parameters. For instance,

$$\int_{y(a)}^{y(b)} \Gamma(y) dy = \int_{y(a)}^{y(b)} f(x, y) dy . \quad (3.19)$$

But as well one can impose "moments" of the form:

$$\int_{y(a)}^{y(b)} \Gamma(y) \cdot y^N dy = \int_{y(a)}^{y(b)} f(x, y) y^N dy \quad (3.20)$$

$$\int_a^b \Gamma(y) \cdot x^N dx = \int_a^b f(x, y) x^N dx \quad (3.21)$$

or of any other form felt suitable to the problem. There is little degree of assurance that in general the "solution" thus obtained is of a desired accuracy, but there is the strict assurance that the approximate result satisfies at least as many integral relations as have been imposed -- relations which the exact solution also would have to satisfy. Intuitively one feels that the procedure here is somewhat akin to the steps taken in performing a Fourier series expansion of a defined function, and that the agreement of the approximate with the exact expression is better on the average with this type of condition imposed than would be expected if a "point expansion" were employed.

In any event, the opportunity to impose an integral rather than a point condition on the solution will not be ignored here. It would be physically pleasing to be able to generate an equation which has some understandable physical interpretation. This could be done, for example, by dividing the energy equation through by T -- on integration

one would obtain a gross entropy-continuity relationship. But it is also important to make the most of the existing knowledge about the flame structure and the processes occurring in the flame. Specifically, it is felt that it is more important to emphasize the dominant hot end of the flame by weighting integrals towards that end than to be able to physically interpret the resulting expression. (To weight the cold end of the flame, division by T would suffice; to weight the "middle" of the flame, multiplication by $\partial T/\partial x$ would do; to weight the hot end of the flame, multiplication by T is implicated.) So for this reason, and because the results are easily managed, the energy equation will be multiplied by the temperature and integrated through the flame. The expression so derived will be a genuine requirement of the solution in an "average" sense, and will be a differential equation relating U_o , U_f , and L_T , vaguely resembling an entropy equation. Writing the energy equation in the form

$$\rho T \bar{C}_p \frac{\partial U}{\partial x} = \frac{\partial}{\partial x} \left(k \frac{\partial T}{\partial x} \right) + \rho n \bar{C}_p (T_f - T_o) W(T), \quad (3.22)$$

multiply both sides by T and integrate.

$$\int_{-L_T}^0 \rho \bar{C}_p T^2 \frac{\partial U}{\partial x} dx = \int_{-L_T}^0 T \frac{\partial}{\partial x} \left(k \frac{\partial T}{\partial x} \right) dx + \rho T \bar{C}_p (T_f - T_o) \int_{-L_T}^0 n W(T) dx \quad (3.23)$$

The mathematical manipulations will require an expression for $U(x/L_T)$, which can be obtained from the continuity equation in the form of (3.18):

$$\frac{d(\rho U)}{d(x/L_T)} = \frac{x}{L_T} \frac{dL_T}{dt} \frac{d\rho}{d(x/L_T)} \quad (3.24)$$

Integrating:

$$\rho U - \rho_0 U_0 = \frac{dL_T}{dt} \int_{-1}^{x/L_T} y \frac{d\rho}{dy} dy = \frac{dL_T}{dt} \left[y\rho \Big|_{-1}^{x/L_T} - \int_{-1}^{x/L_T} \rho dy \right] \quad (3.25)$$

$$\rho U = \rho_0 U_0 + \frac{dL_T}{dt} \left\{ \frac{x}{L_T} \rho + \rho_0 - \int_{-1}^{x/L_T} \rho(y) dy \right\} \quad (3.26)$$

Integrate (3.23) by parts and obtain:

$$\begin{aligned} \rho \bar{C}_p T \left\{ UT \Big|_{-L_T}^0 - \int_{-L_T}^0 U \frac{\partial T}{\partial x} dx \right\} = & - \int_{-L_T}^0 k \left(\frac{\partial T}{\partial x} \right)^2 dx + \\ & + \rho \bar{C}_p T (T_f - T_0) \int_{-L_T}^0 nW(T) dx \end{aligned} \quad (3.27)$$

$$\begin{aligned} \rho T \bar{C}_p \left\{ U_f T_f - U_0 T_0 - \int_{-1}^0 U \frac{dT(y)}{dy} dy \right\} = & - \frac{1}{L_T} \int_{-1}^0 k \left(\frac{dT(y)}{dy} \right)^2 dy + \\ & + \rho T \bar{C}_p (T_f - T_0) \int_{-L_T}^0 nW(T) dx \end{aligned} \quad (3.28)$$

The task at hand is to integrate the term

$$I = \int_{-1}^0 U \frac{dT}{dy} dy \quad (3.29)$$

Using (3.26),

$$I = \int_{-1}^0 \frac{dT(y)}{dy} \left\{ \frac{\rho_0}{\rho(y)} U_0 + \frac{dL_T}{dt} \left(y + \frac{\rho_0}{\rho(y)} - \frac{1}{\rho(y)} \int_{-1}^y \rho(s) ds \right) \right\} dy. \quad (3.30)$$

Therefore

$$I = \rho_0 U_0 \int_{T_0}^{T_f} \frac{dT}{\rho} + \frac{dL_T}{dt} \left\{ T y \Big|_{-1}^0 - \int_{-1}^0 T(y) dy + \rho_0 \int_{T_0}^{T_f} \frac{dT}{\rho} - \int_{-1}^0 \frac{1}{\rho} \frac{dT}{dy} \int_{-1}^y \rho(s) ds dy \right\} \quad (3.31)$$

$$I = \frac{\rho_0 U_0}{\rho_0 T_0} \frac{1}{2} (T_f^2 - T_0^2) + \frac{dL_T}{dt} \left\{ T_0 - \int_{-1}^0 T(y) dy + \frac{\rho_0}{\rho_0 T_0} \frac{1}{2} (T_f^2 - T_0^2) - J \right\} \quad (3.32)$$

Or

$$I = \frac{U_0}{2T_0} (T_f^2 - T_0^2) + \frac{dL_T}{dt} \left\{ T_0 - \int_{-1}^0 T(y) dy + \frac{T_f^2 - T_0^2}{2T_0} - J \right\} \quad (3.33)$$

where

$$J = \int_{-1}^0 \frac{T}{T_0 \rho_0} \frac{dT}{dy} \left(\int_{-1}^y \rho(s) ds \right) dy = \frac{1}{\rho_0 T_0} \left\{ \frac{1}{2} T^2 \int_{-1}^y \rho(s) ds \Big|_{y=-1}^{y=0} - \int_{-1}^0 \frac{1}{2} T^2 \rho dy \right\} \quad (3.34)$$

$$J = \frac{1}{2\rho_o T_o} \left\{ T_f^2 \int_{-1}^0 \rho(y) dy - \left(\int_{-1}^0 T dy \right) \rho_o T_o \right\} =$$

$$= \frac{1}{2} \left\{ T_f^2 \int_{-1}^0 \frac{dy}{T(y)} - \int_{-1}^0 T(y) dy \right\}. \quad (3.35)$$

Hence for I is obtained

$$I = \frac{U_o}{2T_o} (T_f^2 - T_o^2) + \frac{dL_T}{dt} \left\{ \frac{T_f^2 + T_o^2}{2T_o} - \frac{1}{2} \int_{-1}^0 T(y) dy - \frac{T_f^2}{2} \int_{-1}^0 \frac{dy}{T(y)} \right\} \quad (3.36)$$

Using this expression in (3.28) gives

$$\bar{C}_p \rho T \left\{ U_f T_f - U_o T_o - \frac{U_o}{2T_o} (T_f^2 - T_o^2) - \frac{dL_T}{dt} \left(\frac{T_f^2 + T_o^2}{2T_o} - \frac{1}{2} \left[\int_{-1}^0 \left(T + \frac{T_f^2}{T} \right) dy \right] \right) \right\} =$$

$$= -\frac{1}{L_T} \int_{-1}^0 k \left(\frac{dT}{dy} \right)^2 dy + \bar{C}_p \rho T (T_f - T_o) \int_{-1}^0 nW(T) dy \quad (3.37)$$

which simplifies to the form:

$$U_f T_f - U_o \left\{ \frac{T_f^2 + T_o^2}{2T_o} \right\} - \frac{1}{2} \frac{dL_T}{dt} \left\{ \frac{T_f^2 + T_o^2}{T_o} - \int_{-1}^0 \frac{T^2(y) + T_f^2}{T(y)} dy \right\} =$$

$$= -\frac{1}{L_T} \frac{k_f}{\bar{C}_p \rho_f T_f} \int_{-1}^0 K \left(\frac{dT}{dy} \right)^2 dy + (T_f - T_o) \int_{-L_T}^0 nW(T) dy \quad (3.38)$$

This equation, together with the three others derived above, specifies $L_T(t)$, $L_n(t)$, $U_o(t)$, and $U_f(t)$, once the profile $T(x/L_T(t))$ is

known. It must be obvious at this point, however, that no attempt will be made to insert a cumbersome expression for T into the integrands above -- instead, the profile for $T(x)$ will be approximated by some "reasonable looking" functions and the coefficients obtained for the differential equations in that manner. Before this is done, however, it will be necessary to make a more adequate approximation to the highly-sensitive rate integral

$$I_r = \int_{-1}^0 n T^r W(T) d(x/L_T) \quad r = -1, 0 \quad (3.39)$$

which appears so often. It would not be legitimate to ignore the fact that singular nature might be introduced into the steady-state results by virtue of an arbitrary profile inserted into (3.39). Just for tidy house-keeping, however, the set of equations to be solved in the two cases are grouped together and put into a standard form to close this chapter. The dimensionless temperature ratio $T/T_f = \theta$ will be used.

Conservation of mass

$$\left\{ \int_{-1}^0 \frac{\theta_0}{\theta} dy - 1 \right\} \dot{L}_T + \theta_0 U_f - U_0 = 0 \quad (3.40)$$

Conservation of energy

$$U_f - U_0 = (1 - \theta_0) \int_{-L_T}^0 \frac{n}{\theta} W(T) dx \quad (3.41)$$

Conservation of fuel species

(a) Thermal Theory

$$\left\{ \int_{-1}^0 \frac{\theta_0}{\theta} dy - 1 \right\} L_T - \theta_0 \left\{ \int_{-1}^0 (1-n) dy \right\} L_n - U_0 = \theta_0 \int_{-L_T}^0 \frac{n}{\theta} W(T) dx \quad (3.42)$$

(b) Unity Lewis Number

$$L_T = L_n, \quad n = \frac{1-\theta}{1-\theta_0} \quad (3.43)$$

Temperature/Energy moment equation

$$\left\{ \frac{1+\theta_0^2}{2\theta_0} - \int_{-1}^0 \frac{1+\theta^2}{2\theta} dy \right\} L_T - U_f + \left\{ \frac{1+\theta_0^2}{2\theta_0} \right\} U_0 - \frac{k_f L_T^{-1}}{C_p \rho_f} \int_{-1}^0 K(\theta) \left(\frac{d\theta}{dy} \right)^2 dy = -(1-\theta_0) \int_{-L_T}^0 n W(T) dx \quad (3.44)$$

In the following section, the von Kármán type hot-boundary approximation is derived for the two cases, and the rate integrals are expressed in more manageable form.

IV. THE HOT BOUNDARY APPROXIMATIONS

A physical look at the processes occurring in the steady-state laminar flame will be enlightening in the development of the hot boundary approximation. As mentioned above, von Kármán early recognized the significance of the hot boundary in determining the flame speed, so the work of von Kármán and Millán will be duplicated to some extent here to illustrate the reasoning which underlies the approximation. The steady-state equations of importance are written for the thermal theory case:

Continuity of mass

$$\rho U = m = \text{constant} \quad (4.1)$$

Conservation of energy

$$m \bar{C}_p (T - T_o) = k \frac{dT}{dx} - \bar{C}_p (T_f - T_o) m (n-1) \quad (4.2)$$

Conservation of fuel species

$$m \frac{dn}{dx} = - \rho n W(T) \quad (4.3)$$

It is important to recognize at this point the character of $W(T)$. This function, the "reaction rate", is generally expressed as

$$W(T) = B T^r \exp(-T_a/T), \quad (4.4)$$

a semi-empirical expression used to correlate experimental data, usually with $r = \frac{1}{2}$ or 0. The dimensional constant B is a measure of the frequency of collisions between molecules, and is known as the "frequency factor". T_a is the "activation temperature", and in all the work presented herein it is understood that

$$T_a > T_f, \quad T_a \gg T_o. \quad (4.5)$$

Thus $W(T_0)$ is completely negligible and (4.4) has a pronounced endpoint maximum at $T = T_f$. By a consideration of this factor alone it is evident that by far the greatest portion of chemical activity occurs in the region near the hot boundary of the flame. In fact, many theoreticians have based flame speed theories on a "two-zone" calculation founded on the physical model that the early, cold-boundary side of the flame is to be described by a constant-composition gas ($W(T) = 0$, $n = 1$) undergoing preliminary heating, while the later, hot-boundary side of the flame is dominated by chemical heat release balanced by heat conduction. The matching point of such solutions is to be interpreted physically as the point at which the gas is heated to "ignition temperature", after which it can react, but before which it cannot.

Von Kármán reasoned that the "ignition temperature" then, being mostly a mathematical artifice, could have little physical significance and hence the flame speed should be highly insensitive to its assumed value. His calculations verified this.⁽³⁾ Furthermore, as the cold-side temperature profile is so completely established, the success of a theory is generally a monotonic function of how well the hot-side profile is approximated. This, he reasoned, is not accidental -- the unique, identifying (and hence controlling) portion of the flame structure is the chemically-reacting hot boundary zone. The appropriate calculation is therefore one which concentrates on accurately representing the structure of the flame as the composition approaches that of the burnt gas, and the temperature approaches its upper limit.

To effect such a calculation, in light of the above arguments, divide the expression for the composition derivative by the expression for the temperature derivative, obtaining:

$$\frac{m \, dn}{k \, dT} = \frac{-pnW(T)}{m\bar{C}_p [T - T_o - (T_f - T_o)(1-n)]} \quad (4.6)$$

Defining

$$\lambda = \frac{m^2 \bar{C}_p}{k_f \rho_f} \frac{1}{W(T_f)} \cdot W(T) = W(T_f) w(\theta) \quad (4.7)$$

and using the dimensionless temperature notation, this becomes:

$$\lambda \frac{dn}{d\theta} = \frac{-\theta n w(\theta)}{\theta - \theta_o - (1-\theta_o)(1-n)} \cdot \quad (4.8)$$

Equation(4.8) is singular at $\theta = 1$, $n = 0$ it appears, unless the numerator vanishes equally as rapidly as the denominator. Physically, however, a singularity cannot be permitted -- but neither can a zero slope of $n(\theta)$ be permitted if the statement of strong chemical activity in the boundary zone is meaningful. What is required, then, is regularity of (4.8) at the boundary point. Expanding n about $\theta = 1$ gives, then:

$$n \approx 0 + \left(\frac{dn}{d\theta}\right)_{\theta=1} \cdot (\theta - 1) + \dots \quad (4.10)$$

Inserting this expression into (4.8) provides:

$$\left(\frac{dn}{d\theta}\right)_{\theta=1} = -\left(\frac{1+\lambda}{\lambda}\right)(1 - \theta_o)^{-1} \cdot \quad (4.10)$$

Using (4.10) in (4.9) and (4.9) then in (4.2) gives rise to

$$\lim_{\theta \rightarrow 1} \frac{d\theta}{dx} = \frac{m\bar{C}_p}{k} (1 - \theta_o)(1 + \lambda)^{-1} n \cdot \quad (4.11)$$

One can see easily that since $w(\theta)$ has a sharp end-point maximum at $\theta = 1$, the integral of (4.8) will be nearly independent of the lower limit -- i. e., the "ignition temperature." The value of λ is given numerically by integrating both sides of (4.8) with an adequate approximation for $n(\theta)$ near the hot boundary. The approximation

given by (4. 10) is sufficient to give engineering accuracy answers or to serve as a method of correlating experimental data. It is easily recognized that λ is of the order $1/\theta_a$, hence for later simplicity the factor $(1 + \lambda)^{-1}$ in (4. 11) will be taken as unity.* Thus a "zereth approximation" to the ratio of $n/(\frac{d\theta}{dx})$ is:

$$\lim_{n \rightarrow 0} n/(\frac{d\theta}{dx}) = \left\{ \frac{\rho U \bar{C}_p}{k} (1 - \theta_o) \right\}^{-1} \quad (4. 12)$$

for the steady-state case.

At this point another basic step enters the calculation procedure. Since it is desired that the transient flame solution wed smoothly to the steady-state condition (since small disturbances from normal steady conditions were assumed at the outset), and since neither θ nor n was allowed perturbation in profile anyway, the limit (4. 12) will be used to approximate the rate integrals in the thermal theory calculations. Let us see physically to what this corresponds. Writing (4.12) as

$$k \frac{\partial T}{\partial x} = \rho_f U_f \bar{C}_p (T_f - T_o) n \quad (4. 13)$$

its interpretation is clear: heat conduction balances the chemical heat release at the hot boundary. In other words, most of the density variation and fluid acceleration has already been accomplished, rendering convective terms ineffective in transporting heat generated by the reaction, so heat conduction alone remains to do the job. This is not an unappealing picture of the process, and it seems to contain the vital

* $(1 + \lambda)^{-1}$ can be approximated by the term $(1 - \frac{\alpha}{1 - \theta_o})$, where α is $O(1/\theta_a)$, for more accuracy.

mechanism of flame propagation. Applied to the non-steady problem, this relation implies that small time fluctuations of density and velocity are equally ineffective at heat removal, and that time fluctuations of chemical composition contribute negligibly compared to the steady-state heat release.

Next the unity Lewis number case must be considered, and an appropriate hot-end approximation generated. In this case there exists the identity:

$$n = \frac{1 - \theta}{1 - \theta_0} \quad (4.14)$$

which is strikingly similar to the previous case. To derive the appropriate hot-end approximation -- in this case for $(1-\theta)/(\frac{d\theta}{dx})$, look to the energy equation:

$$\frac{\partial}{\partial x} (\rho U \bar{C}_p T) = \frac{\partial}{\partial x} (k \frac{\partial T}{\partial x}) + \rho \bar{C}_p (T_f - T_0) n W(T) . \quad (4.15)$$

On the physical basis that $\partial U/\partial x$ should have small significance at the hot boundary, expand the equation about $T = T_f$, with the left-hand side set equal to zero.

$$0 = k_f \frac{\partial^2 T}{\partial x^2} + \rho_f \bar{C}_p (T_f - T_0) \frac{T_f - T}{T_f - T_0} \left\{ W(T_f) + (T - T_f) W'(T_f) + \dots \right\} \quad (4.16)$$

Ignoring second order terms in $(T - T_f)$ gives

$$k_f \frac{\partial^2 T}{\partial x^2} + \rho_f \bar{C}_p (T_f - T) W_f = 0 , \quad (4.17)$$

the solution to which is an exponential form

$$1 - \theta = A \exp(-bx) \quad (4.18)$$

with

$$b = (W_f \rho_f \bar{C}_p / k_f)^{\frac{1}{2}} . \quad (4.19)$$

Hence the ratio of importance is given by:

$$(1 - \theta) / \left(\frac{\partial \theta}{\partial x} \right) = 1/b = \left(\frac{k_f}{\rho_f \bar{C}_p W_f} \right)^{\frac{1}{2}} . \quad (4.20)$$

Consider now the rate integrals of the previous chapter:

$$I_1 = \int_{-L_T}^0 \frac{n}{\theta} W(T) dx ; \quad I_2 = \int_{-L_T}^0 n W(T) dx . \quad (4.21)$$

In order to evaluate these consistently with the steady-state results of accepted theory, insert the approximate expressions derived above, change to variable of integration to θ , and find:

Thermal Theory

$$I_1 = \int_{\theta_0}^1 \frac{k W(T)}{\theta \rho_f U_f \bar{C}_p (1 - \theta_0)} d\theta = \frac{k_f W_f}{\rho_f U_f \bar{C}_p} \frac{1}{1 - \theta_0} \int_{\theta_0}^1 w(\theta) K(\theta) \frac{d\theta}{\theta} \quad (4.22)$$

$$I_2 = \frac{k_f W_f}{\rho_f U_f \bar{C}_p} \frac{1}{1 - \theta_0} \int_{\theta_0}^1 w(\theta) K(\theta) d\theta \quad (4.23)$$

Unity Lewis Number

$$I_1' = \int_{\theta_0}^1 \frac{(k_f / \rho_f \bar{C}_p W_f)^{\frac{1}{2}}}{(1 - \theta_0) \theta} W(T) d\theta = \left(\frac{k_f W_f}{\rho_f \bar{C}_p} \right)^{\frac{1}{2}} \frac{1}{1 - \theta_0} \int_{\theta_0}^1 \frac{w(\theta) d\theta}{\theta} \quad (4.24)$$

$$I_2' = \left(\frac{k_f W_f}{\rho_f \bar{C}_p} \right)^{\frac{1}{2}} \frac{1}{1 - \theta_0} \int_{\theta_0}^1 w(\theta) d\theta . \quad (4.25)$$

These approximations for the rate integrals are henceforth divorced from the arbitrariness of assumed temperature and composi-

tion profiles. Thus these profiles are relegated to the insensitive role of determining constant coefficients in the differential equations for L_T and L_n . Several profiles will be used for this purpose, and the sensitivity of the results to profile choice will be evaluated. Before passing on to the solution for relaxation time, further use should be made of the result for the thermal theory (4. 10) in justifying the length-scale argument preceding the approximation of (3. 10). Recall that the use of the lower bound estimate of (3. 10) was based on the fact that $L_n < L_T$ by some factor. It is possible now to more nearly prove the statement, since it is required of the profiles that:

$$\left. \frac{dn}{d\theta} \right|_{\text{hot end}} \doteq \frac{-1}{1 - \theta_0} \left(\frac{1 + \lambda}{\lambda} \right) . \quad (4. 26)$$

If the restriction is made that the profile shapes are similar

$$\text{Shape} \left(1 - n(x/L_n) \right) = \text{Shape} \left(\frac{\theta(x/L_T) - \theta_0}{1 - \theta_0} \right) \quad (4. 27)$$

then (4. 26) translates into a requirement on L_n/L_T :

$$\frac{dn}{d\theta} = \frac{\frac{1}{L_n} \frac{dn}{d(x/L_n)}}{\frac{1}{L_T} \frac{d\theta}{d(x/L_T)}} = \frac{L_T}{L_n} \left\{ \frac{-1}{1 - \theta_0} \right\} = \frac{-1}{1 - \theta_0} \left(\frac{1 + \lambda}{\lambda} \right) \quad (4. 28)$$

Hence the restriction:

$$L_T/L_n \approx (1 + \lambda^{-1}) \quad (4. 29)$$

and as $\lambda = O(\theta_a^{-1})$, then L_T is ordinarily about one order of magnitude greater than L_n , as mentioned in defense of (3. 10). This restriction, along with (4. 27), insures that the profiles are compatible with the hot-end conditions and strengthens the assumptions underlying the hot-end calculations by restricting the length scale of chemical

-30-

activity to a region near the hot boundary.

V. SOLUTION FOR RELAXATION TIME

From this point on, the derivation is largely a matter of algebra. All the pertinent physics has been introduced, the approximations exhibited and discussed on physical grounds. What remains is the calculation and presentation of the relaxation time, the flame speed, and the flame thicknesses as they have been specified by the above work. No new concepts, approximations, or interpretations are introduced until the results are discussed in the following section.

The equations to be dealt with are listed below:

Thermal Theory

$$a) \left\{ \int_{-1}^0 \frac{\theta_o dy}{\theta(y)} - 1 \right\} L_T + \theta_o U_f - U_o = 0 \quad (5.1)$$

$$b) U_f - U_o = \frac{k_f W_f}{\rho_f U_f \bar{C}_p} \int_{\theta_o}^1 \frac{K(\theta)w(\theta)}{\theta} d\theta \quad (5.2)$$

$$c) \left\{ \int_{-1}^0 \frac{\theta_o dy}{\theta(y)} - 1 \right\} L_T - \theta_o \left\{ \int_{-1}^0 (1-n(y))dy \right\} L_n - U_o = \frac{\theta_o}{1-\theta_o} \frac{k_f W_f}{\rho_f U_f \bar{C}_p} \int_{\theta_o}^1 \frac{K(\theta)w(\theta)}{\theta} d\theta \quad (5.3)$$

$$d) \left\{ \int_{-1}^0 \left(\frac{1+\theta_o}{2\theta_o} - \frac{1+\theta^2(y)}{2\theta(y)} \right) dy \right\} L_T - U_f + \frac{1+\theta_o^2}{2\theta_o} U_o - \frac{k_f}{\rho_f \bar{C}_p} \int_{-1}^0 K(\theta) \left(\frac{d\theta}{dy} \right)^2 dy / L_T = - \frac{k_f W_f}{\rho_f U_f \bar{C}_p} \int_{\theta_o}^1 K(\theta)w(\theta)d\theta \quad (5.4)$$

Unity Lewis Number

e) same as (a) above

$$f) U_f - U_o = \left(\frac{k_f W_f}{\rho_f \bar{C}_p} \right)^{\frac{1}{2}} \int_{\theta_o}^1 \frac{w(\theta) d\theta}{\theta} \quad (5.5)$$

$$g) L_T = L_n \quad (5.6)$$

$$h) \left\{ \int_{-1}^0 \left(\frac{1+\theta_o^2}{2\theta_o} - \frac{1+\theta^2(y)}{2\theta(y)} \right) dy \right\} L_T - U_f + \frac{1+\theta_o^2}{2\theta_o} U_o$$

$$- \frac{k_f}{\rho_f \bar{C}_p} \int_{-1}^0 K(\theta) \left(\frac{d\theta}{dy} \right)^2 dy / L_T = - \left(\frac{k_f W_f}{\rho_f \bar{C}_p} \right)^{\frac{1}{2}} \int_{\theta_o}^1 w(\theta) d\theta \quad (5.7)$$

In order to facilitate the algebra to follow, a list of abbreviated symbols is given:

$$a_1 = 1 - \theta_o \int_{-1}^0 \frac{dy}{\theta(y)} \quad (5.8)$$

$$a_2 = \frac{1 + \theta_o^2}{2\theta_o} \quad (5.9)$$

$$a_3 = a_2 - \int_{-1}^0 \frac{1 + \theta^2}{2\theta} dy \quad (5.10)$$

$$b_1 = \theta_o \left[\int_{-1}^0 (1 - n(y)) dy \right] \quad (5.11)$$

$$U^2 = \frac{k_f W_f}{\rho_f \bar{C}_p} = \frac{k_f W_f}{\rho_o \bar{C}_p \theta_o} \quad (5.12)$$

$$M_1 = \int_{\theta_0}^1 K(\theta)w(\theta)d\theta \quad (5.13)$$

$$M_2 = \int_{\theta_0}^1 \frac{K(\theta)w(\theta)d\theta}{\theta} \quad (5.14)$$

$$M_3 = \int_{\theta_0}^1 w(\theta)d\theta \quad (5.15)$$

$$M_4 = \int_{\theta_0}^1 \frac{w(\theta)}{\theta} d\theta \quad (5.16)$$

$$N = \int_{-1}^0 K(\theta) \left(\frac{d\theta}{dy} \right)^2 dy \left(\frac{k_f}{\rho_0 \theta_0 C_p} \right) \quad (5.17)$$

In terms of these symbols, the equations are simpler:

$$a) a_1 L_T + U_0 - \theta_0 U_f = 0 \quad (5.18)$$

$$b) U_f - U_0 - \frac{U^2}{U_f} M_2 = 0 \quad (5.19)$$

$$c) a_1 L_T + b_1 L_n + U_0 - \frac{\theta_0}{1-\theta_0} \frac{U^2}{U_f} M_2 = 0 \quad (5.20)$$

$$d) a_3 L_T + a_2 U_0 - U_f - \frac{N}{L_T} + \frac{U^2}{U_f} M_1 = 0 \quad (5.21)$$

$$f) U_0 - U_f + U M_4 = 0 \quad (5.22)$$

$$g) L_T = L_n \quad (5.23)$$

$$h) a_3 L_T + a_2 U_0 - U_f - \frac{N}{L_T} + U M_3 = 0 \quad (5.24)$$

Taking first the set a) - d), note that c) is superfluous to solution for $L_T(t)$. Eliminate U_o from a) and d) by using b).

$$a') \quad a_1 \dot{L}_T + U_f(1-\theta_o) - \frac{U^2}{U_f} M_2 = 0 \quad (5.25)$$

$$d') \quad a_3 \dot{L}_T + U_f(a_2-1) - (a_2 U^2 M_2)/U_f - \frac{N}{L_T} + \frac{U}{U_f} M_1 = 0 \quad (5.26)$$

From these two equations eliminate U_f , leaving

$$\begin{aligned} \{a_1(a_2-1) - a_3(1-\theta_o)\} \dot{L}_T - \{U^2 M_2(a_2-1) - (1-\theta_o)(a_2 U^2 M_2 - U^2 M_1)\} / U_f \\ + \frac{N(1-\theta_o)}{L_T} = 0 . \end{aligned} \quad (5.27)$$

Since by definition

$$a_2 - 1 = (1-\theta_o)^2 / 2\theta_o \quad ; \quad 1 - \theta_o a_2 = (1-\theta_o^2) / 2 \quad , \quad (5.28)$$

a factor cancels from (5.27), leaving

$$\left\{ a_1 \frac{1-\theta_o}{2\theta_o} - a_3 \right\} \dot{L}_T - \left\{ M_1 - M_2 \frac{1+\theta_o}{2} \right\} \frac{U^2}{U_f} + \frac{N}{L_T} = 0 . \quad (5.29)$$

From (5.29)

$$\frac{M_2 U^2}{U_f} = \left\{ \left(\frac{1-\theta_o}{2\theta_o} a_1 - a_3 \right) \dot{L}_T + \frac{N}{L_T} \right\} \left\{ \frac{M_1}{M_2} - \frac{1+\theta_o}{2} \right\}^{-1} \quad (5.30)$$

hence (5.25) becomes:

$$a_1 \dot{L}_T + \frac{(1-\theta_o) M_2 U^2 \left(\frac{M_1}{M_2} - \frac{1+\theta_o}{2} \right)}{\left(\left(\frac{1-\theta_o}{2\theta_o} a_1 - a_3 \right) \dot{L}_T + \frac{N}{L_T} \right)} - \frac{\left(\frac{1-\theta_o}{2\theta_o} a_1 - a_3 \right) \dot{L}_T + \frac{N}{L_T}}{\left(\frac{M_1}{M_2} - \frac{1+\theta_o}{2} \right)} = 0 . \quad (5.31)$$

Further shorthand abbreviation

$$B_1 = \frac{M_1}{M_2} - \frac{1+\theta_o}{2} \quad (5.32)$$

$$B_2 = a_3 - \frac{1-\theta_o}{2\theta_o} a_1 \quad (>0) \quad (5.33)$$

simplifies this to the form

$$a_1 L_T + \frac{(1-\theta_o) M_2 U^2 B_1}{\frac{N}{L_T} - B_2 L_T} - \frac{\frac{N}{L_T} - B_2 L_T}{B_1} = 0. \quad (5.34)$$

Let

$$L_T^2 = 2\psi \quad (5.35)$$

and multiply through by L_T to obtain:

$$a_1 \dot{\psi} + \frac{(1-\theta_o) M_2 U^2 B_1 2\psi}{N - B_2 \dot{\psi}} - \frac{N - B_2 \dot{\psi}}{B_1} = 0 \quad (5.36)$$

Clearing fractions results in:

$$(\dot{\psi})^2 \{-a_1 B_1 B_2 - B_2^2\} + (\dot{\psi}) \{a_1 B_1 + 2B_2\} N + 2(1-\theta_o) B_1^2 M_2 U^2 \psi - N^2 = 0. \quad (5.37)$$

Substituting again,

$$\mu = 2B_1^2 M_2 (1-\theta_o) U^2 \psi - N^2, \quad (5.38)$$

makes the equation take the form

$$-\alpha (\dot{\mu})^2 + 2\beta (\dot{\mu}) + (\mu) = 0 \quad (5.39)$$

where

$$\alpha = \frac{B_2(a_1 B_1 + B_2)}{4(1-\theta_o)^2 B_1^4 M_2 U^4} > 0 \quad (5.40)$$

$$\beta = \frac{(a_1 B_1 + 2B_2)N}{4B_1^2 M_2 (1-\theta_o) U^2} > 0 \quad (5.41)$$

From this equation

$$\mu = \frac{-2\beta + \sqrt{4\beta^2 + 4\alpha\mu}}{-2\alpha} = \frac{\beta}{\alpha} \left[1 + \left(1 + \mu \frac{\alpha}{\beta^2} \right)^{\frac{1}{2}} \right] \quad (5.42)$$

Since the steady-state value of μ is zero from (5.39), the negative sign must be chosen for stability. Hence, setting

$$\xi = 1 - \left(1 + \mu \frac{\alpha}{\beta^2} \right)^{\frac{1}{2}} \quad (5.43)$$

gives the equation

$$-2\beta \dot{\xi} (1 - \xi) = \xi \quad (5.44)$$

Let $\xi_0 = \xi(t=0)$. Then the solution to (5.44) is:

$$\xi \exp(-\xi) = \xi_0 \exp(-\xi_0) \cdot \exp(-t/2\beta) \quad (5.45)$$

Although the functional form of $L_T(t)$ may be mysteriously hidden in this relationship, clearly L_T is a monotonic function of $(t/2\beta)$ and it can be concluded that the "relaxation time" is just 2β . This fact is more transparent when one realizes that μ is proportional to $L_T^2(t) - L_T^{\circ 2}$, where L_T° is the steady-state value, so that for very small disturbances from equilibrium,

$$\frac{d}{dt} \left\{ \frac{L_T(t)}{L_T^{\circ}} - 1 \right\} = -\frac{1}{2\beta} \left(\frac{L_T(t)}{L_T^{\circ}} - 1 \right) \quad (5.46)$$

Going back to (5.38) and the definition of Ψ , it can be seen that

$$(L_T^{\circ})^2 = \frac{N^2}{B_1^2 U^2 M_2 (1 - \theta_0)} \quad (5.47)$$

hence

$$\alpha = \frac{1}{4} \left(\frac{L_T^{\circ}}{N} \right)^4 B_2 (a_1 B_1 + B_2) \quad (5.48)$$

$$\beta = \frac{1}{4} \left(\frac{L_T^{\circ}}{N} \right)^2 (a_1 B_1 + 2B_2) N \quad (5.49)$$

$$\mu = N^2 \left\{ \frac{L_T^2(t)}{L_T^{\circ 2}} - 1 \right\} \quad (5.50)$$

$$\mu\alpha/\beta^2 = \frac{N^2 \left[\frac{L_T^2}{L_T^{\circ 2}} - 1 \right] 4 B_2 (a_1 B_1 + B_2)}{N^2 (a_1 B_1 + 2 B_2)^2} \quad (5.51)$$

$$\mu\alpha/\beta^2 = \left\{ \frac{L_T^2(t)}{L_T^{\circ 2}} - 1 \right\} \left\{ \frac{4 B_2 B_3}{(B_2 + B_3)^2} \right\} \quad (5.52)$$

Since

$$B_3 = a_1 B_1 + B_2 \quad (5.53)$$

clearly $\mu\alpha/\beta^2$ is of the order $(L_T^2(t)/L_T^{\circ 2} - 1)$.

The derivation of (5.46) from (5.42) then follows by assuming

$$\left| \frac{L_T(t)}{L_T^{\circ}} \right| \approx 1 \text{ and linearizing.}$$

The results of these calculations are, then, that the relaxation time, t_R , is given by

$$t_R = 2\beta = \frac{1}{2} (a_1 B_1 + 2 B_2) (L_T^{\circ})^2 / N \quad (5.54)$$

Steady state results follow immediately, giving

$$U_o^{\circ} = \theta_o U_f = U \theta_o \sqrt{\frac{M_2}{1 - \theta_o}} \quad (5.55)$$

$$L_T^{\circ} = \frac{N}{U} \frac{1}{B_1 (M_2 (1 - \theta_o))^{\frac{1}{2}}} \quad (5.56)$$

From these results follow the interesting dimensionless groups:

$$U_o^{\circ} t_R / L_T^{\circ} = \frac{\theta_o}{1 - \theta_o} \left\{ \frac{a_1}{2} + \frac{B_2}{B_1} \right\} \quad (5.57)$$

$$L_T^{\circ} / (k_o / W_f \rho_o \bar{C}_p)^{\frac{1}{2}} = \frac{\int_{-1}^0 \theta^{1/2} (d\theta/dy)^2 dy}{\theta_o^{1/4} (1 - \theta_o)^{1/2} M_2^{1/2} B_1} \quad (5.58)$$

$$U_o^o / (k_o W_f / \rho_o C_p)^{1/2} = \frac{\theta_o^{3/4} M_2^{1/2}}{(1-\theta_o)^{1/2}} \quad (5.59)$$

$$t_R W_f = \frac{1}{1-\theta_o} \left\{ \frac{a_1}{2} + \frac{B_2}{B_1} \right\} \frac{\int_{-1}^0 \theta^{1/2} \left(\frac{d\theta}{dy} \right)^2 dy}{B_1 M_2} \quad (5.60)$$

where the assumption has been made that:

$$k(\theta) = k_f K(\theta) = \theta^{1/2} k_f \quad (5.61)$$

The above expressions are plotted and displayed for a chosen temperature profile. The details of the calculations are discussed in the next section, and await the solution of the unity Lewis number case below.

In the unity Lewis number set of equations, first eliminate U_f from equations a) and h), leaving:

$$a') \quad a_1 L_T + U_o - \theta_o (U_o + U M_4) = 0 \quad (5.62)$$

$$h') \quad a_3 L_T + a_2 U_o - (U_o + U M_4) - \frac{N}{L_T} + U M_3 = 0 \quad (5.63)$$

Using (5.62) to eliminate U_o from (5.63) results in:

$$0 = a_3 L_T - \frac{N}{L_T} + U(M_3 - M_4) + (1-a_2) \left(\frac{a_1 L_T - \theta_o U M_4}{(1-\theta_o)} \right) \quad (5.64)$$

Recalling the definition of a_2 results in some simplification:

$$L_T \left(a_3 - \frac{1-\theta_o}{2\theta_o} a_1 \right) - \frac{N}{L_T} + U \left(M_3 - M_4 \left(\frac{1+\theta_o}{2} \right) \right) = 0 \quad (5.65)$$

Making the substitution

$$N - UL_T \left(M_3 - M_4 \left(\frac{1+\theta_o}{2} \right) \right) = \phi, \quad (5.66)$$

and recalling the definition of B_2 gives then

$$-\frac{B_2 (N - \phi) \dot{\phi}}{U^2 \left(M_3 - M_4 \frac{1 + \theta_o}{2} \right)^2} - \phi = 0 . \quad (5.67)$$

The solution to this equation is

$$\phi e^{-\phi/N} = \phi_o e^{-\phi_o/N} e^{-t/t'_R} \quad (5.68)$$

where the relaxation time t'_R is given by

$$t'_R = \frac{NB_2}{U^2 M_4^2 \left(\frac{M_3}{M_4} - \frac{1 + \theta_o}{2} \right)^2} \quad (5.69)$$

The steady-state thermal length is given by

$$\phi = 0 \Rightarrow L_T^o = \frac{N}{UM_4 \left(\frac{M_3}{M_4} - \frac{1 + \theta_o}{2} \right)} . \quad (5.70)$$

while the flame speed is given by (5.62) as:

$$U_o^o = U \frac{\theta_o M_4}{1 - \theta_o} . \quad (5.71)$$

The dimensionless groups in this case are exhibited:

$$U_o^o t'_R / L_T^o = \frac{\theta_o}{1 - \theta_o} \frac{B_2}{\frac{M_3}{M_4} - \frac{1 + \theta_o}{2}} \quad (5.72)$$

$$U_o^o / (k_o W_f / \rho_o \bar{C}_p)^{1/2} = M_4 \frac{\theta_o^{3/4}}{1 - \theta_o} \quad (5.73)$$

$$L_T^o / (k_o / W_f \rho_o \bar{C}_p)^{1/2} = \frac{\int_{-1}^0 \theta^{1/2} \left(\frac{d\theta}{dy} \right)^2 dy}{\theta_o^{1/4} M_4 \left(\frac{M_3}{M_4} - \frac{1 + \theta_o}{2} \right)} \quad (5.74)$$

$$t'_R W_f = \frac{B_2 \int_{-1}^0 \theta^{1/2} \left(\frac{d\theta}{dy}\right)^2 dy}{M_4^2 \left(\frac{M_3}{M_4} - \frac{1+\theta_o}{2}\right)^2} \quad (5.75)$$

where again it has been assumed that:

$$k(\theta) = k_f K(\theta) = k_f \theta^{1/2} . \quad (5.76)$$

In the following section the integrals employed herein are evaluated, some discussion of accuracy is presented, comparison with steady-state flame theory is effected, the effect of profile choice is estimated, and the expressions given above are plotted for ease of use. It is suggested that the form and content of this analysis and its results best suits it for experimental-result correlation and order-of-magnitude estimate endeavors.

VI. NUMERICAL RESULTS

As indicated above, this section contains primarily the mathematical details of computation. Comparison of flame-speed expressions with more exact steady-state theory is effected at the end of this section, and figures displaying numerical results close the chapter.

In order to evaluate the constants appearing in the results and simultaneously to gauge the sensitivity of the results to profile choice, three temperature profiles are selected:

1) linear

$$\theta = \theta_0 + (1-\theta_0)(1 + x/L_T) \quad (6.1)$$

2) bi-parabolic

$$\theta = \begin{cases} \theta_0 + 2(1-\theta_0)(1 + x/L_T)^2, & \frac{x}{L_T} < -\frac{1}{2} \\ 1 - 2(1-\theta_0)(x/L_T)^2, & \frac{x}{L_T} > -\frac{1}{2} \end{cases} \quad (6.2)$$

3) \cos^2

$$\begin{aligned} \theta &= \theta_0 + (1-\theta_0)\cos^2 \frac{\pi}{2} \frac{x}{L_T} = \\ &= \theta_0 + \frac{1-\theta_0}{2} \left(1 + \cos \left(\frac{\pi x}{L_T} \right) \right) \end{aligned} \quad (6.3)$$

The mean values of θ and θ^{-1} as determined by these profiles are exhibited below:

1) linear

$$\bar{\theta} = \int_{-1}^0 \theta \left(\frac{x}{L_T} \right) d\left(-\frac{x}{L_T} \right) = (1+\theta_0)/2 \quad (6.4)$$

$$\bar{\theta}^{-1} = \int_{-1}^0 \frac{d(x/L_T)}{\bar{\theta}(x/L_T)} = (1-\theta_0)^{-1} \ln(1/\theta_0) \quad (6.5)$$

2) bi-parabolic

$$\bar{\theta} = (1 + \theta_0)/2 \quad (6.6)$$

$$\bar{\theta}^{-1} = \frac{\left\{ \theta_0^{-\frac{1}{2}} \tan^{-1} \left(\left(\frac{1-\theta_0}{2\theta_0} \right)^{\frac{1}{2}} \right) + \tanh^{-1} \left(\left(\frac{1-\theta_0}{2} \right)^{\frac{1}{2}} \right) \right\}}{(2(1-\theta_0))^{\frac{1}{2}}} \quad (6.7)$$

3) \cos^2

$$\bar{\theta} = (1 + \theta_0)/2 \quad (6.8)$$

$$\bar{\theta}^{-1} = \theta_0^{-\frac{1}{2}} \quad (6.9)$$

Since $\bar{\theta}$ is the same in all three cases, clearly only a comparison of the value of $\bar{\theta}^{-1}$ is required to gain some feeling for the sensitivity of the solution to profile choice. The table below is an evaluation of $\bar{\theta}^{-1}$ for the three cases over a wide range of θ_0 , to sliderule accuracy.

$\theta_0 =$	0.10	0.15	0.20	0.25	0.30	0.35	0.40	0.50	0.60
linear	2.56	2.23	2.01	1.85	1.72	1.62	1.53	1.39	1.28
bi-parabolic	3.27	2.65	2.28	2.03	1.85	1.71	1.60	1.42	1.30
\cos^2	3.16	2.58	2.24	2.00	1.83	1.69	1.58	1.40	1.29

Table of Values of $\bar{\theta}^{-1}$ for Three Profiles

Although the maximum difference between the bi-parabolic and \cos^2 profiles is given by

$$(\Delta\theta)_{\max} \approx .028 (1 - \theta_0) \quad (6.10)$$

still the greatest difference in θ^{-1} shown in the table is less than 3.5 per cent. The linear profile is clearly a very poor approximation, and yet the worst discrepancy with the more reasonable bi-parabolic profile is only 22 per cent. Thus a conclusion can be reached that the choice of profile will not affect the results by an order of magnitude, and that a "reasonable" profile will provide results essentially independent of the exact nature of the profile.

Another profile-dependent integral is the expression:

$$I_K(\theta_0) = \int_{-1}^0 \theta^{\frac{1}{2}} \left(\frac{d\theta}{dy} \right)^2 dy \quad (6.11)$$

which is tabulated below for the bi-parabolic profile.

$\theta_0 =$	0.10	0.15	0.20	0.25	0.30	0.35	0.40	0.50	0.60
$I_K(\theta_0) =$.485	.445	.403	.363	.325	.286	.249	.179	.115

Values of $I_K(\theta_0)$ from the Bi-Parabolic Profile

The \cos^2 profile gives an ugly expression, and the linear profile is clearly inadequate for the more sensitive I_K integral.* Because of the similarity of the two results for θ^{-1} , it is probable that the above table is very close to the values that would be given by the \cos^2 profile as well. In fact, the greatest deviation of the integrands for the two

* Yet the difference in values of $I_K(\theta_0)$ from the bi-parabolic values is ≈ 20 per cent everywhere.

cases is given by:

$$\Delta \left\{ \theta^{\frac{1}{2}} \left(\frac{d\theta}{dy} \right)^2 \right\} \leq 0.2 (1 - \theta_0)^2 \quad (6.12)$$

which, if extended over 1/4 of the range of integration, would result in a maximum deviation of I_K 's of about 8.5 per cent to a minimum deviation of about 7.0 per cent. This kind of error can only be deemed inconsequential at the present point in these calculations.

Another integral required to fill out the numerical results is of the form:

$$I_p(\theta_a) = \exp(\theta_a) \int_{\theta_0}^1 \theta^p \exp(-\theta_a/\theta) d\theta \quad (6.13)$$

which is a form resulting from the assumption of the reaction rate formula displayed earlier:

$$w(\theta) = \exp(\theta_a) \theta^r \exp(-\theta_a/\theta). \quad (6.14)$$

With the restriction that

$$\exp(-\theta_a/\theta_0) \ll \exp(-\theta_a), \quad (6.15)$$

the integral of (6.13) may be extended to the lower limit of zero. An asymptotic series for $I_p(\theta_a)$ is obtained by repeated partial integration, given by

$$I_p(\theta_a) \sim \frac{1}{\theta_a} \left\{ 1 - \frac{p+2}{\theta_a} \left(1 - \frac{p+3}{\theta_a} \left(1 - \frac{p+4}{\theta_a} \left(1 - \dots \right. \right. \right. \right. \quad (6.16)$$

which is 'exact' if $p+N$ vanishes for some integer, N , but otherwise a 'best approximation' when terminated at $p+N \approx \theta_a$. In order to present numerical data limited mostly by the accuracy of the theory,

$I_p(\theta_a)$ was evaluated by machine calculation* for the range of p relevant to this work and for $3 \leq \theta_a \leq 15$. The following table displays the results.

θ_a	$p =$	-1	$-\frac{1}{2}$	0	$\frac{1}{2}$	1
3		.2621	.2357	.2137	.1952	.1794
4		.2063	.1893	.1746	.1619	.1508
5		.1704	.1584	.1479	.1386	.1303
6		.1453	.1363	.1284	.1213	.1148
7		.1266	.1197	.1135	.1079	.1027
8		.1123	.1068	.1018	.0972	.0929
9		.1009	.0964	.0922	.0884	.0849
10		.0916	.0878	.0844	.0812	.0782
11		.0838	.0807	.0777	.0750	.0724
12		.0773	.0746	.0721	.0697	.0675
13		.0717	.0694	.0672	.0651	.0632
14		.0669	.0649	.0629	.0611	.0594
15		.0627	.0609	.0592	.0576	.0560

Table of the Integral $I_p(\theta_a)$

For ease of presentation, the \cos^2 profile will be employed for the evaluation of $\bar{\theta}$ and $\bar{\theta}^{-1}$, while the $I_K(\theta_0)$ integral will be understood to be given by the bi-parabolic profile. Furthermore, it will be assumed that $r = \frac{1}{2}$ in the reaction rate expression. Using these

* The author thanks Dr. James R. Lloyd who developed the program in the course of his research and was so kind as to loan it for this evaluation.

restrictions, the constants employed in the results can be written:

$$a_1 = 1 - \theta_o^{\frac{1}{2}} \quad (6.17)$$

$$a_3 - \frac{1 - \theta_o}{2\theta_o} a_1 = (1 - \theta_o^{\frac{1}{2}})^2 / 4 = B_2 \quad (6.18)$$

$$M_1 = I_1(\theta_a) \quad (6.19)$$

$$M_2 = I_0(\theta_a) \quad (6.20)$$

$$M_3 = I_{\frac{1}{2}}(\theta_a) \quad (6.21)$$

$$M_4 = I_{-\frac{1}{2}}(\theta_a) \quad (6.22)$$

$$N = \theta_o^{-\frac{1}{2}} I_K(\theta_o) \frac{k_o}{\rho_o \bar{C}_p} \quad (6.23)$$

$$B_1 = I_1(\theta_a) / I_0(\theta_a) - \left(\frac{1 + \theta_o}{2} \right) \quad (6.24)$$

$$\frac{a_1}{2} + \frac{B_2}{B_1} = \frac{(1 - \theta_o^{\frac{1}{2}})}{2} \left\{ 1 + \frac{1 - \theta_o^{\frac{1}{2}}}{2 \left(\frac{I_1(\theta_a)}{I_0(\theta_a)} - \frac{1 + \theta_o}{2} \right)} \right\} \quad (6.25)$$

Using these expressions, the results of the above calculations become simply:

Thermal Theory

$$U_o^o t_R / L_T^o = \frac{\theta_o}{2(1 + \theta_o^{\frac{1}{2}})} \left\{ 1 + \frac{1 - \theta_o^{\frac{1}{2}}}{2 \left(\frac{I_1(\theta_a)}{I_2(\theta_a)} - \frac{1 + \theta_o}{2} \right)} \right\} \quad (6.26)$$

$$L_T^o (\rho_o \bar{C}_p W_f / k_o)^{\frac{1}{2}} = I_K(\theta_o) \cdot \theta_o^{-\frac{1}{4}} (1 - \theta_o)^{-\frac{1}{2}} I_o^{-\frac{1}{2}}(\theta_o) / \left(\frac{I_1(\theta_a)}{I_0(\theta_a)} - \frac{1 + \theta_o}{2} \right) \quad (6.27)$$

$$U_o^o(\rho_o \bar{C}_p / k_o W_f)^{1/2} = \theta_o^{3/4} I_o^{1/2}(\theta_a)(1-\theta_o)^{-1/2} \quad (6.28)$$

$$t_R W_f = \frac{I_K(\theta_o)}{I_o(\theta_a)} \left\{ 1 + \frac{1 - \theta_o^{1/2}}{2 \left(\frac{I_1(\theta_a)}{I_o(\theta_a)} - \frac{1+\theta_o}{2} \right)} \right\} \left(2(1+\theta_o^{1/2}) \right)^{-1} \left(\frac{I_1(\theta_a)}{I_o(\theta_a)} - \frac{1+\theta_o}{2} \right)^{-1} \quad (6.29)$$

Unity Lewis Number

$$U_o^o t'_R / L_T^o = \frac{\theta_o}{4} \frac{1 - \theta_o^{1/2}}{1 + \theta_o^{1/2}} \left\{ \frac{I_{1/2}(\theta_a)}{I_{-1/2}(\theta_a)} - \frac{1+\theta_o}{2} \right\} \quad (6.30)$$

$$U_o^o(\rho_o \bar{C}_p / k_o W_f)^{1/2} = \frac{\theta_o^{3/4} I_{-1/2}(\theta_a)}{1 - \theta_o} \quad (6.31)$$

$$L_T^o(\rho_o \bar{C}_p W_f / k_o)^{1/2} = \theta_o^{-1/4} I_K(\theta_o) I_{-1/2}^{-1}(\theta_a) \left(\frac{I_{1/2}(\theta_a)}{I_{-1/2}(\theta_a)} - \frac{1+\theta_o}{2} \right)^{-1} \quad (6.32)$$

$$t'_R W_f = \left(\frac{1 - \theta_o^{1/2}}{2} \right)^2 I_K(\theta_o) I_{-1/2}^{-2}(\theta_a) \left\{ \frac{I_{1/2}(\theta_a)}{I_{-1/2}(\theta_a)} - \frac{1+\theta_o}{2} \right\}^{-2} \quad (6.33)$$

Recalling the definition of λ in equation (4.7),

$$\lambda = \frac{\rho_o U_o^2 \bar{C}_p}{\theta_o^{3/2} k_o W_f} \quad (6.34)$$

it can be written now as:

$$\lambda = I_o(\theta_a) / (1 - \theta_o). \quad (6.35)$$

Thus the length scale ratio for the thermal theory may be expressed as (see (4.29)):

$$L_T^o / L_n^o = 1 + (1 - \theta_o) / I_o(\theta_a). \quad (6.36)$$

All of the expressions above which involve the function $I_p(\theta_a)$ can be simply modified to include the case of $r = 0$ for the temperature

exponent in the reaction rate expression by the expedient of replacing $I_p(\theta_a)$ by $I_{p-\frac{1}{2}}(\theta_a)$. A glance at the table of $I_p(\theta_a)$ will convince the reader, however, that the difference is slight.

Before closing this chapter with a graphical presentation of results, the comparisons with flame propagation theory that are possible should be made to gain some idea of the accuracy with which the steady-state situation is described. Fortunately, it is possible to compare directly the expression for steady flame speed in the unity Lewis number case with an equivalent expression given in reference 2. The von Kármán "zerth approximation" developed on the assumption of unity Lewis number, first order reaction, and $r = 0$ in the reaction rate expression, is given by

$$U_{K_o} = \frac{\theta_o^{\frac{1}{2}}}{1-\theta_o} \left(\frac{k_f W_f}{\rho_o C_p} \right)^{\frac{1}{2}} (2\Omega)^{\frac{1}{2}} \quad (6.37)$$

where

$$\Omega = \exp(\theta_a) \int_{\theta_o}^1 (1-\theta) \exp(-\theta_a/\theta) d\theta \quad (6.38)$$

The comparable expression from this chapter would be

$$U_o^o = \frac{\theta_o^{\frac{1}{2}}}{1-\theta_o} \left(\frac{k_f W_f}{\rho_o C_p} \right)^{\frac{1}{2}} I_{-1}(\theta_a) \quad (6.39)$$

The ratio of the two expressions is given, in this notation, by:

$$U_o^o / U_{K_o} = I_{-1}(\theta_a) / (2I_o(\theta_a) - 2I_1(\theta_a))^{\frac{1}{2}} \quad (6.40)$$

which is tabulated below for easy reference.

$\theta_a =$	3	5	7	9	11	13	15
$U_o^o/U_{K_o} =$	1.04	0.91	0.86	0.84	0.81	0.80	0.80

Tabular Comparison of Theoretical Flame Speeds

On the basis of the above comparison and the expressions given in reference 2, it is evident that the U_o^o generated herein is never more than 30 per cent in error of the "exact" solution over the range $3 \leq \theta_a \leq 15$, and is indeed a better approximation than the first iteration of Boys and Corner as reported in reference 2.

One further comparison with independent theory is possible, this being for the thermal theory flame speed. Kármán and Penner⁽¹⁾ detail a thermal theory calculation of the steady-state flame speed for the ozone decomposition flame, the results of which can be hammered into the form

$$U_{Kp} = \left(\frac{\theta_o}{1-\theta_o} \right)^{\frac{1}{2}} \left(\frac{k_f W_f}{\rho_o C_p} \right)^{\frac{1}{2}} J^{\frac{1}{2}}, \quad (6.41)$$

without changing any of their analysis or definitions.

$$J_{Kp} = \theta_a \exp(\theta_a) \cdot \left(-Ei(-\theta_a) \right) / \left((1-\theta_a \exp(\theta_a)) \left(-Ei(-\theta_a) \right) / (1-\theta_o) \right) \quad (6.42)$$

and Ei is the exponential integral

$$-Ei(-x) = \int_x^{\infty} t^{-1} \exp(-t) dt. \quad (6.43)$$

The thermal theory result derived here gives a value of

$$J_o = I_o(\theta_a), \quad (6.44)$$

so the ratio of the flame speeds, in this notation, is simply:

$$U_o^o/U_{Kp} = \left\{ I_o(\theta_a)(1 - I_{-1}(\theta_a))/(1 - \theta_o)/I_{-1}(\theta_a) \right\}^{\frac{1}{2}} \quad (6.45)$$

This is tabulated below for an unfavorable value of $\theta_o = 1/3$.

$\theta_a =$	3	5	7	9	11	13	15
$U_o^o/U_{Kp} =$	0.70	0.81	0.86	0.88	0.90	0.91	0.92

Comparison of Theoretical Flame Speeds. ($\theta_o = 1/3$)

For larger values of θ_o (which are less likely), the agreement is slightly worse, but for smaller values it is slightly better. For the limiting case $\theta_o = 0$, the comparison is not much different:

$\theta_a =$	3	5	7	9	11	13	15
$U_o^o/U_{Kp} =$	0.78	0.85	0.89	0.91	0.92	0.93	0.94

Comparison of Theoretical Flame Speeds. ($\theta_o \rightarrow 0$)

The Kármán - Penner solution for the ozone flame speed is shown in reference 1 to be highly accurate as compared to numerical integration of the equations, so the result derived here (which is essentially a "zereth order" approximation, whereas the Kármán - Penner result is a "first order" approximation) is not far in error of the accurate solution to the steady-state equations.

A comparison of flame thicknesses would be interesting and informative, but theoretical estimates were not discovered in the literature. Measurements, however, have been made on a reasonably

extensive scale^(18, 19, 22), so a comparison with experimental data is carried out below. A word of caution, however; the indefiniteness of the flame "boundaries" is well known, and the measured thickness of a flame is by no means independent of the method by which it was measured. But in any case, one should expect order-of-magnitude agreement and proper "trends".

Comparison of relaxation time expressions is not carried out because no similar expression was found with which to compare. Experimental data on relaxation time are sparse^(23, 24).

In the comparison of flame thicknesses effected below, it was not possible to obtain an appropriate value for W_f (it seldom is in complicated processes) so it had to be deduced by using the measured value of flame speed and the known value of thermal diffusivity in conjunction with the theoretical value of $U_o^o (\rho_o \bar{C}_p / k_o W_f)^{\frac{1}{2}}$ given by θ_o and θ_a . Furthermore, θ_a was calculated on the assumption that the activation temperature for methane combustion is = 13,000°K.

This procedure exemplifies the greatest value of an analysis such as this one -- it can be used to correlate and cross-check experimental data after a few basic parameters are measured. In this case, one requires any four parameters to deduce the other three. The graphs are constructed in such a form as to expedite such procedure.

The table below lists experimental values of θ_o , U_o^o , and L_T^o for three flames taken from reference 24. ρ_o and \bar{C}_p were measured by the same authors, but k_o was estimated from data in reference 25, and the activation energy of 26 K cal/mole was adopted

from reference 26. Each of the flames is fed by a stoichiometric mixture of oxygen and methane, with sufficient inert diluent gas added to bring the proportions of the inert gas and oxygen to that of air (O₂ and N₂). Thus each pre-mixed gas contains 10 per cent CH₄, 18.4 per cent O₂, and 71.6 per cent diluent by volume.

Diluent	$K^E = \frac{k_o}{\rho_o \bar{C}_p} \text{ (cm}^2/\text{sec)}$	$U_o^E \text{ (cm/sec)}$	θ_o^E	θ_a^E	$L_T^E \text{ (cm)}$
N ₂	0.195	36.3	0.13	6.0	0.0482
A	0.191	77.3	0.11	5.5	0.0292
He	0.762	126	0.11	5.4	0.0465

Tabulation of Experimental and Estimated Data

As five quantities are available here, there are many ways the data could be used. If the symbols

$$(A_1, A_2) \xrightarrow{T} (B_1, B_2) \quad (6.46)$$

are read "A₁ and A₂ can be used by the theory, T, to provide B₁ and B₂", then the following relations hold:

$$(K^E, U_o^E, \theta_o^E, \theta_a^E) \xrightarrow{T} (L_T^O, W_f, t_R) \quad (6.47)$$

$$(K^E, U_o^E, \theta_o^E, L_T^E) \xrightarrow{T} (\theta_a, W_f, t_R) \quad (6.48)$$

$$(K^E, U_o^E, \theta_a^E, L_T^E) \xrightarrow{T} (\theta_o, W_f, t_R) \quad (6.49)$$

$$(K^E, \theta_o^E, \theta_a^E, L_T^E) \xrightarrow{T} (U_o^O, W_f, t_R) \quad (6.50)$$

$$(U_o^E, \theta_o^E, \theta_a^E, L_T^E) \xrightarrow{T} (K, W_f, t_R) \quad (6.51)$$

where, of course, there are two theories (two T's) -- the thermal theory and the unity Lewis number theory. Of the above possible procedures, (6.47) and (6.50) appear the most reasonable. Employing the graphs at the end of this chapter, the following tables can then be constructed.

Diluent	$W_f (\mu\text{sec}^{-1})$	$t_R (\mu\text{sec})$	$L_T^O (\text{cm})$	$L_T^E (\text{cm})$
N ₂	0.12	58	.023	.048
A	0.54	13	.011	.029
He	0.36	19	.028	.047

Procedure (6.47) T = Thermal Theory

Diluent	$W_f (\mu\text{sec}^{-1})$	$t_R (\mu\text{sec})$	$L_T^O (\text{cm})$	$L_T^E (\text{cm})$
N ₂	0.78	34	.026	.048
A	2.8	6.6	.012	.029
He	1.9	11	.031	.047

Procedure (6.47) T = Unity Lewis Number

Diluent	$W_f (\mu\text{sec}^{-1})$	$t_R (\mu\text{sec})$	$U_O^O (\text{cm/sec})$	$U_O^E (\text{cm/sec})$
N ₂	.019	300	15	36.3
A	.052	96	25	77.3
He	.083	60	64	126

Procedure (6.50) T = Thermal Theory

Diluent	$W_f (\mu\text{sec}^{-1})$	$t_R (\mu\text{sec})$	$U_o^O (\text{cm/sec})$	$U_o^E (\text{cm/sec})$
N ₂	13	161	17	36.3
A	34	58	28	77.3
He	53	36	72	126

Procedure (6.50) T = Unity Lewis Number Theory

Clearly the above tables do not show striking accuracy in the comparison of predicted and observed values -- but the trends are correct, and nowhere is there an order-of-magnitude disagreement. Little else was asked of this theory at the outset. Now, in defense of the further accuracy of the theory, the following obvious points of discrepancy and sources of error should be noted:

- 1) The relevant reaction is probably not first order -- i. e., the rate-controlling step may not be proportional to CH₄ concentration.
- 2) The effective θ_a is not known to general satisfaction⁽²⁷⁾. An estimate was substituted for knowledge, and the curves are fairly sensitive to the value of θ_a used.
- 3) The precise physical interpretation of the measured value of L_T is uncertain to some degree, and procedure (6.50) is very sensitive to the value of L_T used.

In any event, the above example of the use of the curves illustrates the main purpose of the calculations -- to provide a method of correlation and to produce order-of-magnitude estimates quickly, on

the basis of known data. The graphical presentation of results which follows has been constructed with ease of such use in mind. An index to the figures is given below.

Index to Figures

- 6.1 Steady state flame speed for thermal theory versus flame temperature ratio, with activation temperature ratio as parameter.
 $U_o \cdot (\rho_o \bar{C}_p / k_o W_f)^{\frac{1}{2}}$ vs. $(\theta_o; \theta_a)$.
- 6.2 Same as 6.1, but for unity Lewis number theory.
- 6.3 Thermal length (L_T) in terms of flame speed and thermal diffusivity versus flame temperature ratio with activation temperature ratio as parameter -- for thermal theory.
 $\rho_o U_o \bar{C}_p L_T / k_o$ vs. $(\theta_o; \theta_a)$.
- 6.4 Same as 6.3, but for unity Lewis number theory.
- 6.5 L_T / L_n versus $(\theta_o; \theta_a)$ -- for thermal theory.
- 6.6 Relaxation time in terms of flame speed and thermal thickness versus flame temperature ratio with activation temperature ratio as parameter -- for thermal theory.
 $U_o t_R / L_T$ vs. $(\theta_o; \theta_a)$.
- 6.7 Same as 6.5, but for unity Lewis number theory.

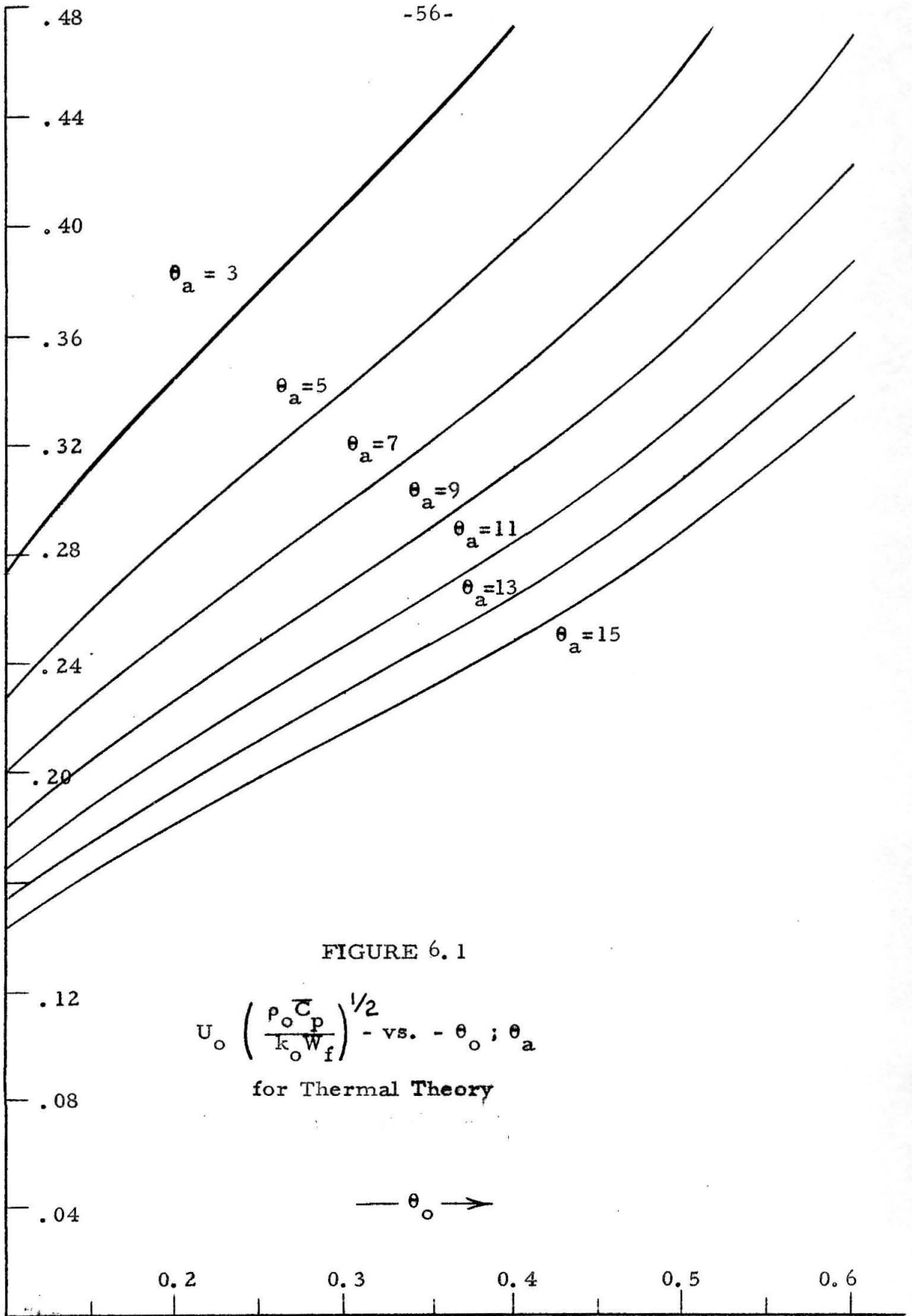
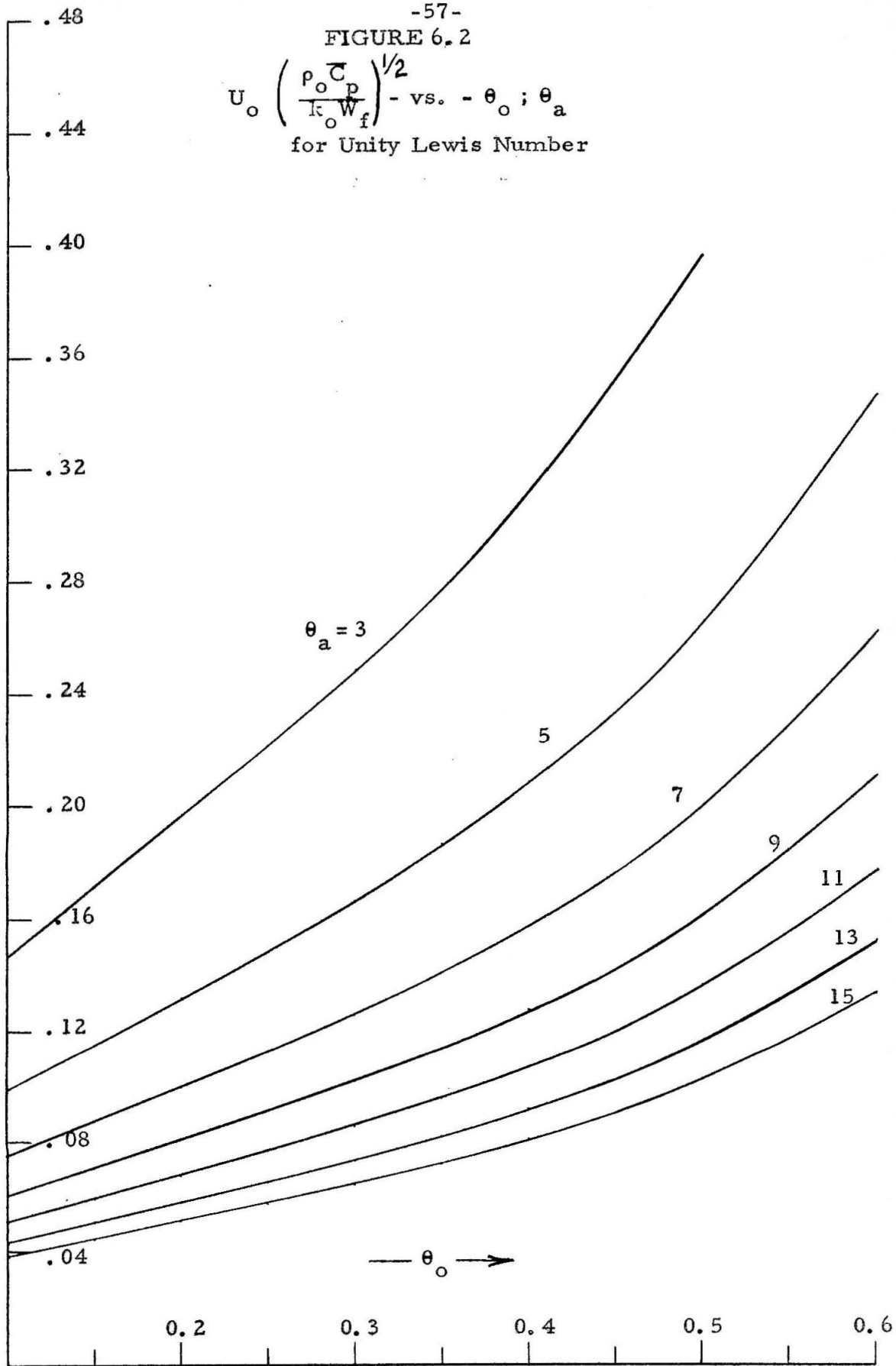


FIGURE 6.2

$U_o \left(\frac{\rho_o \bar{c}_p}{k_o W_f} \right)^{1/2}$ - vs. $-\theta_o$; θ_a
for Unity Lewis Number



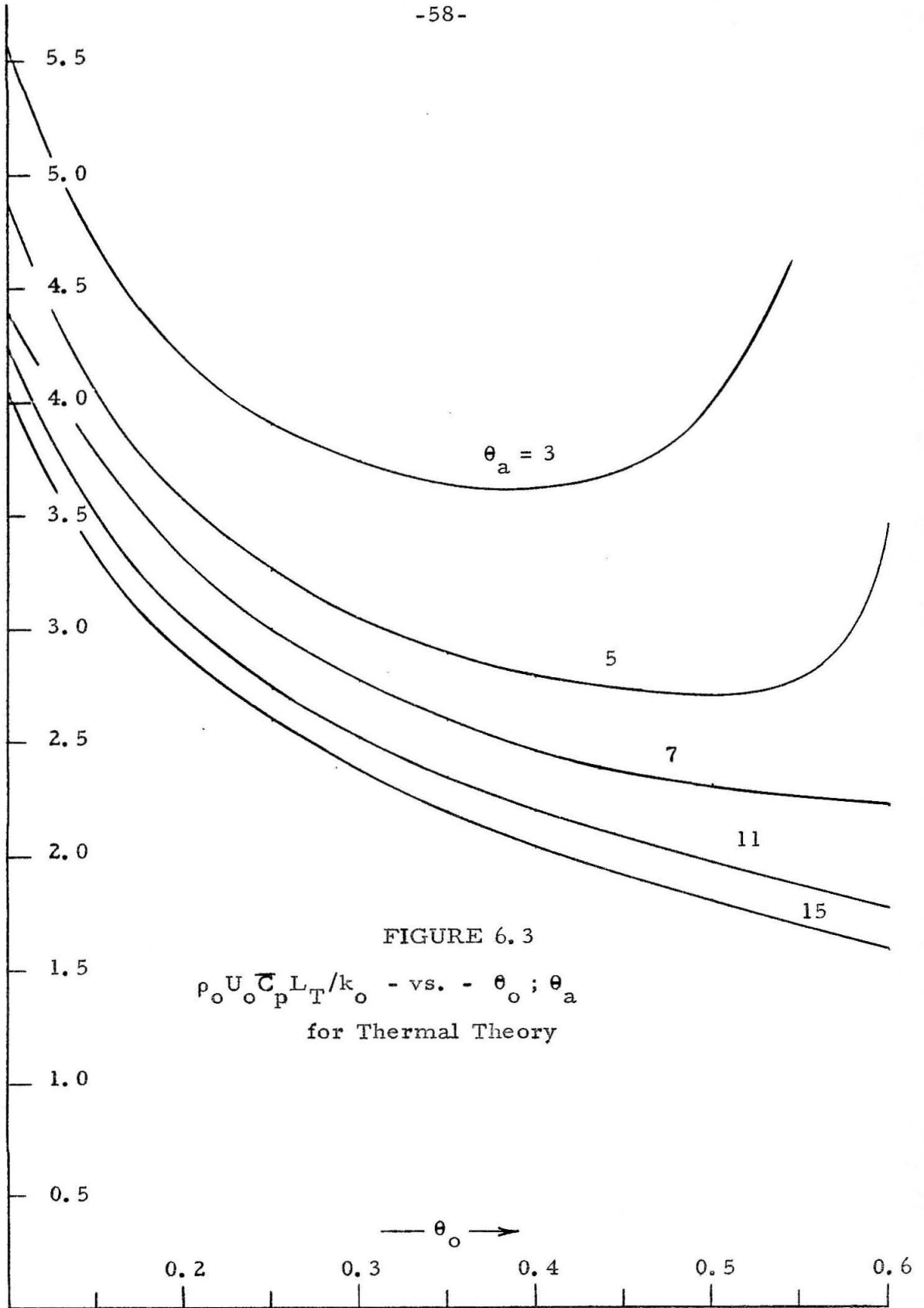


FIGURE 6.3
 $\rho_0 U_0 \bar{C}_p L_T / k_0$ - vs. - θ_0 ; θ_a
for Thermal Theory

FIGURE 6.4

$\rho_o U_o \bar{C}_p L_T / k_o$ - vs. $-\theta_o ; \theta_a$
for Unity Lewis Number

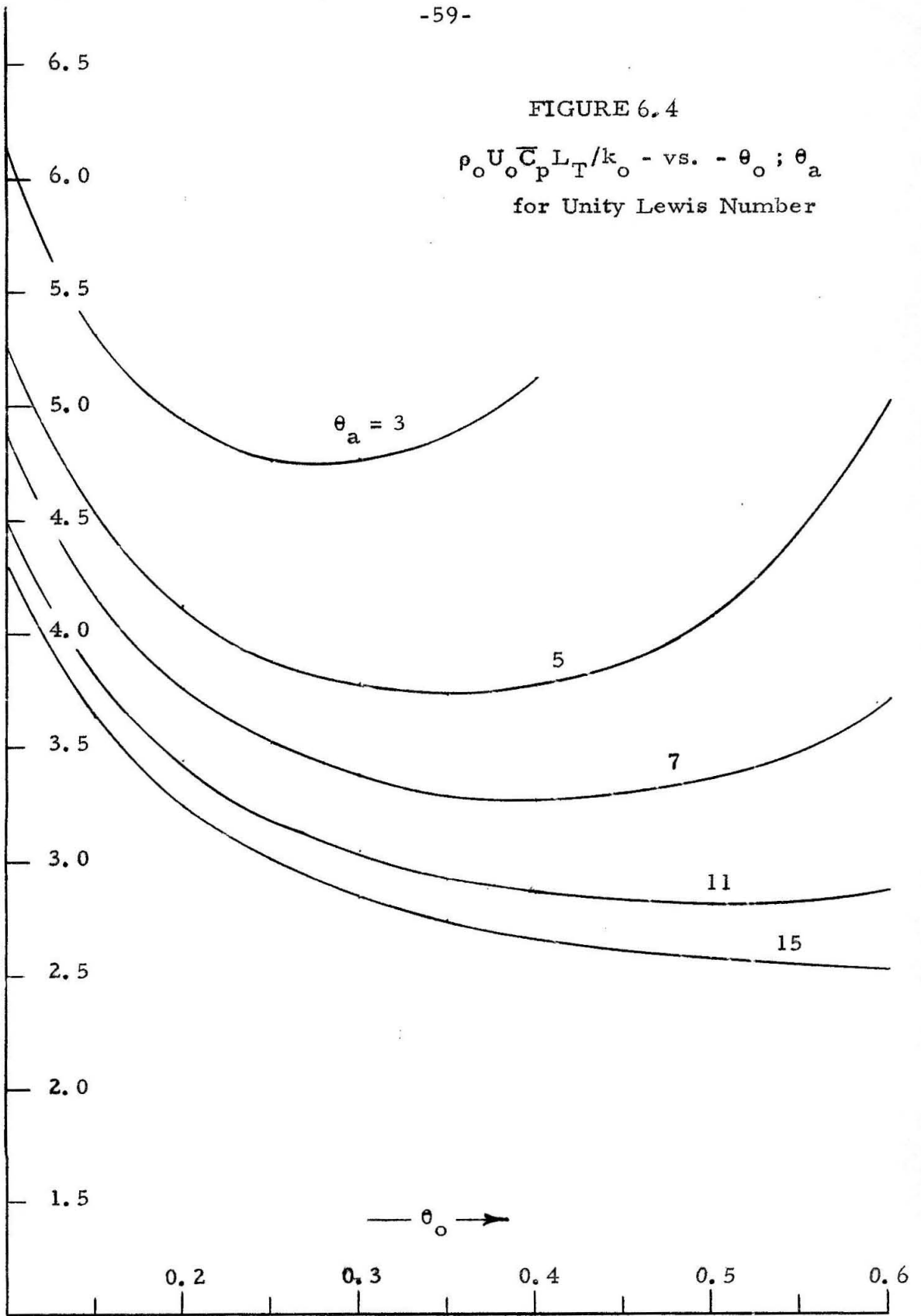


FIGURE 6.5
 L_T/L_η - vs. $\theta_o; \theta_a$
for Thermal Theory

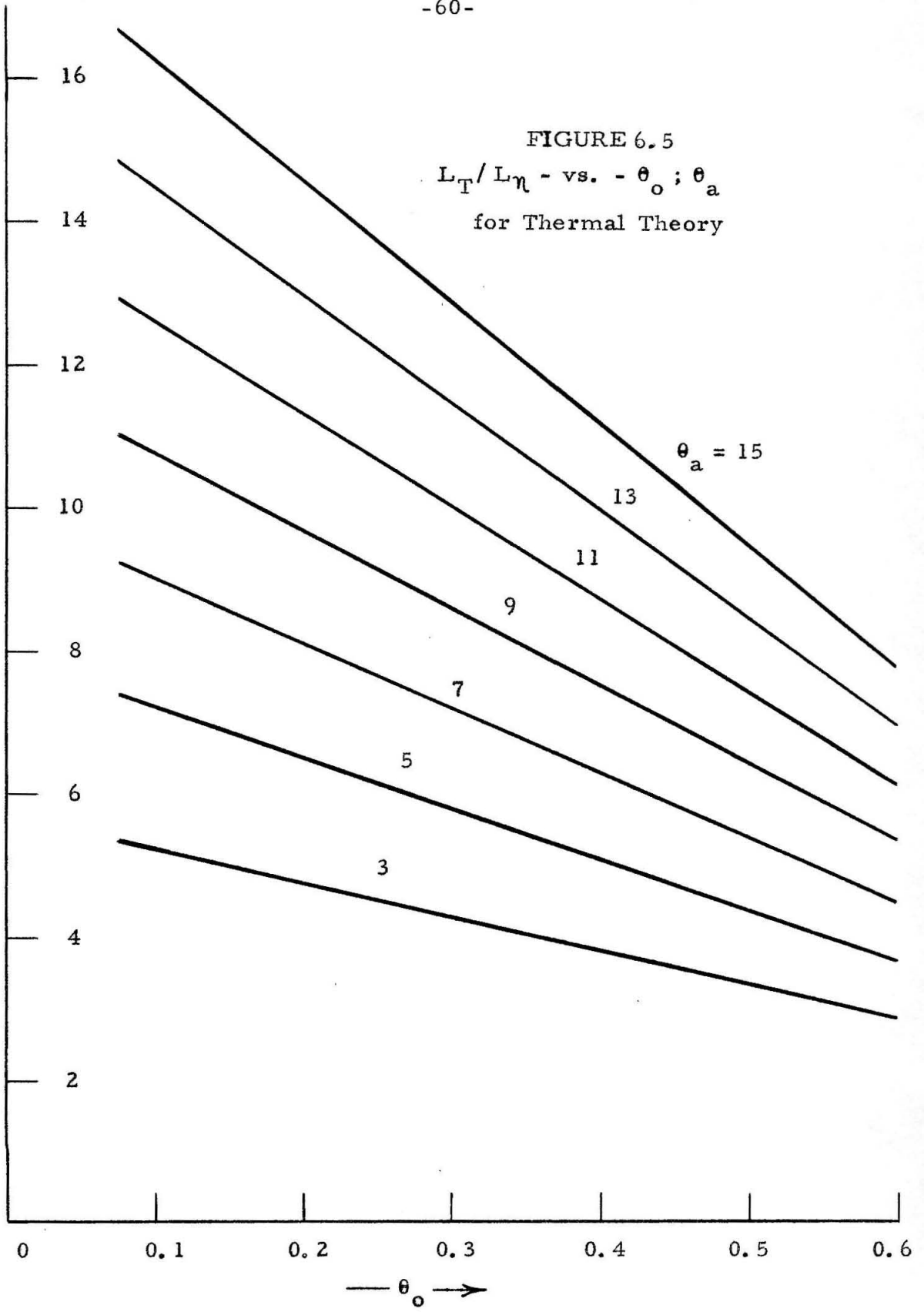


FIGURE 6.6
 $U_o t_R / L_T$ - vs. $-\theta_o$; θ_a
for Thermal Theory

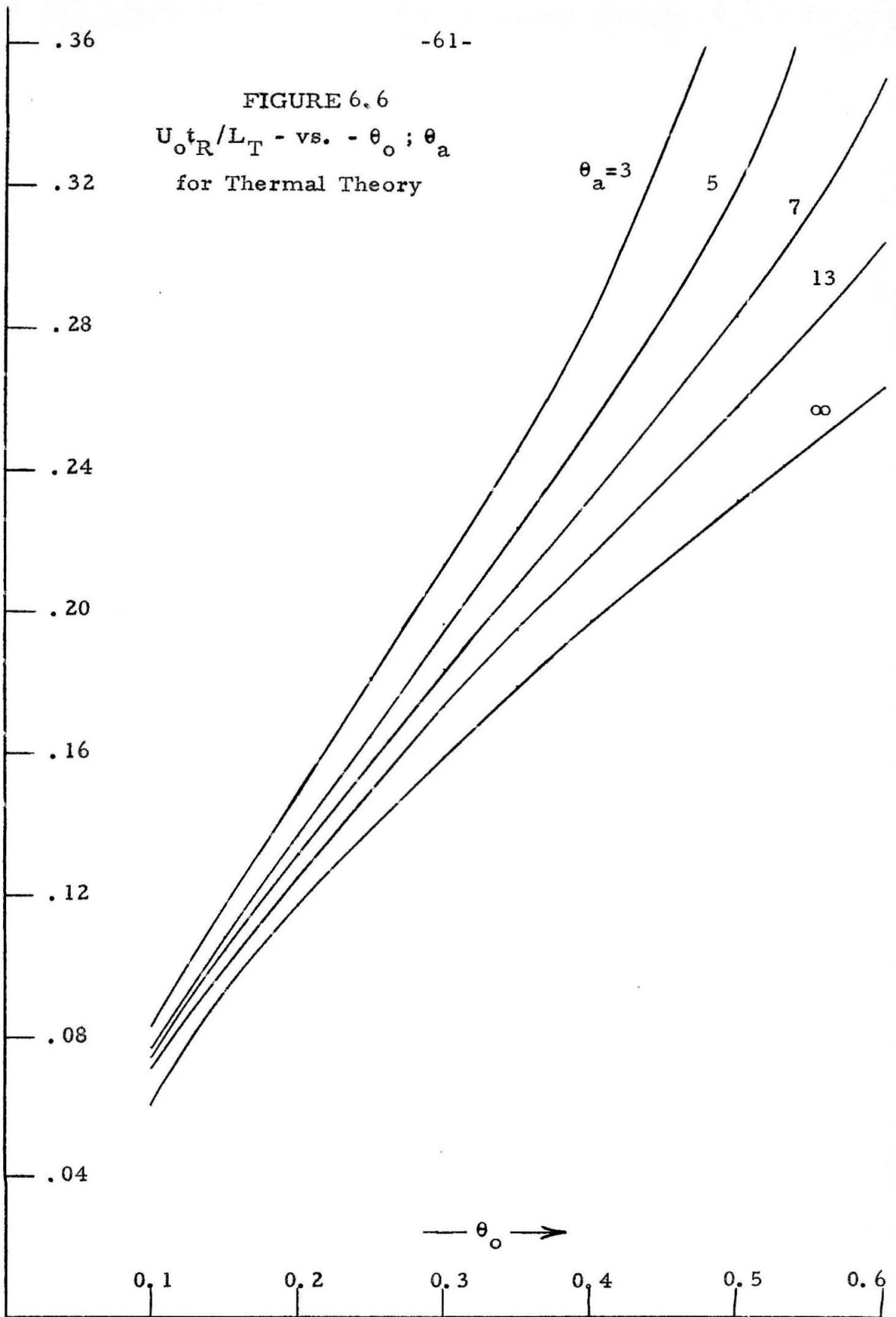
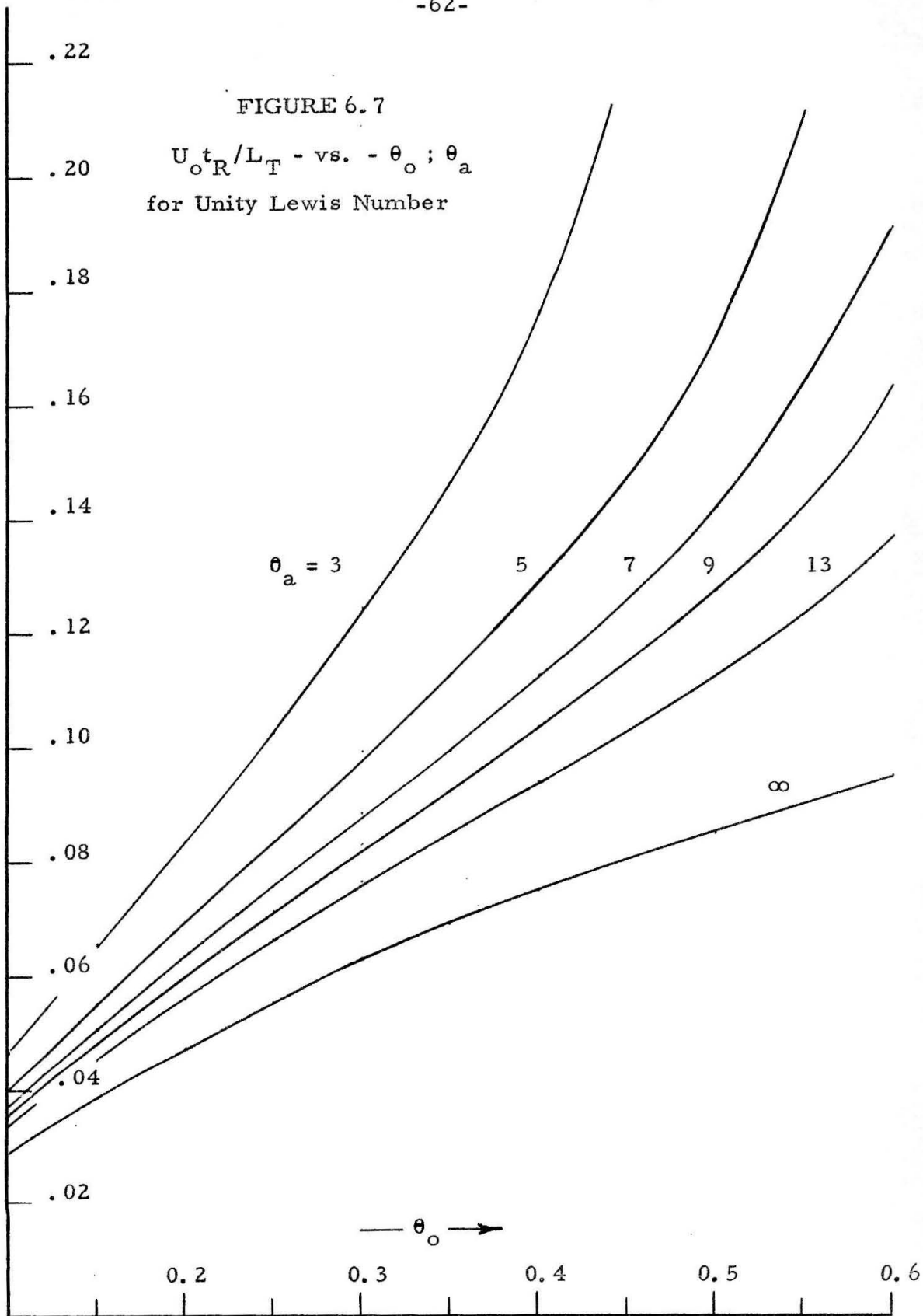


FIGURE 6.7
 $U_o t_R / L_T$ - vs. $-\theta_o ; \theta_a$
for Unity Lewis Number



VII. CONCLUDING REMARKS

In the preceding work, a method for computing the relaxation time of a first-order reaction laminar deflagration has been developed, for restricted perturbations. The restrictions are not seen as severe, and indeed the relevant physical processes are not curtailed -- only the ability of the simplified physical model used to describe the processes is limited. The results depicted graphically permit rapid experimental data reduction and estimation of unmeasured quantities. Only one major item remains to be discussed; the physical interpretation of the relaxation time. From a cursory look at the values of $U_o t_R / L_T$ one must realize that t_R cannot be far removed from the time it takes some fraction of the gas to pass through the flame. This is the interpretation espoused here. It is felt that the relaxation time is the time required for the "reacting" gas to flow through the remainder of the flame and be burnt. In other words, if L^* is the distance from the hot boundary to the peak of chemical activity (maximum of $\rho n W(T)$) then $U_f t_R / L^*$ should be approximately unity. Fortunately this is calculable fairly simply in the unity Lewis number case, if a temperature profile is chosen. Taking the \cos^2 profile as an approximation to the temperature profile, the quantity L^* was computed, and $U_f t_R / L^*$ evaluated. Figure 7.1 shows the value of this group for various θ_o , θ_a , and confirms that it is near unity in all cases. This physical interpretation is appealing, for it is only within the rapidly-reacting zone that small fluctuations of ρ , T , or n can have great influence -- in the upstream part of the flame, the highly-damped heat conduction equation predominates, rendering small fluctuations inef-

fectual. (12, 13, 14) This interpretation should serve to reinforce the arguments set forth for accurate representation of the hot boundary zone as the dominating region.

It might be argued that the analysis herein is highly restrictive, so that the results are of little usefulness. However, the analysis does provide reasonably accurate (order of magnitude, at least) answers to the problem considered. Now, since it is valid for small perturbations a fortiori, the results must be quite close to the result which would be obtained from a perturbation analysis under the same restrictions and assumptions. But it is a generally-accepted principle that the characteristic decay time computed from perturbation (linear) analysis is at worst a weak function of the restrictions and initial conditions assumed, i. e. the relaxation time is provided by the equations and not the conditions on the solutions. Therefore, one must conclude that the relaxation time computed here can be no less reliable than one given by a perturbation analysis of the same situation. The generality and accuracy of the results are felt not to be restricted severely by the method, but rather by the approximations and weaknesses admitted for the sake of tractable analysis.

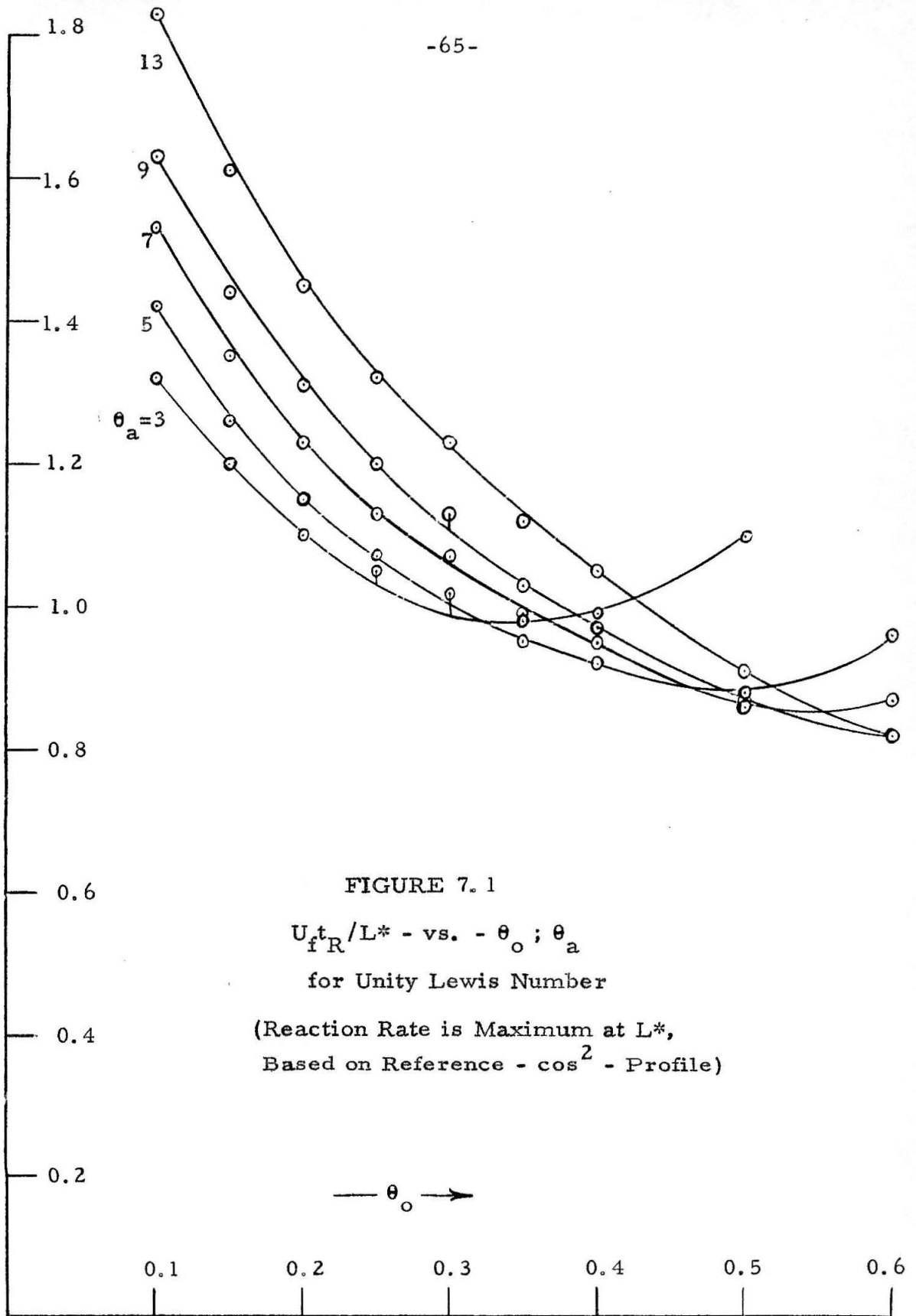


FIGURE 7.1

$U_f t_R / L^*$ - vs. $-\theta_0 ; \theta_a$

for Unity Lewis Number

(Reaction Rate is Maximum at L^* ,
Based on Reference $-\cos^2$ - Profile)

$\theta_0 \rightarrow$

VIII. ANNOTATED BIBLIOGRAPHY

1. von Kármán, Th., and S. S. Penner, "Fundamental Approach to Laminar Flame Propagation." Presented at the Colloquium held by the Advisory Group for Aeronautical Research and Development, North Atlantic Treaty Organization, Cambridge, U. K., Dec. 7-11, 1953, (available from AGARD in monograph form). Most of this material is also available in S. S. Penner, "Chemistry Problems in Jet Propulsion," Fergamon Press, London (1957).

This work contains a general and rigorous development of the complete equations describing constant-pressure deflagration, including all chemical kinetic processes. Some degree of clarity is lost in the encumbering notation required for such generality, in spite of full development of the thermal theory and unity Lewis number cases. Specific calculations of the hydrazine and ozone decomposition flames illustrate the theory and to a large extent rectify possible obscurity (in the textbook numerous other examples reinforce this).

2. von Kármán, Th., "The Present Status of the Theory of Laminar Flame Propagation," pg. 1, Sixth International Symposium on Combustion, Reinhold Publishing Co., New York (1957).

A lucid survey article bringing together and evaluating existent flame propagation theories. Many references are cited.

3. von Kármán, Th., and G. Millán, "The Thermal Theory of Constant Pressure Deflagration," pg. 55, C. B. Biezeno Anniversary Volume of Applied Mechanics, N. V. De Technische Uitgeverij H. Stam., Haarlem; March, 1953.

This article, with characteristic clarity and simplicity, presents a concise development of the thermal theory for one-step reactions and a logical development of the hot boundary approximation. A physical discussion of the "ignition temperature" concept is included and a mathematical demonstration of the insensitivity of the results to its assumed value.

4. Penner, S. S., and F. A. Williams, "The Theory of Steady, One-Dimensional, Laminar Flame Propagation for One-Step Chemical Reactions", Astronautica Acta, VII, 171 (1961).

This is an excellent survey article, covering especially the unimolecular decomposition reaction with unity Lewis number. Various theories are compared with the exact solution in lucid graphical form.

5. Richardson, J. M., "The Existence and Stability of Simple, One-Dimensional, Steady-State Combustion Waves," pg. 182, Fourth International Symposium on Combustion, Williams and Wilkins Co., Baltimore (1953).

This is an only slightly obscure proof of the existence and stability of a steady-state solution to the accepted flame equations, under the assumption $W(T_0) \equiv 0$. Many such papers have been written, and controversy has raged for years among the mathematically-oriented concerning the existence, uniqueness, and stability questions. This particular paper is referenced (as are several others) as background material representative of the types of arguments and analyses employed in the controversy. Most of the furor has centered about the (physically unimportant) cold boundary problem ($W(T_0) \neq 0$), and Richardson sees fit to just postulate its nonexistence.

6. Berlad, A. L., and C. H. Yang, "On the Existence of Steady-State Flames," Combustion and Flame, 3, 447 (1959).

This article is representative of the mathematical treatments of the cold boundary difficulty. The authors scrutinize this disturbing feature of the equations and convince themselves that no steady-state solutions exist. To reconcile this conclusion with experimental data, they argue that "quasi-steady" (but unstable) solutions exist if a heat sink is provided at the cold boundary. (The heat sink has been shown to be equivalent to an "ignition temperature" assumption.)

7. Rosen, J. B., "Theory of Laminar Flame Stability I. Analytic Stability Condition", J. Chem. Phys., 22, 733 (1954).

In this paper Rosen formulates the perturbation equations for a transient description of a general laminar flame. He immediately restricts the perturbation to a temperature (heat release) pulse applied at the inflection point of the steady temperature profile, which is also the origin of his coordinate system.* An appropriate solution is effected by assuming mass flux and fuel concentration perturbations to be negligible.** Despite boundary conditions applied at $+\infty$, Rosen assumed the coefficients of the differential equation to be constant except over a narrow zone describing the flame thickness. His results imply the possibilities of oscillation, exponential-like decay to steady state, and runaway instability interpreted as transition to detonation.

* See remarks under Barenblatt and Zel'dovich reference.

** See remarks under Menkes reference.

8. Rosen, J. B., "Theory of Laminar Flame Stability II. General Numerical Method and Application to Typical System," Journal of Chemical Physics, 22, 743 (1954).

In this companion paper Rosen displays the results of numerical integration of the perturbation equations. He finds a posteriori justification of approximations in the calculations of Part I. He finds oscillatory solutions, damped decay, and runaway instability in the range of calculations performed. His analysis has been criticized by Barenblatt and Zel'dovich and by Menkes on different grounds, but neither seems aware of the fact that the temperature perturbation imposed by Rosen in this numerical work is inordinately large. As mentioned in the text, the perturbation must be restricted to keep the perturbed reaction rate much smaller than the steady-state reaction rate. Rosen's perturbation results in a reaction rate perturbation term approximately six times larger than the steady-state reaction rate! On this fact a fundamental objection to the results is voiced, and no comparison with this work was carried out here.

9. Rosen, J. B., "Stability of the Ozone Flame Propagation," pg. 236, Sixth International Symposium on Combustion, Reinhold Publishing Co., New York (1957).

This article presents another numerical integration of the perturbation equations as above, with more details of the numerical procedure. It is interesting to note that Rosen was forced to restrict the steady-state profiles to a finite zone, and assumed the perturbation quantities all to have zero slope at the endpoints of this zone. The remarks above apply here also.

10. Rosen, J. B., "Combustion Wave Stability and Flammability Limits," J. Chem. Phys., 22, 750 (1954), Letter to Editor.

By applying a transformation on the perturbation energy equation, Rosen reduces the equation to a second order, linear, wave-like homogeneous equation. Then by an (unnecessary) analogy to the Schrödinger equation of wave mechanics, the stability limits of the solution are deduced. He illustrates the procedure by approximating the "wave number function" with a square well profile and deducing a flammability limit. The method is clever and original, but interpretation is difficult -- in addition the "wave number function" must be reasonably accurately approximated or the conclusions would be spurious.

11. Wehner, J. F., and J. B. Rosen, "Temperature Stability of the Laminar Combustion Wave," Combustion and Flame, 1, 339 (1957).

This paper presents what is essentially an amplification and refinement of the method discussed by Rosen in the 1954 Letter to the Journal of Chemical Physics. The Schrödinger wave equation analogy is more fully developed and discussed.

12. Zel'dovich, Ya. B., and G. I. Barenblatt, "Theory of Flame Propagation," Combustion and Flame, 3, 61 (1959).

In this paper the authors present and discuss (with examples) a numerical integration procedure for obtaining flame speed as the asymptotic solution to the transient flame equations with a characteristic variable $(x - V_0 t)$. The authors suspect the work of J. B. Rosen as having found a spurious solution which represents translation of the flame structure at flame speed. They show that all flames are stable under temperature perturbation for unity Lewis number. They state that for a Lewis number different from unity only very small and rapidly-damped differences would be observable, so the conclusion of stability is not influenced.

13. Menkes, J., "On the Stability of a Plane Deflagration Wave," Proc. Roy. Soc., A253, 380 (1959).

Menkes effects an analytical solution to the perturbation equations for a general global reaction rate term under the unity Lewis number assumption, by choice of a specific, reasonable temperature profile function for steady state. He concludes that laminar deflagration is always stable, but the generation of relaxation time or other observable variables from his solution is virtually impossible. In this paper the author references earlier work of his which shows that the effect of Lewis number slightly different from unity is second order in perturbation quantities -- a conclusion with which Barenblatt and Zel'dovich would concur.

In this paper the author criticizes the work of J. B. Rosen for incompleteness in restricting the species perturbation term to be zero. This criticism was met in later numerical work by Rosen and shown to be unjustified, as instabilities were still observed with this term included.

14. Layzer, D., "Theory of Linear Flame Propagation I. Existence, Uniqueness, and Stability of the Steady State," J. Chem. Phys., 22, 222 (1954).

An integral method is employed in this fundamental investigation, and much emphasis is placed on physical arguments concerning expansion and contraction of the length scale (flame thickness). Layzer employs a non-inertial coordinate system as was done above, after discussing the constant pressure assumption. He formulates and discusses the basic equations and boundary conditions, dismissing the cold boundary difficulty after due consideration. He deduces that the flame thickness should be of the order of, but larger than, the ratio of thermal diffusivity to flame speed (a result borne out above) and observes that a sinusoidal perturbation will have its greatest effect if the wavelength of the perturbation is of the order of the flame thickness. Heat conduction and species diffusion will

quickly dampen higher frequency disturbances, and the flame will react quasi-steadily to lower frequencies. This conjecture is borne out to a large extent by the relaxation times computed herein. He concludes the existence and stability of laminar deflagration, and poses some conjectures concerning inflammability limits.

15. Layzer, D., "Theory of Linear Flame Propagation II. Structure of the Steady Flame," J. Chem. Phys., 22, 229 (1954).

In this companion paper, Layzer continues his investigation of laminar flames. His abstract speaks well in description:

"A quantitative approximate theory of flame structure in the steady state, including formulas for the determination of flame speeds, is set forth. The theory predicts that in a first approximation, the sensitivity of a steady deflagration wave to external perturbations depends upon the shape of the temperature profile but not upon the speed or width of the wave, or the pressure. It is shown that the sensitivity increases with increasing dilution of the explosive mixture, in agreement with the explanation of inflammability limits suggested in Part I."

For the unity Lewis number case, Layzer seeks to improve the von Kármán hot boundary approximation by assuming a species flux rate proportional to θ^N . This leads him to a quite credible temperature profile:

$$\theta = e^{\xi} \left(1 + e^{(N-1)\xi} \right)^{- (1/N-1)}$$

where

$$\xi = \rho U C_p x / k .$$

16. Spalding, D. B., "Approximate Solutions of Transient and Two-Dimensional Flame Phenomena; Constant Enthalpy Flames," Proc. Roy. Soc., A245, 352 (1958).

Spalding, taking his cue from the Marble-Adamson integral treatment of the laminar mixing zone ignition problem, treats several initial-value combustion problems by an integral method. He deals only with the temperature equation and uses the unity Lewis number restriction for simplicity. He treats the propagation of a flame away from a cold catalytic wall which ignites it, the formation and propagation of a flame from a surface of contact between combustible cold gas and hot burnt gas, and the consumption by flame of a cold, planar slab of combustible gas immersed in a medium of hot, burnt gas.

The paper serves well as an example of what Spalding calls "profile techniques", but fares not so well in treating the specific problems attacked. The major objection is that the method will not provide a decision as to whether or not ignition

occurs. Although Spalding states (on the basis of comparison of the linear, bi-parabolic and \cos^2 profile integrals) that the method is accurate to within 20 per cent, the writer feels that this has not been sufficiently demonstrated. Spalding makes a profile similarity assumption in his analysis which is quite similar to the assumption employed herein, and though his integrals extend to infinity in some cases, he uses flame thickness as a basic dependent variable.

17. Marble, F. E., and T. C. Adamson, Jr., "Ignition and Combustion in a Laminar Mixing Zone," Jet Propulsion (J. Amer. Rocket Soc.), pg. 85 (March-April, 1954).

An elegant application of the integral method (with similarities to boundary-layer integrals) to the problem of heat and species transfer in a laminar mixing zone, leading to ignition and combustion. This work exemplifies the inherent "physical picture" nature of the integral method and allows a thorough comprehension of the process at each step of the analysis.

18. Levy, A., and F. J. Weinberg, "Optical Flame Structure Studies," Combustion and Flame, 3, 229 (1959).

This paper is a study in experimental care and precision. A careful preparation of extremely lean and flat ethylene-air flames permits the rigorous interpretation of optical data. A highly exact (and exacting) ray-tracing procedure leads to density/distance profiles, hence temperature/distance profiles. These, coupled with a modicum of theory provide heat-release-rate profiles and concentration profiles. In the words of the authors, their results "simultaneously justify the chemist's disdain for and the engineer's use of a 'global reaction'." This may be the first such direct experimental evidence of high accuracy.

19. Friedman, R., "Measurement of the Temperature Profile in a Laminar Flame," pg. 259, Fourth International Symposium on Combustion, Williams and Wilkins Company, Baltimore (1953).

Friedman, in a characteristically careful and accurate manner, presents the results of temperature profile measurements in very lean propane/air flames. The flames employed are flat by virtue of special burner apparatus, and are traversed by very small coated thermocouples. Radiation-corrected data then are reduced as $\rho U C_p x/k$ versus T curves. Friedman calculates a profile, including all temperature-dependent properties, for the cold end of the flame under the assumption of a negligible reaction rate, and compares this with the experimental results. The comparison is strikingly successful. His result for this flame is a "thickness" which is approximately twice the value computed herein, and a perusal of his error analysis places the source of discrepancy in the inadequacy of the theory here developed. It should be pointed out,

however, that the major source of the 'extra thickness' is the exponential cold-boundary temperature decay, which has been artificially truncated here.

20. Friedman, R., "Kinetics of the Combustion Wave," A. R. S. Journal, 23, 349 (1953).

In this survey-type article Friedman reviews structure and flame speed calculations in elementary systems. A point of interest is the presentation of a value for $\rho_0 U_0 \bar{c} L_T / k_f = 2.0$ obtained by numerical integration for the case of unity Lewis number, $\theta_0 \approx 0.2$, $\theta_a \approx 10$. The same case treated here gives a value of 1.6 -- i. e. about 25 per cent low. In light of the fact that the U_0 computed herein is known to be ~ 20 per cent low or more, the implication of greater accuracy for L_T is apparent. Friedman's experimental results are not so encouraging, however.

21. Emmons, H. W., J. Haar, and P. Strong, "Thermal Flame Propagation," monograph issued Feb. 1950 by Computation Laboratory of Harvard University, Cambridge, Mass. (under contract AT(30-1)-497.)

A detailed discussion of numerical integration of the steady-state laminar flame equations, demonstrating a high degree of insensitivity of flame speed to initial temperature slope and "ignition temperature".

22. Morgan, G. H., and W. R. Kane, "Some Effects of Inert Diluents on Flame Speeds and Temperatures," pg. 313, Fourth International Symposium on Combustion, Williams and Wilkins Co., Baltimore (1953).

The authors present measurements of flame speed and thickness for a very large range of mixtures of gases. Methane and oxygen in stoichiometric proportions are diluted with inert gases (N_2 , A, He) in various concentrations. Flame speeds are computed as the ratio of volumetric flow rates to cone areas of bunsen flames, and thicknesses are measured by the density changes visible in Schlieren photographs of the flames. Quenching effects are severe in some cases, and temperature measurements do not stand the test of consistency in all cases, but the limitations and inaccuracies of the data are intelligently discussed by the authors.

23. Schalla, Rose L., "Perturbation Studies of Flames by Changes in Composition," Combustion and Flame, 5, 45 (1961).

This paper presents results of studies conducted in a closed combustion tube, with the flame traversing a change in composition of the combustible gas. Pressure oscillations, two-dimensional disturbances, and insufficient equipment

response-time render the interpretation of the data nearly unmanageable. No deduction of flame relaxation time appears possible from these data.

24. Zucrow, M. J., J. R. Osborn, and A. C. Pinchak, "Luminosity and Pressure Oscillations Observed with Longitudinal and Transverse Modes of Combustion Instability," J. Am. Rocket Soc., 30, 758 (1960).

This paper presents the results of experimental investigations on ethylene-air (premixed)- burning rocket chambers which exhibited high-frequency combustion fluctuations. "Transverse" and "longitudinal" pressure-wave oscillations were accompanied by fluctuations of luminosity of the reacting gas mixture. Measurement of the phase shift between the time histories of pressure and luminosity variations indicated a relaxation time of $\sim 95 \mu\text{sec}$ for the combustion zone in the "transverse" mode.

25. Clingman, W. H., R. S. Brokaw, and R. N. Pease, "Burning Velocities of Methane with Nitrogen-Oxygen, Argon-Oxygen, and Helium-Oxygen Mixtures," pg. 310, Fourth International Symposium on Combustion, Williams and Wilkins Co., Baltimore (1953).

A careful experimental investigation of flame speeds and a comparison with various theoretical predictions.

26. Fenn, J. B., and H. F. Calcote, "Activation Energies in High Temperature Combustion," pg. 231, Fourth International Symposium on Combustion, Williams and Wilkins Co., Baltimore (1953).

27. Vandenberg, H., R. Corbeels, and A. van Tiggelen, "Activation Energy and Reaction Order in Methane-Oxygen Flames," Combustion and Flame, 4, 253 (1960).

This paper describes experimental measurements of flame speeds for diluted oxygen-methane flames, and subsequent deduction of activation energy and reaction order. The results differ rather severely from other sources consulted, with activation energy estimated at 38 k cal/mole, and flame speeds several times higher than "usual". It is interesting to note that use of this high value of activation energy in the data reduction carried out in the text would cause greater divergence of experimental and theoretical results.

II. REFLECTION AND TRANSMISSION OF ELECTROMAGNETIC
WAVES AT ELECTRON DENSITY GRADIENTS

ACKNOWLEDGMENT

The author expresses sincere appreciation of the many hours of discussion and encouragement afforded him by Professor Robert G. Jahn, without whose physical insight this effort might have been completely misdirected, and to the Daniel and Florence Guggenheim Foundation, for the fellowship which made continued graduate study possible.

ABSTRACT

The interaction of an electromagnetic wave with a mildly ionized gas is described by an ensemble average treatment of electron motion, and under this description, electromagnetic wave propagation parameters are derived. Motivated by the fact that mildly ionized gases in general exhibit inhomogeneous boundary regions, exemplary transition zones are described in terms of varying electron density but constant collision frequency, in order to simplify the solution of wave problems. The half-space reflection problem with a linear transition zone is solved exactly and under two approximations. It is discovered that the reflection and transmission coefficients are strong functions of zone thickness for thin zones. A piecewise-linear transition zone solution exemplifies the procedure for constructing an approximate solution to an arbitrary profile and illustrates the relative insensitivity of reflection and transmission coefficients to detailed zone structure. The "slab" reflection problem with symmetrical, linear transition zones is solved exactly, and it is discovered that the basic periodicity of reflection and transmission coefficients with slab thickness is unchanged, although shifted to higher values of slab thickness/wavelength. The text is supported by fairly extensive graphical presentation of results.

TABLE OF CONTENTS

<u>Chapter</u>	<u>Title</u>	<u>Page</u>
	Acknowledgment	75
	Abstract	76
	Table of Contents	77
IX.	INTRODUCTION	78
X.	FORMULATION OF PROBLEMS	93
XI.	THE LINEAR RAMP PROBLEM	103
	Figures, Chapter XI	118
XII.	THE KINKED RAMP PROBLEM	134
	Figures, Chapter XII	141
XIII.	THE TRAPEZOID PROBLEM	157
	Figures, Chapter XIII	167
XIV.	SUMMARY	215
	References	219

IX. INTRODUCTION

In the recent history of engineering, extreme gas temperatures have forced to the forefront of investigation a hybrid electrical-aerodynamic medium, the mildly-ionized gas. Such a body of ionized gas expelled from a rocket nozzle forms a "cloud" behind the propelled vehicle at high altitude, which may interfere with telemetry and radio-guidance signals. The mildly-ionized gas formed behind a strong bow shock wave of a hypersonic vehicle may alter heat transfer rates and cause shorting of transmitting antennae. The weakly-ionized gas formed by shock-heated air and by ablated material from a re-entry projectile may provide a wake visible to radar, much like the meteor's trail which is similarly visible. The ionized gas composing the atmospheres of stars provides the signals attended by radio astronomers, and the Earth's own ionosphere provides a low-frequency radio-propagation path around the world. Such research devices as shock tubes, fusion plasma confiners, plasma accelerators, ion engines, magneto-hydrodynamic generators, etc., all employ in various forms, an ionized gas. In short, there is ample incentive for basic study of the properties of an ionized gas.

Perhaps the most important of the properties of an ionized gas is its ability to interact strongly with electromagnetic waves and fields. This interaction is fundamental to the operation of most plasma accelerators and generators, and is intrinsic to much telemetry and communications engineering. It also provides the basis of a useful experimental tool for investigation of ionized gases, i. e., the microwave probe. An ionized gas, generally, displays a lower limit frequency for propagation

of electromagnetic waves, and a phase velocity greater than the vacuum speed of light, properties of considerable academic interest in addition to obvious practical importance.

Unfortunately, most practical situations of electromagnetic wave interaction with a mildly-ionized gas (mig) are complicated by the existence of indistinct boundaries. Even when the mig is confined by a physical container, the interaction of the wall with the gas produces a region of inhomogeneity, or "transition", which complicates exact calculations, and obscures the validity of various approximations which might be considered.

The object of this investigation will be to solve exactly and evaluate numerically certain problems concerned with electromagnetic wave propagation through and reflection from such transition zones. The purpose in doing so is first to attempt to understand physically the processes occurring, and second to develop criteria for application of approximate procedures.

In order to illustrate some of the points mentioned above and to lay the groundwork for later development, the following description of the interaction of an electromagnetic wave with a mig is presented. The basic assumptions underlying the development include those listed below:

- (1) The mig can be considered locally isotropic. In other words, a sufficiently small region of the mig will exhibit constant, scalar, electrical parameters, yet contain a sufficient number of ionized particles upon which to base the calculation of such parameters in an average sense. This assumption is strictly analogous to the "particle of fluid" semi-atomistic description of continuum fluid mechanics.

(2) The fields are not so strong as to produce velocity changes in the charged particles which approach the mean thermal velocity.

(3) The gas is weakly ionized, i. e., the number of neutral atoms is far greater than the number of ionized atoms. Hence, the local fields may be assumed to provide the only significant disturbing forces, i. e., large-scale coherent plasma oscillation, streaming, and interparticle long-range forces will be neglected.

Under the restrictions listed above, the interaction can be described in terms of local average motions of the particles. * If the ensemble average vector velocity of the electrons in a typical semi-infinitesimal volume is computed, one must conclude that without an applied field, such an average would be zero. But if an electric field, \vec{E} , is applied, each particle of charge q will feel a force.

$$\vec{F} = q \vec{E}$$

Since the fields exist as propagating waves here, the Lorentz force due to the concomitant magnetic field, \vec{B} , and the velocity, \vec{V} ,

$$\vec{F}' = q \vec{V} \times \vec{B}$$

will be of the order of $(|\vec{V}|/c)$ times the electric force, where c is the speed of light. Therefore, this force is neglected on the condition that the speed of the particle is negligible compared to the speed of light.

Thus each charged particle, to a high degree of approximation, will experience acceleration

* More rigorous (and more complex) analyses of the field-mig interaction process are to be found in references (1) - (4), which exemplify the more basic attacks on the electron distribution function.

$$m \frac{d\vec{V}}{dt} = \vec{F} = q \vec{E} \quad (9.1)$$

under the influence of the electromagnetic wave. Before integrating this equation to find the velocity, however, it is important to look ahead to what is required. The net motion of charged particles, in classical electromagnetic theory, represents a "convection current,"⁽⁵⁾ the area density (\vec{J}) of which is given by a sum over all particle types, i , and all velocities.

If, of the particles i (N_i per unit volume), the j^{th} member moves with the velocity \vec{V}_{ij} , the current density is given in the form of a sum

$$\vec{J} = \sum_i q_i \sum_{j=1}^{N_i'} \vec{V}_{ji}$$

where N_i' is the total number of particles i in a unit infinitesimal volume. In other words, an ensemble average flux density is required:

$$\vec{J} = \sum_i N_i q_i \overline{(\vec{V}_i)}^E \quad (9.2)$$

where $\overline{\quad}^E$ implies ensemble average.

Under the ensemble average, then, the random, thermal velocity will vanish. But since equation (9.1) applies to every charged particle in the small region, it appears that under a steady electric field, eventually the \vec{J} of equation (9.2) will become infinite. This is clearly not an accurate picture of the process, for collisions with the neutral atoms present impede the "flow" of the charge carriers. It is a well established experimental fact that in a weak electric field, the charge carri-

ers will attain a mean "drift" velocity proportional to the field strength,⁽⁶⁾ the constant of proportionality being called the "mobility", K :

$$\overline{(\vec{V}_i)}^E = K_i (\vec{E})_{\text{steady}} \quad (9.3)$$

To effect such a steady solution, it is mandatory that the momentum gained by the particle between collisions be rendered up in the following collision, on the average. If τ is the ensemble mean time between collisions, then the momentum gained from the field force between collisions is

$$\vec{F}_i \tau_i = \Delta \vec{p}_i = q_i \vec{E} \tau_i .$$

But the number of collisions per second per particle of mean speed $\overline{|\vec{C}_i|}^E$ is $\overline{\mu}_i^E$, where

$$\overline{\mu}_i^E = N_n \Omega_n \overline{|\vec{C}_i|}^E = 1/\tau_i$$

and N_n is the neutral number density, Ω_n the collision cross section. Making the hypothesis that on the (ensemble) average, all momentum gained between collisions is lost in each collision, then the rate of loss of momentum by an (ensemble) average charge carrier is

$$\frac{\overline{\Delta(\vec{p}_i)}^E}{\tau_i} = \overline{\mu}_i^E (m_i \overline{\vec{V}_i}^E) .$$

Therefore

$$\overline{\mu}_i^E m_i \overline{(\vec{V}_i)}^E = q_i \vec{E} , \quad (9.4)$$

and thus

$$K_i = \frac{q_i}{m_i} \frac{1}{\mu_i} E = \frac{q_i \tau_i}{m_i} \quad (9.5)$$

Hence it can be concluded that there is indeed a term missing from (9.1) if it is to be interpreted in an ensemble average sense, and the appropriate equation for the ensemble average velocity of particles i is:

$$m_i \frac{d \overline{V}_i}{dt} + m_i \nu_{c_i} \overline{V}_i = q_i \overline{E} \quad (9.6)$$

where ν_{c_i} is defined to be equal to $\frac{1}{\mu_i} E$.

The integration of (9.6) is straightforward, and on the assumption of harmonic time dependence of the applied field of the form

$$\vec{E} = \vec{E}_0(x, y, z) e^{i\omega t},$$

the ensemble average velocity is given by:

$$\overline{V}_i = \frac{q_i \vec{E}_0 e^{i\omega t}}{m_i \nu_{c_i} + i\omega m_i} \quad (9.7)$$

Noting the proportionality is inverse in the mass of the particle, it is clear that electrons will contribute to \vec{J} the most by at least three orders of magnitude, hence (9.2) becomes, to a good approximation,

$$\vec{J} = N_e q_e \left\{ \frac{q_e \vec{E}_0 e^{i\omega t}}{m_e \left\{ \nu_{c_e} + i\omega \right\}} \right\} \quad (9.8)$$

where the subscript e implies electron. By analogy to Ohm's law for conducting media, a conductivity σ can be defined then for the ionized gas:

$$\sigma = \frac{N_e q_e^2}{m_e \nu_c} \left\{ 1 + i \frac{\omega}{\nu_c} \right\}^{-1} \quad (9.9)$$

The fact that σ is complex is to be interpreted in the straightforward manner that part of the current is in phase, and part of it out of phase with the driving field.

There is another way of looking at the wave-mig interaction, and that is to regard the displacement of the electrons from a "neutral" position as generating a polarization within the medium. This seems physically a bit wide of the mark, but mathematically the treatment is identical. This will become clear in the development of wave equations below.

The validity of Maxwell's equations is postulated:

$$\begin{aligned} \nabla \times \vec{E} &= - \frac{\partial \vec{B}}{\partial t} \\ \nabla \times \vec{H} &= \vec{J} + \frac{\partial \vec{D}}{\partial t} \end{aligned}$$

and the constitutive equations of the weakly ionized gas are assumed to be those of a conductor with vacuum permittivity and permeability:

$$\begin{aligned} \vec{B} &= \mu_0 \vec{H} \\ \vec{D} &= \epsilon_0 \vec{E} \\ \vec{J} &= \sigma \vec{E} \end{aligned}$$

The parameters ϵ_0 , μ_0 , and σ are independent of time, and only σ might be a function of position. Assuming harmonic time dependence for all vectors leads to the pair of equations:

$$\nabla \times \vec{E} = -i\omega\mu_0 \vec{H} \quad (9.10)$$

$$\nabla \times \vec{H} = (\sigma + i\omega\epsilon_0) \vec{E} \quad (9.11)$$

At this point the change in notation will be made, which implies the second interaction interpretation mentioned above. On the right hand side of (9.11), let

$$(\sigma + i\omega\epsilon_0) = i\omega\epsilon_0 \left(1 + \frac{\sigma}{i\omega\epsilon_0}\right) = i\omega\epsilon_0 K^*$$

where K^* can be called a complex dielectric constant by analogy to the nomenclature for lossy dielectrics. The division of σ by $i\omega$ implies the next integration of equation (9.7) leading to the second interpretation berated above. From equation (9.9) it is clear that

$$K^* = 1 + \left(\frac{N_e q_e^2}{\omega\epsilon_0 m_e}\right) \frac{1}{i\nu_c - \omega}$$

which can be written in the dimensionless ratio form

$$K^* = 1 - \left(\frac{\omega_p}{\omega}\right)^2 \left(1 + i\frac{\nu_c}{\omega}\right) \left(1 + \left(\frac{\nu_c}{\omega}\right)^2\right)^{-1} . \quad (9.12)$$

The term $\omega_p = (N_e q_e^2 / m_e \epsilon_0)^{\frac{1}{2}}$ in equation (9.12) is called the "plasma frequency" and has a definite physical meaning, evident from consideration of that class of solutions to Maxwell's equations which exhibits no magnetic field. Such solutions are "electrostatic" in a sense, ⁽⁷⁾ and could consist of symmetrical volumetric oscillations and the like. The equations for such motions are:

$$\begin{aligned} \nabla \times \vec{E} &= 0 \\ \vec{J} + \frac{\partial \vec{D}}{\partial t} &= 0 \end{aligned}$$

Writing $N_e q_e \vec{V}$ for \vec{J} , and differentiating the second equation with respect to time gives

$$\frac{\partial}{\partial t} (N_e q_e \vec{V}) + \epsilon_0 \frac{\partial^2 \vec{E}}{\partial t^2} = 0 . \quad (9.13)$$

For simplicity assume N_e constant and $\nu_c \rightarrow 0$ (a highly diffuse gas), thus obtaining from (9.6):

$$N_e q_e \left(\frac{q_e}{m_e} \right) \vec{E} + \epsilon_0 \frac{\partial^2 \vec{E}}{\partial t^2} = 0$$

or

$$\frac{\partial^2 \vec{E}}{\partial t^2} + \omega_p^2 \vec{E} = 0. \quad (9.14)$$

Thus ω_p is the natural frequency of "electrostatic" plasma oscillations. More complete (and much more complicated) derivations of the equivalent of (9.14) have been given^(4, 7, 8), including gradients in N_e and a pressure term in the electron-ensemble equation of motion. The upshot of all this is that ω_p is found to be a lower bound for the natural frequency of "electrostatic" oscillations -- the more accurate expressions include a temperature-dependent correction term.

The mig/electromagnetic wave interaction is to be described under the assumptions above by the equations

$$\nabla \times \vec{E} = -i\omega\mu_0 \vec{H}$$

$$\nabla \times \vec{H} = i\omega\epsilon_0 K^* \vec{E}$$

where K^* is defined in equation (9.12). Assuming for the moment that K^* is constant (homogeneous medium), the equation of propagation can be written:

$$\nabla \times \nabla \times \vec{G} = \omega^2 \epsilon_0 \mu_0 K^* \vec{G}$$

where \vec{G} is \vec{E} , \vec{B} , \vec{D} , or \vec{H} . Since in this situation all field vectors are solenoidal,

$$(\nabla^2 + k_0^2 K^*) \vec{G} = 0 \quad (9.15)$$

where $\omega^2 \epsilon_0 \mu_0 = \omega^2 / c_0^2 = (2\pi / \lambda_0)^2 = k_0^2$, the wave number squared. If $\nu_c / \omega \ll 1$, then $K^* = 1 - (\omega_p / \omega)^2$, and the peculiar nature of mig propagation becomes apparent from the simple plane wave solution:

$$G_z = G_{z_0} \exp \left(-ik_0 x \sqrt{1 - \left(\frac{\omega_p}{\omega}\right)^2} \right). \quad (9.16)$$

Equation (9.16) exhibits a phase velocity c_ϕ greater than the vacuum velocity of light c_0 ,

$$c_\phi = c_0 \left(1 - \left(\frac{\omega_p}{\omega}\right)^2 \right)^{-\frac{1}{2}} \quad (9.17)$$

while the group velocity c_g (as ordinarily defined by $\frac{d\omega}{d(\omega/c_\phi)}$) is less than the velocity of light:

$$c_g = c_0 \left(1 - \left(\frac{\omega_p}{\omega}\right)^2 \right)^{\frac{1}{2}} = c_0^2 / c_\phi. \quad (9.18)$$

Equation (9.16) also exhibits the lower limit of frequency for which propagation is possible. Clearly if $\omega > \omega_p$, the wave exists, propagates with $c_\phi > c_0$, and has a wavelength greater than the vacuum wavelength. As ω is decreased, the phase velocity increases and the wavelength increases, until finally a "wavelength" no longer exists, c_ϕ becomes a pure imaginary, and the "propagation" is evanescent. To insure the proper choice of sign in $\sqrt{K^*}$, recall that K^* as given in (9.12) is restricted to the lower half plane of complex numbers, so

$$(K^*)^{\frac{1}{2}} = |K^*|^{\frac{1}{2}} \exp \left(-\frac{1}{2} |\arg K^*| \right); \quad 0 \leq |\arg K^*| \leq \pi.$$

Further, it is physically obvious that when $\nu_c \neq 0$, the forward-going wave ($\exp(-ikx)$) must decrease in amplitude as x increases.

In general, then, for $\omega < \omega_p$, the medium is almost purely reactive (for small ν_c/ω) and propagation is evanescent, but for $\omega > \omega_p$, the medium acts essentially like a dielectric and dispersion is normal. For rapid, rule-of-thumb calculations, the critical frequency is given by

$$f_c = \frac{\omega_p}{2\pi} \doteq 9 \sqrt{N_e} \text{ KCPS} \quad (9.19)$$

where N_e is measured in cm^{-3} .

It is interesting to note that as $\omega_p/\omega \rightarrow \infty$, equation (9.16) becomes independent of the driving frequency

$$A_z = A_{z_0} \exp(-\omega_p x/c_0)$$

which implies a "skin depth" for a mig given by

$$\delta = c_0/\omega_p = 3.33 \times 10^6 / N_e^{1/2} \text{ cm.} \quad (9.20)$$

for waves of frequency $\ll f_c$ of equation (9.19). Note that δ is the wavelength that an electromagnetic wave of frequency f_c would have in vacuum.

These facets of mig/electromagnetic wave interaction are intriguing and suggestive, but as mentioned above, the mig, by its very nature is a medium of limited extent but indistinct boundaries. Thus an electromagnetic wave, if generated outside the mig, must negotiate an inhomogeneous region of transition to enter the mig. In point of fact, this transition is not peculiar to the mig, but is a universal characteristic of wave interaction with any material medium. Maxwell's equations are, strictly speaking, not applicable to regions of discontinuity in constitutive parameters, nor are constitutive parameters definable on an

atomic scale in which macroscopic discontinuities vanish. Thus the same sort of arguments as outlined above prior to the derivation of σ for the mig must be applied to any material body, and its "boundary conditions" derived from a limiting process about a narrow transition zone. An important distinction of the mig problem, however, is the breadth of the transition region, which may be comparable with, or exceed, the incident wavelength. Thus it is not possible in such cases to relegate the changes in the wave, produced by the region of inhomogeneous propagation, to a "boundary condition".

Unfortunately, this modification, although in concept almost trivial, introduces considerable mathematical difficulty into the problem. One obvious aspect of the transition zone's influence is that the wavelength must change continuously from one edge to the other, rather than discontinuously at an "interface". Likewise, the phase and amplitude of the wave must vary smoothly over the transition zone. In similar manner, one would anticipate that wave polarization, if required to change in the limiting "boundary value" problem (such as obliquely reflected waves from dielectrics or conductors) must then change continuously in the transition zone. These expectations will be displayed in the mathematical considerations below.

The propagation equation for the electric vector is given by

$$\nabla \times \nabla \times \vec{E} = k_0^2 K^* \vec{E} .$$

Since

$$\nabla \times \nabla \times \vec{E} = \nabla(\nabla \cdot \vec{E}) - \nabla^2 (\vec{E}) ,$$

an equation similar to the familiar Helmholtz equation (9.15) would be forthcoming if $\nabla \cdot \vec{E}$ were zero. But, taking the divergence of the

second Maxwell equation gives

$$\nabla \cdot (K^* \vec{E}) = K^* \nabla \cdot \vec{E} + \vec{E} \cdot \nabla K^* = 0,$$

which shows that $\nabla \cdot \vec{E}$ does not vanish unless \vec{E} has no component parallel to the gradient in K^* . The more general equation is:

$$\nabla^2 \vec{E} + k_0^2 K^* \vec{E} + \nabla \left\{ \frac{\nabla K^* \cdot \vec{E}}{K^*} \right\} = 0. \quad (9.21)$$

The analogous equation for the magnetic field is similar:

$$\nabla^2 \vec{H} + k_0^2 K^* \vec{H} + \nabla K^* \times \left\{ \frac{\nabla \times \vec{H}}{K^*} \right\} = 0. \quad (9.22)$$

The appearance of the unusual terms in the above equations precludes the possibility of waves of constant polarization, as neither equation can be satisfied, in general, by a constant vector multiplied by a scalar point function. Thus one can deduce the essence of the speculations above:

(1) The fact that K^* is function of position implies that phase, amplitude, and "wavelength" vary continuously from point to point in the region of transition.

(2) The appearance of the "dyadic" terms in the propagation equation produces a continuous change in the state of polarization in the region of transition.

It is possible to reduce the degree of complexity of (9.21) and (9.22) in some cases. Consider, for example, the case in which K^* is a function of only one Cartesian position variable. In this case ∇K^* is constant in direction, and the fields everywhere can be resolved into components parallel and perpendicular to this fixed direction:

$$\vec{E} = \vec{E}_{\parallel} + \vec{E}_{\perp} \quad (9.23)$$

$$\vec{H} = \vec{H}_{\parallel} + \vec{H}_{\perp} \quad (9.24)$$

where the subscripts refer to the orientation of the \vec{E} vector with respect to this direction. If, furthermore, the total fields are formed from the use of Maxwell's equations:

$$\vec{E} = \vec{E}_{\perp} + \frac{\nabla \times \vec{H}_{\parallel}}{i \omega \epsilon_0 K^*} \quad (9.25)$$

$$\vec{H} = \vec{H}_{\parallel} - \frac{\nabla \times \vec{E}_{\perp}}{i \omega \mu_0} \quad (9.26)$$

then only the two simple equations reducible to scalar form need be solved,

$$(\nabla^2 + k_0^2 K^*) \begin{Bmatrix} \vec{E}_{\perp} \\ \vec{H}_{\parallel} \end{Bmatrix} = 0 . \quad (9.27)$$

This reduction illustrates the intuitively obvious fact that polarization rotation is due to phase and amplitude differences in the two modes of propagation.

Another mathematical difficulty occurs in the region of $K^* = 0$, for the electric field may be singular there. Physically, such difficulties are superficial (clearly the linear constitutive parameters do not apply for extremely high field strengths) and they may be avoided mathematically by excluding the origin of the K^* complex plane from consideration. But it is nonetheless troublesome and sometimes difficult to interpret physically when situations arise in which K^* apparently has a zero in the zone of transition.

In the following work, several situations will be analyzed involving transition zones. For the sake of conceptual and analytical simplicity, polarization-rotating propagation will not be considered. Attention

will be focused on the other basic effects outlined above. The purpose of the analysis, as stated above, is to provide exact answers in an attempt to understand more fully the physical processes and to provide the rigorous basis on which to test proposed approximate procedures.

Physical descriptions of the transition zone problems to be considered, and rigorous mathematical statements of the problems are the subject of the next brief section.

X. FORMULATION OF PROBLEMS

The central theme of the computations to follow is the evaluation of the effect of finite transition zones in which K^* varies continuously between two specified values. Since

$$K^* = 1 - \left(\frac{\omega_p}{\omega}\right)^2 \frac{1 + i \frac{\nu_c}{\omega}}{1 + \left(\frac{\nu_c}{\omega}\right)^2}$$

it appears that the variation of K^* is largely due to variation of ω_p -- i. e., the electron number density. For example, because simple kinetic theory implies that ν_c is independent of electron number density⁽⁹⁾, it is a reasonably good approximation for many physical situations to assume that the collision frequency is a constant through the transition zone. Such an assumption would be appropriate so long as the temperature and neutral number density were constant (or nearly so) through the transition. In the case of extreme changes of density, such an idealization might not be possible, but for a constant-pressure transition zone in local thermal equilibrium characterized by a temperature gradient, it is shown below that the sensitivity of K^* is far greater to changes in N_e than to variations of ν_c . Form the ratio

$$\xi = \frac{\left(\frac{\partial K^*}{\partial x}\right) \nu_c}{\left(\frac{\partial K^*}{\partial x}\right) \omega_p}$$

which is a measure of the sensitivity of K^* to the two variations.

If both ω_p and ν_c are functions of the temperature and density, and the pressure is held constant, then

$$\xi = \left(\frac{\partial K^*}{\partial N_e} \right)_{\nu_c} \left(\frac{\partial N_e}{\partial T} \right)_p \left(\frac{dT}{dx} \right) / \left(\frac{\partial K^*}{\partial \nu_c} \right)_{\omega_p} \left(\frac{\partial \nu_c}{\partial T} \right)_p \left(\frac{dT}{dx} \right).$$

The equilibrium ionization (electron) density in a mildly-ionized, monatomic gas is given in this case approximately by⁽¹⁰⁾

$$N_e / N_{e_{\max}} = (T / T_{\max})^{1/4} \exp(-V/2kT + V/2kT_{\max})$$

where V is the ionization potential and k is Boltzmann's constant, while the collision frequency is given by

$$\nu_c = N_n \bar{C}_{\max} (T_{\max} / T)^{1/2} Q_n(T)$$

where $Q_n(T)$ is the (appropriately averaged) neutral/electron collision cross section and \bar{C} is the electron mean speed.

Hence it is apparent that

$$\frac{\partial N_e}{\partial T} = \left(\frac{1}{4T} + \frac{V}{2kT^2} \right) N_{e_{\max}}$$

$$\frac{\partial \nu_c}{\partial T} = \left(-\frac{1}{2T} + \frac{Q_n'(T)}{Q_n(T)} \right) \nu_{c_{\max}}$$

$$\left(\frac{\partial K^*}{\partial N_e} \right)_{\nu_c} = -\frac{q^2}{m \epsilon_0 \omega^2} \frac{1}{1 - i \frac{\nu_c}{\omega}}$$

$$\left(\frac{\partial K^*}{\partial \nu_c} \right)_{N_e} = \left(\frac{\omega_p}{\omega} \right)^2 \frac{i}{\omega} \left(\frac{1}{1 - i \frac{\nu_c}{\omega}} \right)^2$$

Therefore

$$\xi = \frac{-\left(\frac{\omega_p}{\omega}\right)^2_{\max} \left(\frac{1}{4T} + \frac{V}{2kT^2}\right) \frac{1}{1 - i \frac{\nu_c}{\omega}}}{-\left(\frac{i\nu_c}{\omega}\right)_{\max} \left(\frac{1}{2T} - \frac{Q_n'(T)}{Q_n(T)}\right) \left(\frac{\omega_p}{\omega}\right)^2 \frac{1}{\left(1 - i \frac{\nu_c}{\omega}\right)^2}}$$

or, simplified:

$$\xi = \frac{1 - i \frac{\nu_c}{\omega}}{i \left(\frac{\nu_c}{\omega}\right)_{\max}} \left(\frac{N_{e\max}}{N_e}\right) \frac{1}{2} \frac{1 + \frac{2V}{kT}}{1 - 2 \frac{d \ln Q(T)}{d \ln T}} \quad (10.1)$$

The assumption of mild ionization requires $V \gg kT$, and by virtue of the averaging process $d \ln Q / d \ln T$ cannot be large except in very peculiar circumstances. As $N_e \leq N_{e\max}$ and $(1 - i \frac{\nu_c}{\omega}) / (i \frac{\nu_c}{\omega})$ is bounded between ∞ and 1 in modulus, it is clear that $|\xi| \gg 1$ in general. In other words, the electromagnetic equations are in general much more sensitive to the variations of N_e than to variations in ν_c under constant pressure equilibrium conditions. These conditions might be apropos for free surfaces, boundary layers, shear layers, and diffusion/heat conduction problems.

Under the assumption of constant temperature but variable pressure, the equivalent expression to (10.1) is

$$\xi = \frac{1 - i \frac{\nu_c}{\omega}}{-2i \frac{\nu_c}{\omega}} \quad (10.2)$$

which does not necessarily imply the predominance of electron concentration sensitivity implied by (10.1).

In any case, it may be seen that the greater part of problems

concerned with mig transition zones may be adequately approximated by considering γ_c constant and N_e the variable parameter determining the propagation conditions. This approximation leads to considerable simplification in specifying and solving certain problems, for under the assumption, the parameter K^* can be written

$$K^* = 1 - (1 - K^2) \Psi \quad (10.3)$$

In the above equation,

$$K^2 = 1 - \left(\frac{\omega_p^o}{\omega} \right)^2 \left/ \left(1 + i \frac{\gamma_c}{\omega} \right) \right. \quad (10.4)$$

$$(\omega_p^o)^2 = N_{e_{\max}} q_e^2 / m_e \epsilon_0 \quad (10.5)$$

$$\Psi = N_e / N_{e_{\max}} \quad (10.6)$$

and thus the problem depends on the specification of the parameter K and the "distribution function" $\Psi(x, y, z)$, the normalized electron concentration.

The problems of concern here are the following three:

- (1) A mig half space and a vacuum half space meet at a transition zone. Waves are incident from vacuum normally onto the mig half space. The transition layer is characterized by a linear variation of electron density.
- (2) The transition layer of problem (1) is considered to be made of a piecewise linear variation of electron density.
- (3) A finite plane slab of mig, with symmetrical transition zones of linearly-varying electron density is illuminated at normal incidence from vacuum.

In each case the special conditions for constant polarization propagation are met, and the electron density gradient is along the z -axis. The equation of propagation for the electric vector thus takes the form:

$$\frac{d^2 \vec{E}}{dz^2} + k_0^2 (1 - (1 - K^2) \Psi(z)) \vec{E} = 0. \quad (10.7)$$

In each problem, K is a loose parameter, and the shape of $\Psi(z)$ specifies the electron geometry. In the first case, the linear ramp, Ψ is given by:

$$\Psi_1 = \begin{cases} 0 & z \leq 0 \\ z/z_0 & 0 \leq z \leq z_0 \\ 1 & z \geq z_0 \end{cases}$$

In the second case, the kinked ramp, is given by:

$$\Psi_2 = \begin{cases} 0 & z \leq 0 \\ \psi_A z/z_0 & 0 \leq z \leq z_0 \\ \psi_A + (1 - \psi_A) \frac{z - z_0}{z_1 - z_0} & z_0 \leq z \leq z_1 \\ 1 & z \geq z_1 \end{cases}$$

where z_0 and ψ_A have now been introduced as separate parameters.

In the third case, the trapezoid geometry, Ψ is given by

$$\Psi_3 = \begin{cases} 0 & z \leq 0 \\ z/z_0 & 0 \leq z \leq z_0 \\ 1 & z_0 \leq z \leq z_t - z_0 \\ (z_t - z)/z_0 & z_t - z_0 \leq z \leq z_t \\ 0 & z \geq z_t \end{cases}$$

These electron distributions are displayed graphically in figures 10. 1, 10. 2, and 10. 3; the nomenclature is more obvious from the illustrations. The figures also include the incident, reflected, and transmitted waves. The propagation exponent is given by Kk_0 in the regions of $\psi = 1$, as is evident from (10. 7). The incident wave is assumed to be of amplitude one.

The problem statement then is as follows. It is desired to evaluate the complex coefficients R and T , the reflection and transmission coefficients, as functions of the parameter K and the other defining dimensionless numbers, viz., $k_0 z_0$, $k_0 z_1$, $k_0 z_t$, and ψ_A , or their equivalents. To do so, it is required to find solutions of the propagation equation:

$$\frac{d^2 \vec{E}}{dz^2} + k^2(z) \vec{E} = 0 \quad (10.8)$$

for all values of z , and apply the conditions of continuity to the field vectors \vec{E} and \vec{H} at each boundary. The continuity of \vec{H} reduces to the requirement of continuity of $d\vec{E}/dz$.

Another aim is the generation of graphical results and a discussion of the physical interpretation thereof. Furthermore, approximate solutions to the linear ramp case are to be generated and compared to the exact results, in order to determine, at least crudely, what type of approximation is best suited to the problem and to estimate its accuracy.

Each of the three geometries indicated in the figures will be analyzed and discussed under separate headings below. Much of what follows is essentially algebraic, and the notation developed for the linear ramp case will be carried over into the other problems. For this reason, the reader who intends to follow the development closely is advised

that the following chapter is the most informative and complete.

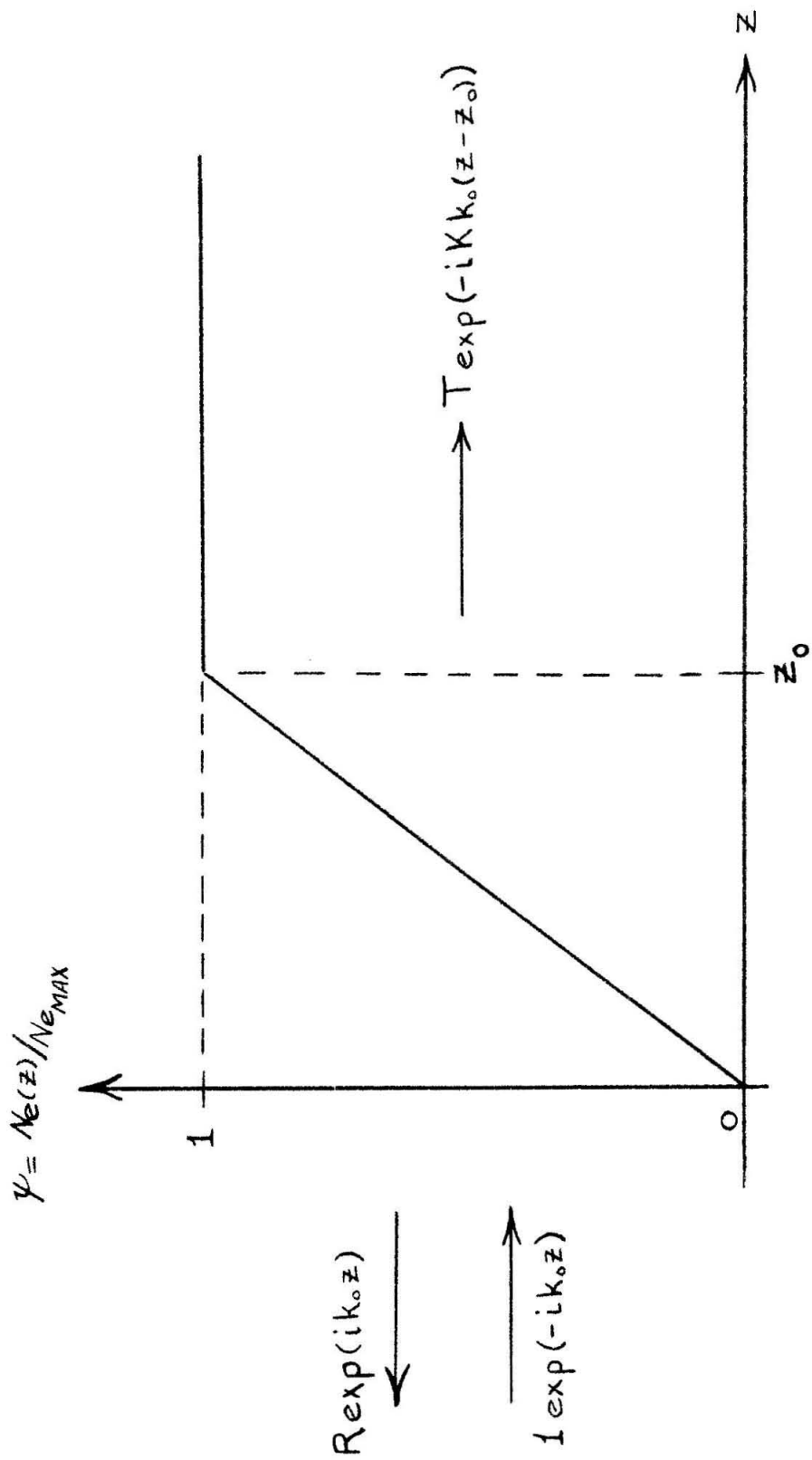


Figure 10.1 The Linear Ramp Transition Zone.

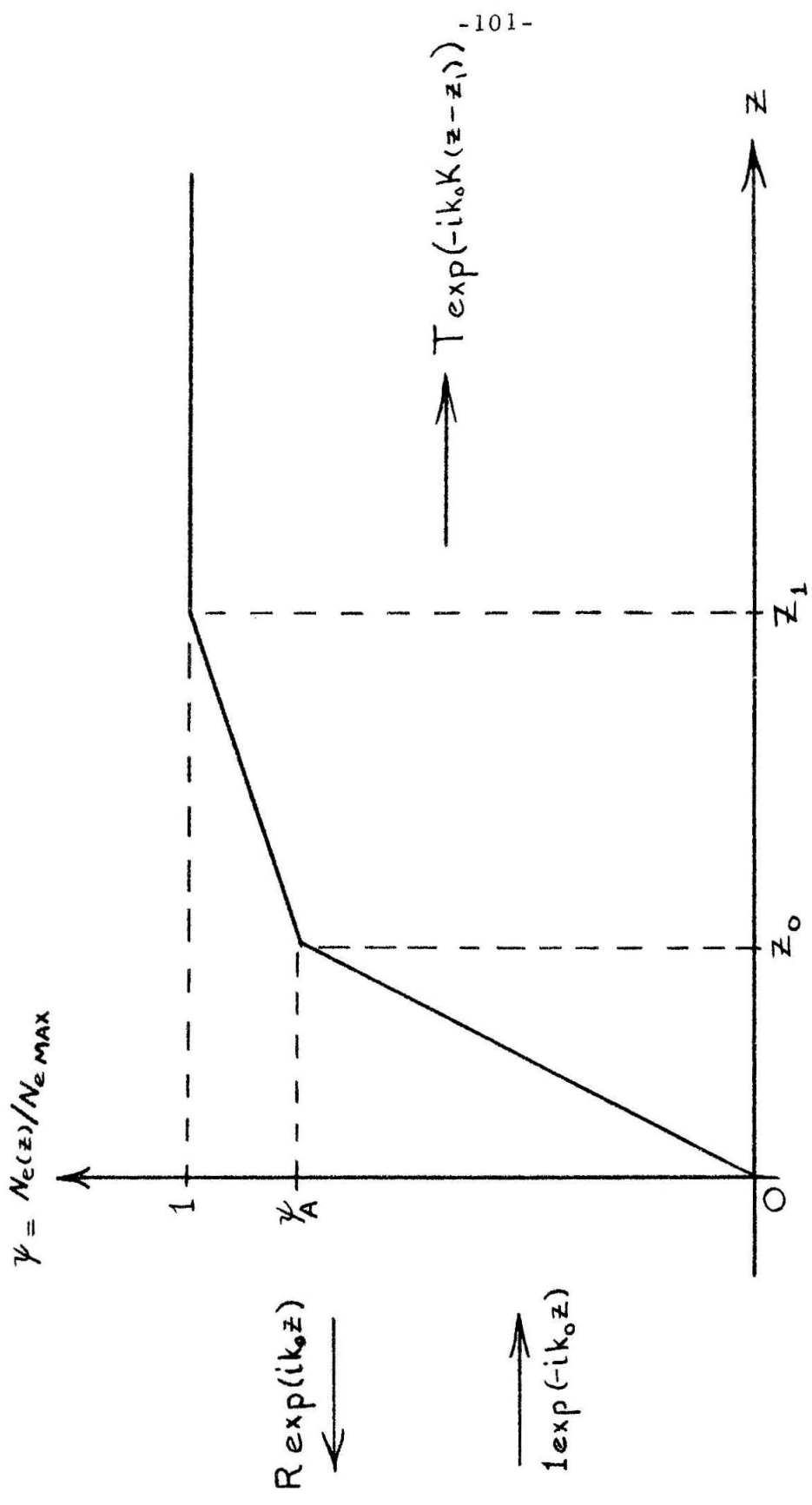


Figure 10.2 The "Kinked Ramp" Transition Zone.

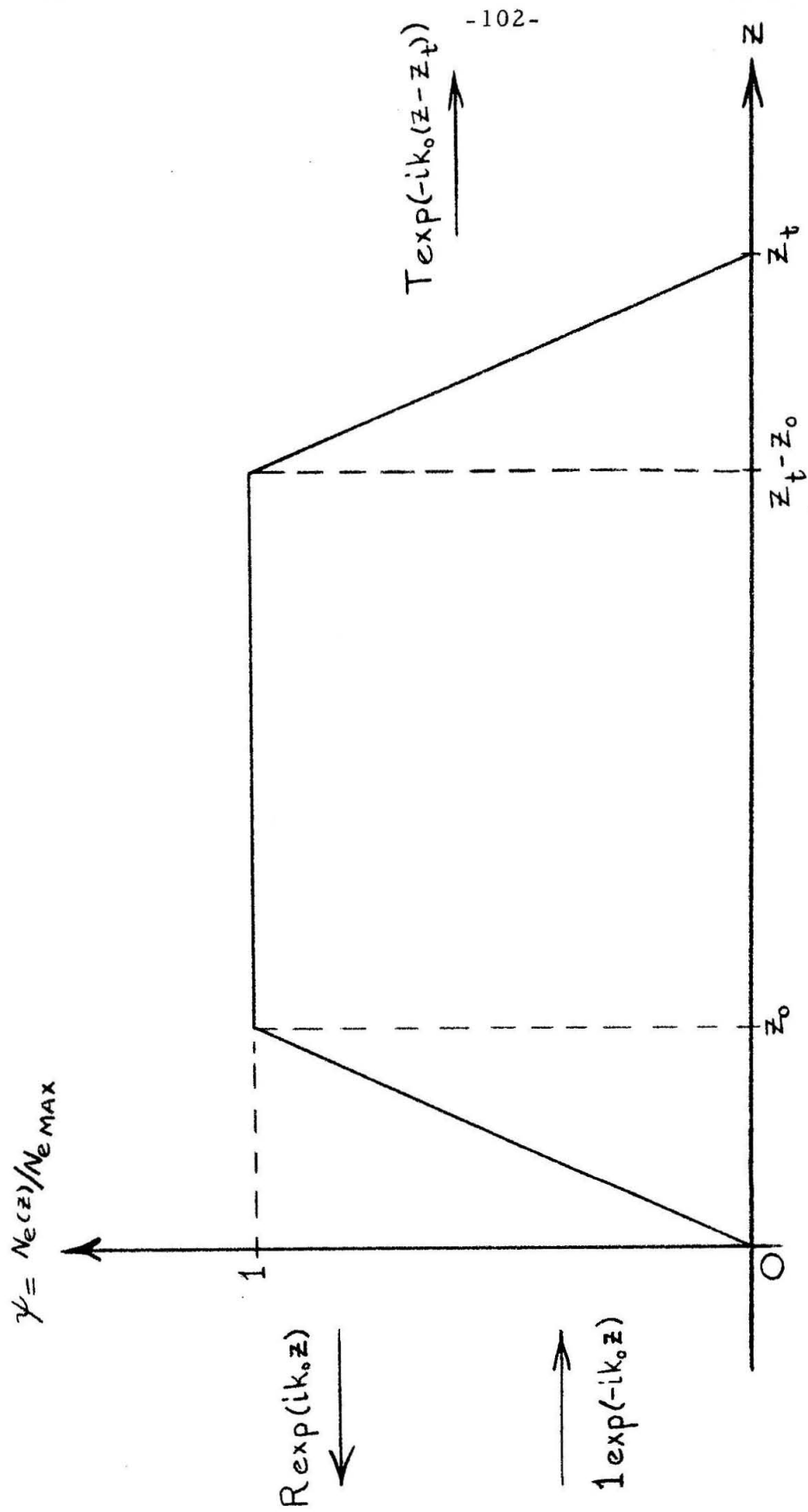


Figure 10.3 The "Trapezoid" Generalization of the Slab Problem.

XI. THE LINEAR RAMP PROBLEM

The linear ramp (see figure 10.1) problem requires the solution of

$$\frac{d^2 E}{dz^2} + k_o^2 \left(1 - (1 - K^2) z/z_o \right) E = 0 \quad (11.1)$$

and the matching of the following boundary conditions:

$$E(0) = 1 + R$$

$$\left. \frac{dE}{dz} \right|_0 = -ik_o (1 - R)$$

$$E(z_o) = T$$

$$\left. \frac{dE}{dz} \right|_{z_o} = -ik_o K T$$

Equation (11.1) can be reduced by the substitution

$$v = - \left(\frac{k_o z_o}{1 - K^2} \right)^{2/3} \left(1 - (1 - K^2) z/z_o \right) \quad (11.2)$$

to the form

$$\frac{d^2 E}{dv^2} = v E \quad (11.3)$$

This form is standard, and solutions are available as tabulated Airy functions of the first and second kind⁽¹¹⁾:

$$E = A \cdot Ai(v) + B \cdot Bi(v) \quad (11.4)$$

where A and B are unspecified constant coefficients.

The matching of the boundary conditions is most handily represented in terms of the dimensionless constant ϕ , where

$$\phi = -i \left(\frac{k_o z_o}{1 - K^2} \right)^{1/3} = e^{-i\pi/2} \left(\frac{k_o z_o}{1 - K^2} \right)^{1/3} \quad (11.5)$$

The boundary condition equations become simply

$$1 + R = A (A_i(\phi^2)) + B (B_i(\phi^2)) \quad (11.6)$$

$$\phi(1 - R) = A (A_i'(\phi^2)) + B (B_i'(\phi^2)) \quad (11.7)$$

$$T = A (A_i(K^2\phi^2)) + B (B_i(K^2\phi^2)) \quad (11.8)$$

$$K\phi T = A (A_i'(K^2\phi^2)) + B (B_i'(K^2\phi^2)) \quad (11.9)$$

where a prime denotes differentiation with respect to the argument.

From the form of (11.3), the Wronskian of the two solutions is evidently a constant. To be consistent with tabulated values, this constant is chosen to be π^{-1} , although the solution for R and T must be independent of such choices.

$$W(A_i, B_i) = A_i B_i' - B_i A_i' = \pi^{-1} \quad (11.10)$$

In the solution of (11.6) - (11.9), a combination occurs in terms of which the values of R and T can be expressed. Defining

$$A^{\pm}(\xi) = A_i(\xi^2) \pm \xi A_i'(\xi^2) \quad (11.11)$$

$$B^{\pm}(\xi) = B_i(\xi^2) \pm \xi B_i'(\xi^2) \quad (11.12)$$

it is found by direct computation that

$$A^+(\xi) B^-(\xi) - B^+(\xi) A^-(\xi) = 2\xi/\pi \quad (11.13)$$

and by inspection

$$A^-(\xi) = A^+(-\xi) \quad (11.14)$$

$$B^-(\xi) = B^+(-\xi) \quad (11.15)$$

In terms of these functions it follows directly that

$$R = \frac{A^-(\phi) B^-(K\phi) - A^-(K\phi) B^-(\phi)}{A^-(K\phi) B^+(\phi) - A^+(\phi) B^-(K\phi)} \quad (11.16)$$

$$T = \frac{-2\phi/\pi}{A^-(K\phi) B^+(\phi) - A^+(\phi) B^-(K\phi)} \quad (11.17)$$

These solutions, of course, could have been derived in terms of cylinder functions* of order $\pm 1/3$, but the Airy functions are available in tabular form in the complex plane, whereas complex-valued cylinder functions of fractional order are rare.

$$\text{Ai}(-z) = \frac{1}{3} z^{1/2} \left\{ J_{-1/3} \left(\frac{2}{3} z^{3/2} \right) + J_{1/3} \left(\frac{2}{3} z^{3/2} \right) \right\}$$

$$\text{Bi}(-z) = \left(\frac{z}{3} \right)^{1/2} \left\{ J_{-1/3} \left(\frac{2}{3} z^{3/2} \right) - J_{1/3} \left(\frac{2}{3} z^{3/2} \right) \right\}$$

An integral representation for $\text{Ai}(z)$ is available and is useful in generating asymptotic formulae:

$$\text{Ai}(z) = \frac{z^{1/2}}{2\pi} \int_{-\infty}^{+\infty} \exp \left(i z^{3/2} \left(t + t^3/3 \right) \right) dt \quad (11.18)$$

where the path of integration is suitably chosen by deforming the contour of integration for complex values of z . The second Airy function can be written in terms of the first by the identity⁽¹⁴⁾:

$$\text{Bi}(z) = iw \left(w \text{Ai}(w^2 z) - \text{Ai}(wz) \right), \quad w = \exp(2\pi i/3). \quad (11.19)$$

The reflection and transmission coefficients given by (11.16) and (11.17) are plotted in the figures at the end of this chapter**, both in absolute value and in phase. In general, for a given value of

* Such solutions were employed by Poincelot, references (12, 13), in generating the reflection coefficient from a linear density distribution model of the ionosphere.

** The expressions in this and other chapters were evaluated on the I. B. M. 709 digital computer at the Western Data Processing Center, Graduate School of Business Administration, U. C. L. A. The machine was programmed to compute the Airy functions in the entire complex plane to .01 per cent accuracy by series expansion. All arithmetic was carried out in Argand form, and the results converted to polar form for ease of presentation.

$K = K_r - iK_i$, $K_r \neq 0$, the behavior of the coefficients as a function of $k_0 z_0 = 2\pi z_0 / \lambda$ appears quite reasonable. At the limit $z_0 / \lambda = 0$, the coefficients approach the values given by the solution of the problem as a discontinuity in K^* , i. e.,

$$R_0 = \frac{1 - K}{1 + K} \quad , \quad T_0 = \frac{2}{1 + K} \quad (11.20)$$

The magnitude of the reflection coefficient approaches $|R_0|$ with zero slope, but $|T|$ comes to $|T_0|$ with a slope dependent on K_i , as one might anticipate. For real values of K , $|R| \rightarrow 0$ and $|T| \rightarrow K^{-\frac{1}{2}}$ as $k_0 z_0 \rightarrow \infty$. $|T|$ is reasonably well behaved, showing mild oscillations as it approaches this limiting value. For $K_i \neq 0$, $|T|$ shows an exponential decay typical of wave propagation in a linear, lossy medium. The phase of T is pleasantly monotonic in z_0 / λ , and is quite accurately represented by an approximate expression derived below.

The reflection coefficient decays in modulus fairly rapidly from its value at $z_0 / \lambda = 0$, and begins a quasi-periodic oscillation tending towards zero at $z_0 / \lambda \rightarrow \infty$. The most significant changes in $|R|$ occur in a relatively short distance ($z_0 / \lambda < 1$), and the asymptotic character of both R and T is fairly well established beyond $z_0 = \lambda$.

The origin of the behavior of R and T versus z_0 / λ can be visualized in the following ways. From an atomic point of view, it appears that the spreading out of the "interface" into a finite transition zone spoils the coherence (relative phase and amplitude) of the re-radiated fields from the individual electrons, thus diminishing the strength of the total signal reflected. The transmitted wave, on the other hand, is given a finite distance to adjust its phase velocity to match that of the medium (assumed lossless for the moment) into which it is

propagating, thus diminishing the "mis-match" between propagation parameters for any two nearby stations; in this manner the ramp provides a lesser barrier to penetration of the wave. When the "dielectric constant" is complex, however, the transmitted wave is continually being weakened by loss of energy to the medium, and of course decreases in amplitude with thickness of the transition zone.

Note that for the special case of K purely imaginary, both $K\phi$ and ϕ^2 are purely real, ϕ being imaginary. In that case, the ratio A/B is real from (11.8) and (11.9), and $(1-R)/(1+R)$ is imaginary from (11.6) and (11.7), as A_i and B_i are real for real argument (or could be chosen so in any case). Thus $|R|$ is unity for imaginary K , and hence no power can be transmitted into a purely reactive medium, regardless of the transition zone thickness. In this case, T does not vanish, but the Poynting vector in the second medium has no real part, i. e., there is no propagation, only reactive (stored) energy exists there.

Although the expressions computed above are exact, they do not lend themselves to easy computation, nor can the general behavior of R and T be deduced from inspection. Thus asymptotic behavior, expressed in simple form, would be desirable; expansions for R and T for both large and small values of $(k_0 z_0)/(1-K^2)$ are generated below.

Approximate Expressions

To generate the small argument expansion, one could solve (11.1) by truncated power series substitution (a polynomial approximation), proceed to match boundary conditions, and arrive at expressions for R and T . Or one could substitute the power series expansions of the

Airy functions into (11. 16) and (11. 17). Providing the same order of accuracy were maintained, the results would be identical in the expressions for R and T. (The obvious but important point being made here is that the solution of the problem is not dependent upon the choice of solutions to the differential equation; this fact will be used to great advantage in the large argument expansion.) Another and perhaps more direct attack is the insertion into (11. 16) and (11. 17) of series expansions for A^+ and B^+ . This approach will be taken here. The functions $A^+(\xi)$ and $B^+(\xi)$ are linearly independent solutions to the equation:

$$\frac{d^2 F^+}{d\xi^2} = (4\xi^2 + 6\xi) F^+ \quad (11. 19)$$

where the definitions of A^+ and B^+ have been employed, along with the basic differential equation (11. 3). Solving (11. 19) by a power series substitution

$$F^+(\xi) = \sum_{n=0}^{\infty} a_n^+ \xi^n \quad (11. 20)$$

leads to the relationships:

$$a_0^+, a_1^+ \quad \text{arbitrary} \quad (11. 21)$$

$$\left. \begin{aligned} a_2^+ &= 0 \\ a_3^+ &= + a_0^+ \\ a_4^+ &= + \frac{1}{2} a_1^+ \\ a_5^+ &= 0 \\ a_j^+ + 6 &= \frac{4 a_j^+ + 6 a_{j+3}^+}{(j+6)(j+5)} \end{aligned} \right\} \quad (11. 22)$$

Therefore, two linearly independent solutions are given by

$$F_1^+(\xi) = \xi + \frac{1}{2}\xi^4 + \frac{1}{6}\xi^7 + \frac{1}{30}\xi^{10} + \frac{1}{180}\xi^{13} + \dots \quad (11.23)$$

$$F_2^+(\xi) = 1 + \xi^3 + \frac{1}{3}\xi^6 + \frac{1}{12}\xi^9 + \frac{1}{72}\xi^{12} + \dots \quad (11.24)$$

The task remaining at this point is the assurance that

$$A^+(x)B^-(x) - A^-(x)B^+(x) = \frac{2x}{\pi} \quad (11.25)$$

since this fact has been used in the derivation of (11.16) and (11.17).

Note also that (11.25) requires (11.10), which was used earlier in the derivation. Thus, other than the requirement of (11.25), one could substitute F_1^+ for A^+ and F_2^+ for B^+ in (11.16) and (11.17). Noting the definitions (11.11) and (11.12), it is required that

$$A^-(x) = -q F_2^+(x) + p F_1^+(x) \quad (11.26)$$

$$B^-(x) = 3^{\frac{1}{2}} \left\{ q F_2^+(x) + p F_1^+(x) \right\} \quad (11.27)$$

where

$$p = Ai(0) = 3^{-\frac{1}{2}} Bi(0) \quad (11.28)$$

$$q = Ai'(0) = 3^{-\frac{1}{2}} Bi'(0) \quad (11.29)$$

Thus all conditions leading to (11.16) and (11.17) have been satisfied, and the results may be expressed as:

$$T = \frac{2\phi}{F_1^+(\phi) F_2^-(K\phi) + F_1^-(K\phi) F_2^+(\phi)} \quad (11.30)$$

$$R = \frac{F_1^-(K\phi) F_2^-(\phi) - F_1^-(\phi) F_2^-(K\phi)}{F_1^+(\phi) F_2^-(K\phi) + F_1^-(K\phi) F_2^+(\phi)} \quad (11.31)$$

It should be noted that (11.30) and (11.31) are essentially the expressions evaluated by machine computation. They are exact, but very slowly convergent; in general, the accuracy of the machine computation

is limited to seven decimals, so whenever two of the series expressions for $F_{1,2}^+$ become simultaneously large and approximately equal, the accuracy is destroyed. For this reason, some of the figures show truncated plots of R and T. Expressed in terms of $k_0 z_0$ and K, the above expressions, to three terms, are given by:

$$T = T_0 (1 + ik_0 z_0 (1+K)/2 - (k_0 z_0)^2 (1+K+K^2)/6 \dots)^{-1} \quad (11.32)$$

$$R = \frac{R_0 (1 - ik_0 z_0 (1-K)/2 - (k_0 z_0)^2 (1 - K + K^2)/6 \dots)}{(1 + ik_0 z_0 (1+K)/2 - (k_0 z_0)^2 (1 + K + K^2)/6 \dots)} \quad (11.33)$$

Recall the following limiting expressions towards which these expansions must tend:

for K real,

$$\left. \begin{array}{l} T \rightarrow K^{-\frac{1}{2}} \\ R \rightarrow 0 \end{array} \right\} \text{ as } k_0 z_0 \rightarrow \infty$$

for K imaginary,

$$\left. \begin{array}{l} T \rightarrow 0 \\ |R| \equiv 1 \end{array} \right\} \text{ as } k_0 z_0 \rightarrow \infty$$

which indicates the sensitivity of the expressions to $\arg K$. Expressions (11.32) and (11.33) are superposed on the plot of an exact evaluation of $|R|$ and $|T|$ for a typical case, to show the range of validity expected from a polynomial solution. Shown also on these plots are evaluations of the asymptotic forms generated below, valid for large ϕ and $K\phi$.

Two linearly independent solutions to (11.3) for very large v have the asymptotic representations⁽¹⁵⁾:

$$E \sim v^{-1/4} \exp(\pm 2/3 v^{3/2}) \{ 1 \pm O(0.1 v^{-3/2}) \} \quad (11.34)$$

In restricted sectors, these are representations of the Airy functions:

$$Ai(v) \longrightarrow (4\pi)^{-1/2} v^{-1/4} \exp(-2/3 v^{3/2}) \quad (11.35)$$

$$v \longrightarrow \infty, \quad -\pi < \arg v < \pi$$

$$Bi(v) \longrightarrow (\pi)^{-1/2} v^{-1/4} \exp(2/3 v^{3/2}) \quad (11.36)$$

$$v \longrightarrow \infty, \quad -\pi/3 < \arg v < \pi/3$$

The representation for $Bi(v)$ in other sectors can be generated from identities relating Ai and Bi (14, 15), but in point of fact this is unnecessary for the generation of asymptotic formulae for R and T . To demonstrate this, proceed as follows.

Consider the two functions* :

$$Aa(z) = (4\pi)^{-1/2} z^{-1/4} \exp(-2/3 z^{3/2})$$

$$Ba(z) = \pi^{-1/2} z^{-1/4} \exp(2/3 z^{3/2})$$

Differentiating twice gives, for $F = Aa$ or Ba :

$$\frac{d^2 F}{dz^2} - z F = \frac{5}{16} \frac{F}{z^2} \quad (11.37)$$

Thus for some region in which $|z^3| \gg 1$

$$\frac{d^2 F}{dz^2} - z F \approx 0 \quad (11.38)$$

Furthermore

$$Aa(z) Ba'(z) - Ba(z) Aa'(z) = 1/\pi \quad (11.39)$$

Therefore, for sufficiently large $|v|$, Aa and Ba can be chosen as two linearly independent approximate solutions to (11.3). Since (11.39) is formally the same as (11.10), it is only required to substitute Aa for

* These are the WKB (Wentzel-Kramers-Brillouin) solutions to (11.3). See references (15) and (16) for a discussion of the method and some of its subtleties, and reference (14) for discussion pertinent to the following work.

Ai and Ba for Bi in (11.11) and (11.12) respectively, and then evaluate R and T. By this means

$$\begin{aligned} A^+(z) &= -Aa(z^2)/4z^2 \\ A^-(z) &= -Aa(z^2)(2z - 1/4z^2) \\ B^+(z) &= Ba(z^2)(2z - 1/4z^2) \\ B^-(z) &= -Ba(z^2)/4z^2 \end{aligned}$$

Substituting

$$\begin{aligned} J_1 &= Aa(\phi^2) Ba(K^2\phi^2) \\ J_2 &= Aa(K^2\phi^2) Ba(\phi^2) \end{aligned}$$

the resulting expressions for R and T can be written:

$$R \rightarrow \frac{(1 + 8\phi^3) J_1 - (1 + 8K^3\phi^3) J_2}{(1 + 8K^3\phi^3)(1 - 8\phi^3)J_2 - J_1} \quad (11.40)$$

$$T \rightarrow \frac{-32 K^2 \phi^5 / \pi}{(1 + 8K^3\phi^3)(1 - 8\phi^3)J_2 - J_1} \quad (11.41)$$

Since

$$\begin{aligned} J_1 &= (2\pi\phi K^{\frac{1}{2}})^{-1} \exp\left(-2/3 \phi^3 (1-K^3)\right) \\ J_2 &= (2\pi\phi K^{\frac{1}{2}})^{-1} \exp\left(2/3 \phi^3 (1-K^3)\right) \end{aligned}$$

it is clear that for $\text{Im}(K) \neq 0$,

$$\frac{J_2}{J_1} = \exp\left(\frac{4}{3} \phi^3 (1-K^3)\right) = \exp\left(\frac{4}{3} i k_o z_o \left(1 + \frac{K^2}{1+K}\right)\right) \quad (11.42)$$

will grow exponentially large. Furthermore, as $|\phi|$ and $|K\phi|$ have been assumed large at the outset, even if $\text{Im}(K)$ is zero, it is evident that

$$R \rightarrow \frac{1 - \frac{J_2 (1 + 8K^3 \phi^3)}{J_1 (1 + 8\phi^3)}}{\frac{J_2 (1 - 8\phi^3)(1 + 8K^3 \phi^3)}{J_1 (1 + 8\phi^3)} - \frac{1}{1 + 8\phi^3}} \rightarrow \frac{1 - K^3 \frac{J_2}{J_1}}{-8K^3 \phi^3 \frac{J_2}{J_1} \left\{ 1 + \frac{1 - K^3}{8K^3 \phi^3} \right\}}$$

$$R \rightarrow \frac{1}{8\phi^3} \left\{ 1 - K^{-3} \frac{J_1}{J_2} \right\}$$

$$R \rightarrow -i \left(\frac{1 - K^2}{8k_o z_o} \right) \left(1 - K^{-3} \exp \left(-\frac{4}{3} i k_o z_o \left(1 + \frac{K^2}{1 + K} \right) \right) \right) \quad (11.43)$$

Likewise, with $\xi = (2/3)\phi^3 (1 - K^3) = (2/3) i k_o z_o \left(1 + \frac{K^2}{1 + K} \right)$,

$$T \rightarrow \frac{-32 K^2 \phi^5 / \pi}{(2\pi \phi K^{\frac{1}{2}})^{-1} e^{\xi} \left\{ (1 + 8K^3 \phi^3)(1 - 8\phi^3) - e^{-2\xi} \right\}}$$

$$T \rightarrow \frac{-64 \phi^6 K^{5/2} e^{-\xi}}{-64 K^3 \phi^3 + 8 \phi^3 (K^3 - 1)}$$

$$T \rightarrow K^{-\frac{1}{2}} \left\{ 1 + i \frac{(1 - K^2)(1 - K^3)}{8K^3 k_o z_o} \right\} \exp \left(\frac{2}{3} i k_o z_o \left(1 + \frac{K^2}{1 + K} \right) \right) \quad (11.44)$$

The convergence of these expressions is clearly a function of the validity of the approximation of large $|v|$. Thus the case of purely imaginary K is not accurately represented, since $|v|$ goes to zero in the range of integration. But the case of purely real K is valid à fortiori, and indeed the limit $K = 1$ is exact,

$$T_1 = \exp(-i k_o z_o)$$

$$R_1 = 0$$

as is the case of $k_o z_o \rightarrow \infty$

$$T_2 = K^{-\frac{1}{2}}$$

$$R_2 = 0.$$

It is clear from the small argument approximations (11.32) and (11.33) that as $k_0 z_0$ goes to zero, the coefficients approach the "interface" values in modulus.

$$|R| \longrightarrow |R_0| ; \left. \frac{d|R|}{d(k_0 z_0)} \right|_0 = 0 \quad (11.45)$$

$$|T| \longrightarrow |T_0| ; \left. \frac{d|T|}{d(k_0 z_0)} \right|_0 = |T_0| \operatorname{Im}(K) \quad (11.46)$$

The phase, on the other hand, is more sensitive near the origin:

$$\left. \frac{d(\arg R)}{d(k_0 z_0)} \right|_0 = - \left. \frac{d}{d\xi} (\tan^{-1}(\xi)) \right|_{\xi=0} = -1 \quad (11.47)$$

$$\left. \frac{d(\arg T)}{d(k_0 z_0)} \right|_0 = - \left. \frac{d}{d\xi} \left(\tan^{-1} \frac{\xi(1+\operatorname{Re} K)}{1-\xi \operatorname{Im} K} \right) \right|_{\xi=0} = -(1 + \operatorname{Re} K) \quad (11.48)$$

Thus to the order of $k_0 z_0$, the small argument approximations can be written

$$\begin{aligned} R &\longrightarrow R_0 e^{-i k_0 z_0} \\ T &\longrightarrow T_0 e^{-i k_0 z_0 (1+K)} \end{aligned}$$

uniformly in $\arg K$.

One further approximation is developed, which provides a highly accurate fit to the exact data. The phase of the transmitted wave ($\arg T$), plotted against $k_0 z_0$, is a remarkably straight line, decaying from $\arg T_0$ with a slope dependent upon the real part of K only (see plotted results). Taking this as an established generality, it would be pleasant to determine the slope analytically. Following the intuitive approach, it is assumed that the phase is to be given by the average of the real part of the propagation exponent:

$$\arg T - \operatorname{Re} \overline{(k(z))} z_0 = - \operatorname{Re} \left(\frac{2}{3} k_0 z_0 \left(1 + \frac{K^2}{1+K} \right) \right) \quad (11.49)$$

The slope so determined agrees very accurately with the exact results. The only adjustment required to make (11.49) almost coincident with the exact results is the addition of the constant $\arg T_0$, for coincidence at $z_0 = 0$. Thus

$$\arg T \doteq \arg T_0 - \frac{2}{3} k_0 z_0 \left[1 + \operatorname{Re} \left(\frac{K^2}{1+K} \right) \right] \quad (11.50)$$

where $\arg T_0 = - \arg (1+K)$.

As (11.50) is linear in z_0 , the transmitted wave has the same relative phase as if it had passed through an interface located at z_e such that

$$\arg T_0 - k_0 z_e - k_0 \operatorname{Re}(K)(z_0 - z_e) = \arg T. \quad (11.51)$$

The value of z_e is given by solving (11.51) and (11.50):

$$\frac{z_e}{z_0} = \frac{\frac{2}{3} - \operatorname{Re} \left\{ \frac{K}{3} \left(1 + \frac{2}{1+K} \right) \right\}}{1 - \operatorname{Re}(K)}. \quad (11.52)$$

Thus for K real, z_e is confined between the two limits

$$1/3 \leq z_e/z_0 \leq 2/3, \quad (11.53)$$

the lower limit being $K \rightarrow \infty$, and the upper limit being $K \rightarrow 0$.

Note that (11.50) is essentially the real part of the exponent in the asymptotic form for T as given by (11.44). It would be fatuous to concern oneself with the factor $K^{-\frac{1}{2}}$ in (11.44) as it contributes to phase, for both (11.44) and (11.50) are approximate, and it would be only fortuitous if they agreed exactly. It is required, however, that the two expressions for $\arg T$ give approximately the same value for the number of 2π revolutions (the number of wavelengths of relative phase),

and this they do with the common term $\text{Re}(\bar{k}z_0)$.

The phase of the reflected wave, $\arg R$, is also nearly a straight line for small values of $k_0 z_0$, thus providing a fairly accurate representation in this region by the expression

$$\arg R \doteq \arg R_0 - k_0 z_0 . \quad (11.54)$$

This expression clearly implies an "equivalent interface" reflection, with the interface located at

$$z_e' = \frac{1}{2} z_0 . \quad (11.55)$$

The straight line approximation for $\arg R$, however, falls rapidly as $k_0 z_0$ approaches unity (the breakdown of the approximation is clearly a function of K ; $k_0 z_0 \rightarrow 1$ is the limit for the samples displayed in the figures here). The somewhat pathological behavior of $\arg R$ versus $k_0 z_0$ for large $k_0 z_0$ can be seen to be required to make the polar plot of R versus $k_0 z_0$ a smooth curve. Thus reference to the $|R|$ curves always shows $|R| \sim 0$ in the neighborhood of a rapid change in $\arg R$.

To sum up the findings of this chapter, the following observations are listed:

- (1) There is a marked dependence of R and T upon the transition zone thickness, particularly for small values of thickness/wavelength ratio.
- (2) For large values of thickness/wavelength ratio and/or small values of $|1 - K^2|$, the asymptotic formulae adequately describe both R and T . However, the accuracy of the description is a function of the argument of K , being very good for real K and poor for K imaginary.
- (3) The small argument (polynomial) approximation is adequate

only for very small values of thickness/wavelength, and the accuracy is again a function of $\arg K$.

(4) The argument of T (phase of transmitted wave) is accurately approximated by the sum of the interface-induced phase change, $\arg T_0$, and the phase shift due to the average real part of the propagation exponent, $\text{Re}(\bar{K}z_0)$.

(5) The phase of R is much more sensitive for large and intermediate values of thickness/wavelength ratio, but for fractional values, is given fairly accurately by the extension of the slope at the origin. The almost pathological behavior of $\arg R$ can be explained by reference to the curve of $|R|$ and visualization in polar form.

The conclusions which may be drawn from this analysis are that:

(a) Approximate expressions can be generated by either polynomial expansion or the WKB-type integral expansion*, but both these methods fail to describe accurately the region of greatest sensitivity of $|R|$ and $|T|$ -- namely the region $z_0 \sim \lambda/2$.

(b) The strong dependence of R and T on transition zone thickness requires that a further investigation be made to estimate the sensitivity of R and T to the detailed structure of the transition zone. This is the subject of the next chapter.

* See Hall (reference 17) for an iterative approximation procedure for real K .

Figure 11.1 Linear Ramp

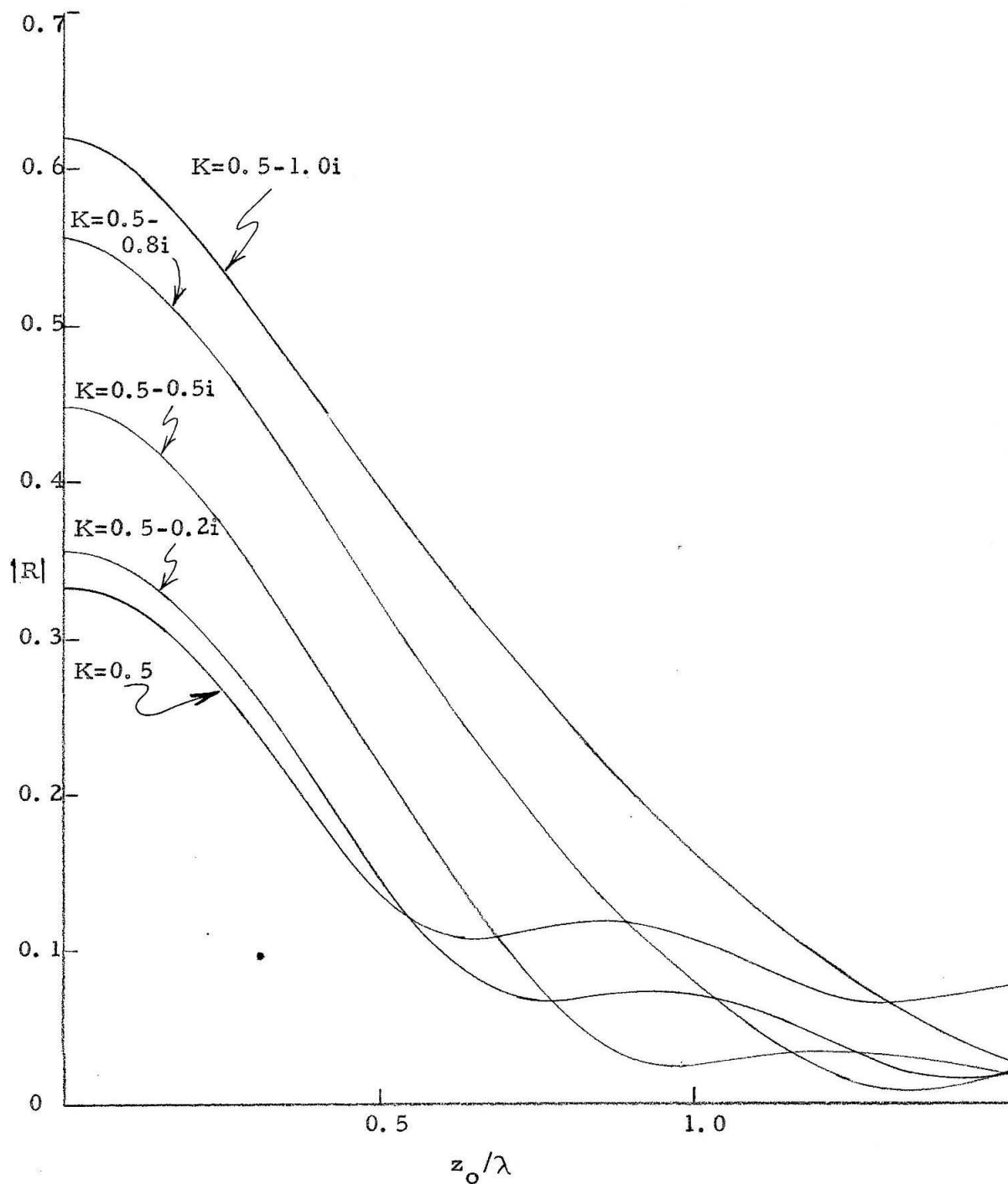


Figure 11.2 Linear Ramp

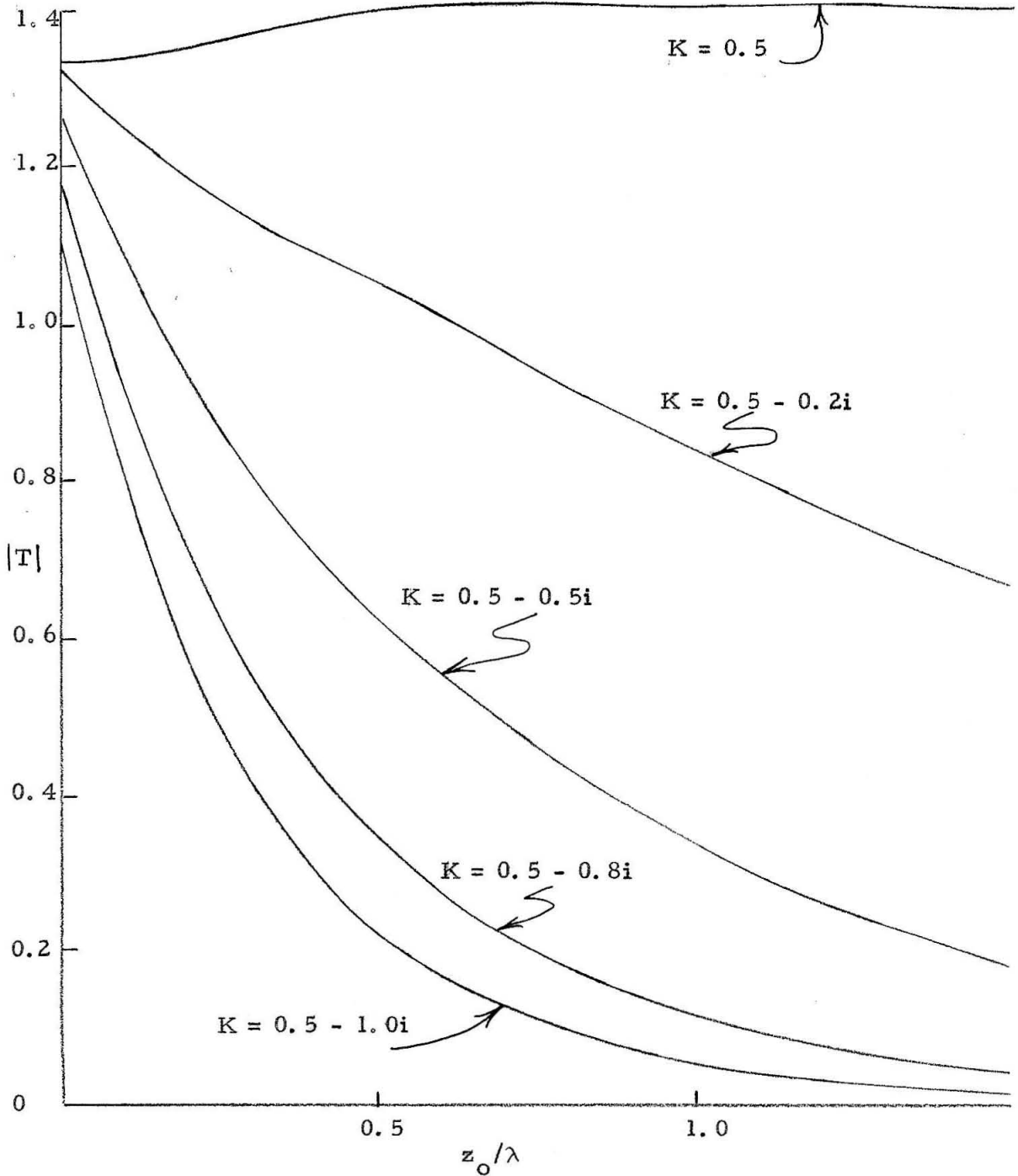


Figure 11.3 Linear Ramp

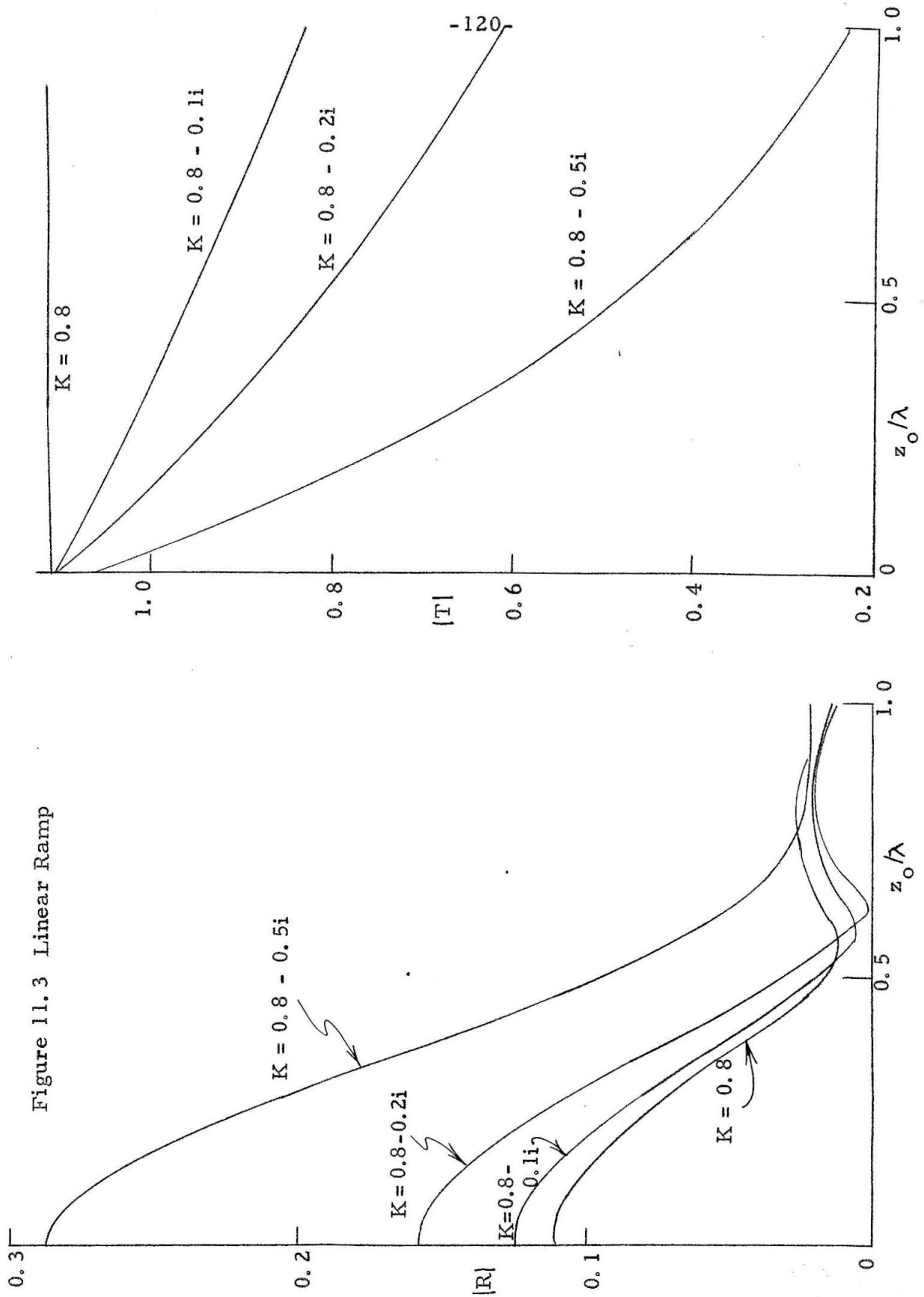


Figure 11.4 Linear Ramp

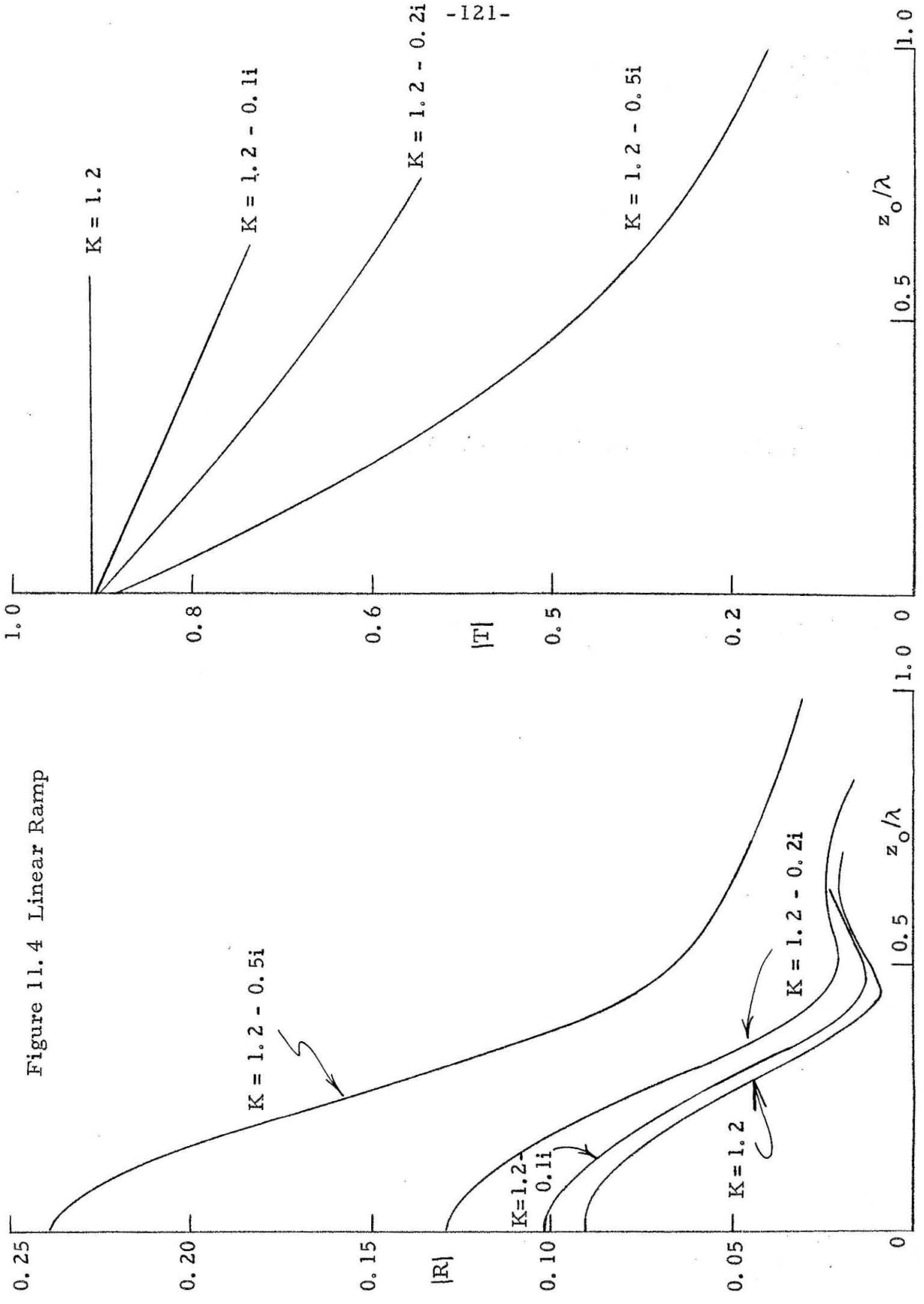


Figure 11.5 Linear Ramp

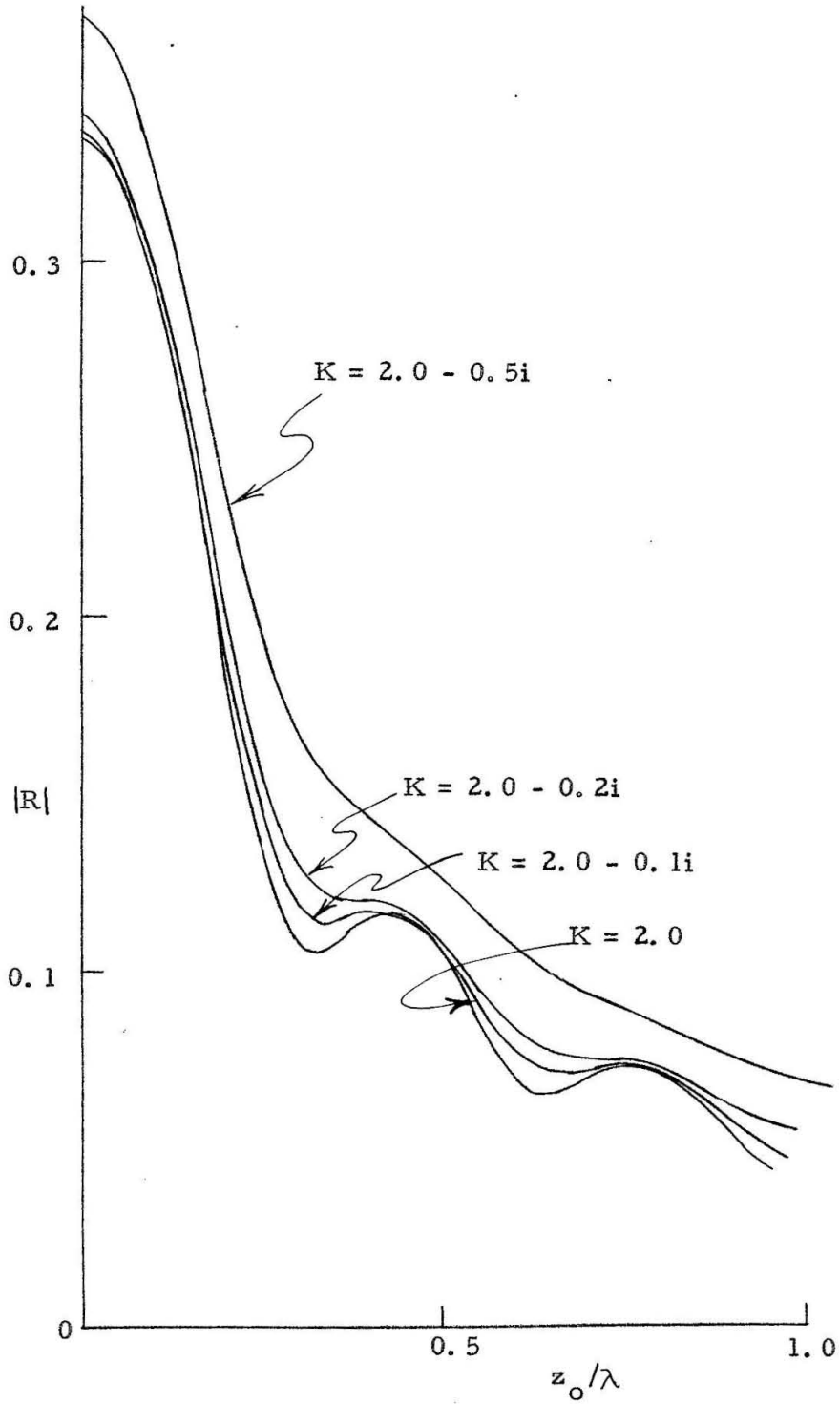


Figure 11.6 Linear Ramp

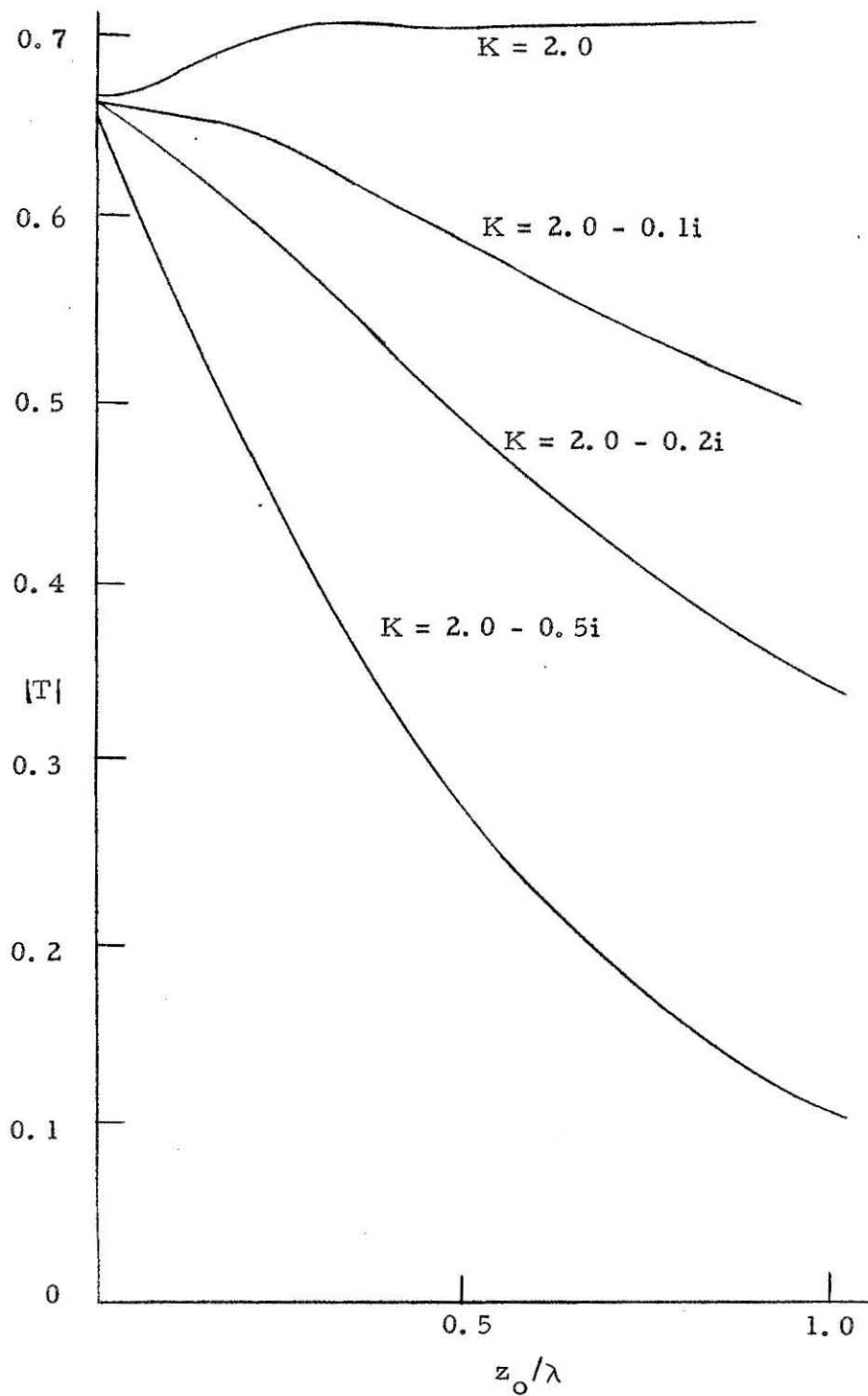


Figure 11.7 Linear Ramp

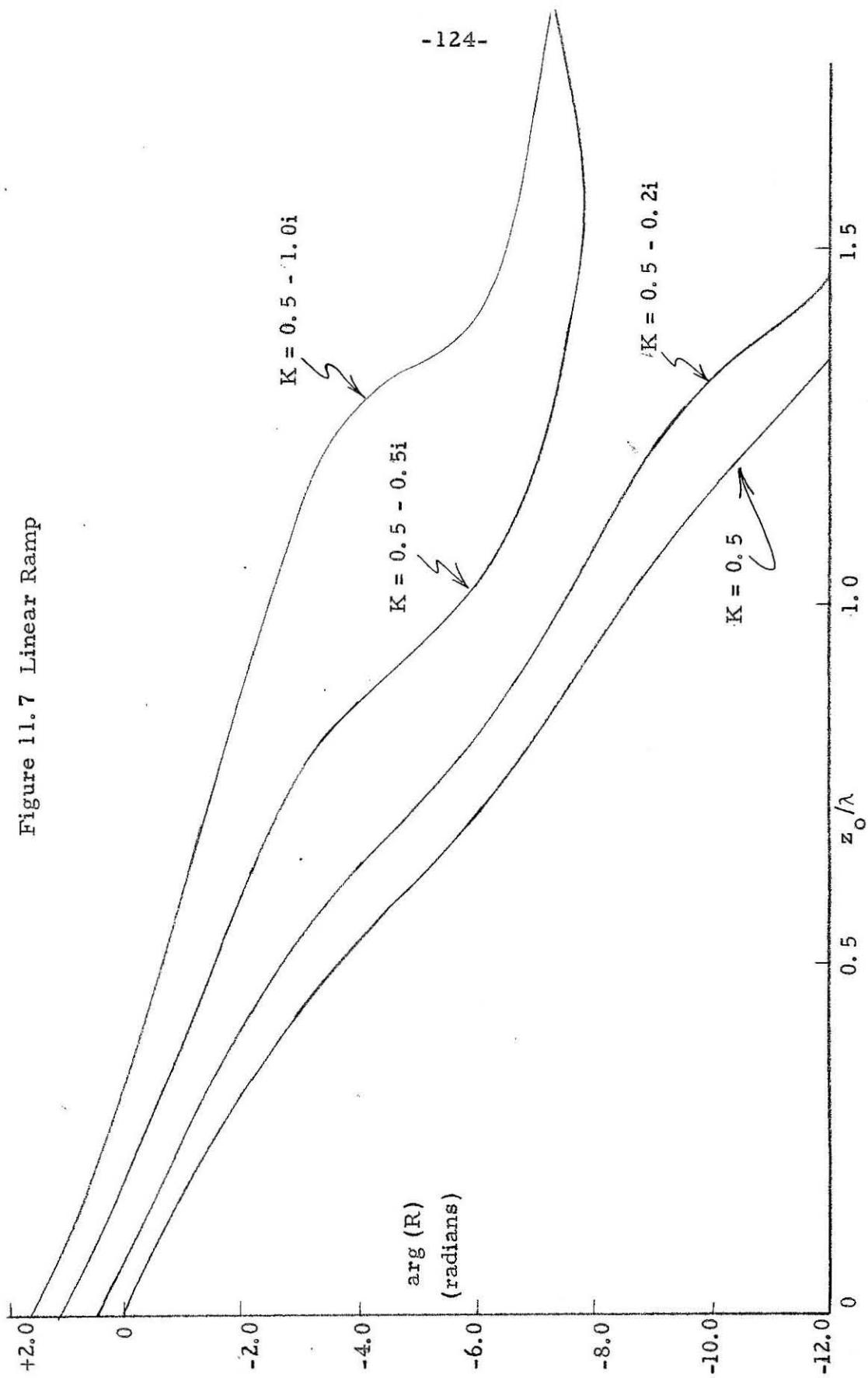


Figure 11.8 Linear Ramp

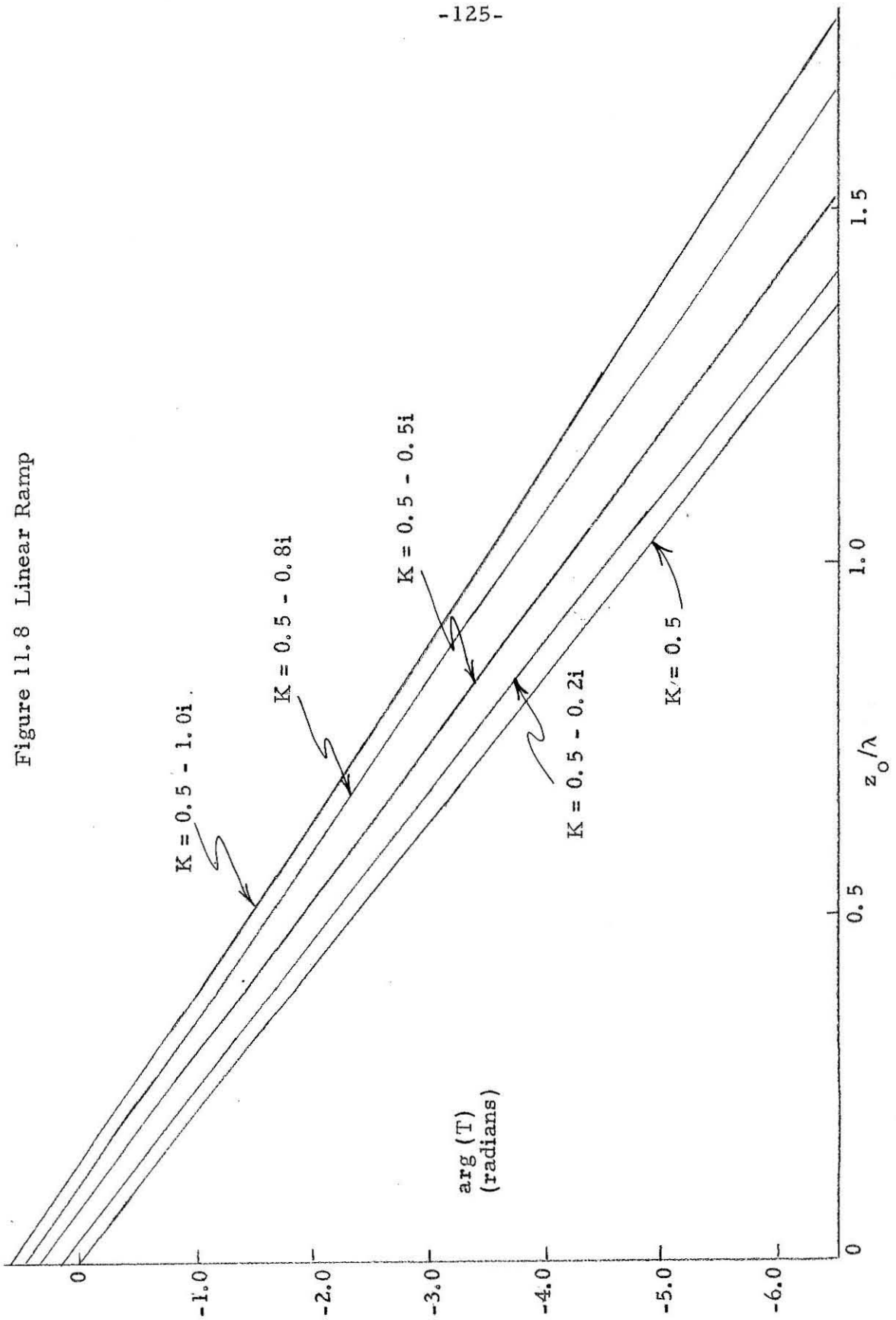


Figure 11.9 Linear Ramp

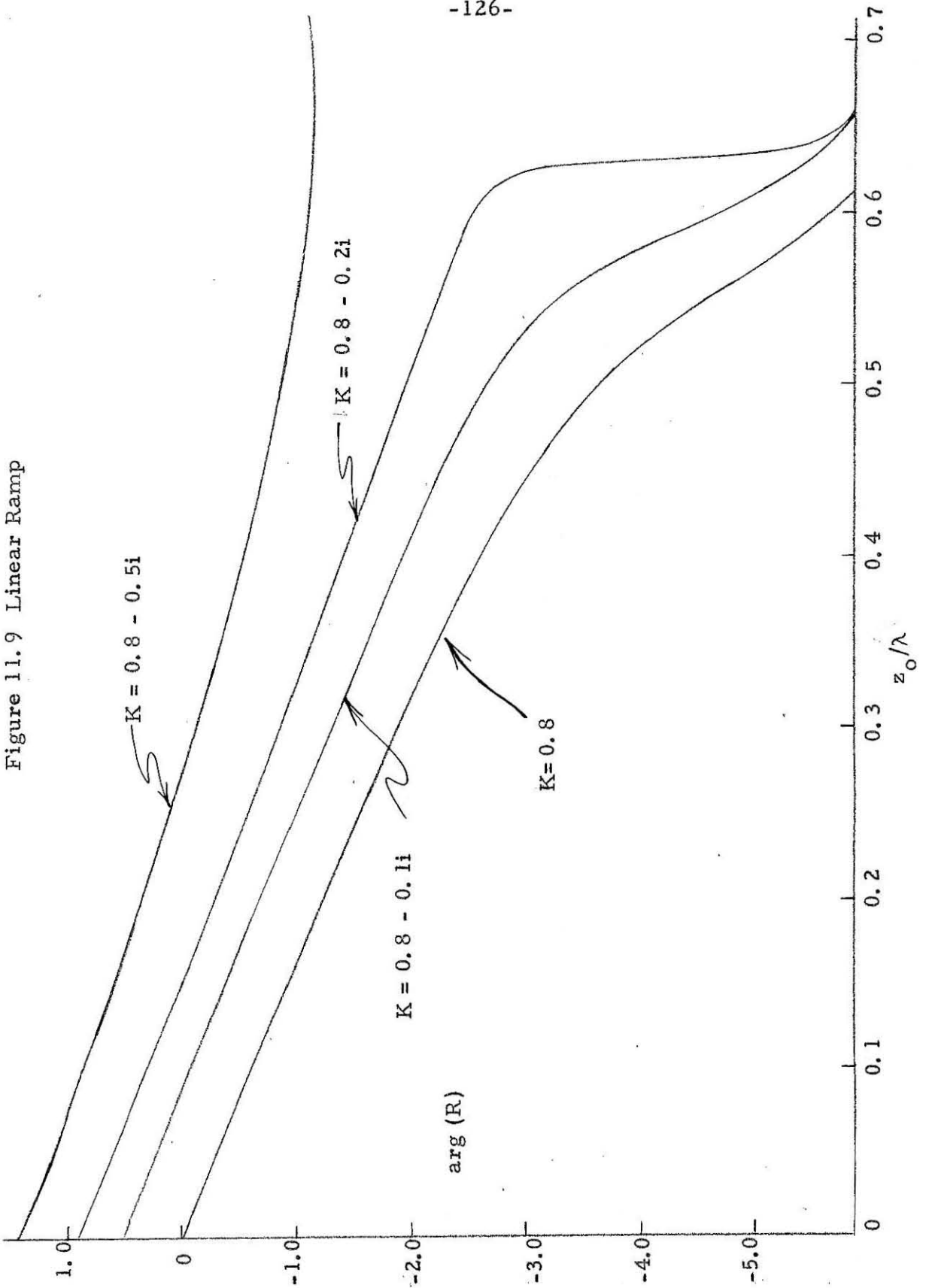


Figure 11.10 Linear Ramp

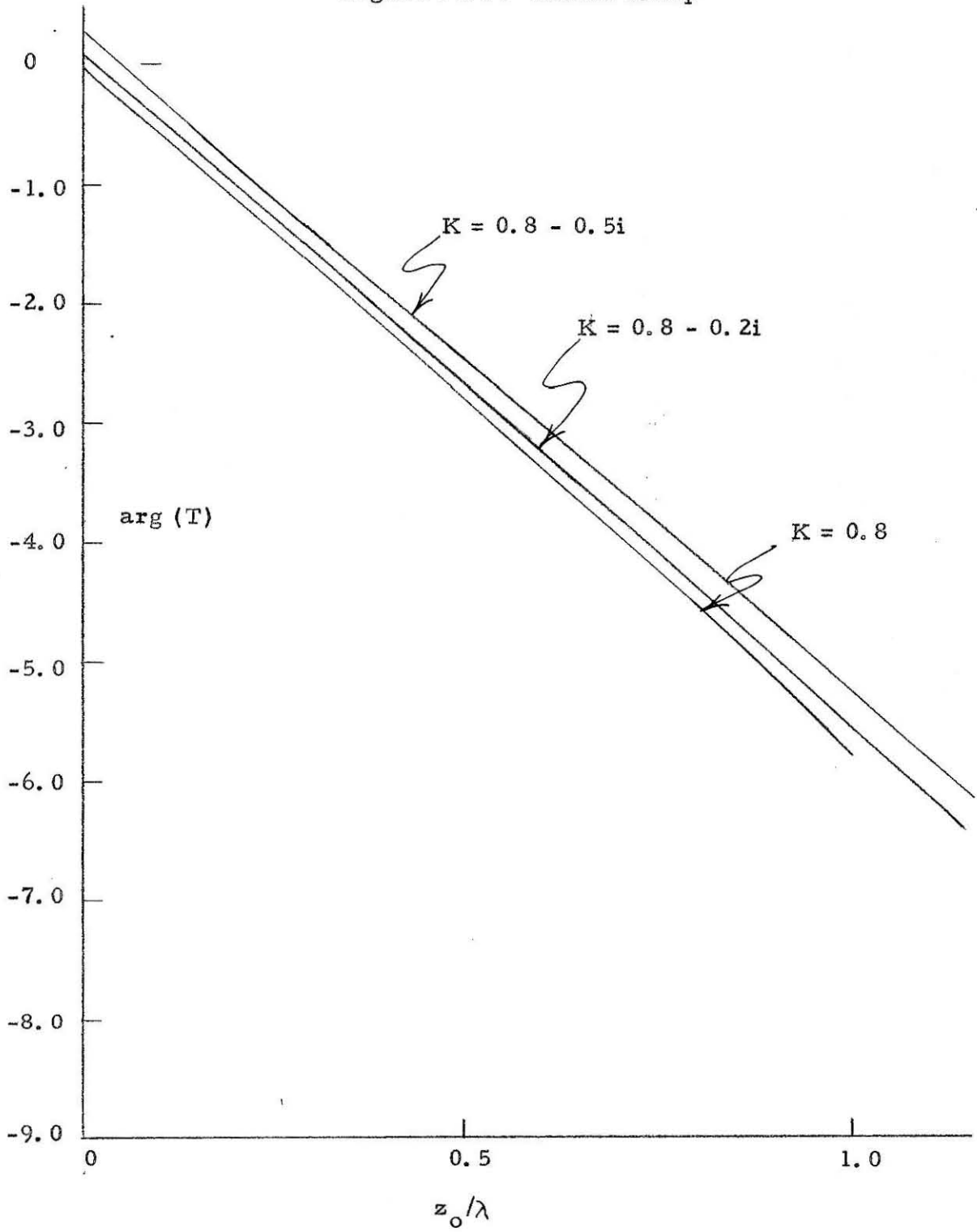


Figure 11.11 Linear Ramp

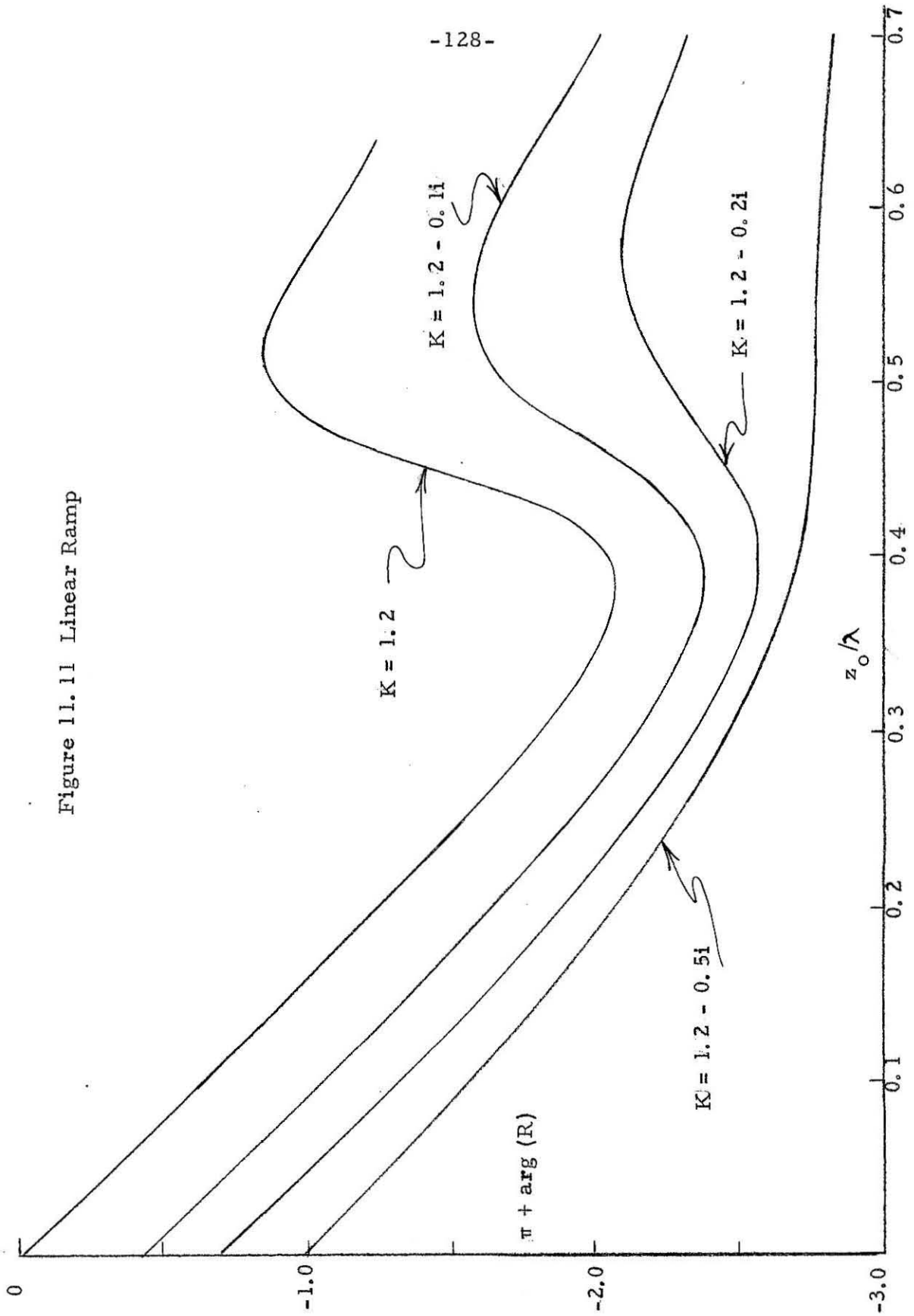


Figure 11.12 Linear Ramp

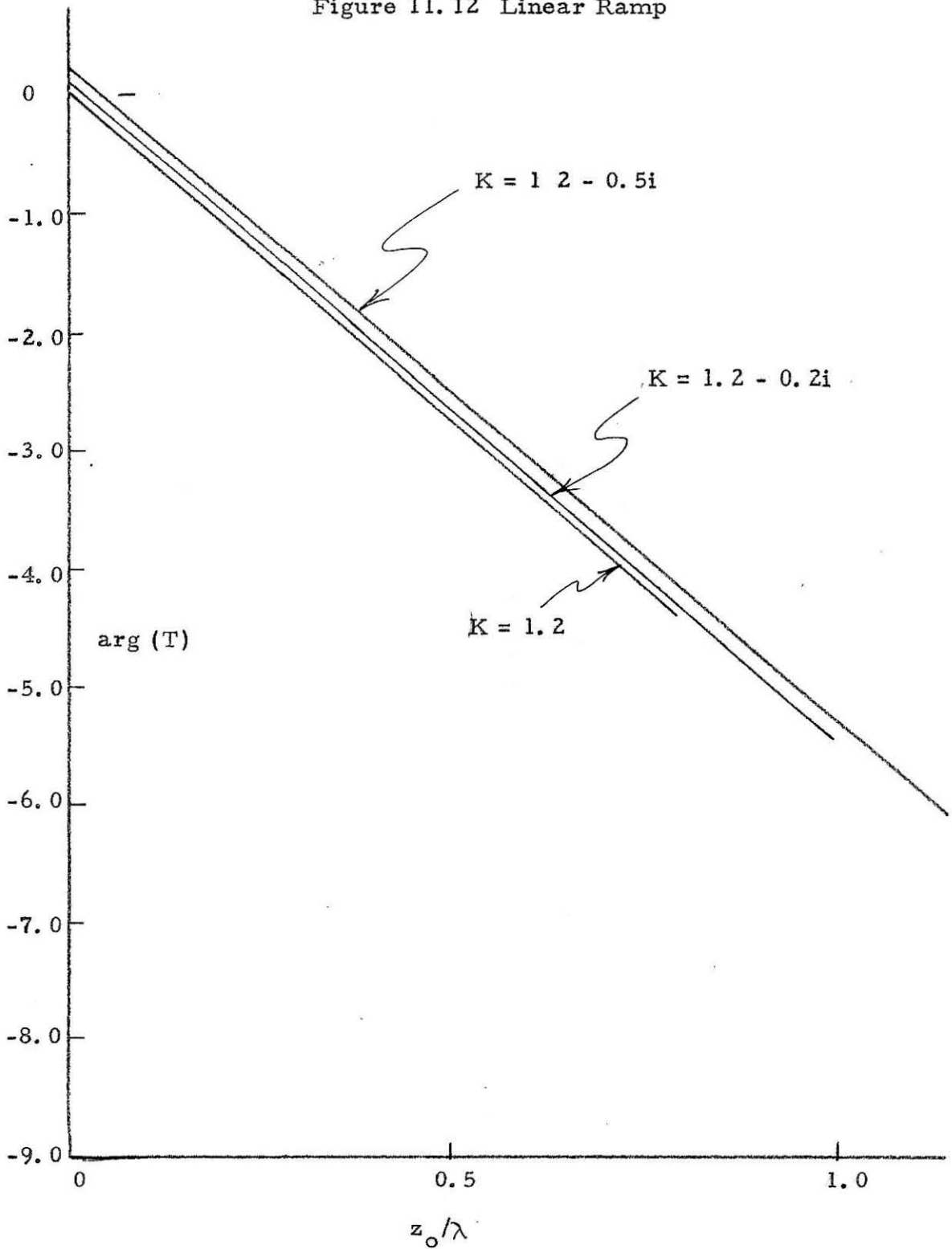


Figure 11.13 Linear Ramp

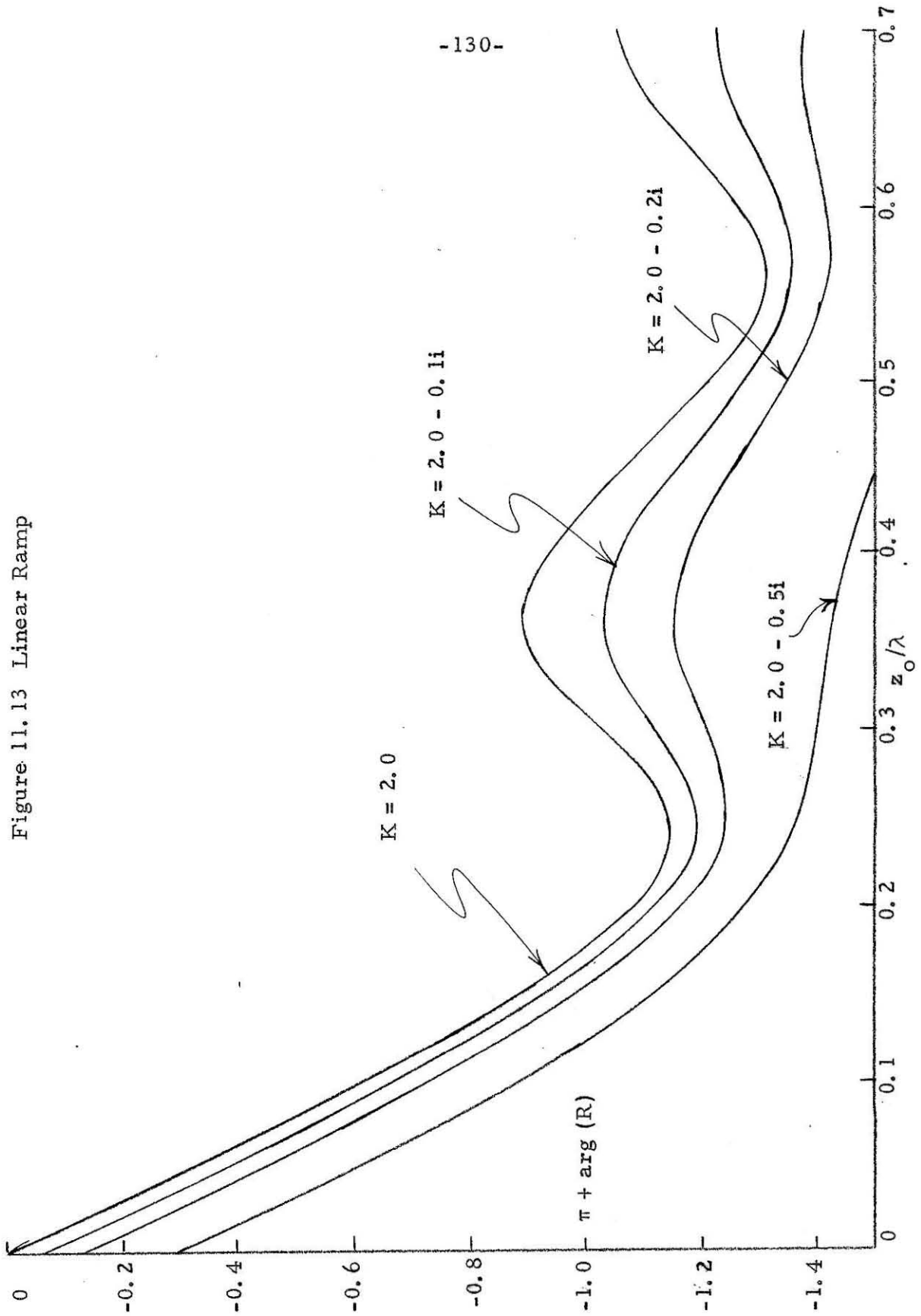


Figure 11.14 Linear Ramp

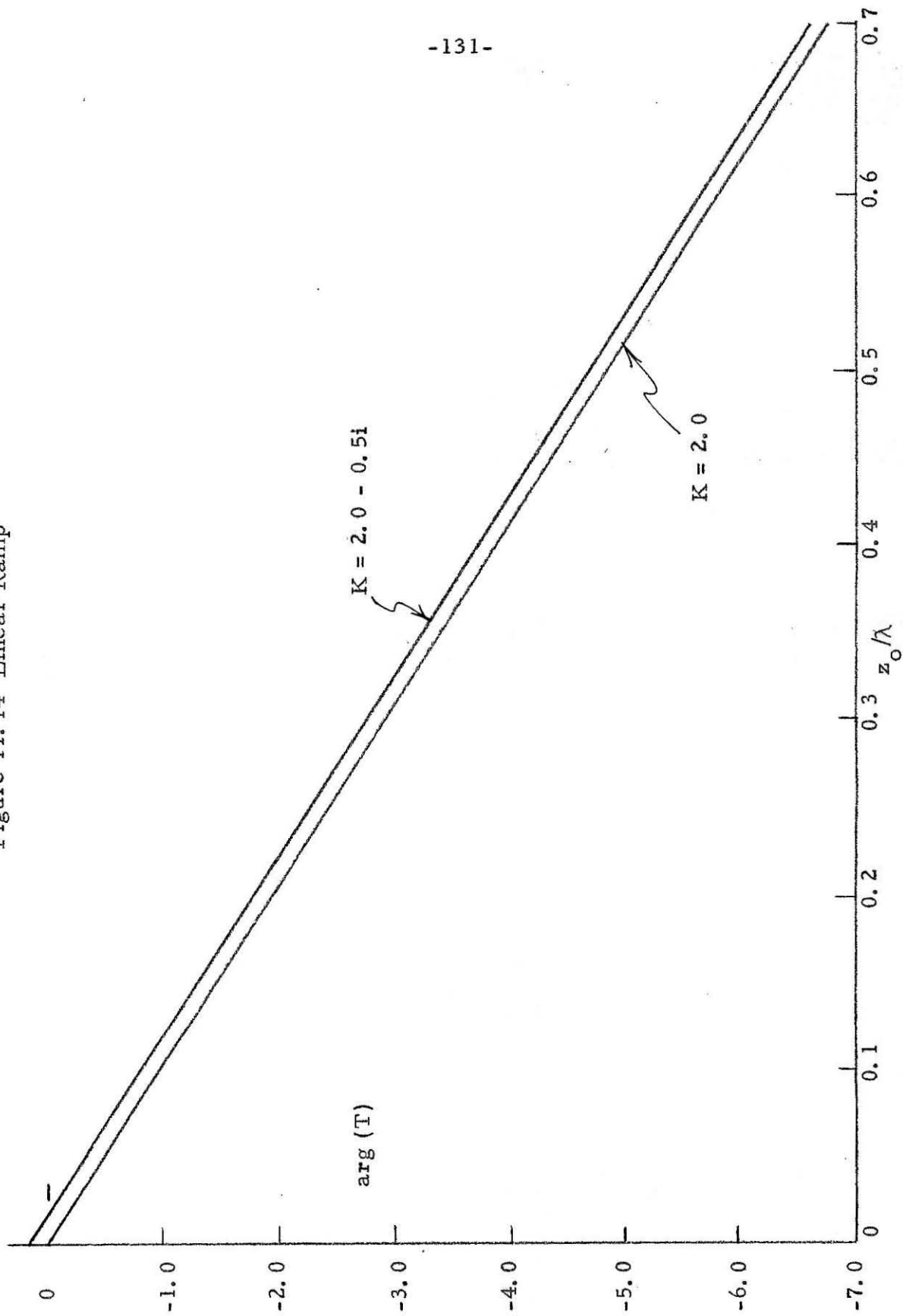


Figure 11.15 Linear Ramp
Comparison of Approximate and Exact
Expressions for $|R|$ at $K = 0.5 - 0.1i$

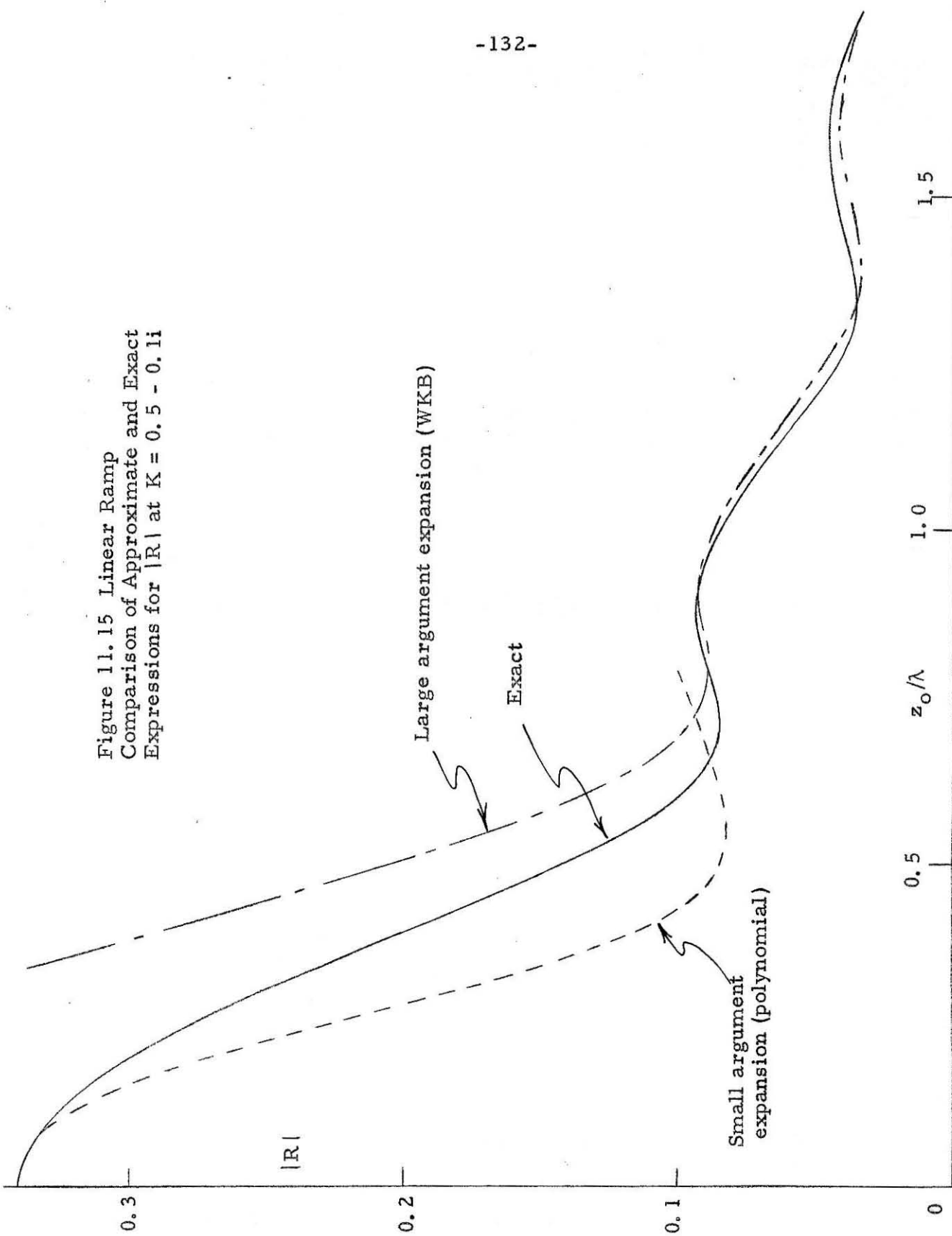
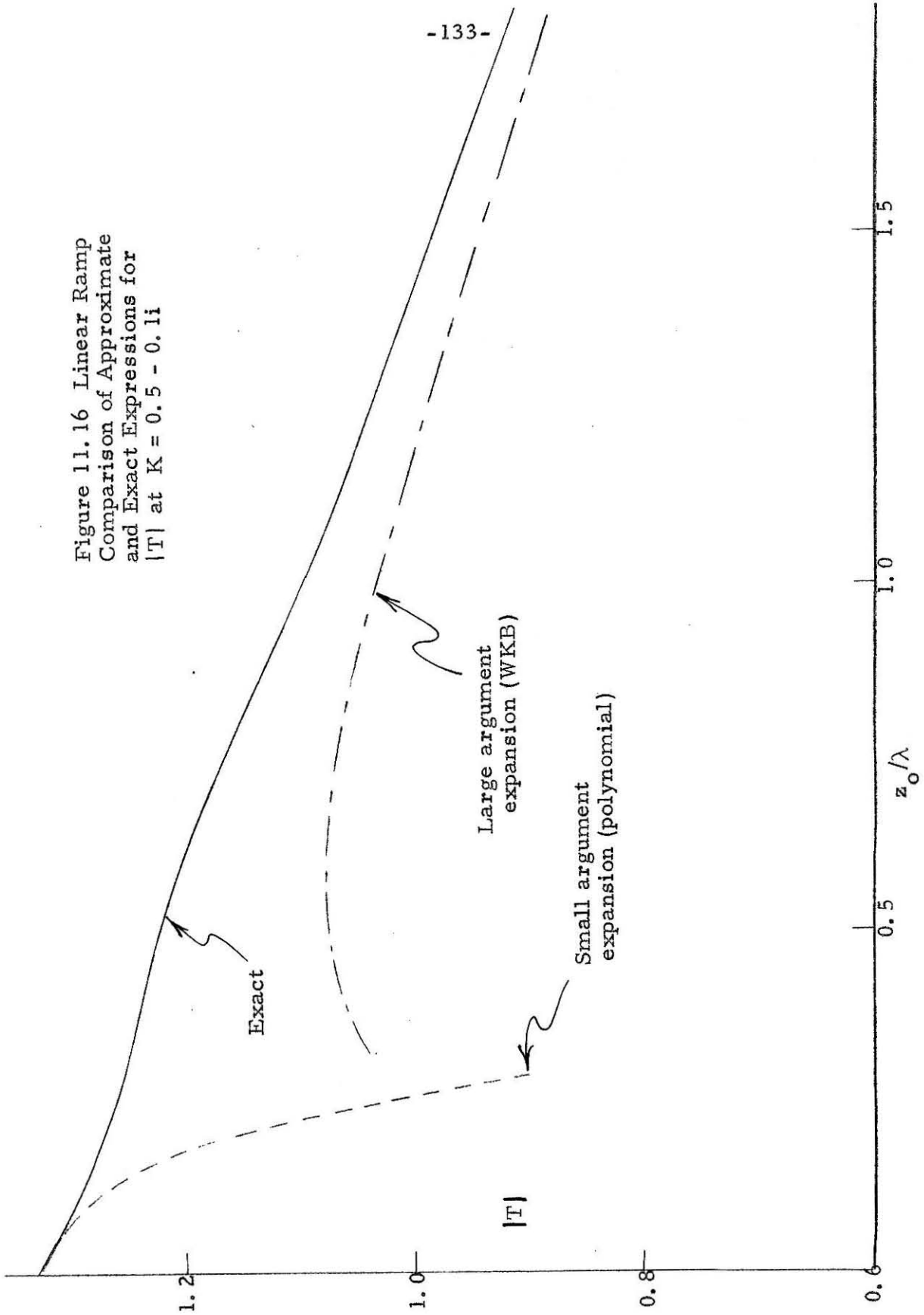


Figure 11.16 Linear Ramp
Comparison of Approximate
and Exact Expressions for
 $|T|$ at $K = 0.5 - 0.1i$



XII. THE KINKED RAMP PROBLEM

The strong influence of transition zone thickness evidenced by the results of the previous chapter certainly justifies some investigation of the sensitivity to the transition zone structure. The discovery of this sensitivity is the goal of this chapter*. The piecewise-linear transition zone (a kinked ramp, see figure 10.2) may serve as a second approximation to a smoother profile of electron density.

Writing the form of (10.7) valid for each of the four regions of space gives:

$$\frac{d^2 E}{dz^2} + k_0^2 E = 0, \quad z \leq 0 \quad (12.1)$$

$$\frac{d^2 E}{dz^2} + k_0^2 \left[1 - (1 - K_0^2) \frac{z}{z_0} \right] E = 0, \quad 0 \leq z \leq z_0 \quad (12.2)$$

$$\frac{d^2 E}{dz^2} + k_0^2 \left[K_0^2 - (K_0^2 - K_1^2) \frac{z - z_0}{z_1 - z_0} \right] E = 0, \quad z_0 \leq z \leq z_1 \quad (12.3)$$

$$\frac{d^2 E}{dz^2} + k_0^2 K_1^2 E = 0, \quad z \geq z_1 \quad (12.4)$$

where z_0 is the abscissa of the kink and z_1 is the thickness of the complete transition zone. K_0 is "dielectric constant" at z_0 , and K_1 is equal to the K of Chapter XI. In terms of the dimensionless electron density, ψ , of figure 9.2, and the K of Chapter X,

$$(1 - K^2) \psi_A = (1 - K_0^2) \quad (12.5)$$

* The analysis of Wallot (reference 18) for a smooth transition zone characterized by a polynomial of order n is not applicable for two reasons: first, the "dielectric constant" is a function of n explicitly, and second, the electron density would need be complex to make the end points of the transition region correct, for $n > 1$.

$$K = K_1 \quad (12.6)$$

The solutions to these equations may be derived as in Chapter XI, in terms of Airy functions in the linear variation regions.

$$E = e^{-ik_0 z} + R e^{ik_0 z} \quad z \leq 0 \quad (12.7)$$

$$E = A \cdot Ai(v) + B \cdot Bi(v) \quad 0 \leq z \leq z_0 \quad (12.8)$$

$$E = C \cdot Ai(w) + D \cdot Bi(w) \quad z_0 \leq z \leq z_1 \quad (12.9)$$

$$E = T e^{-ik_0 K(z-z_1)} \quad z \geq z_1 \quad (12.10)$$

where

$$v = - \left(\frac{k_0 z_0}{1-K_0^2} \right)^{2/3} \left\{ 1 - (1 - K_0^2) z/z_0 \right\} \quad (12.11)$$

$$w = - \left(\frac{k_0(z_1-z_0)}{K_0^2 - K_1^2} \right)^{2/3} \left\{ K_0^2 - (K_0^2 - K_1^2) \frac{z-z_0}{z_1-z_0} \right\} \quad (12.12)$$

Writing K_0 in terms of ψ_A and K , the arguments can be evaluated at the end points of the linear ranges:

$$v(0) = - \left(\frac{k_0 z_0}{1-K_0^2} \right)^{2/3} = - \left(\frac{k_0 z_1}{1-K^2} \right)^{2/3} \left(\frac{z_0}{z_1} \frac{1}{\psi_A} \right)^{2/3}$$

$$v(z_0) = - \left(\frac{k_0 z_0}{1-K_0^2} \right)^{2/3} K_0^2 = - \left(1 - (1-K^2)\psi_A \right) \left(\frac{z_0}{z_1} \frac{1}{\psi_A} \right)^{2/3} \left(\frac{k_0 z_1}{1-K^2} \right)^{2/3}$$

$$w(z_0) = - \left(\frac{k_0(z_1-z_0)}{K_0^2 - K^2} \right)^{2/3} K_0^2 = - \left(1 - (1-K^2)\psi_A \right) \left(\frac{1 - z_0/z_1}{1 - \psi_A} \right)^{2/3} \left(\frac{k_0 z_1}{1-K^2} \right)^{2/3}$$

$$w(z_1) = - \left(\frac{k_0(z_1-z_0)}{K_0^2 - K^2} \right)^{2/3} K_1^2 = - K^2 \left(\frac{1 - z_0/z_1}{1 - \psi_A} \right)^{2/3} \left(\frac{k_0 z_1}{1-K^2} \right)^{2/3}$$

More simply, in terms of the variable of the preceding section, let

$$\phi_0 = -i \left(\frac{k_0 z_0}{1-K^2} \right)^{1/3} \quad (12.13)$$

and introduce the "slope ratio" parameter, S ,

$$S = \left[(\psi_A/z_0) / \{ (1 - \psi_A)/(z_1 - z_0) \} \right]^{1/3} \quad (12.14)$$

which is the cubic root of the ratio of the normalized density profile

slopes in the two linear segments. In terms of these variables:

$$v(0) = \phi_0^2, \quad v(z_0) = (K_0 \phi_0)^2 \quad (12.15)$$

$$w(z_0) = (SK_0 \phi_0)^2, \quad w(z_1) = (SK\phi_0)^2 \quad (12.16)$$

$$\frac{dv}{dz} = -ik_0/\phi_0, \quad \frac{dw}{dz} = -ik_0/\phi_0 S \quad (12.17)$$

where

$$\phi_0 = -i \left(\frac{k_0 z_1}{1-K^2} \right)^{1/3} \left(\frac{z_0}{z_1} \frac{1}{\psi_A} \right)^{1/3}, \quad (12.18)$$

$$K_0 = \left(1 - (1-K^2)\psi_A \right)^{1/2}. \quad (12.19)$$

Thus the basic parameters of the problem can be visualized quickly.

They are:

- (1) $(k_0 z_1 / (1-K^2))$, the transition zone thickness measured in wavelengths divided by the total change in "dielectric constant", as before;
- (2) ψ_A , the ordinate of the discontinuity in profile slope;
- (3) z_0/z_1 , the abscissa of the discontinuity in profile slope.

The convenient parameter S allows easy transition to the simple ramp problem, as is shown in the boundary condition equations below. Matching the boundary conditions of continuity on E and dE/dz requires:

$$\begin{aligned} 1 + R &= A \text{Ai}(\phi_0^2) + B \text{Bi}(\phi_0^2) \\ \phi_0(1-R) &= A \text{Ai}'(\phi_0^2) + B \text{Bi}'(\phi_0^2) \end{aligned}$$

$$\begin{aligned}
 A \operatorname{Ai}(K_0^2 \phi_0^2) + B \operatorname{Bi}(K_0^2 \phi_0^2) &= C \operatorname{Ai}(S^2 K_0^2 \phi_0^2) + D \operatorname{Bi}(S^2 K_0^2 \phi_0^2) \\
 S(A \operatorname{Ai}'(K_0^2 \phi_0^2) + B \operatorname{Bi}'(K_0^2 \phi_0^2)) &= C \operatorname{Ai}'(S^2 K_0^2 \phi_0^2) + D \operatorname{Bi}'(S^2 K_0^2 \phi_0^2) \\
 T &= C \operatorname{Ai}(S^2 K_0^2 \phi_0^2) + D \operatorname{Bi}(S^2 K_0^2 \phi_0^2) \\
 SK_0 T &= C \operatorname{Ai}'(S^2 K_0^2 \phi_0^2) + D \operatorname{Bi}'(S^2 K_0^2 \phi_0^2)
 \end{aligned}$$

From these equations it is clear that when S is unity, i. e., $\psi_A = z_0/z_1$, the equations reduce to those of the linear ramp problem. Manipulation of the first two equations yields

$$\begin{aligned}
 R A^+(\phi_0) + A^-(\phi_0) &= -B/\pi \\
 R B^+(\phi_0) + B^-(\phi_0) &= A/\pi
 \end{aligned}$$

while the last two give

$$\begin{aligned}
 T A^-(SK_0 \phi_0) &= -D/\pi \\
 T B^-(SK_0 \phi_0) &= C/\pi
 \end{aligned}$$

where the A^+ , B^+ functions are as defined in the previous chapter.

The remaining two equations link A and B to C and D . The reader is spared the remaining algebra; the resulting expressions for R and T may be written in the form:

$$R = \frac{\alpha B^-(\phi_0) - \beta A^-(\phi_0)}{\beta A^+(\phi_0) - \alpha B^+(\phi_0)} \quad (12.20)$$

$$T = \frac{2 \phi_0 / \pi^2}{\beta A^+(\phi_0) - \alpha B^+(\phi_0)} \quad (12.21)$$

The functions α and β are most compactly expressed by repeated matrix operations:

$$\begin{Bmatrix} \beta \\ \alpha \end{Bmatrix} = \begin{bmatrix} \operatorname{Bi}'(x) & -\frac{1}{S} \operatorname{Bi}(x) \\ \operatorname{Ai}'(x) & -\frac{1}{S} \operatorname{Ai}(x) \end{bmatrix} \cdot \begin{bmatrix} \operatorname{Ai}(y) & \operatorname{Bi}(y) \\ \operatorname{Ai}'(y) & \operatorname{Bi}'(y) \end{bmatrix} \cdot \begin{Bmatrix} B^-(u) \\ -A^-(u) \end{Bmatrix} \quad (12.22)$$

where

$$x = (K_0 \phi_0)^2$$

$$y = (S K_0 \phi_0)^2$$

$$u = (S K \phi_0)$$

The expressions for R and T were evaluated by machine computation as in the previous case, and representative examples are presented graphically at the end of this chapter. For each value of K, the position of the "kink" was established at 12 distinct locations, and four degenerate, "smooth ramp" locations, as given by the coordinates:

$\psi_A = 0.2, 0.4, 0.6, \text{ and } 0.8$; $z_0/z_1 = 0.2, 0.4, 0.6, \text{ and } 0.8$. In general, the behavior of the curves of |R| and |T| are essentially the same as for the linear ramp degenerate case; only minor shifts of the relative minima and maxima occur in many cases, while in others it is clear that the first or second portion of the ramp is dominating the behavior, introducing only a scaling effect in the plot versus $k_0 z_1$. In most cases, the solutions are largely independent of the kink coordinates over the first few tenths of wavelengths, indicating a relative insensitivity to the detailed structure of the transition zone for narrow zones. For large values of z_1/λ , the asymptotic forms are again similar in periodicity and amplitude, as would be anticipated by an integral approximation of the WKB type.

Two examples of the phase of the reflected and transmitted waves are included in the plots. Much like the linear ramp, prominent periodicities are evident in $\arg(R)$ while $\arg(T)$ is nearly a straight line. As before, the real part of the average value of $K(z)$ provides an

excellent approximation for the slope of the $\arg(T)$ versus z_1/λ curves.

$$\arg(T) \doteq -\arg(1+K) - \operatorname{Re} \left[\frac{2}{3} \frac{k_o z_o}{1-K_o} \left(1 - S^3 (K^3 - K_o^3) \right) \right]$$

The success of an integral approximation procedure in this case can be anticipated from the accuracy of the $\arg(T)$ approximation, but approximations are not developed for this case because of the complexity. The reader is asked to observe that in such cases as it would be appropriate to consider the simple ramp as a zeroth approximation, and the kinked ramp as a first approximation, to an unspecified smooth profile, there is little difference between the zeroth and first approximation results. This implies that the major effects of the transition zone are contained in the linear model, these being based largely on the value of transition zone thickness (in wavelengths) and the total change in "dielectric constant". The relative insensitivity of the reflection coefficient to detailed zone structure in a dielectric gas has been noted by Greene and Hornig⁽¹⁹⁾ in numerical calculations for shock-wave thickness measurements using optical techniques; indeed, the strong dependence of reflectance on transition zone thickness furnished the basis for their experiments.

With the above observations, the essential effort of this chapter is fulfilled, i. e., the discovery of the sensitivity of the reflection and transmission coefficients to the detailed structure of the transition. The next effort is the computation of R and T for the more practical problem of a mig slab bounded by symmetrical linear transition zones. Having established the validity of some linear transition as a reasonable approximation to the true electron density profile, one may then employ

these results with the assurance that first order effects are not being neglected or spuriously introduced by the profile choice. The "trapezoid" geometry of the following section is then perhaps the most useful case considered, so several examples will be plotted.

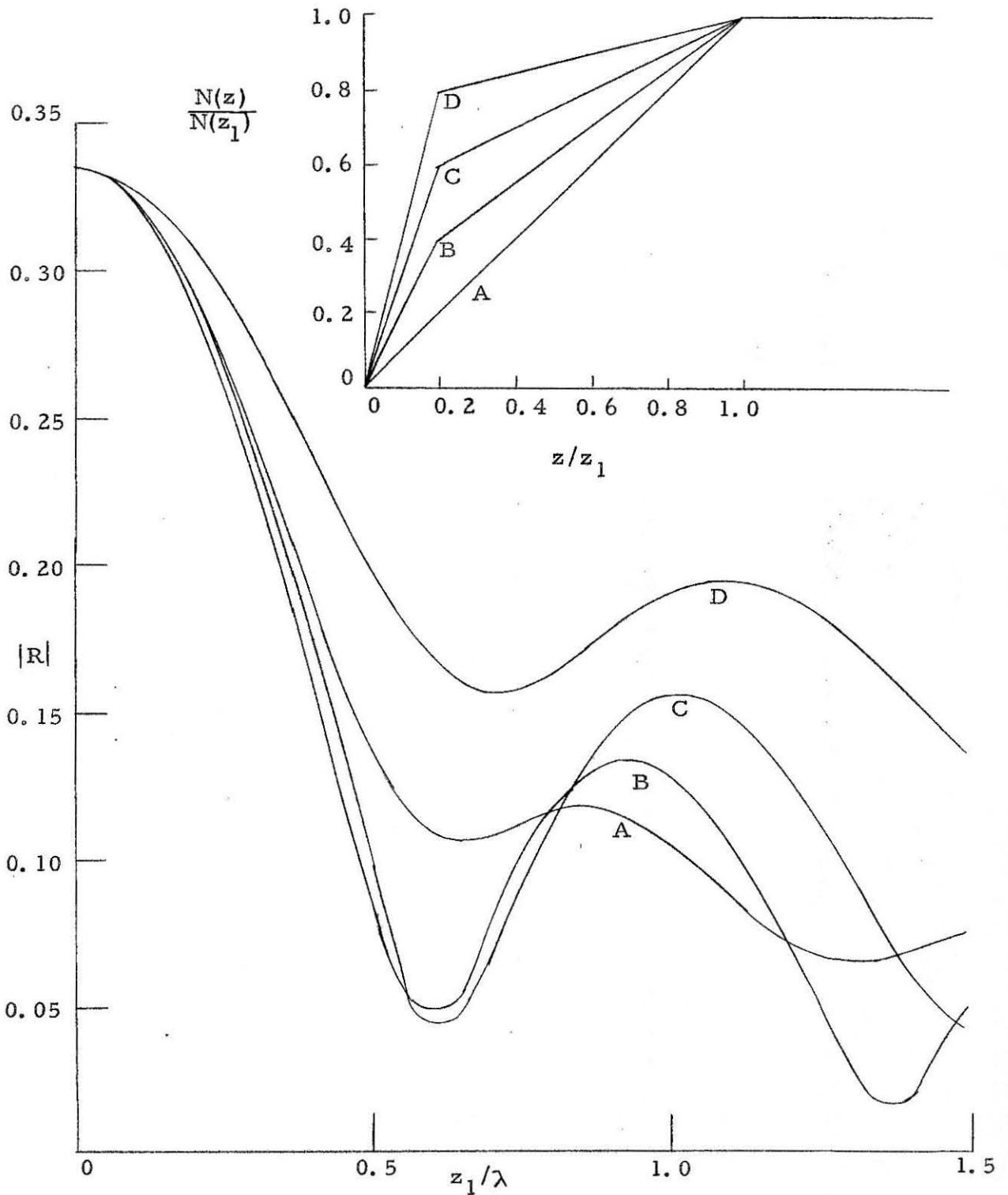


Figure 12.1 Kinked Ramp, $K = 0.5$

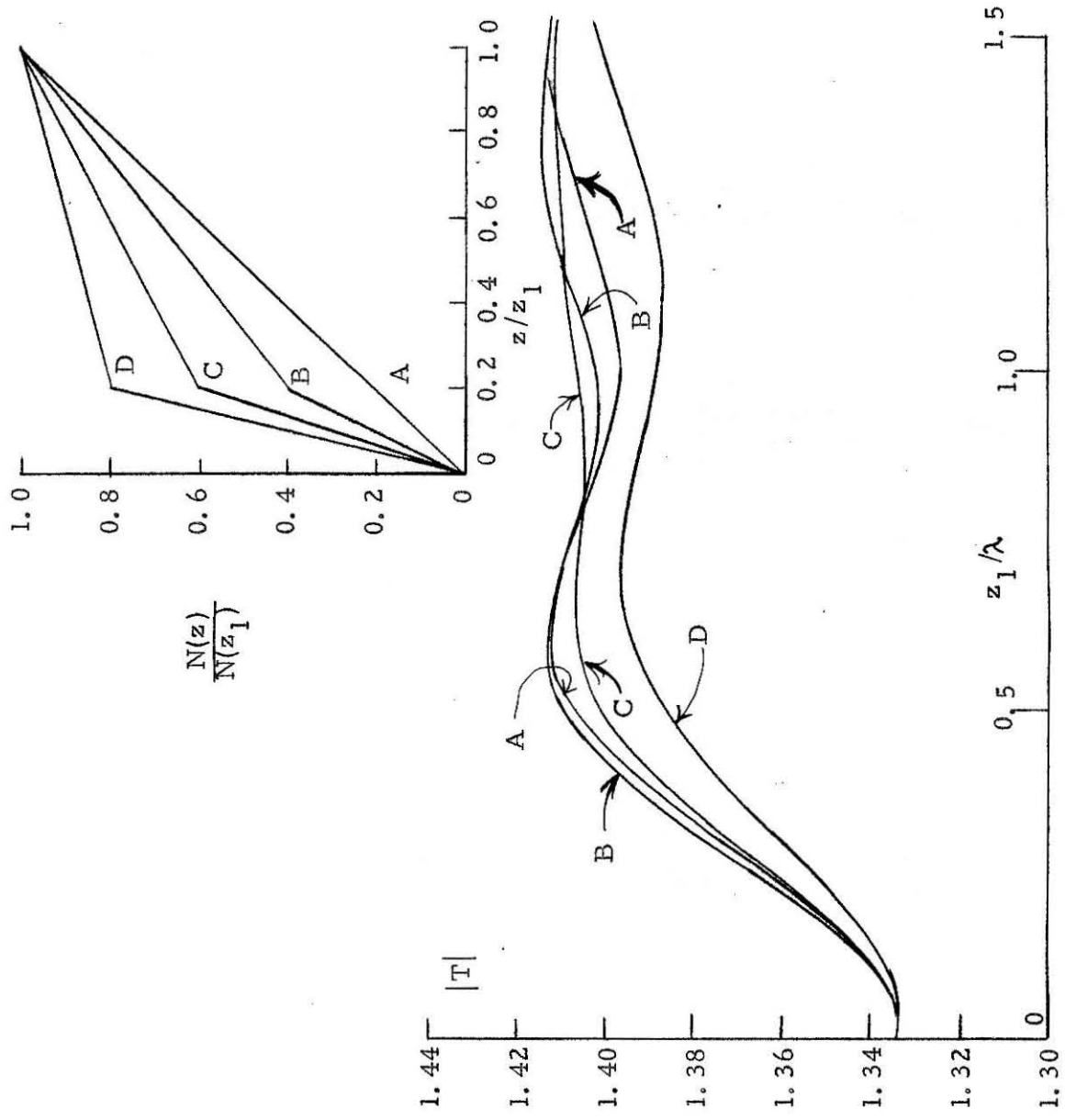


Figure 12.2 Kinked Ramp, $K = 0.5$

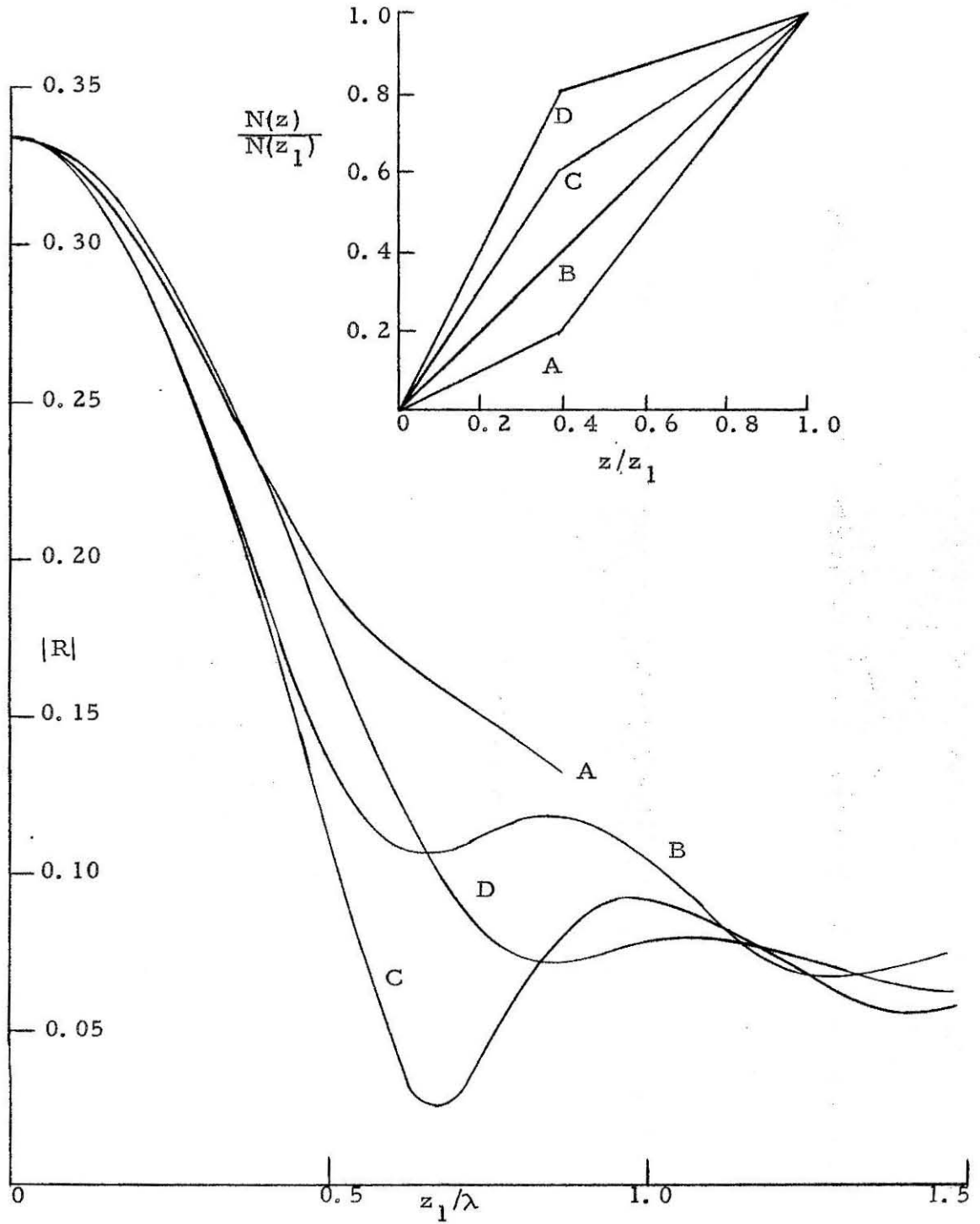


Figure 12.3 Kinked Ramp, $K = 0.5$

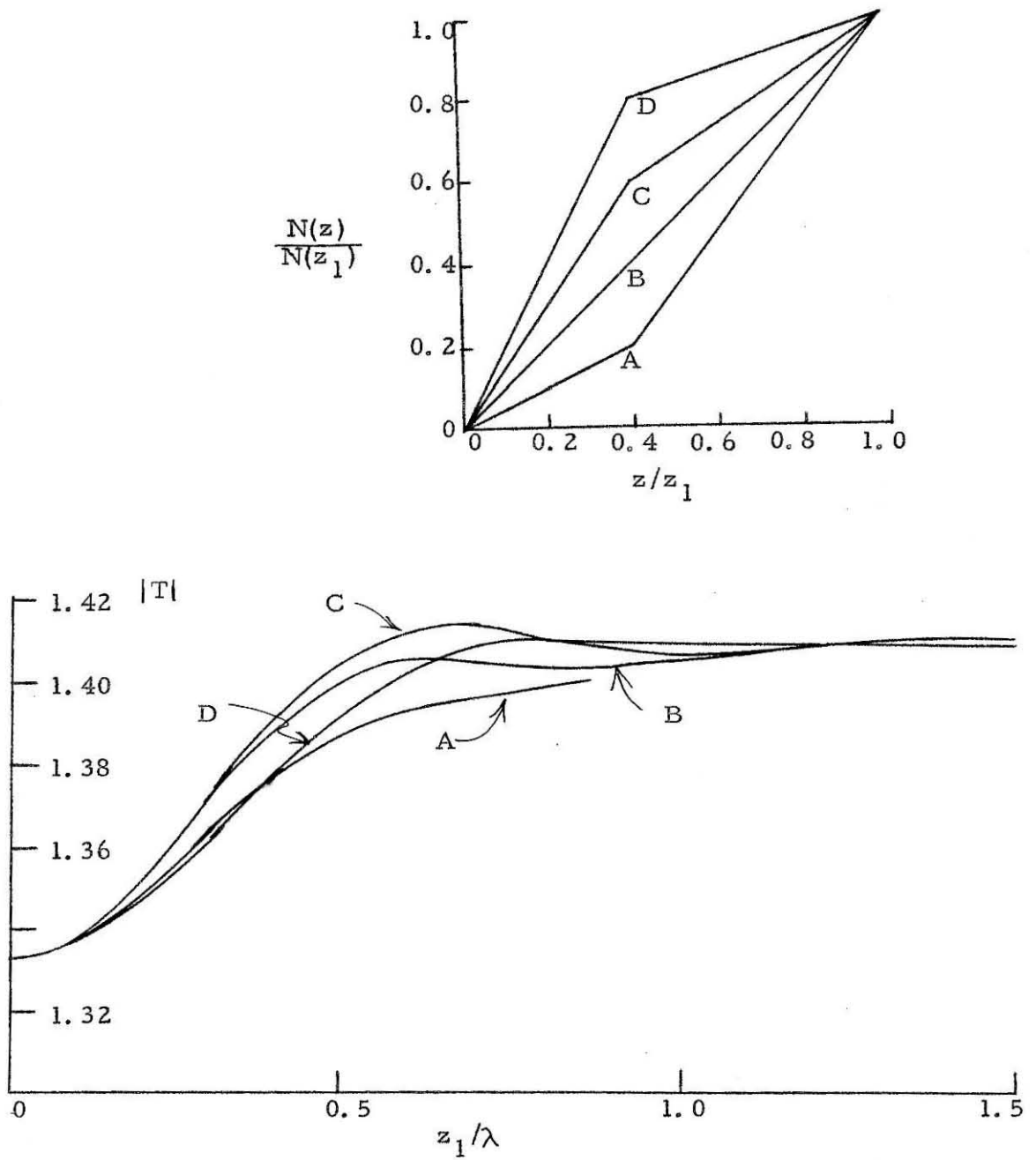


Figure 12.4 Kinked Ramp, $K = 0.5$

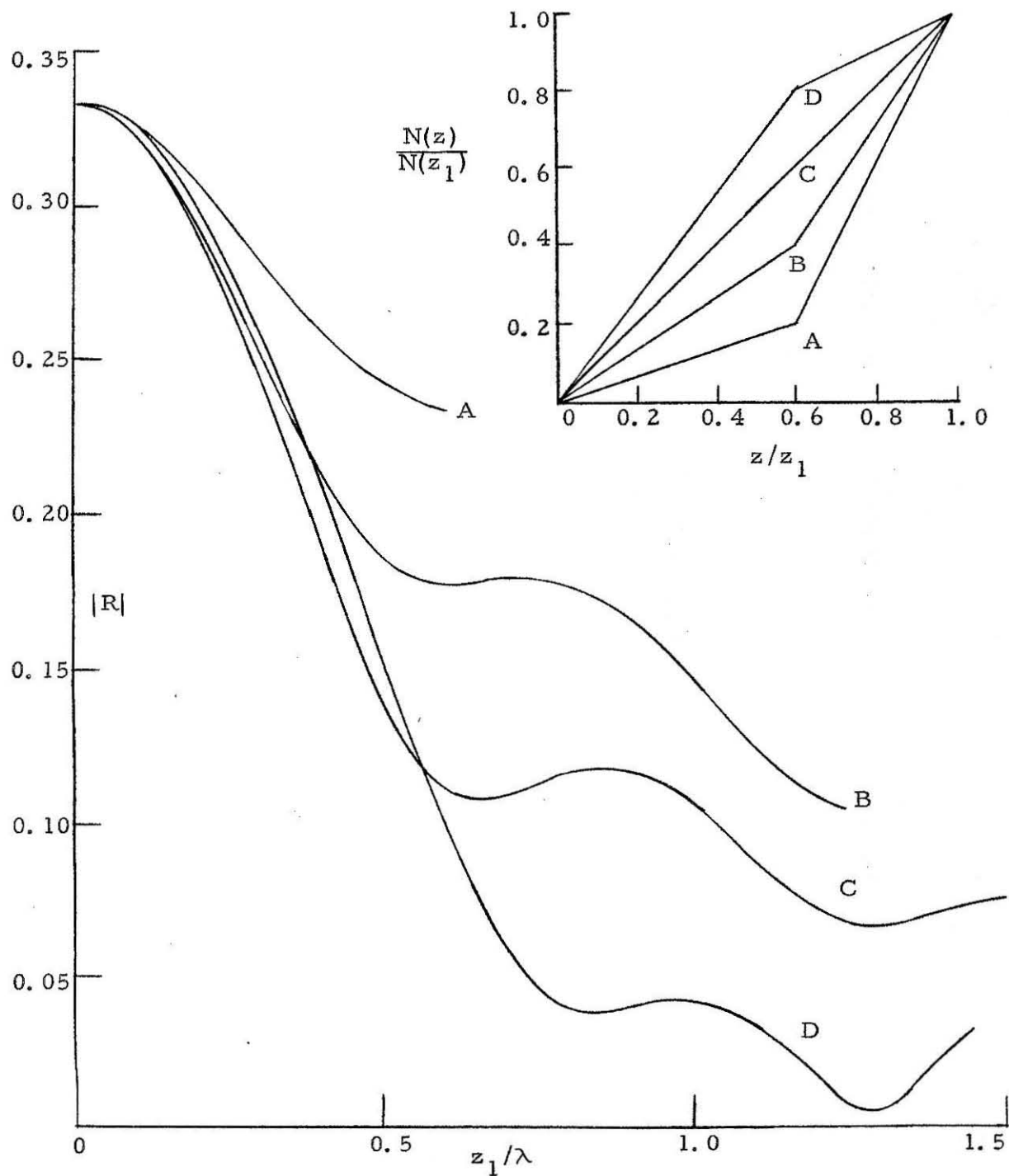


Figure 12.5 Kinked Ramp, $K = 0.5$

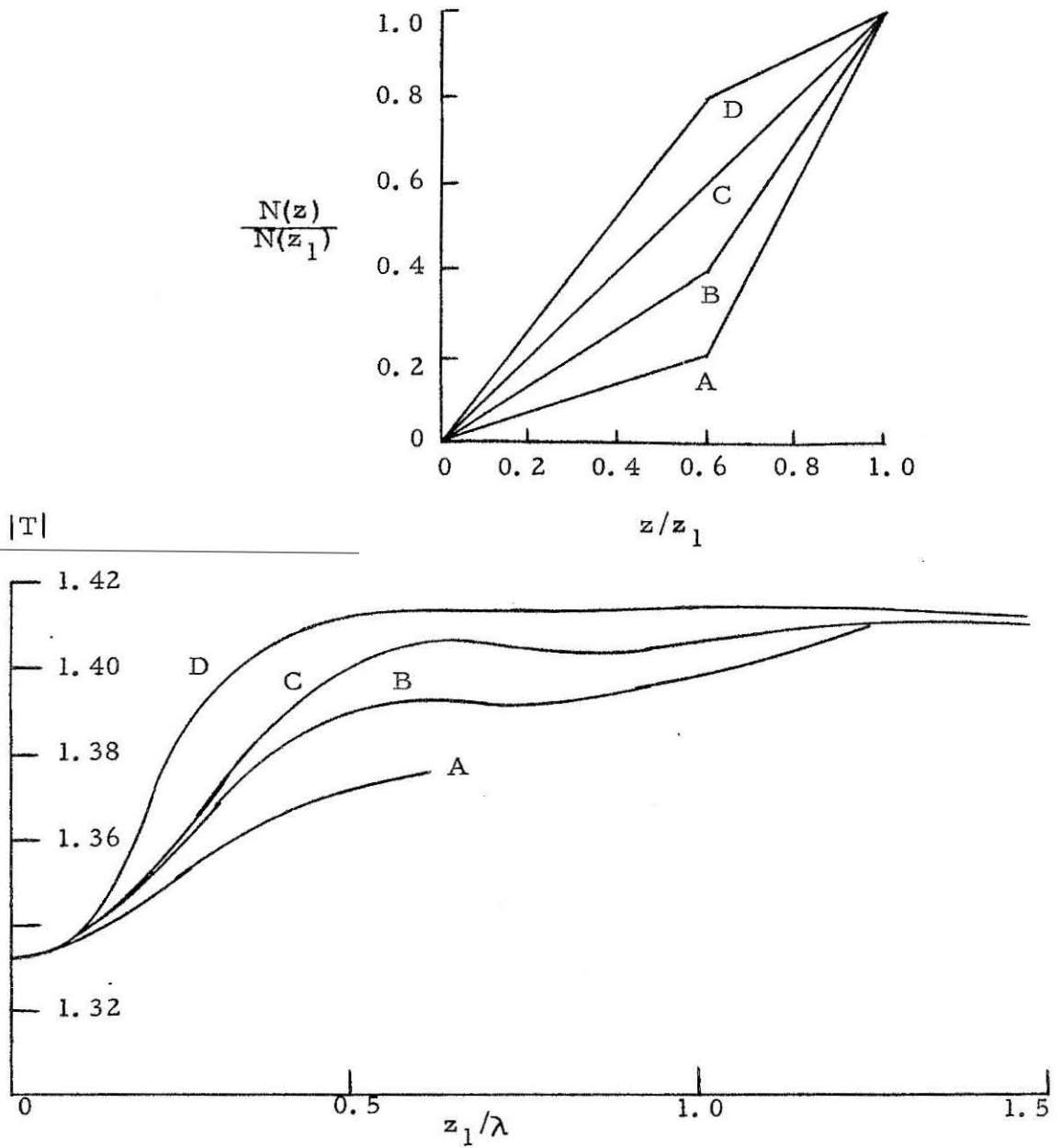


Figure 12.6 Kinked Ramp, $K = 0.5$

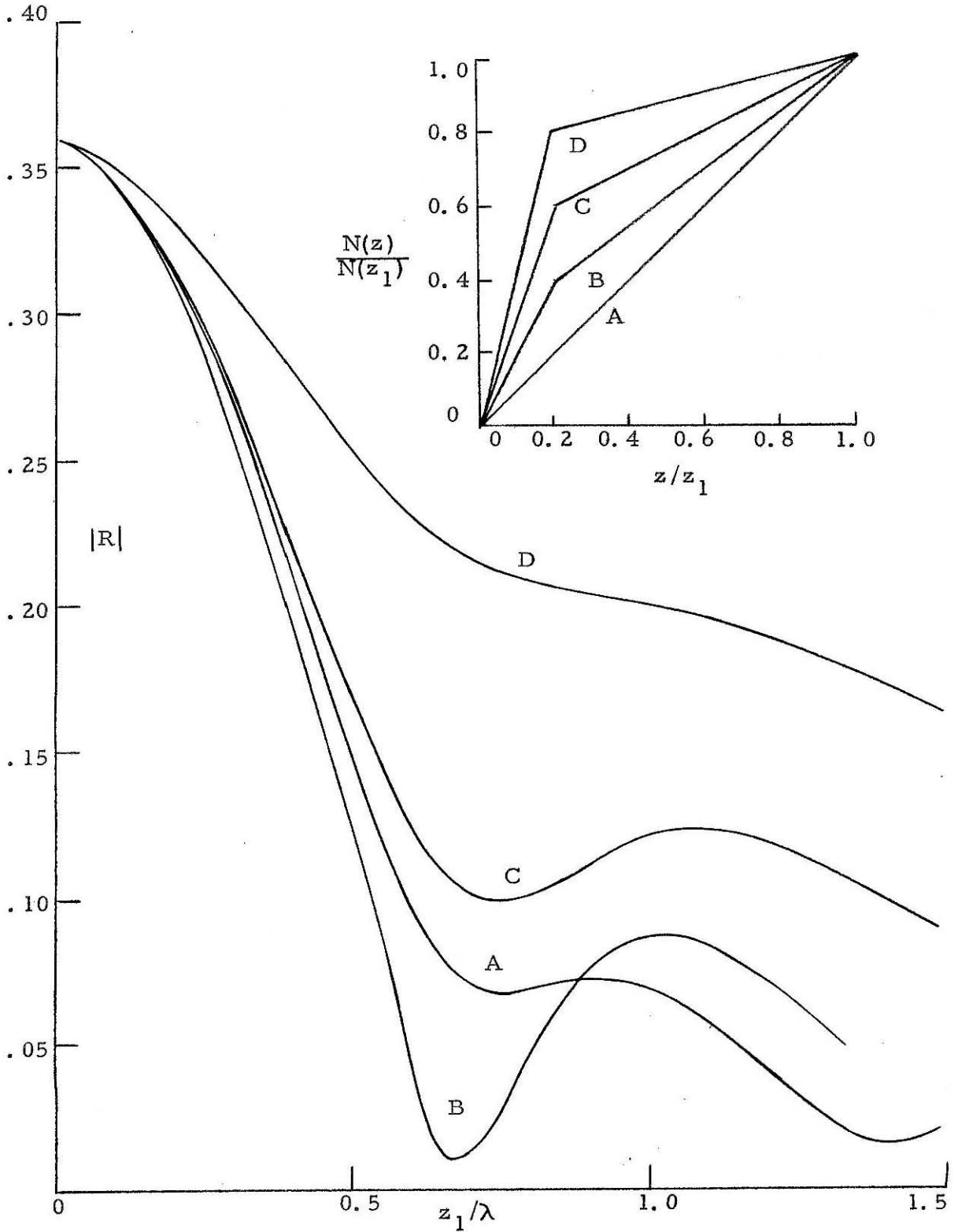
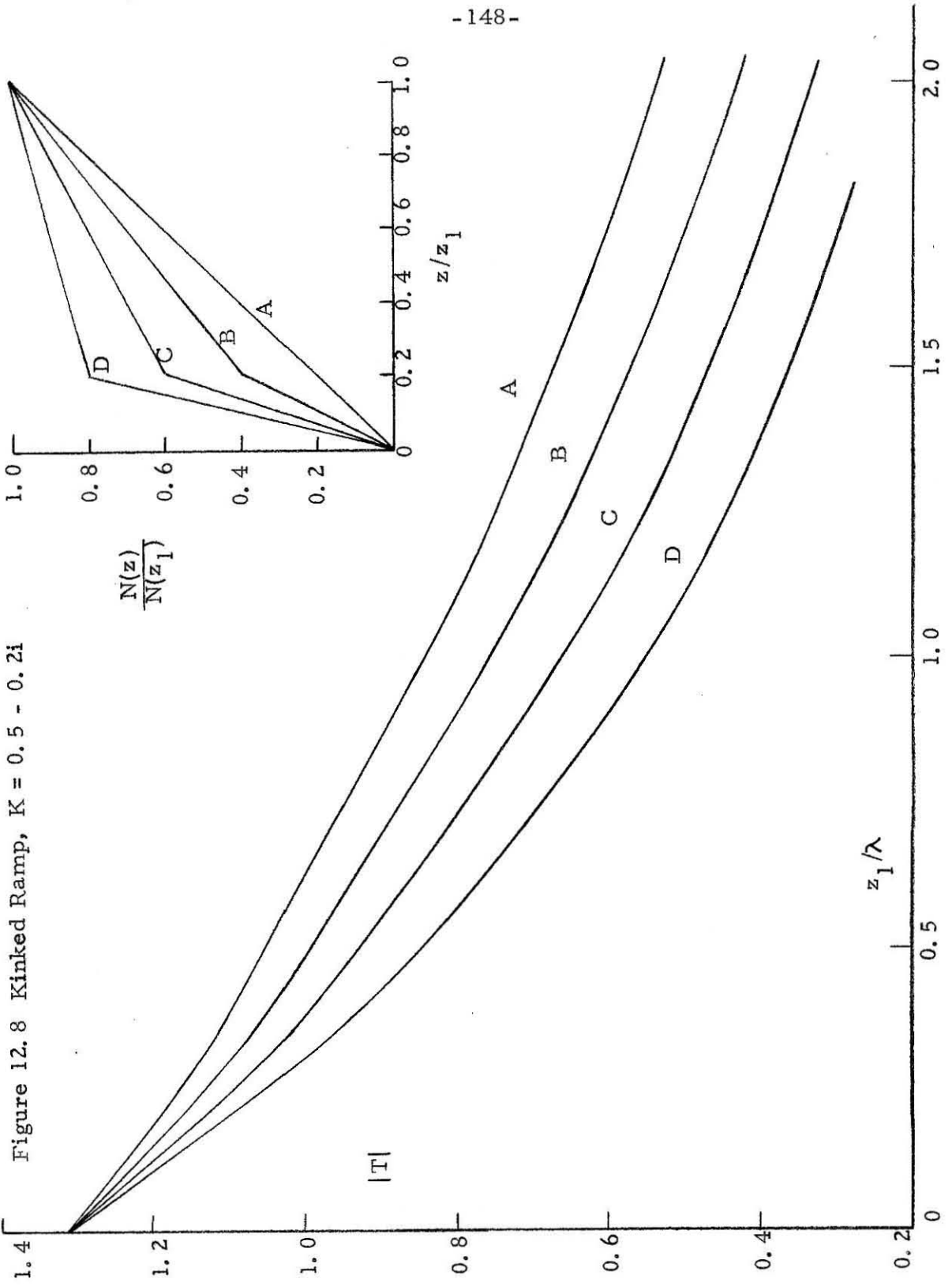


Figure 12.7 Kinked Ramp, $K = 0.5 - 0.2i$

Figure 12.8 Kinked Ramp, $K = 0.5 - 0.2i$



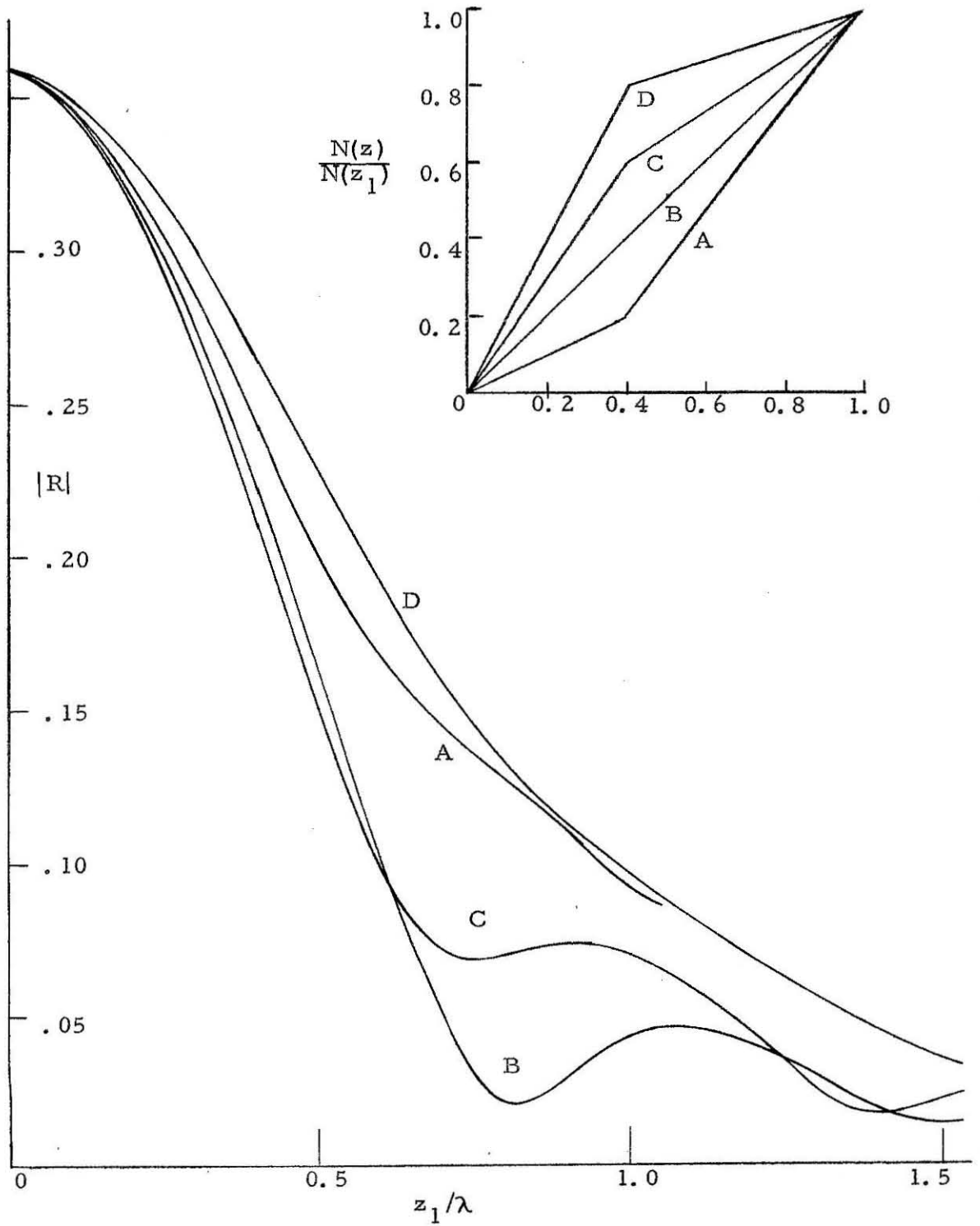


Figure 12.9 Kinked Ramp, $K = 0.5 - 0.2i$

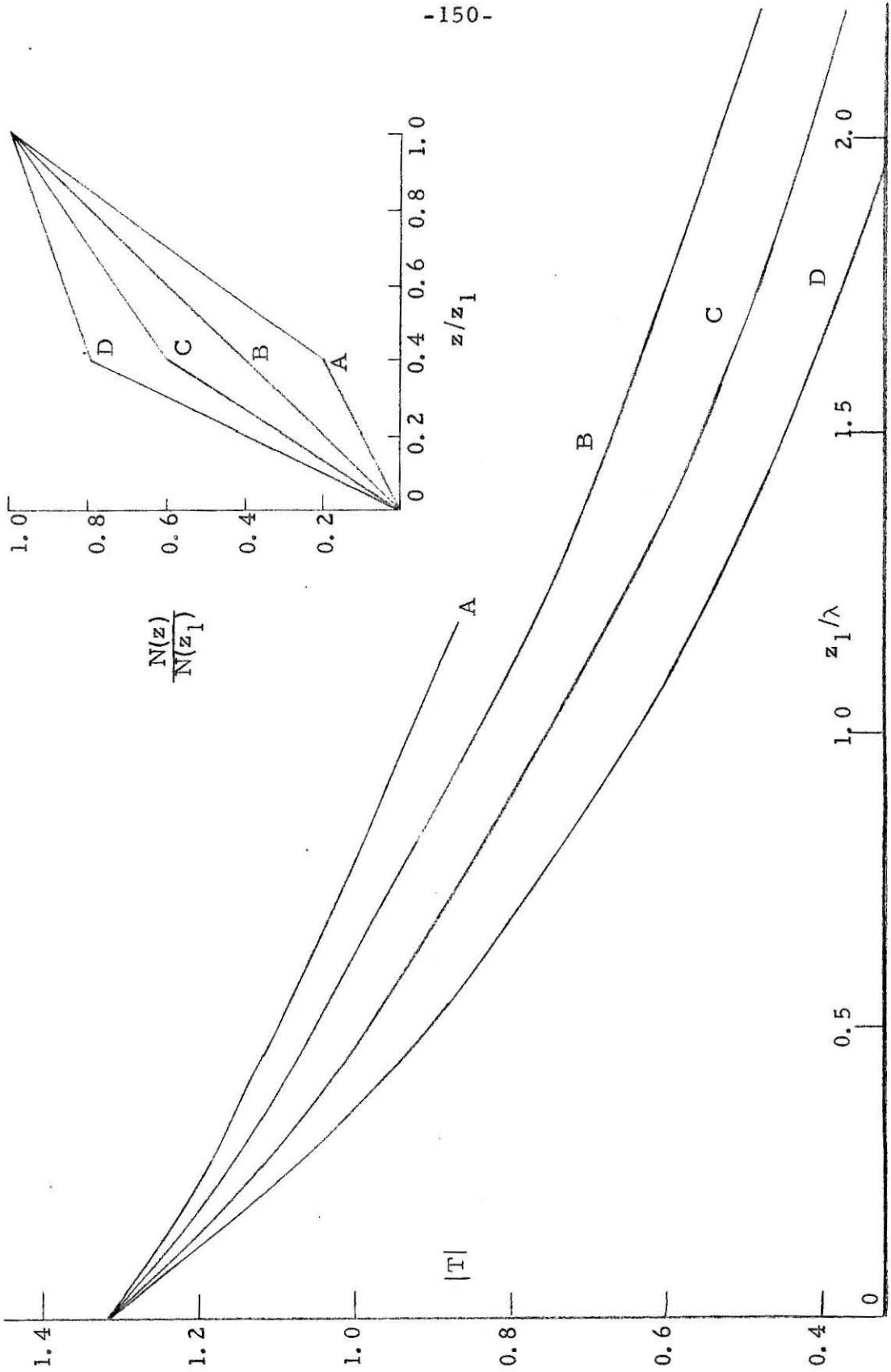


Figure 12.10 Kinked Ramp, $K = 0.5 - 0.2i$

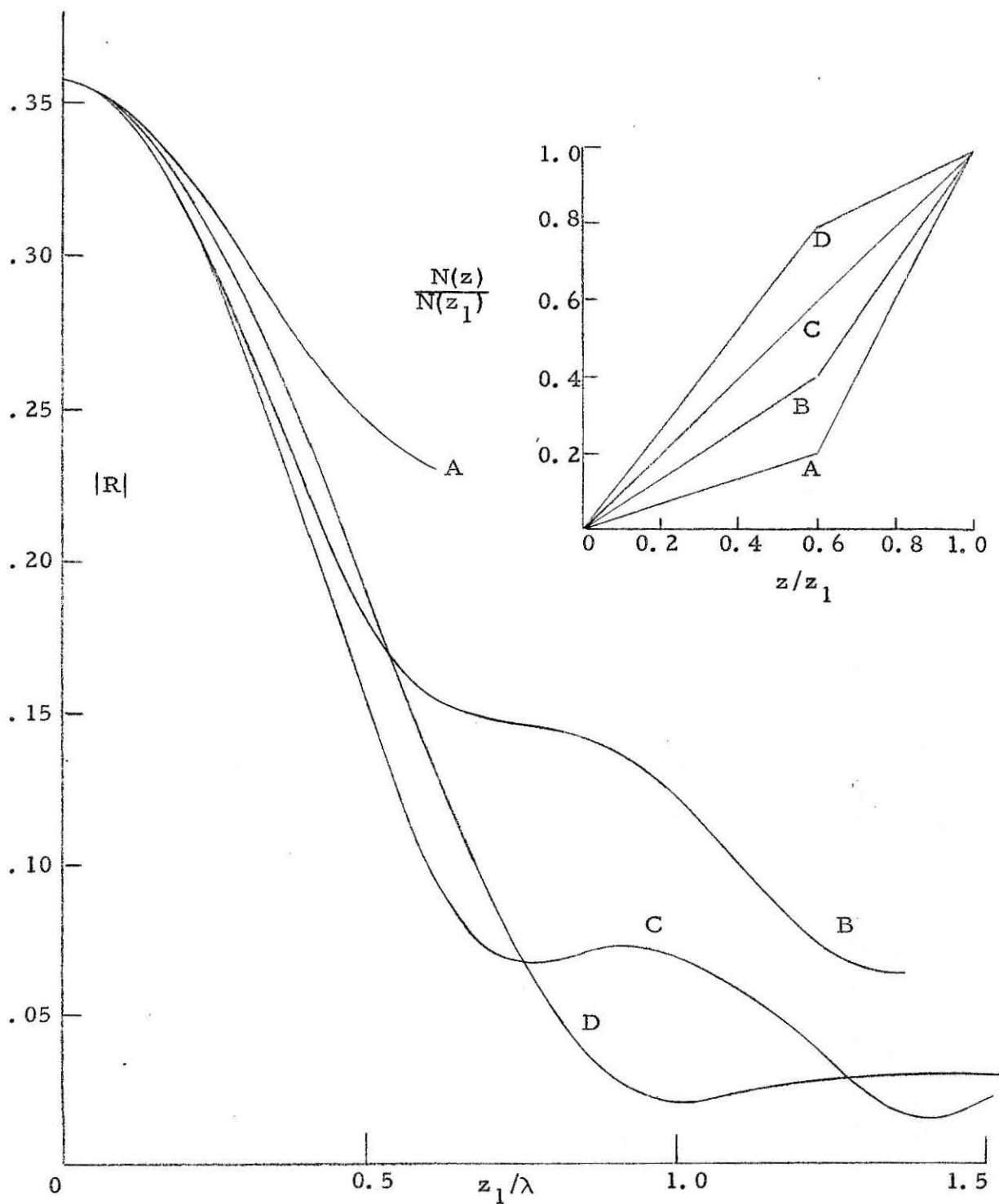
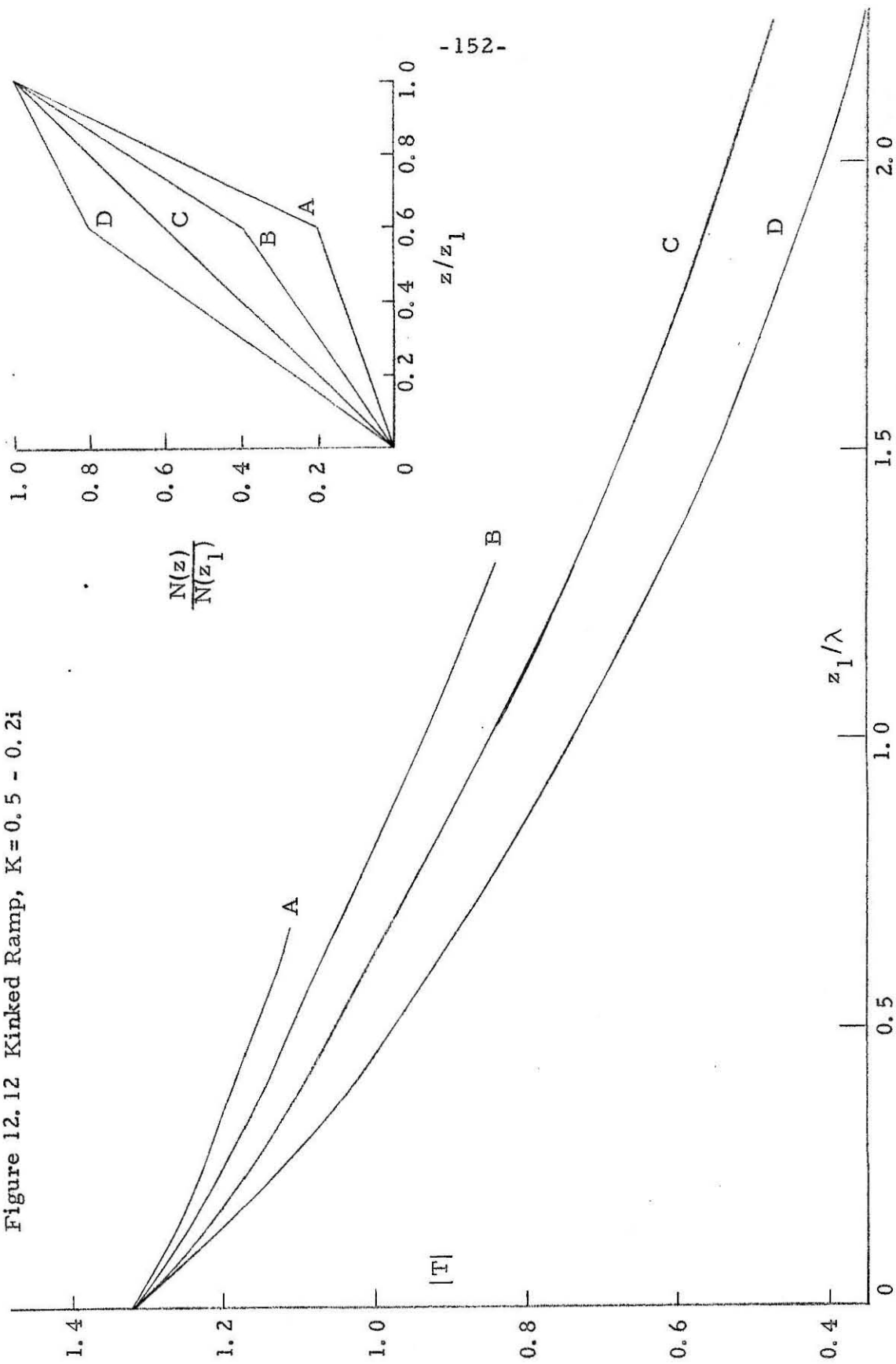


Figure 12.11 Kinked Ramp, $K = 0.5 - 0.2i$

Figure 12.12 Kinked Ramp, $K = 0.5 - 0.2i$



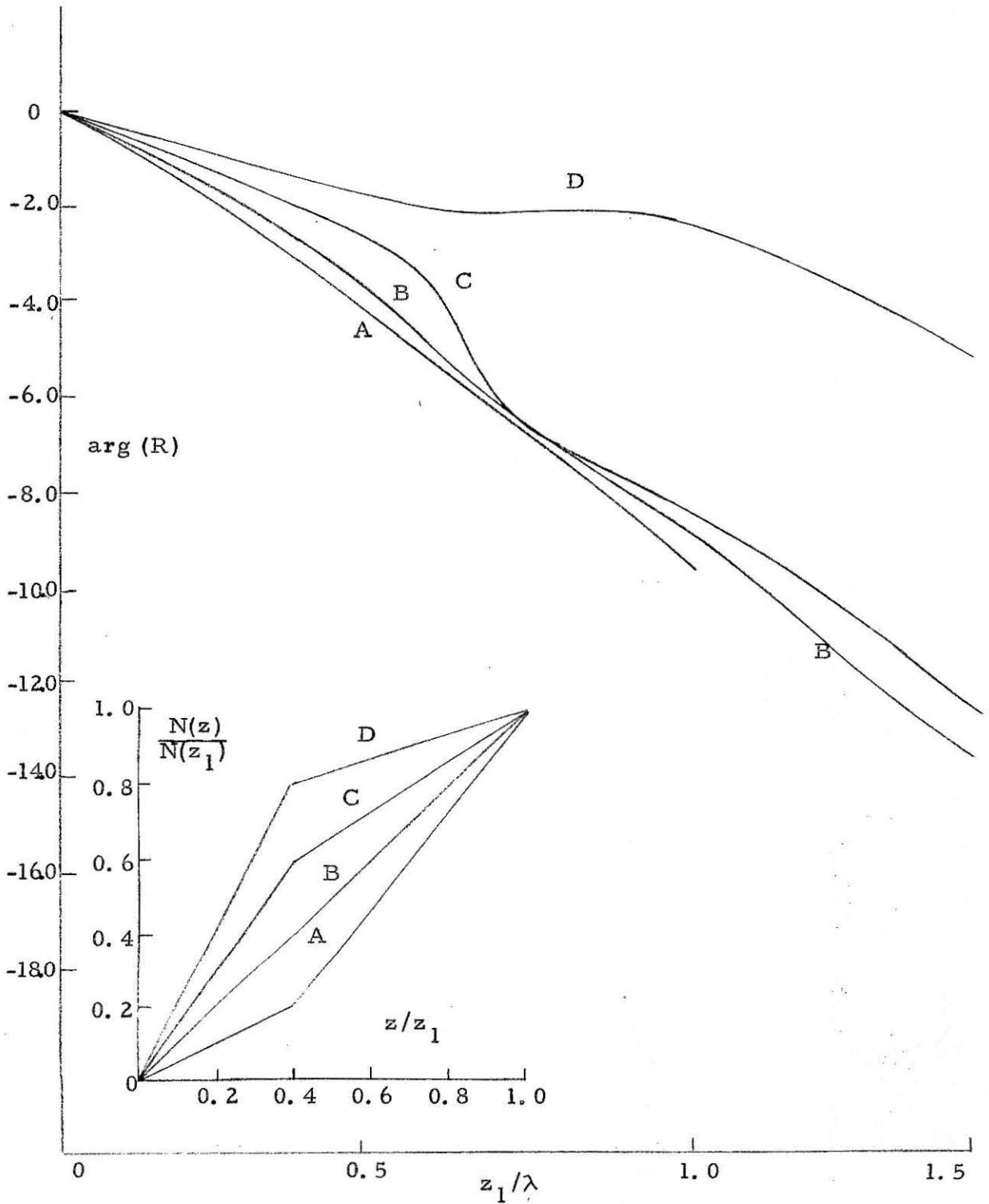


Figure 12.13 Kinked Ramp, $K = 0.5$

Figure 12.14 Kinked Ramp, $K = 0.5$

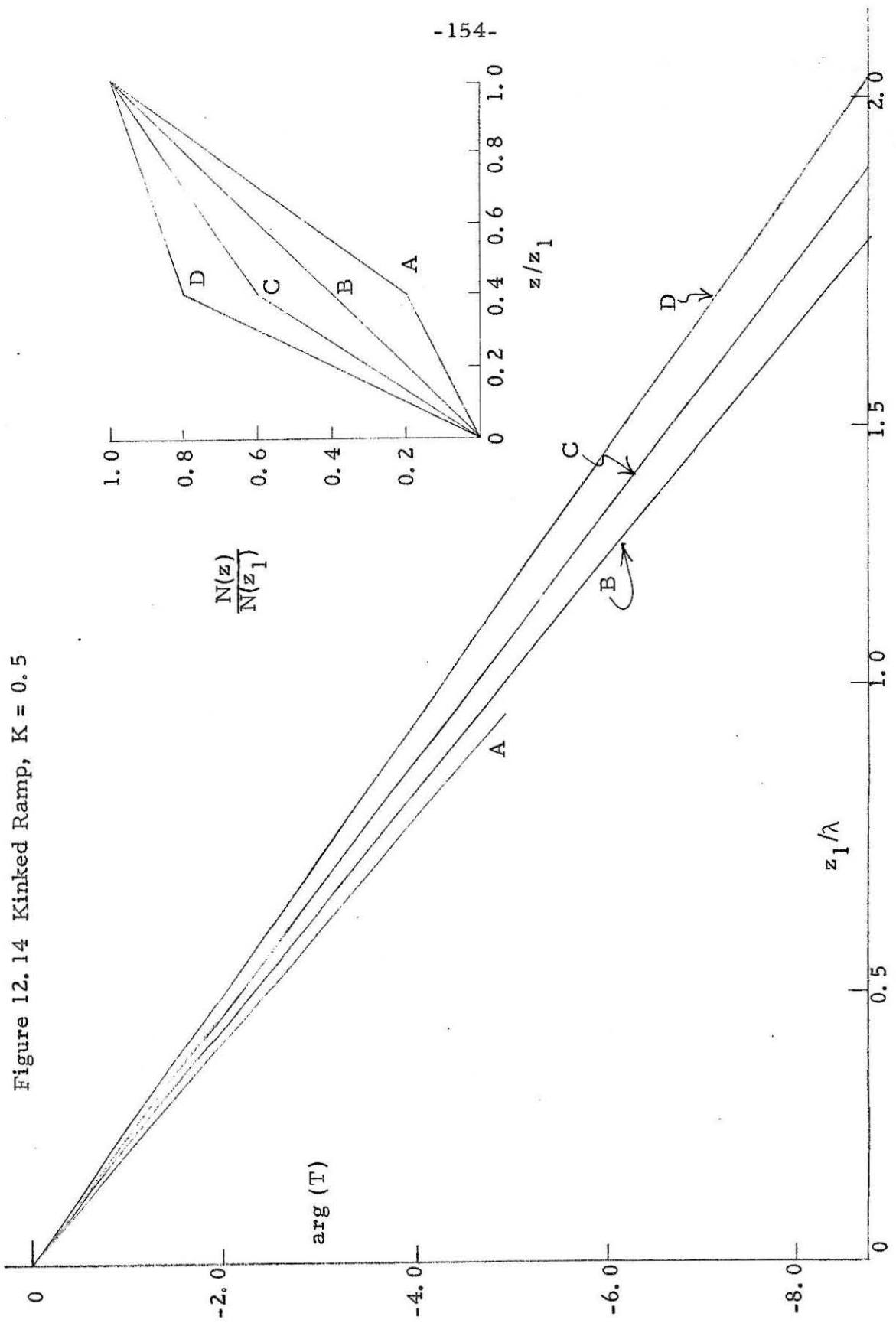


Figure 12.15 Kinked Ramp, $K = 0.5 - 0.2i$

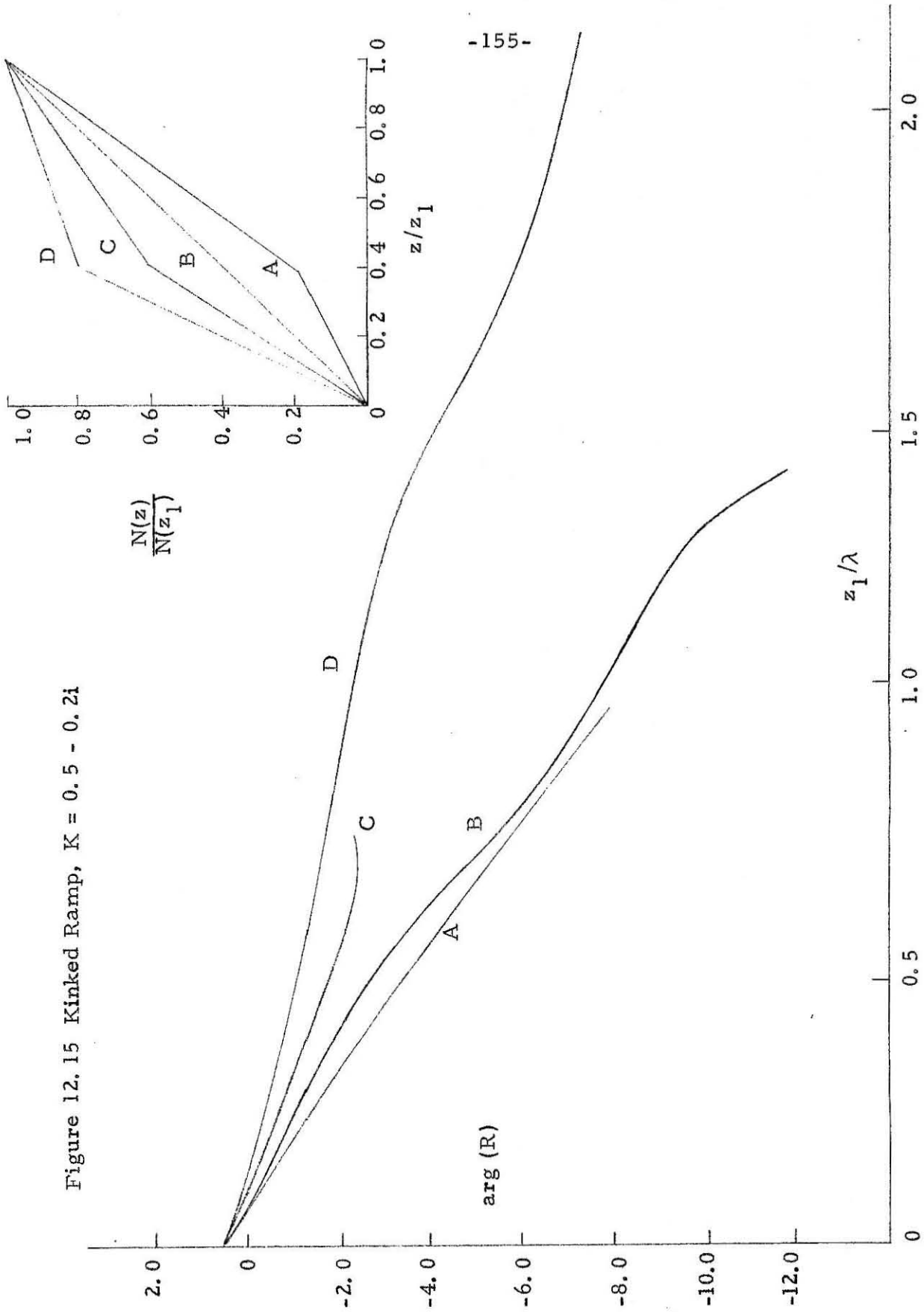
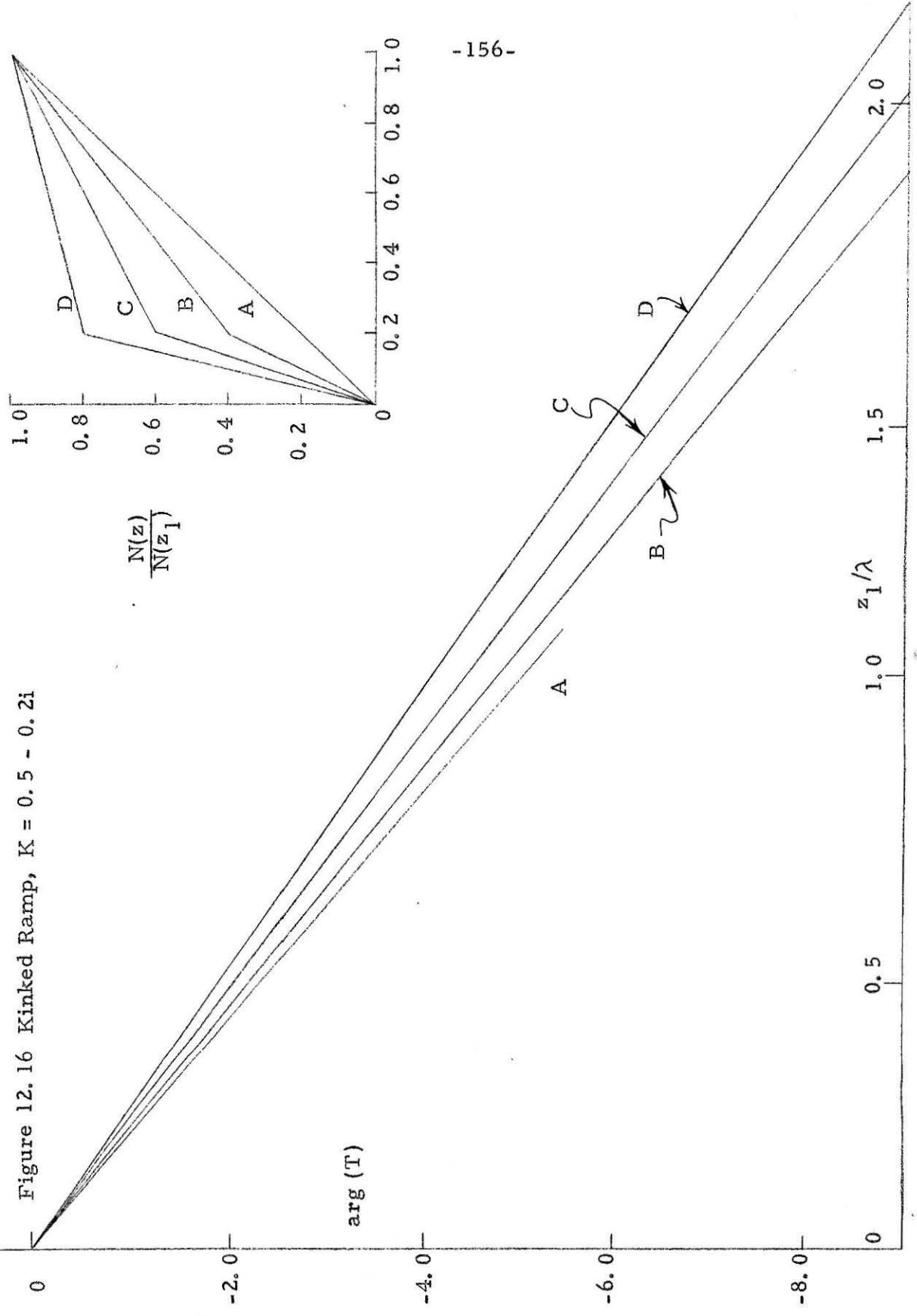


Figure 12.16 Kinked Ramp, $K = 0.5 - 0.2i$



XIII. THE TRAPEZOID PROBLEM

The essential feature of the mig "trapezoid" geometry (see figure 10.3) is the presence of a second boundary region to which the incident wave may penetrate. In this problem, further interference-type interactions can be anticipated, and a more pronounced periodicity in the modulus of R and T . The practical importance of this geometry is clearly greater than either of the previous two cases treated, so more numerical results will be displayed for this case.

The general features of the results of this chapter can be anticipated from the solution of the "slab" problem, i. e., the limiting case of zero thickness transition zones. The "slab" problem has the solution⁽⁵⁾:

$$R = R_0 (1 - \gamma_S^2) / (1 - \gamma_S^2 R_0^2) \quad (13.1)$$

$$T = T_0^2 K \gamma_S / (1 - \gamma_S^2 R_0^2) \quad (13.2)$$

where, in the notation of figure 9.3 and the preceding chapters,

$$\gamma_S = \exp(-ik_0 K z_t)$$

$$R_0 = (1-K)/(1+K)$$

$$T_0 = 2/(1+K)$$

For real K , the periodicity of $|R|$ and $|T|$ is evident from the above formulae; for complex K , the very thick slab clearly returns the interface solution (R_0) for R , and suppresses $|T|$ to zero. Note that R will be periodically zero for any real K , i. e. when $2Kz_t/\lambda = N$, an integer, and $|R|$ will be periodically maximum, when $2Kz_t/\lambda = (2M+1)/2$, one half of an odd integer. Likewise $|T|$ will be periodically maximum (unity) and minimum ($1-|R|^2$), with its maxima and minima precisely out of phase with $|R|$. In fact, for real K , the polar plot of R

is a circle, with center at $R_o/(1+R_o^2)$ and radius $R_o/(1+R_o^2)$, since R may be written as

$$R = \frac{R_o}{1+R_o^2} \left\{ 1 - \frac{\gamma_S^2 - R_o^2}{1 - \gamma_S^2 R_o^2} \right\}. \quad (13.3)$$

Since T may also be written as

$$T = \gamma_S \left\{ \frac{1 - R_o^2}{1 - \gamma_S^2 R_o^2} \right\} \quad (13.4)$$

or
$$T = \frac{(1 - R_o^4)}{(1+R_o^4 - 2R_o^2 \cos \theta)} \left\{ \frac{1-R_o^2}{1+R_o^2} \cos \theta + i \sin \theta \right\}; \theta = \arg \gamma_S \quad (13.5)$$

Writing $T = a(b \cos \theta + i \sin \theta) = \text{Re}(T) + i \text{Im}(T)$, (13.6)

it is clear that

$$\left(\frac{\text{Re}(T)}{a b} \right)^2 + \left(\frac{\text{Im}(T)}{a} \right)^2 = 1. \quad (13.7)$$

Thus the locus of T is an ellipse with center at the origin, with semi-major axis of 1, along the real axis, and semi-minor axis of $(1-R_o^2)/(1+R_o^2)$, along the imaginary axis. These observations are shown schematically in figure 13.1. The parameter $(k_o K z_t)$ which generates the circle and ellipse, is to be measured off along the loci, starting at the x . Note that R completes two circuits of its locus while T makes one circuit.

The behavior of R and T when K is slightly complex should be obvious from the sketches and the equations for these quantities. T plots into an elliptical spiral, terminating at the origin, while R becomes a circular spiral, terminating at R_o . When K is markedly complex, T spirals in more quickly from one to zero; for the limiting case $(K \rightarrow -i \infty)$ T shrinks from +1 along the real axis to zero. Likewise for markedly complex K , R traces a Cornu-like spiral from the

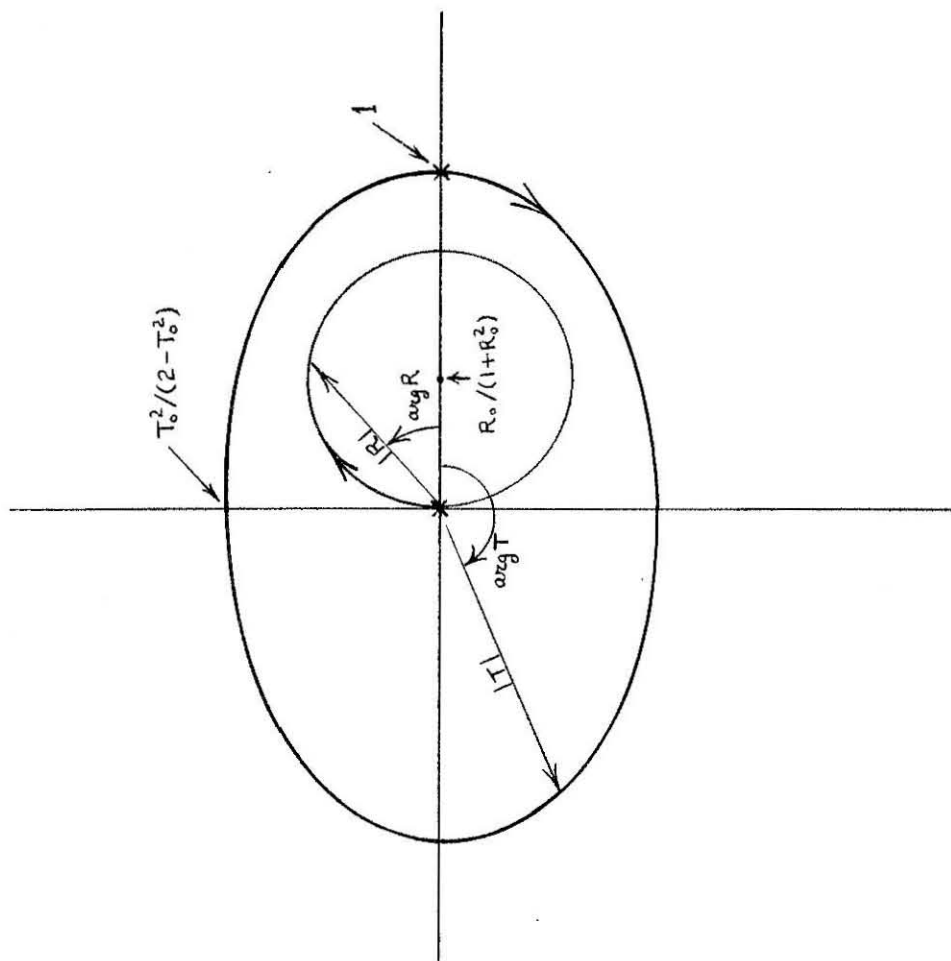


Figure 13.1 Schematic plot of loci of R and T versus slab thickness. Thickness, as $k_o z_t$, is measured from x on locus, increasing in the direction of the arrow. Plot shown is for K real and less than one.

origin to R_0 which for K imaginary is on the unit circle; in the limit of $K \rightarrow -i\infty$, R runs along the real axis from the origin to minus one. Keeping these behaviors in mind will greatly simplify the understanding of the plots of modulus and argument presented at the end of the chapter. Figures 13.2 and 13.3 show $|R|$ and $|T|$ for typical "slab" problem parameters.

With the introduction of transition zones into the slab geometry, the behavior of R and T will be modified. Considering first the case of purely real K , it is clear that $|T|$ should tend to increase (see the discussion under linear ramp) while $\arg T$ should be slightly larger due to the lower value of \bar{K} . But the basic character of T as lying on or near an ellipse should not be altered. Apparently, the ellipse might enlarge in area, rotate, and alter in proportions (eccentricity), but the underlying structure should remain. Likewise, the R circle should still touch the origin, but its center may rotate and move towards the origin. The locus of the R circle center might be traced as the locus of R for the linear ramp of the same initial geometry, for as the back boundary recedes to infinity, an unmeasurably small imaginary part of K will reduce the problem to that of Chapter XI. The behavior for complex values of K then follows by considerations analogous to those in the "slab" problem.

The analysis below gives the values of R and T in explicit, if slightly obscure, form, and discussion of special cases with reference to the plotted results justifies the speculations above.

The equations to be solved in this case are:

$$\frac{d^2 E}{dz^2} + k_0^2 E = 0, \quad z \leq 0; \quad z \geq z_t \quad (13.8)$$

$$\frac{d^2 E}{dz^2} + k_0^2 \left(1 - (1-K^2)z/z_0\right) E = 0, \quad 0 \leq z \leq z_0 \quad (13.9)$$

$$\frac{d^2 E}{dz^2} + k_0^2 K^2 E = 0, \quad z_0 \leq z \leq z_t - z_0 \quad (13.10)$$

$$\frac{d^2 E}{dz^2} + k_0^2 \left[1 - (1-K^2) \frac{z_t - z}{z_0}\right] E = 0, \quad z_t - z_0 \leq z \leq z_t \quad (13.11)$$

Note that on replacing $z_t - z$ by ξ in (13.11), the equation becomes identical to (13.9):

$$\frac{d^2 E}{d\xi^2} + k_0^2 \left[1 - (1-K^2)\xi/z_0\right] E = 0, \quad 0 \leq \xi \leq z_0 \quad (13.12)$$

The solutions are given below for the different zones

$$E = e^{-ik_0 z} + R e^{ik_0 z} \quad z \leq 0$$

$$E = A \text{Ai}(v) + B \text{Bi}(v) \quad 0 \leq z \leq z_0$$

$$E = C e^{-ik_0 K(z-z_0)} + D e^{ik_0 K(z+z_0-z_t)} \quad z_0 \leq z \leq z_t - z_0$$

$$E = F \text{Ai}(w) + G \text{Bi}(w) \quad z_t - z_0 \leq z \leq z_t$$

$$E = T e^{-ik_0(z-z_t)} \quad z \geq z_t$$

where

$$v = - \left(\frac{k_0 z_0}{1-K^2}\right)^{2/3} \left(1 - (1-K^2)z/z_0\right)$$

$$w = - \left(\frac{k_0 z_0}{1-K^2}\right)^{2/3} \left(1 - (1-K^2) \frac{z_t - z}{z_0}\right)$$

With the previous definition of ϕ , the boundary conditions may be matched by the equations:

$$1 + R = A \text{Ai}(\phi^2) + B \text{Bi}(\phi^2)$$

$$\phi(1 - R) = A \text{Ai}'(\phi^2) + B \text{Bi}'(\phi^2)$$

$$\begin{aligned}
 C + D\gamma &= A \operatorname{Ai}(K^2\phi^2) + B \operatorname{Bi}(K^2\phi^2) \\
 K\phi(C - D\gamma) &= A \operatorname{Ai}'(K^2\phi^2) + B \operatorname{Bi}'(K^2\phi^2) \\
 C\gamma + D &= F \operatorname{Ai}(K^2\phi^2) + G \operatorname{Bi}(K^2\phi^2) \\
 -K\phi(C\gamma - D) &= F \operatorname{Ai}'(K^2\phi^2) + G \operatorname{Bi}'(K^2\phi^2) \\
 T &= F \operatorname{Ai}(\phi^2) + G \operatorname{Bi}(\phi^2) \\
 -\phi T &= F \operatorname{Ai}'(\phi^2) + G \operatorname{Bi}'(\phi^2)
 \end{aligned}$$

where

$$\gamma = \exp(-ik_0 K z_t (1 - 2z_0/z_t)) \quad (13.13)$$

Employing the previous definitions of $A^\pm(\phi)$, etc., the above equations can be cast in the form

$$R B^+(\phi) + B^-(\phi) = A/\pi \quad (13.14)$$

$$R A^+(\phi) + A^-(\phi) = -B/\pi \quad (13.15)$$

$$A A^+(K\phi) + B B^+(K\phi) = 2K\phi C \quad (13.16)$$

$$A A^-(K\phi) + B B^-(K\phi) = -2\gamma K\phi D \quad (13.17)$$

$$F A^+(K\phi) + G B^+(K\phi) = 2K\phi D \quad (13.18)$$

$$F A^-(K\phi) + G B^-(K\phi) = -2\gamma K\phi C \quad (13.19)$$

$$F A^+(\phi) + G B^+(\phi) = 0 \quad (13.20)$$

$$F A^-(\phi) + G B^-(\phi) = -2\phi T \quad (13.21)$$

Employing the abbreviations

$$P^\pm = A^\pm(K\phi)B^\pm(\phi) - A^\pm(\phi)B^\pm(K\phi) \quad (13.22)$$

$$Q^\pm = A^\pm(K\phi)B^\mp(\phi) - A^\mp(\phi)B^\pm(K\phi) \quad (13.23)$$

The coefficients R and T are found to be

$$R = \frac{\gamma^2 P^+ Q^+ - P^- Q^-}{(Q^-)^2 - \gamma^2 (P^+)^2} \quad (13.24)$$

$$T = \frac{\gamma K (2\phi/\pi)^2}{(Q^-)^2 - \gamma^2 (P^+)^2} \quad (13.25)$$

An identity which is useful in deriving (13. 24) and (13. 25) is

$$P^+P^- - Q^+Q^- = K(2\phi/\pi)^2 \quad (13. 26)$$

The only limiting situation to which it is relatively easy to pass is that of $\gamma \rightarrow 0$ (i. e., the slab is absorbent, and the exponent $\exp(-ik_0 Kz_t)$ is vanishingly small), for which

$$R \rightarrow -\frac{P^-}{Q^-} \quad (13. 27)$$

$$T \rightarrow 0 \text{ as } \gamma \quad (13. 28)$$

Note that (13. 27) is the linear ramp result, while (13. 28) is physically a reasonable result. The limit $z_0/z_t \rightarrow 0$ cannot be easily extracted from (13. 24) and (13. 25), but note from the set of equations preceding (13. 13), if functions of $(K\phi)$ are equated to functions of (ϕ) , there results the simpler set:

$$1 + R = C + D\gamma$$

$$1 - R = K(C - D\gamma)$$

$$T = C\gamma + D$$

$$T = K(C\gamma - D)$$

where, as $z_0/z_t \rightarrow 0$, $\gamma \rightarrow \gamma_S$. This set is exactly that of the "slab" problem. The limit $K \rightarrow 1$ must be approached much more cautiously, as this simultaneously lets $K\phi \rightarrow \phi$, but $\phi \rightarrow \infty$. If one arbitrarily assumes $K\phi$ to equal ϕ and K to equal one, then the "slab" equations return, but with the solutions:

$$R = 0 \quad , \quad T = \gamma$$

which is wrong for $\arg T$ by a factor of $2k_0 z_0$. The error lies in not differentiating between the rates at which ϕ and $K\phi$ go to infinity -- they must go at such a rate as to make

$$P^+ \rightarrow 0$$

but

$$(\Omega^-)^2 \longrightarrow (-2\phi/\pi e^{ik_0 z_0})^2.$$

The phase shift factor in Ω^- must therefore arise from the different rates at which $K\phi$ and ϕ go to infinity. It can be seen from the asymptotic developments in Chapter III that Ω^- is of the proper form to provide this effect, so the matter will not be pursued here further.

Note that the pronounced periodicity of the "slab" results with $\arg(\gamma_S)$ is not exactly duplicated in this case, as P and Q are in general complex. However, for real K , ϕ is purely imaginary, hence A^- is the conjugate to A^+ and B^- is the conjugate to B^+ . Thus P^- is conjugate to P^+ and Q^- is conjugate to Q^+ . Furthermore, for K and z_0 fixed, R and T are solely functions of z_t , through γ^2 . Viewing (13.24) as a linear fractional transformation of the form

$$R = \frac{\alpha\beta\xi - \bar{\alpha}\bar{\beta}}{(\bar{\beta})^2 - \alpha^2\xi} \quad (13.29)$$

where $|\xi| = 1$, then, as this transformation maps circles onto circles⁽²⁰⁾, a definite periodicity of R with γ (thus z_t) is to be anticipated. In fact, when $\xi = (\bar{\alpha}\bar{\beta})/(\alpha\beta)$, R will be zero, so the transformed circle touches the origin. When K is complex, however, the above simplifications do not obtain. The "spiral" nature of R 's locus with z_t has been discussed above for the slab problem, and this character is preserved in the trapezoid problem. In the trapezoid problem, however, the end point of the spiral is not R_0 , but the reflection coefficient for the linear ramp, R_L .

When K is purely imaginary, ϕ is purely imaginary, so that $\overline{Q^-} = P^+$, where the bar denotes complex conjugation. Using this fact, and also (13.27) it is easily shown that R is of the form

$$R = R_L \left\{ \frac{1 - \gamma^2 \left(\frac{a}{b} \right) \left(\frac{a}{b} \right)}{1 - \gamma^2 \left(\frac{a}{b} \right)^2} \right\} \quad (13.30)$$

where R_L is the linear ramp reflection coefficient, which for this case is of modulus one (see Chapter XI). As γ is a monotonic-decreasing exponential function, the character of R is apparent from this formulation. The form of T is apparent from (13.25), i. e., $|T|$ is nearly dominated by γ , thus exponentially decreasing, with oscillations superposed upon the decay.

The above observations and special cases are informative, but the practical problem of evaluating R and T for the trapezoid geometry and an arbitrary, complex value of K is still prodigious. To generate the curves presented at the end of this chapter, the digital computer was again employed, and (13.24) and (13.25) evaluated accurately. The details of computation will not be discussed, but sufficient accuracy was ensured to make the graphical results exact to within plotting capability. No approximations were generated for this case, as the procedure is essentially identical to that of Chapter XI and would thus not render any new insight. The main distinguishing features of the trapezoid results are the shifting of the relative maxima and minima of $|R|$ and $|T|$ to higher values of z_t/λ and the degradation of $|R|$, with increased $|T|$. It is apparent from the plots that for small values of z_0/λ (say ≤ 0.1), the result is essentially obtained by shifting the "slab" curves to the right by the value of z_0/λ , degrading $|R|$ proportionally to the value given by the linear ramp problem (or the small-argument expansion thereof), and increasing $|T|$ likewise. This procedure is almost an intuitive one; the analysis and evaluation demon-

strates its validity. The utility of the results of this chapter (and the others) and the significance of the major effects discovered is discussed in the following chapter.

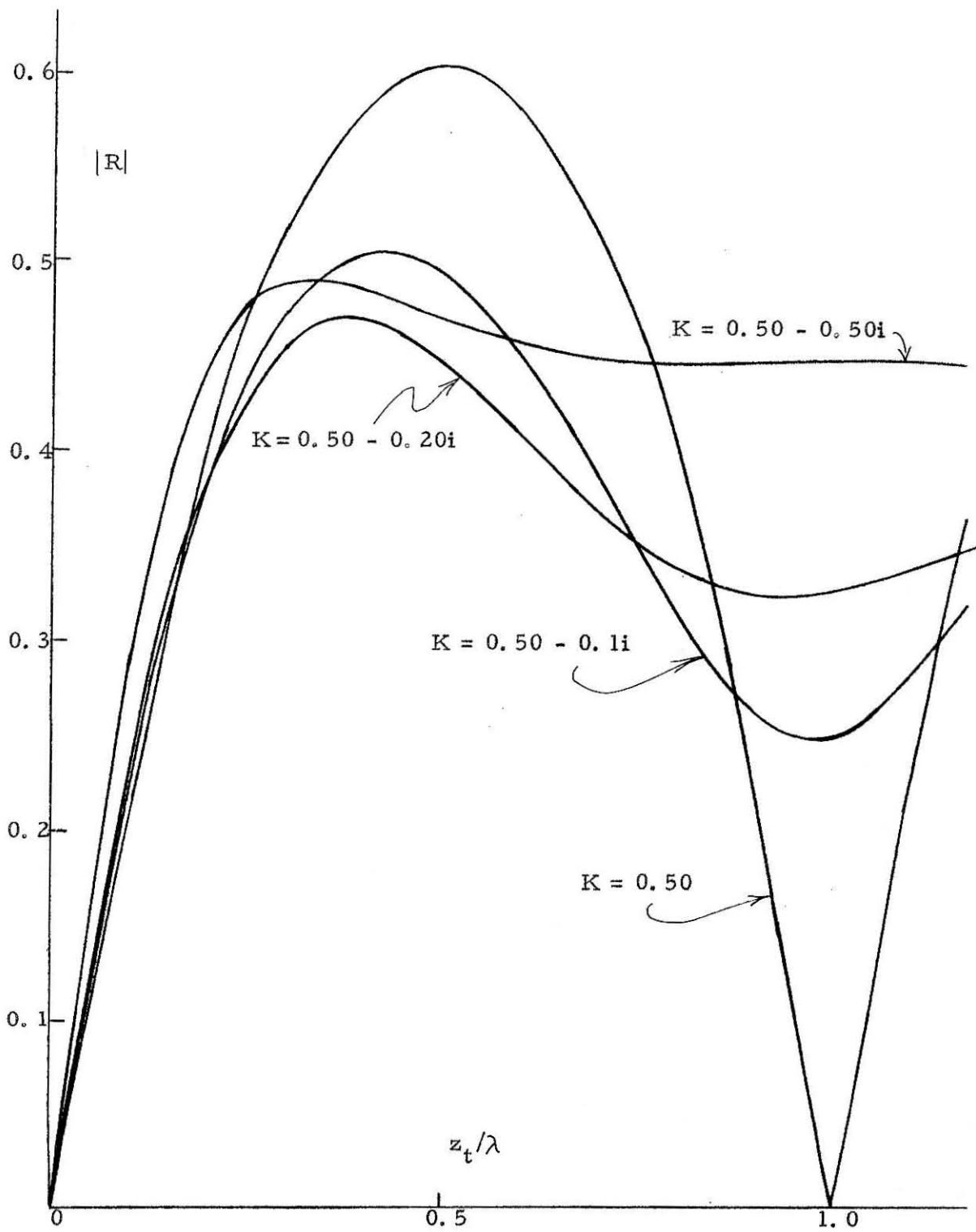


Figure 13.2 Slab Problem Reflection for Various K

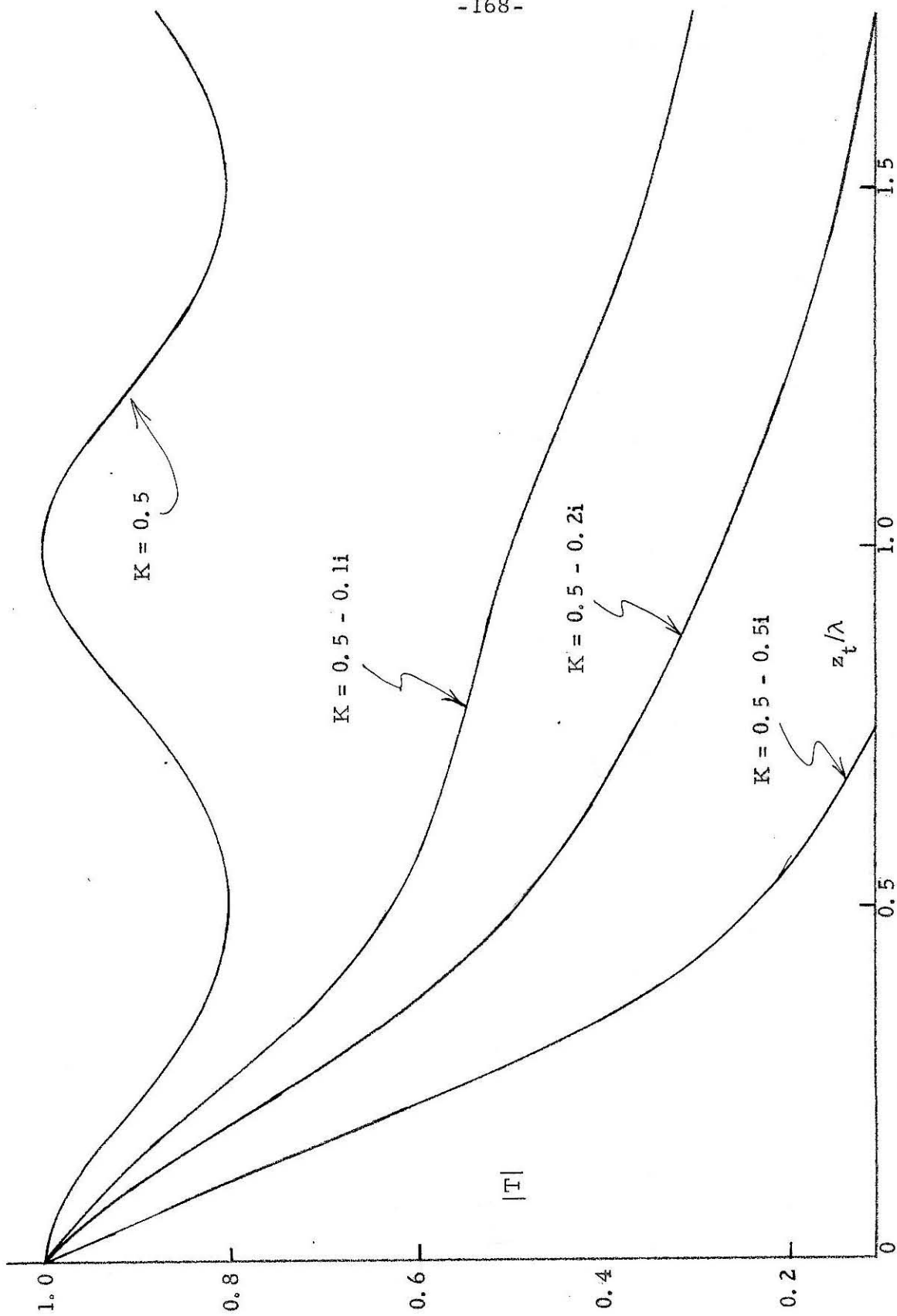


Figure 13.3 Slab Problem Transmission for Various K

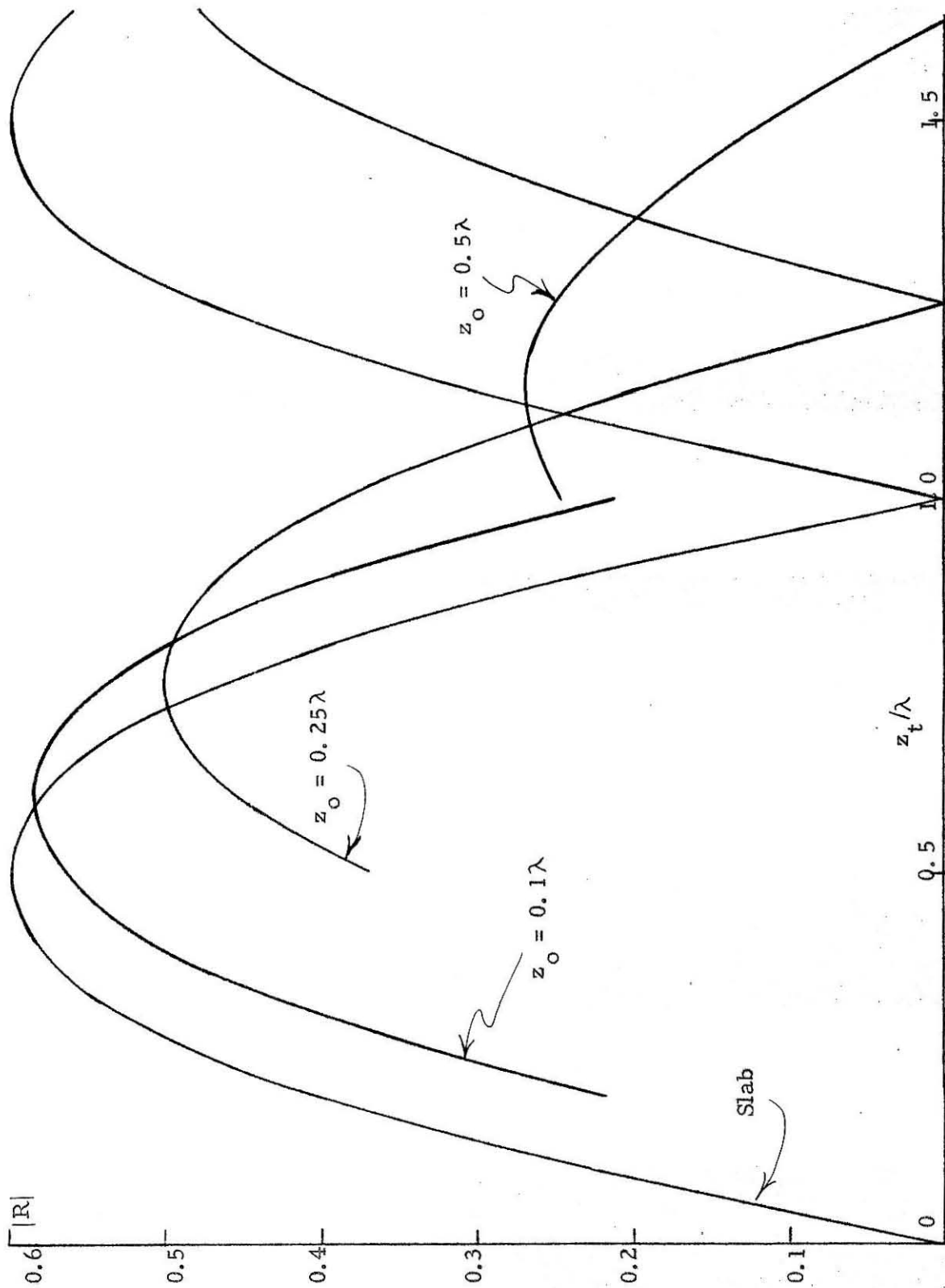


Figure 13.4 Trapezoid, $K = 0.5$

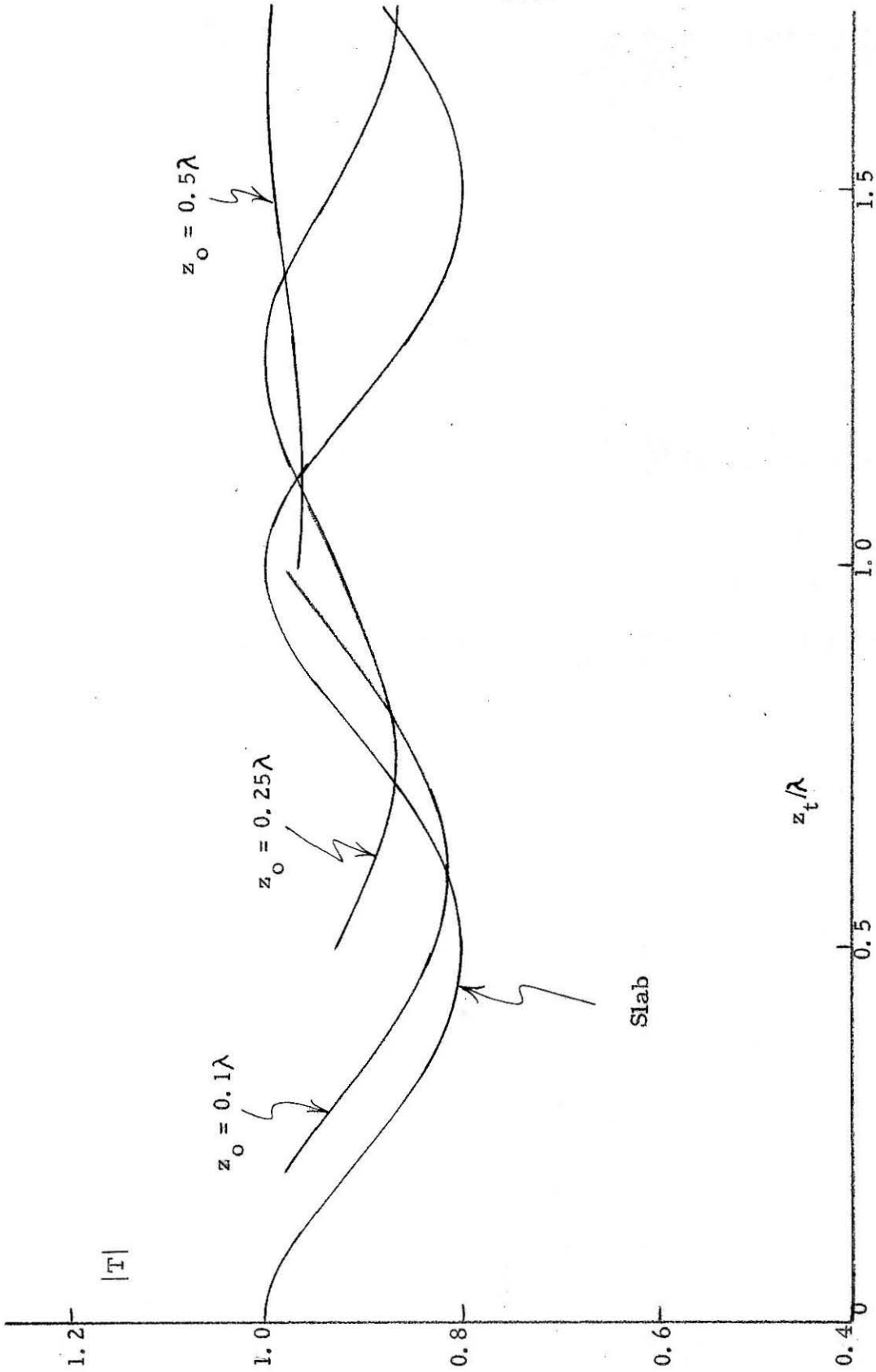


Figure 13.5 Trapezoid, $K = 0.5$

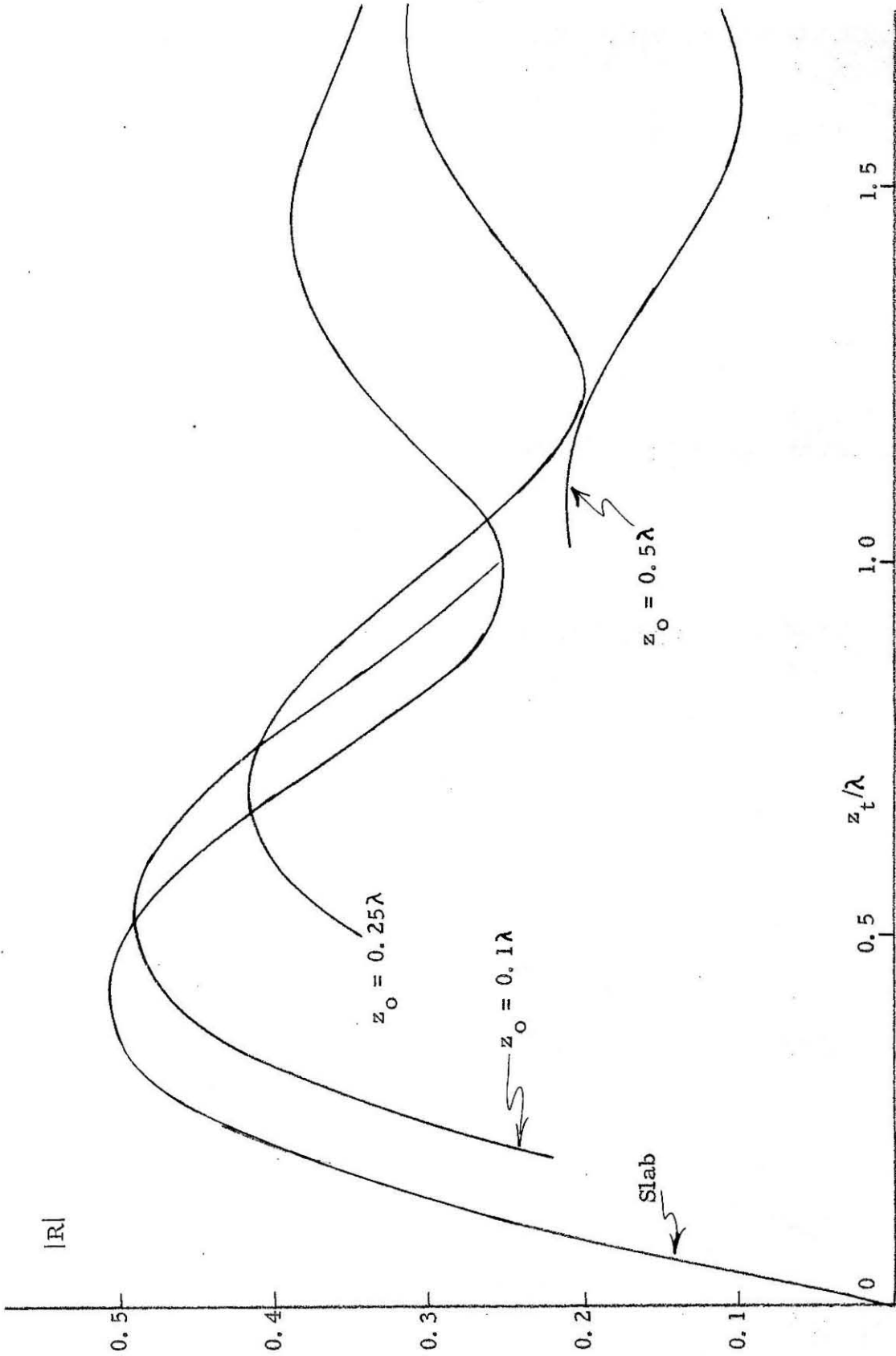


Figure 13.6 Trapezoid, $K = 0.5 - 0.11$

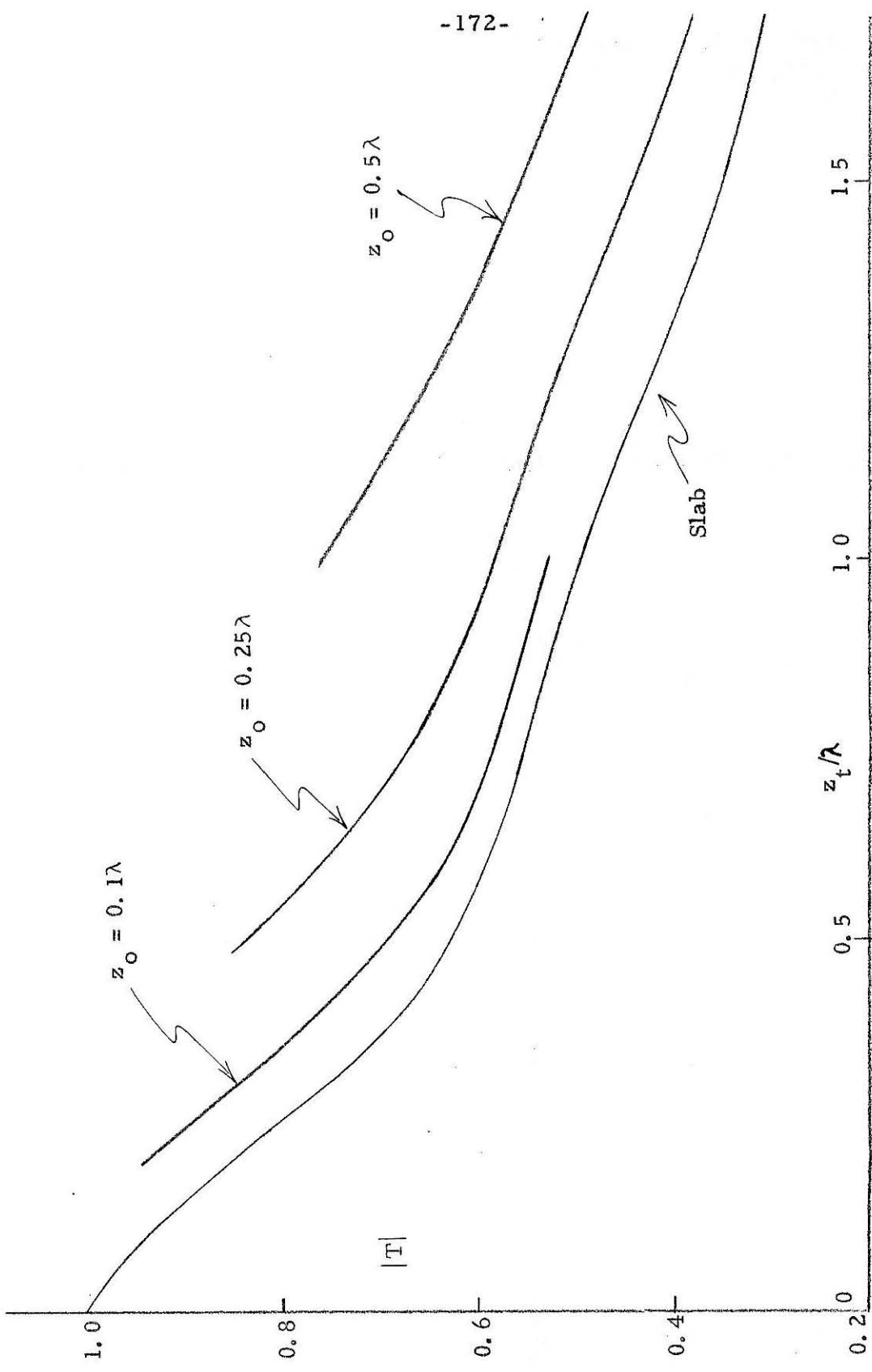


Figure 13.7 Trapezoid, $K = 0.5 - 0.1i$

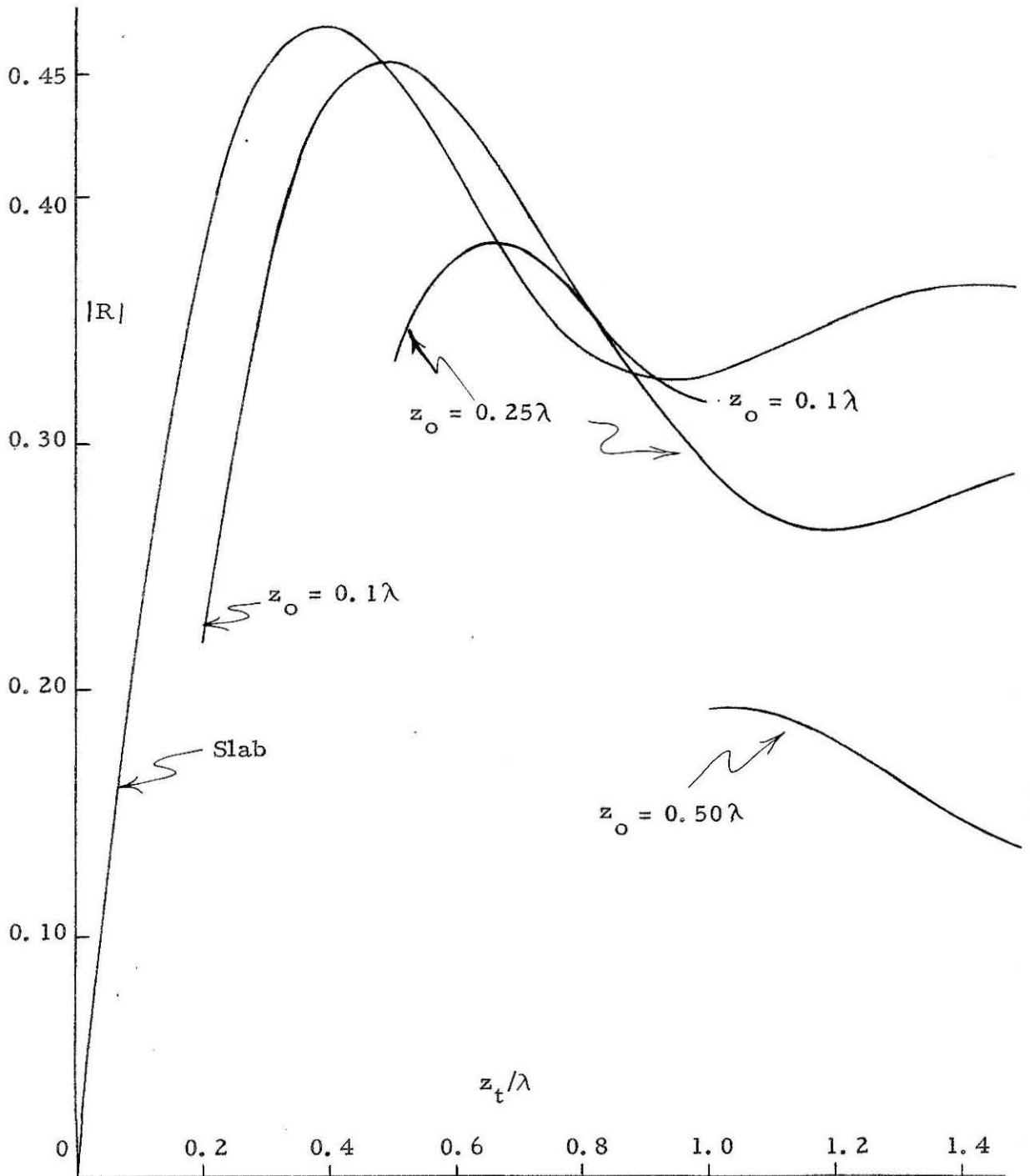


Figure 13.8 Trapezoid, $K = 0.5 - 0.2i$

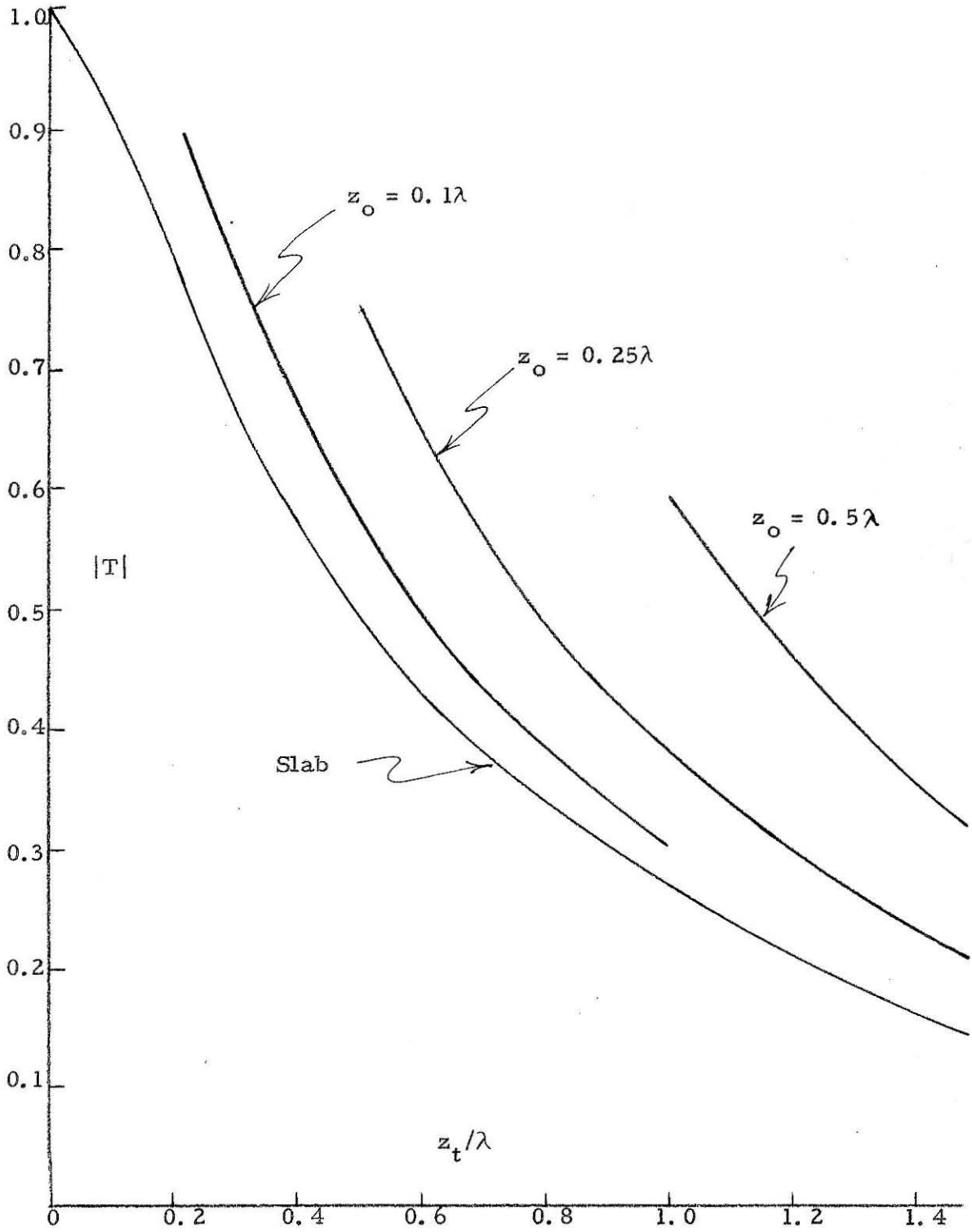


Figure 13.9 Trapezoid, $K = 0.5 - 0.2i$

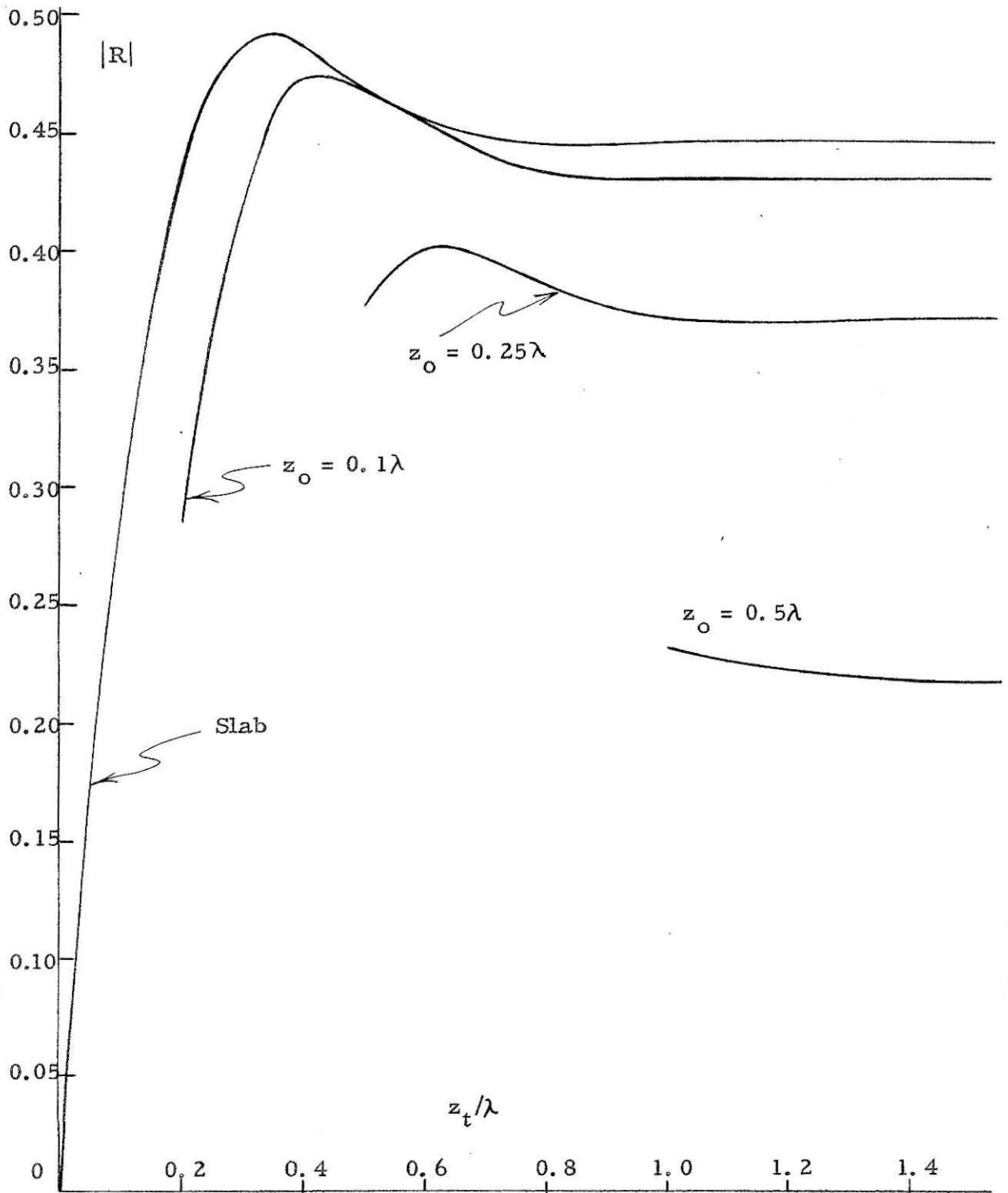


Figure 13.10 Trapezoid, $K = 0.5 - 0.5i$

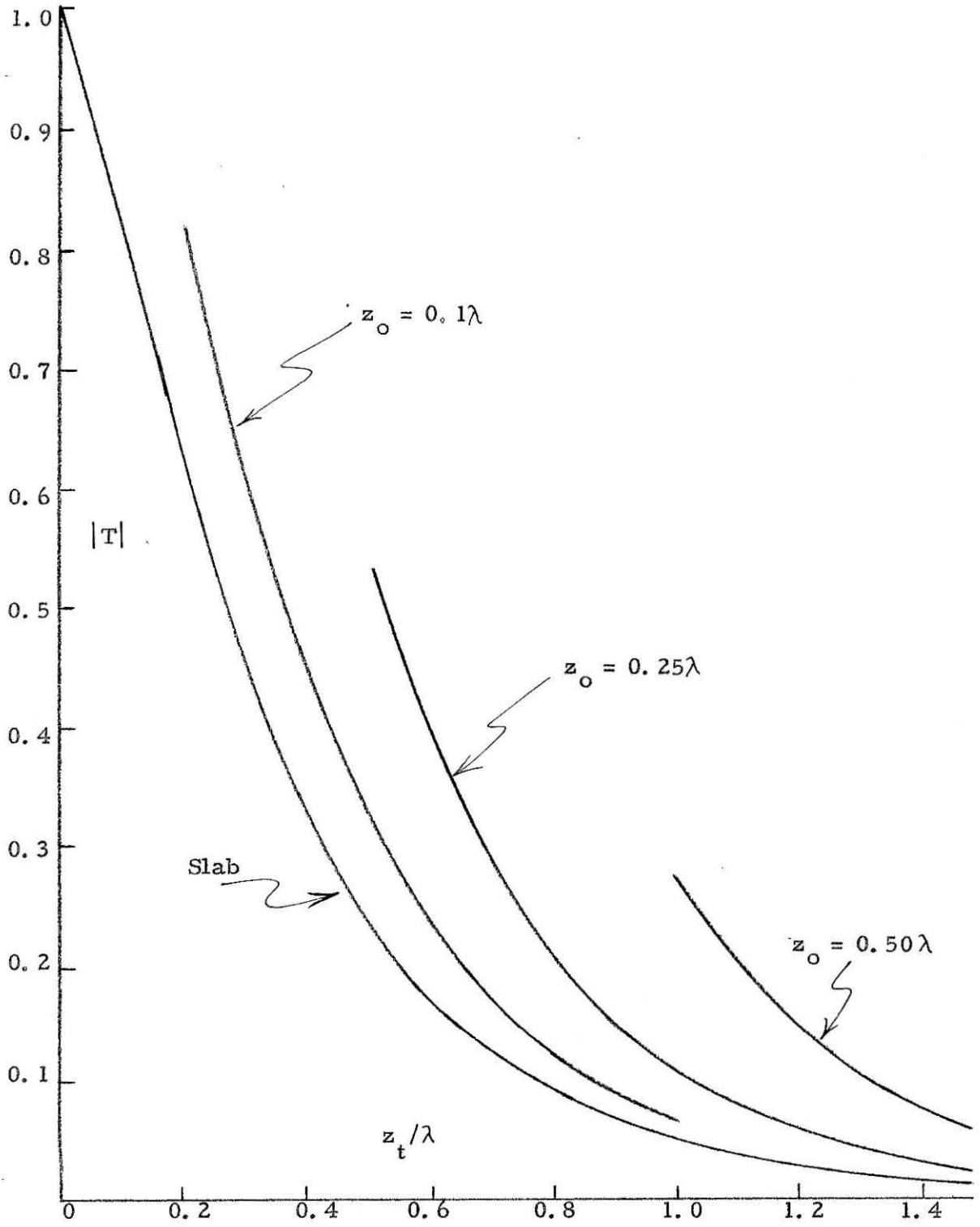


Figure 13.11 Trapezoid, $K = 0.5 - 0.5i$

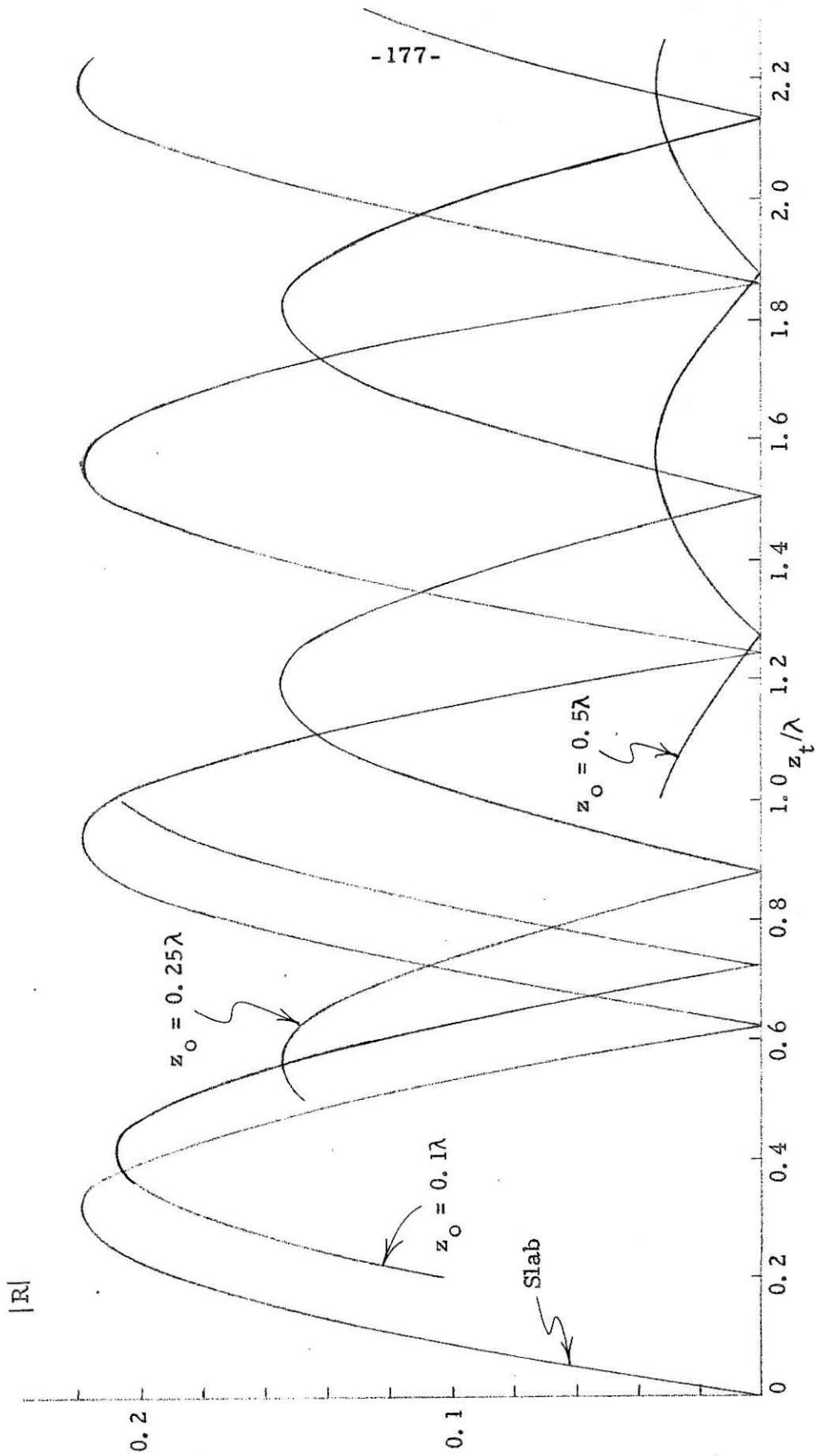


Figure 13.12 Trapezoid, $K = 0.8$

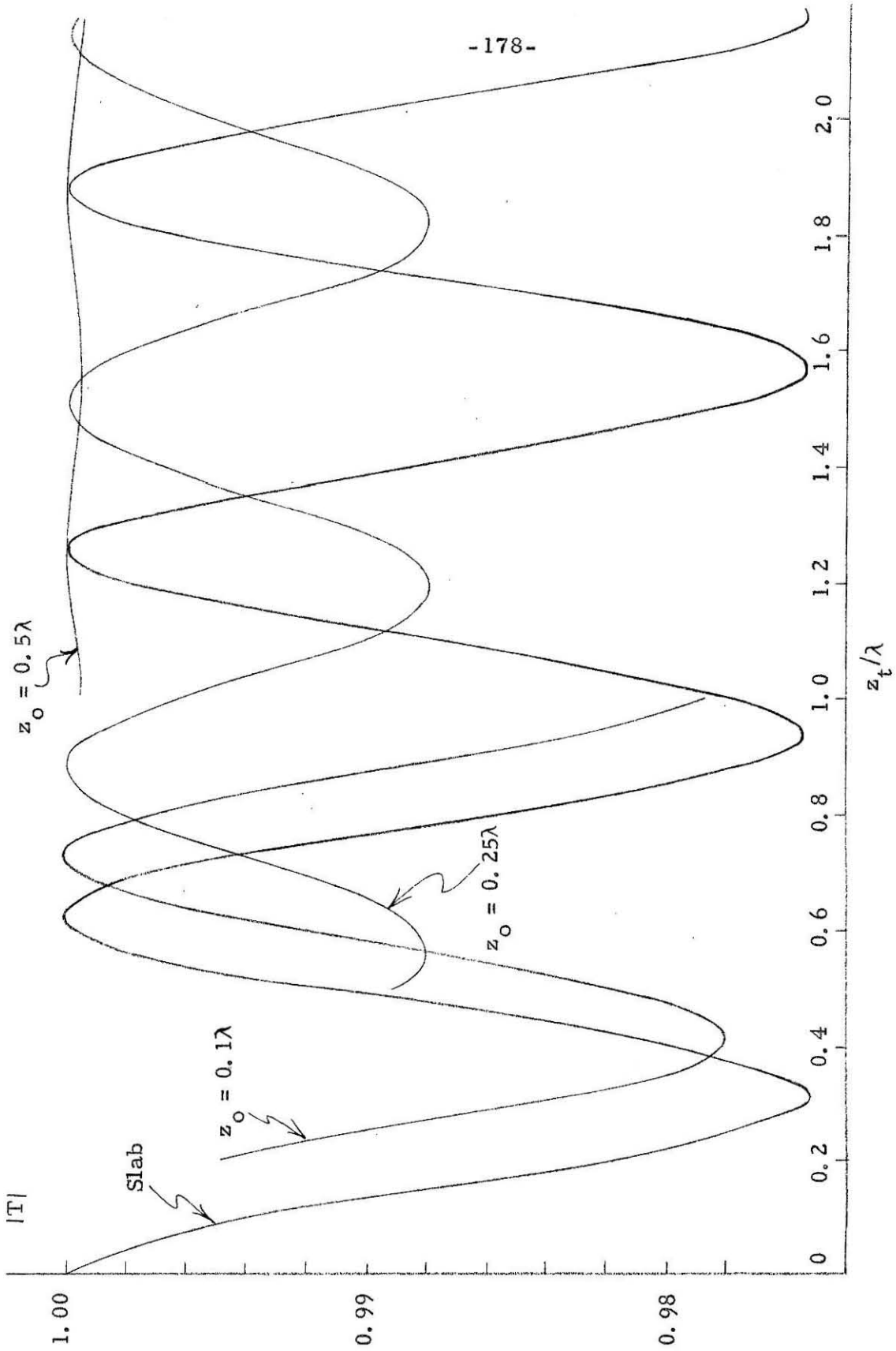


Figure 13.13 Trapezoid, $K = 0.8$

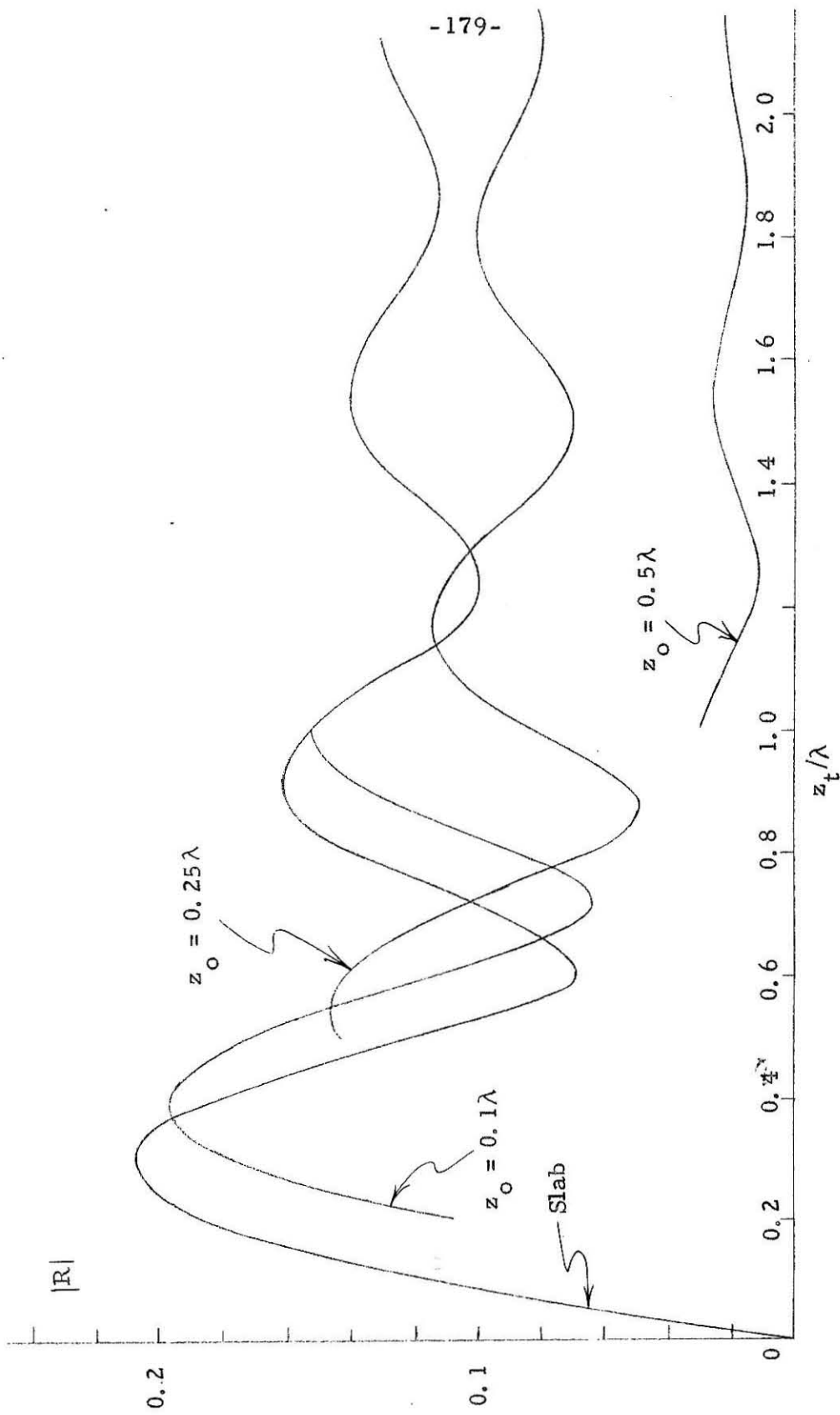


Figure 13.14 Trapezoid, $K = 0.8 - 0.1i$

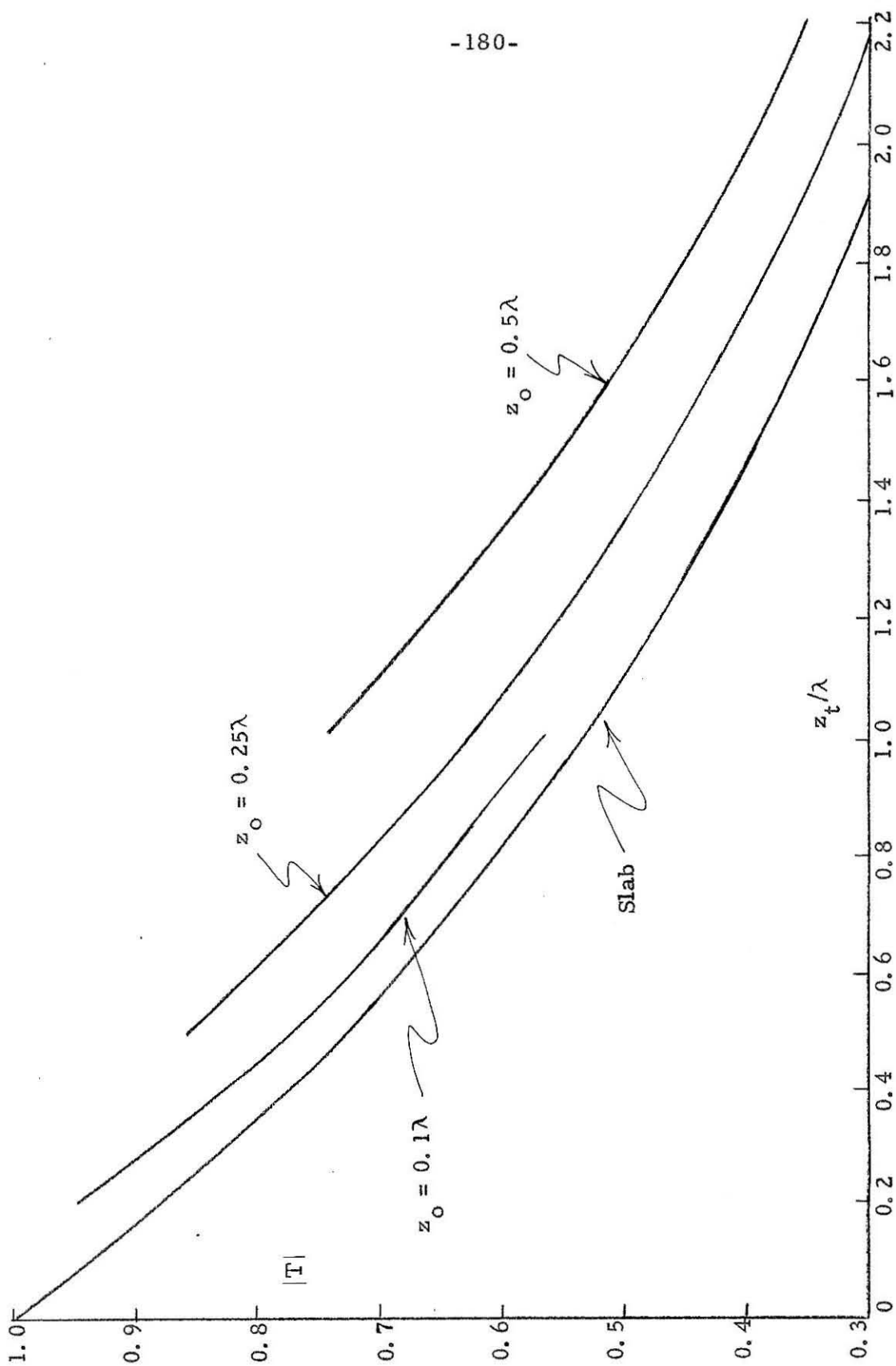


Figure 13.15 Trapezoid, $K = 0.8 - 0.11$

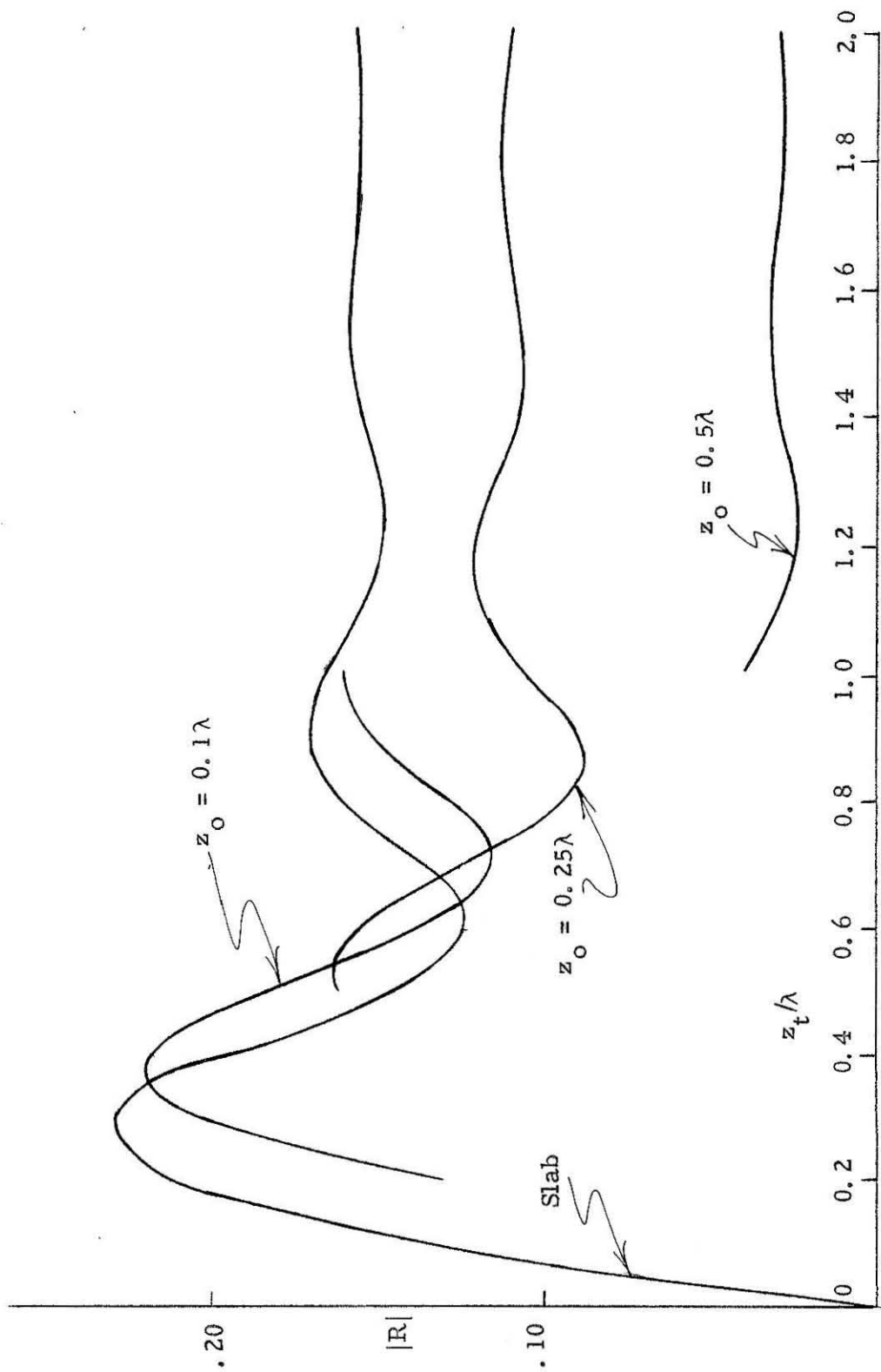


Figure 13.16 Trapezoid, $K = 0.8 - 0.2i$

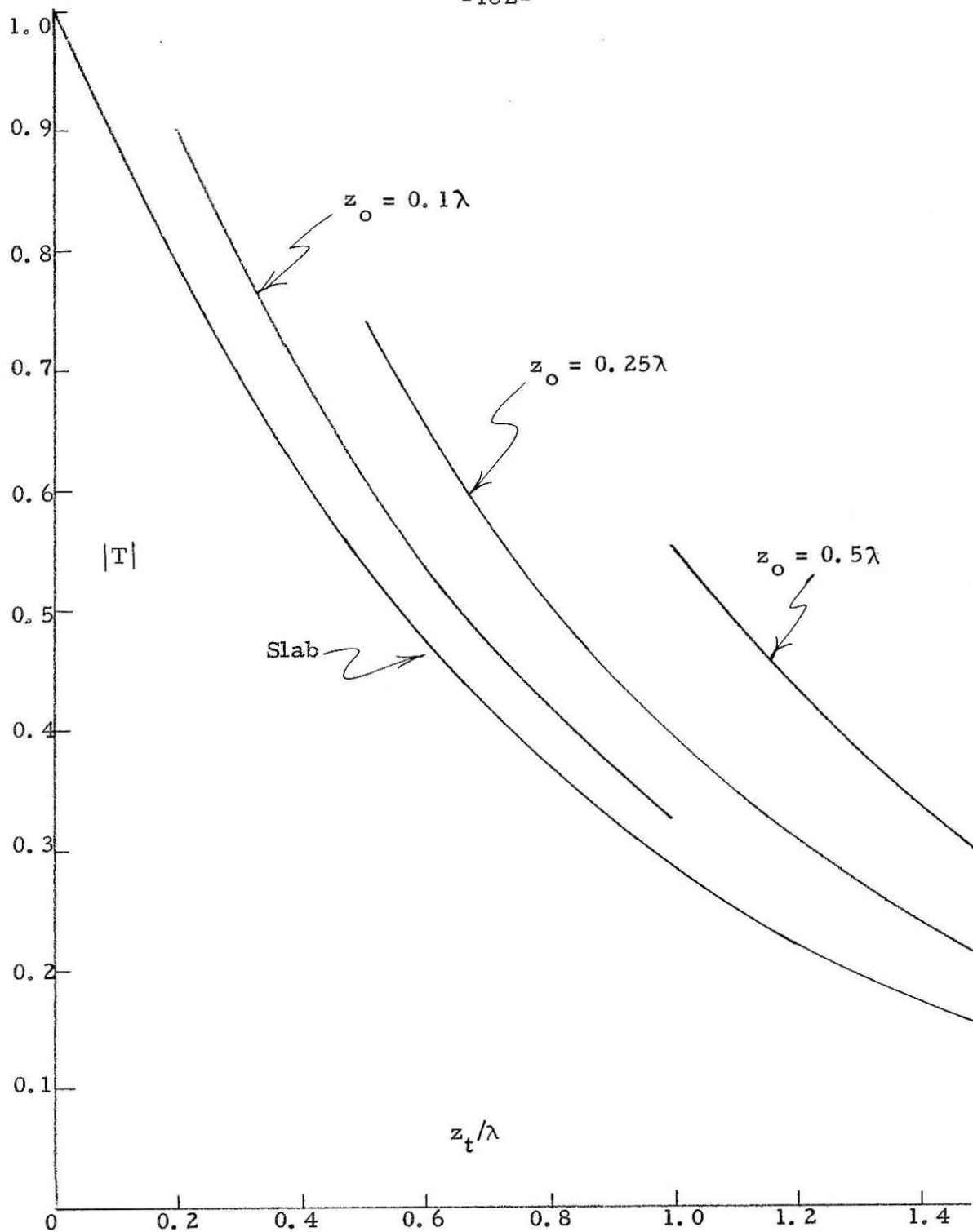


Figure 13.17 Trapezoid, $K = 0.8 - 0.2i$

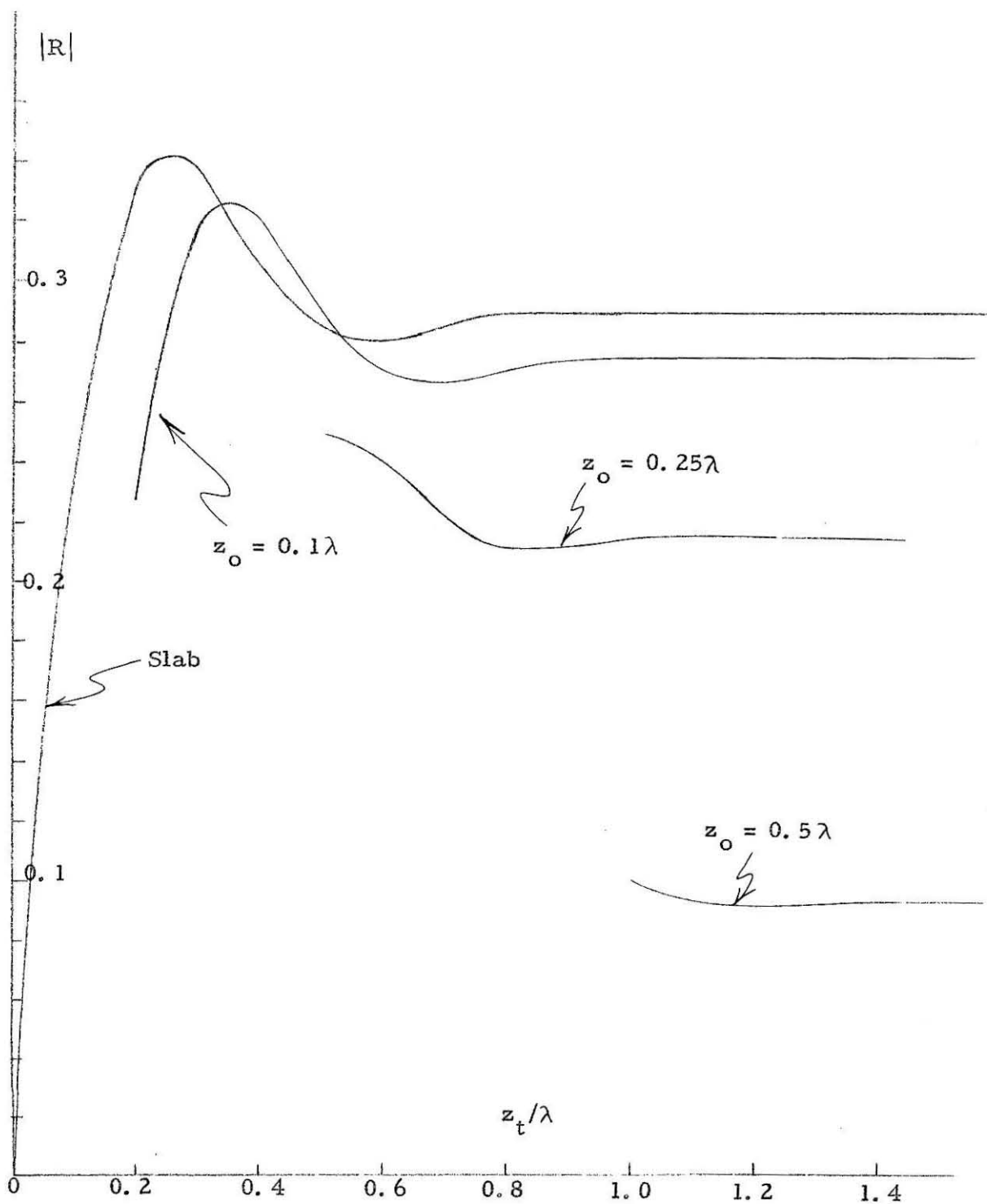


Figure 13.18 Trapezoid, $K = 0.8 - 0.5i$

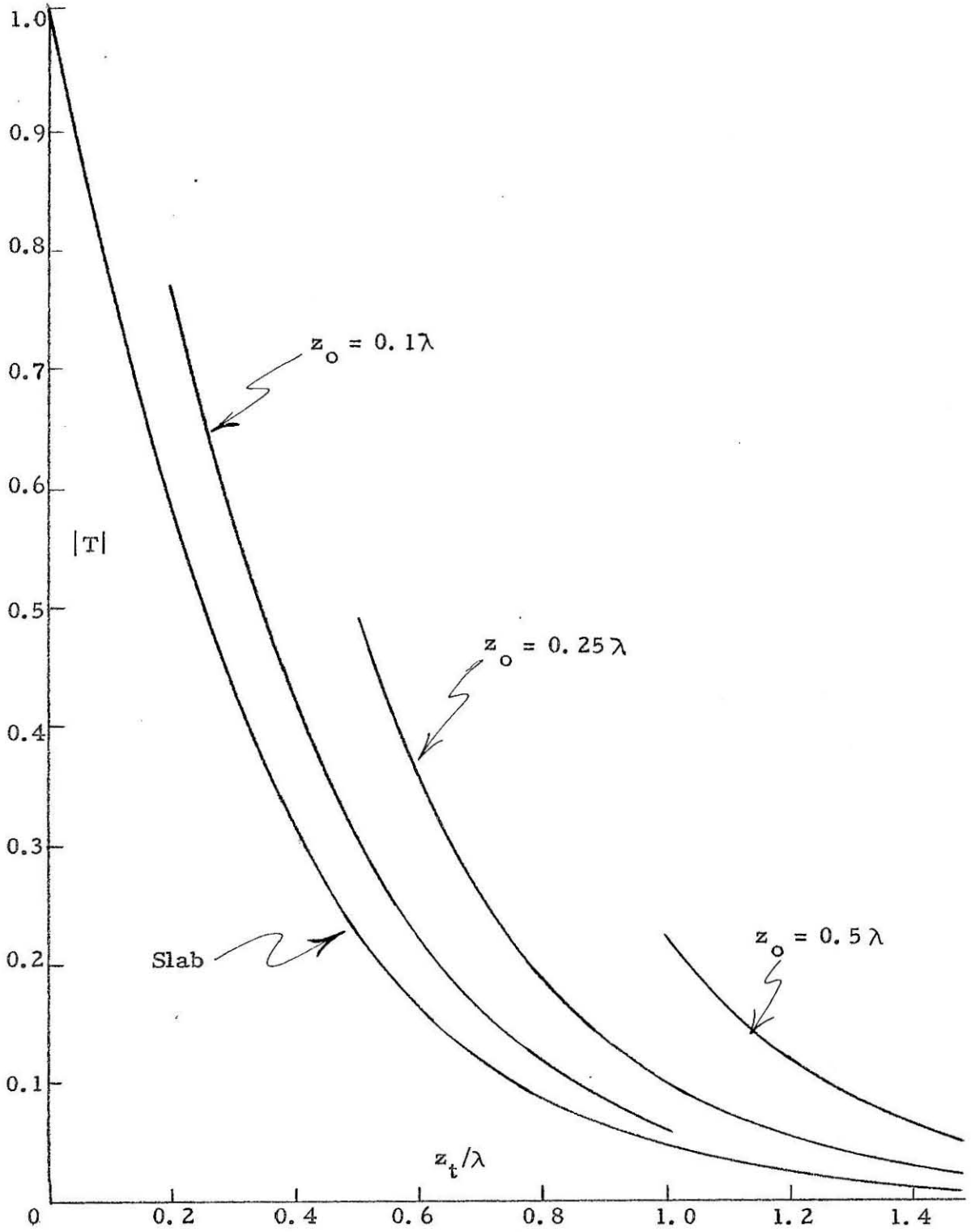


Figure 13.19 Trapezoid, $K = 0.8 - 0.5i$

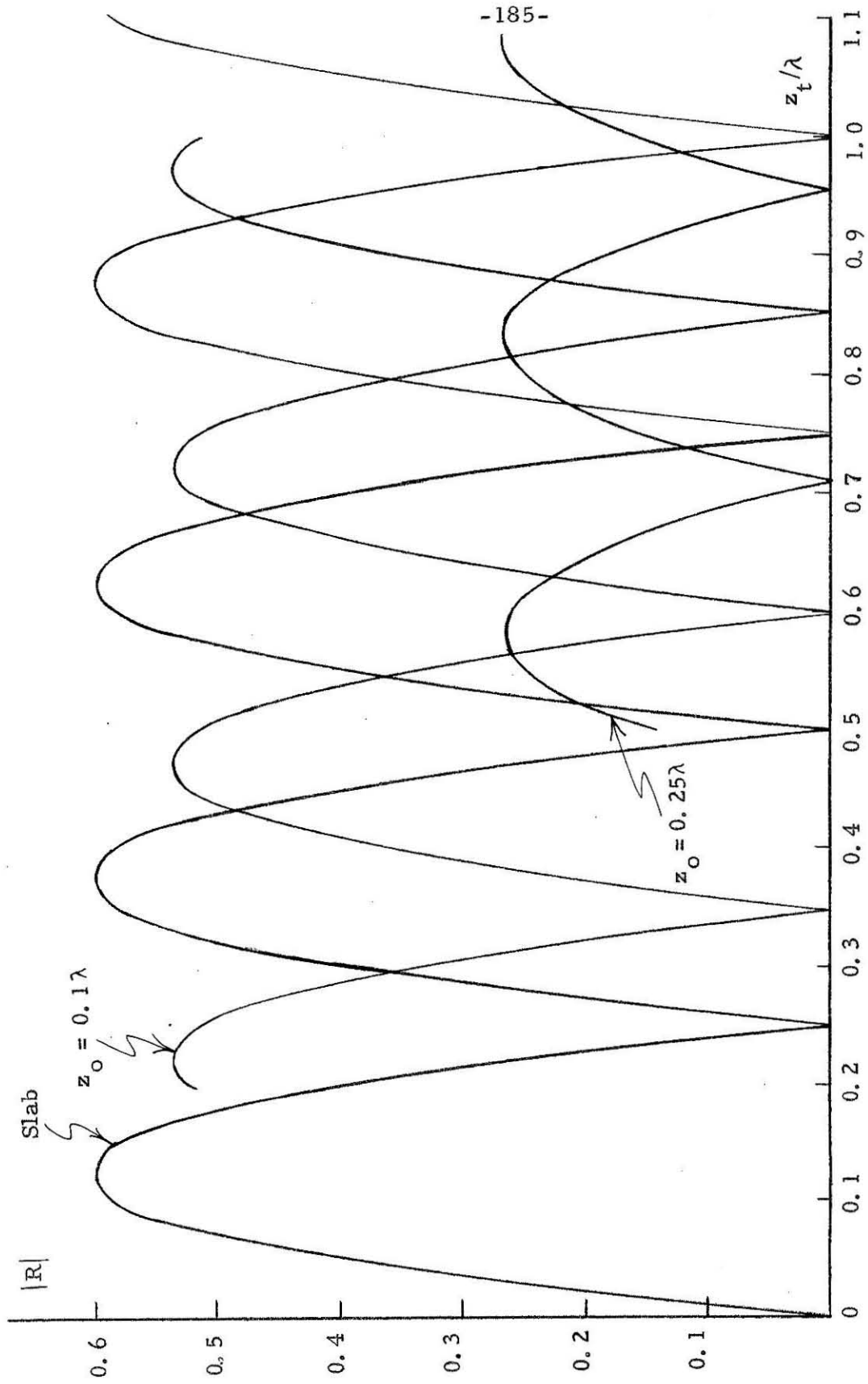


Figure 13.20 Trapezoid, $K = 2.0$

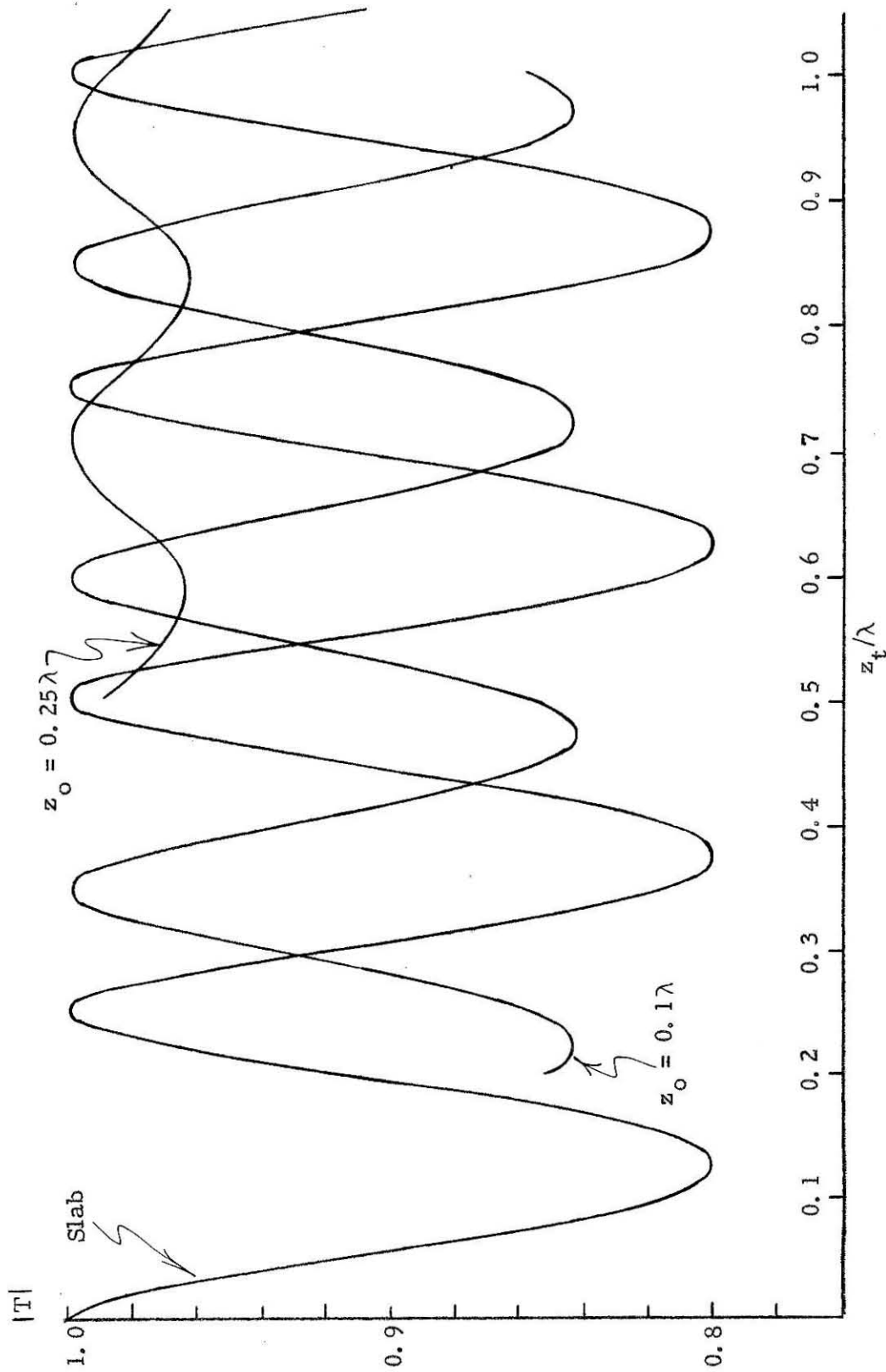


Figure 13.21 Trapezoid, $K = 2.0$

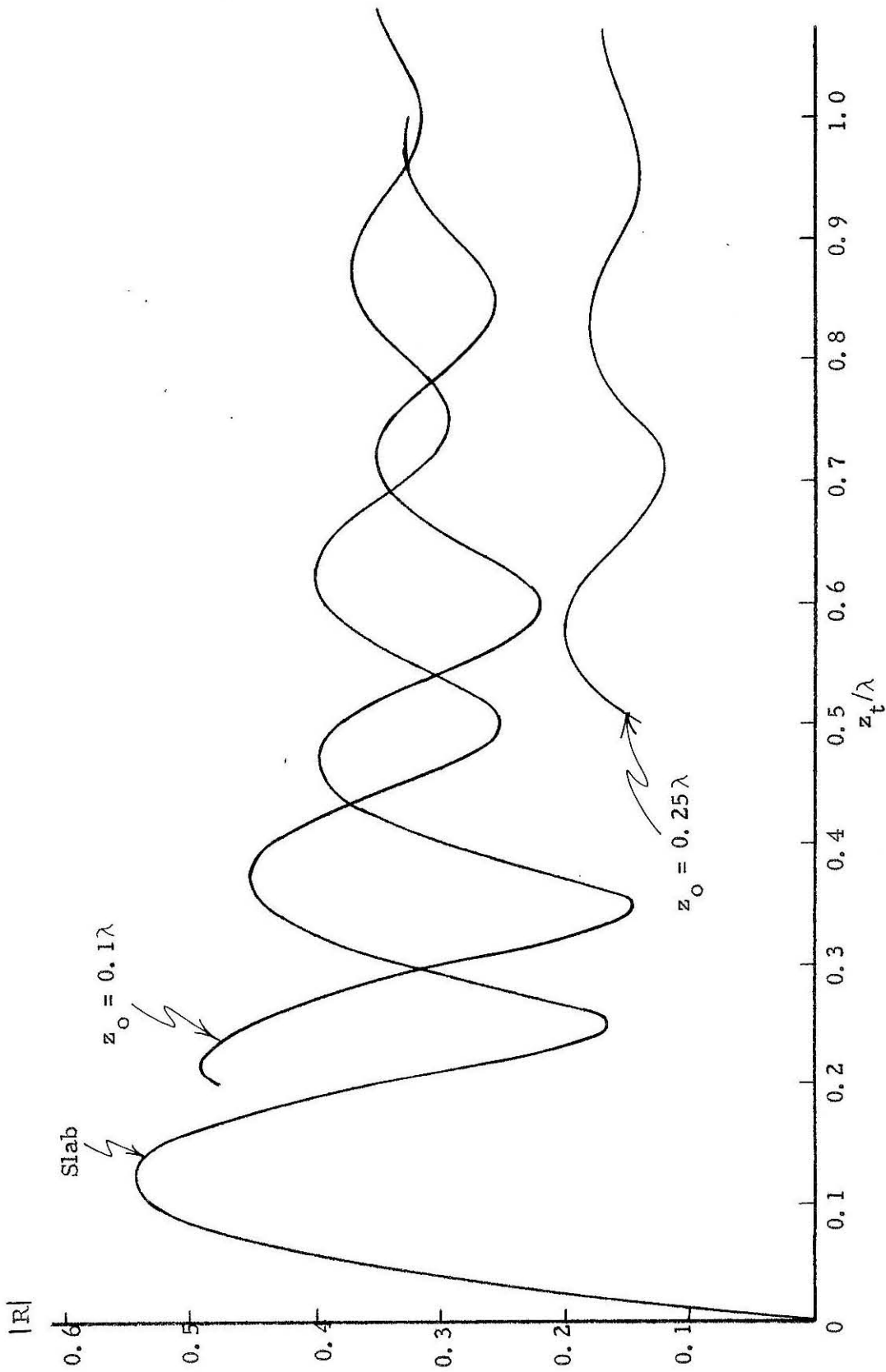
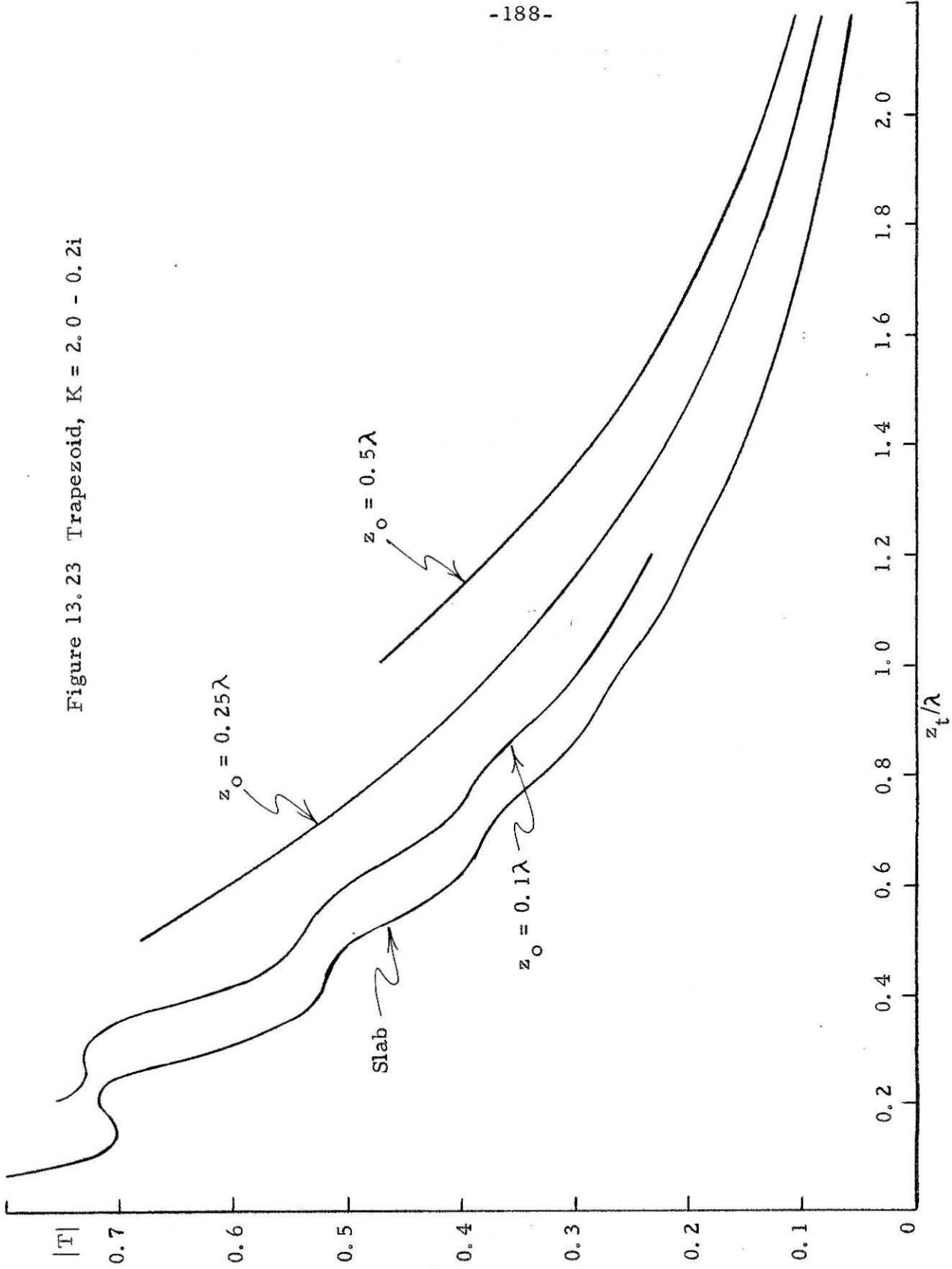


Figure 13.22 Trapezoid, $K = 2.0 - 0.2i$

Figure 13.23 Trapezoid, $K = 2.0 - 0.2i$



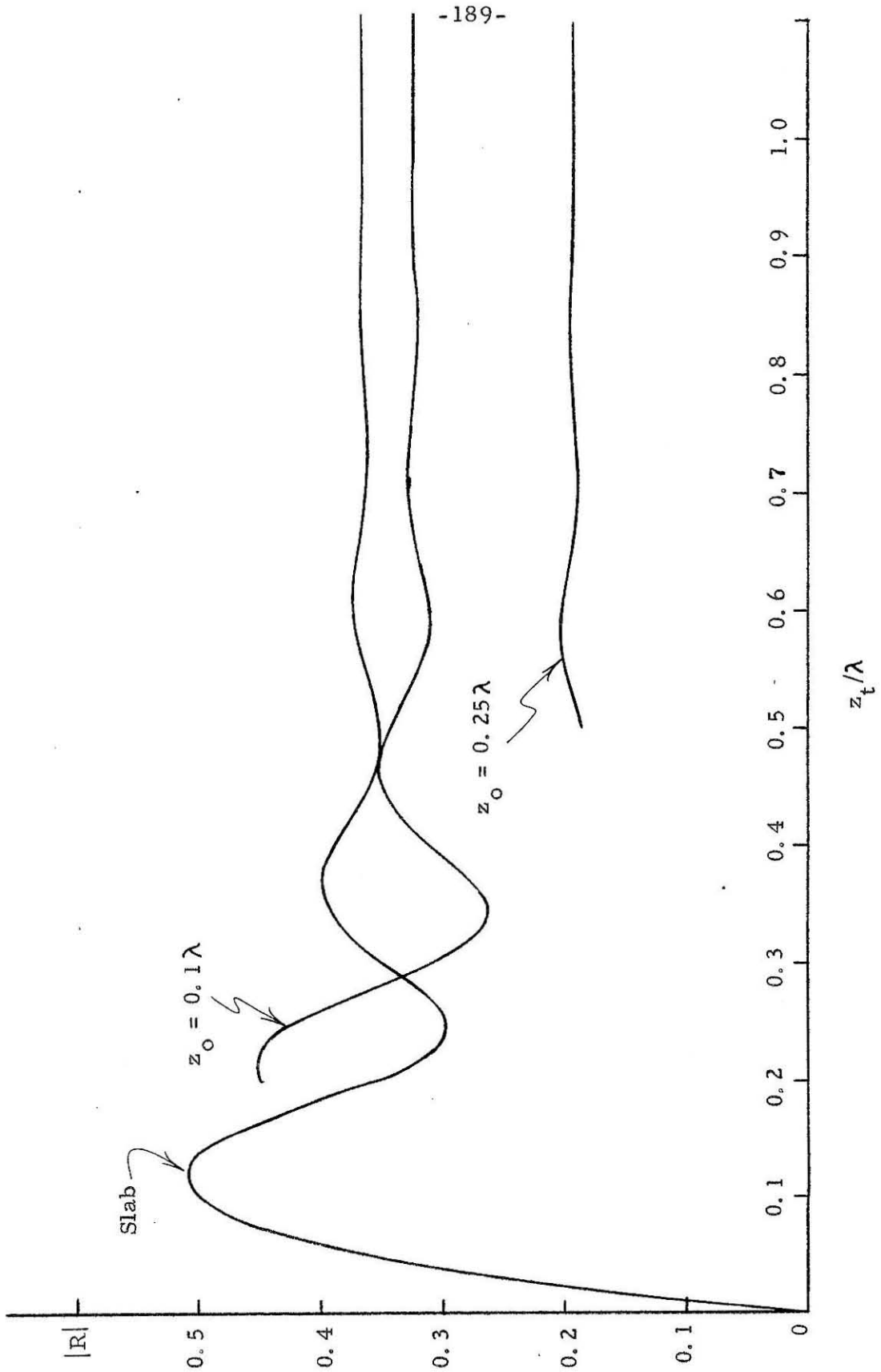


Figure 13.24 Trapezoid, $K = 2.0 - 0.5i$

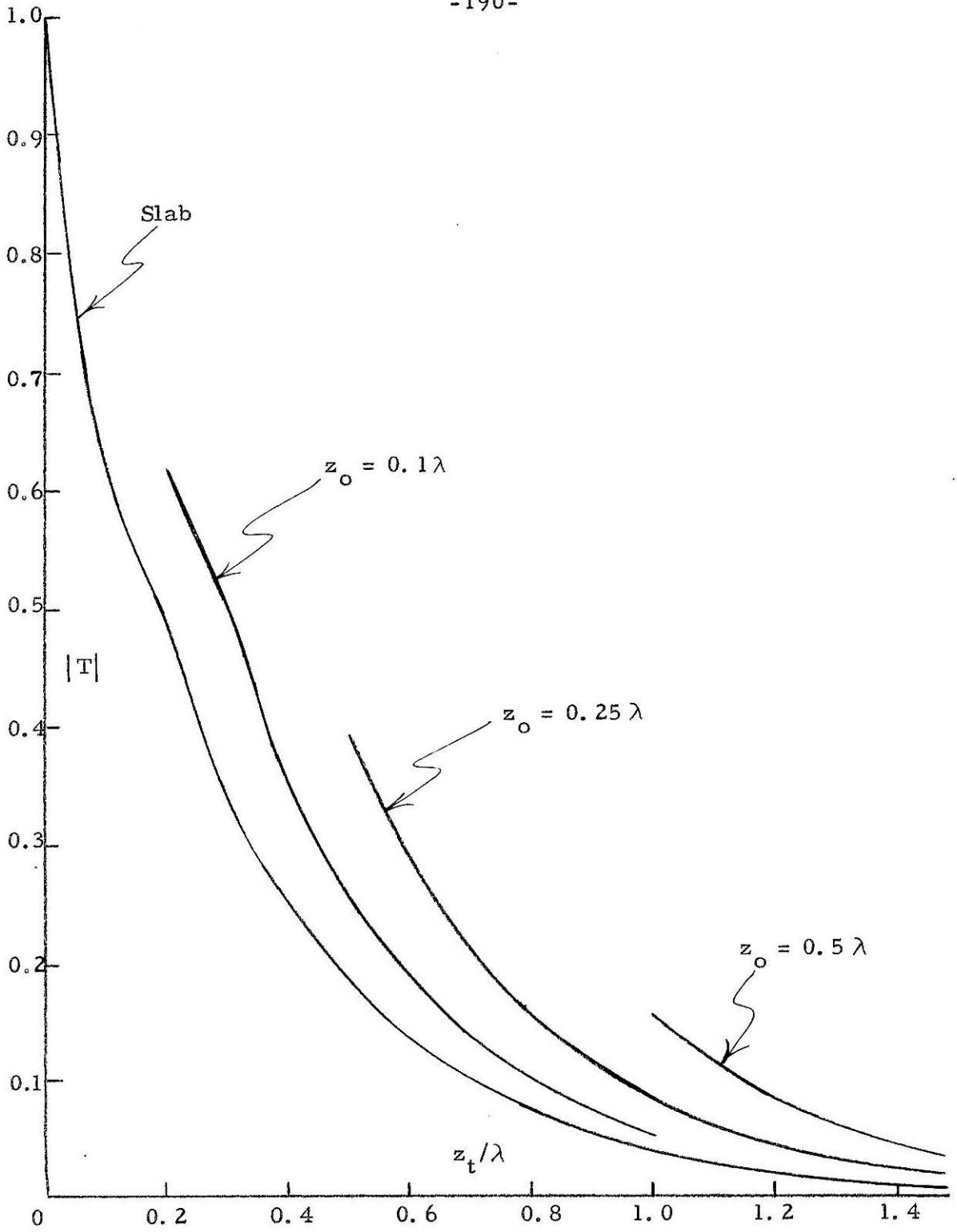


Figure 13.25 Trapezoid, $K = 2.0 - 0.5i$

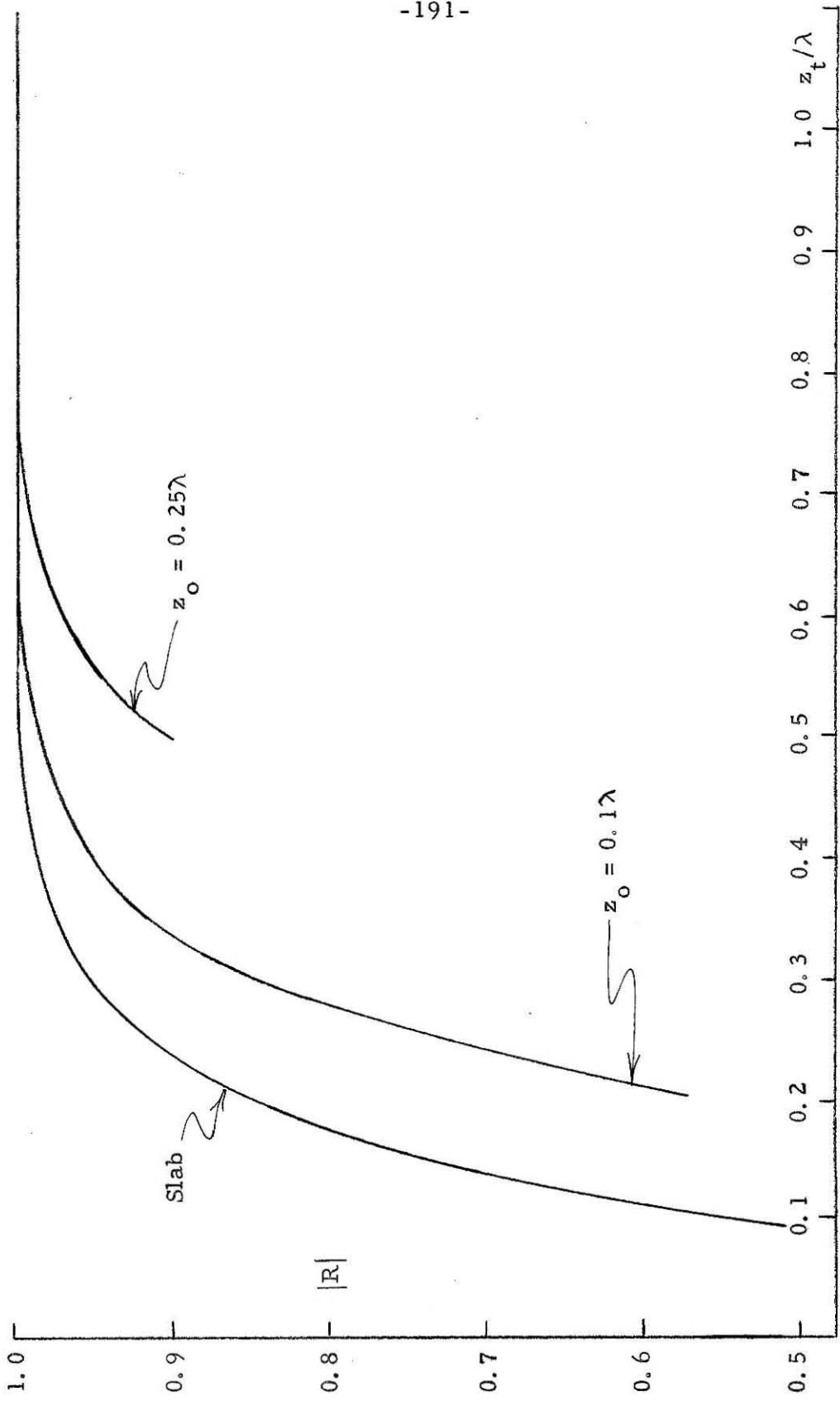


Figure 13.26 Trapezoid, $K = 0 - 1.0i$

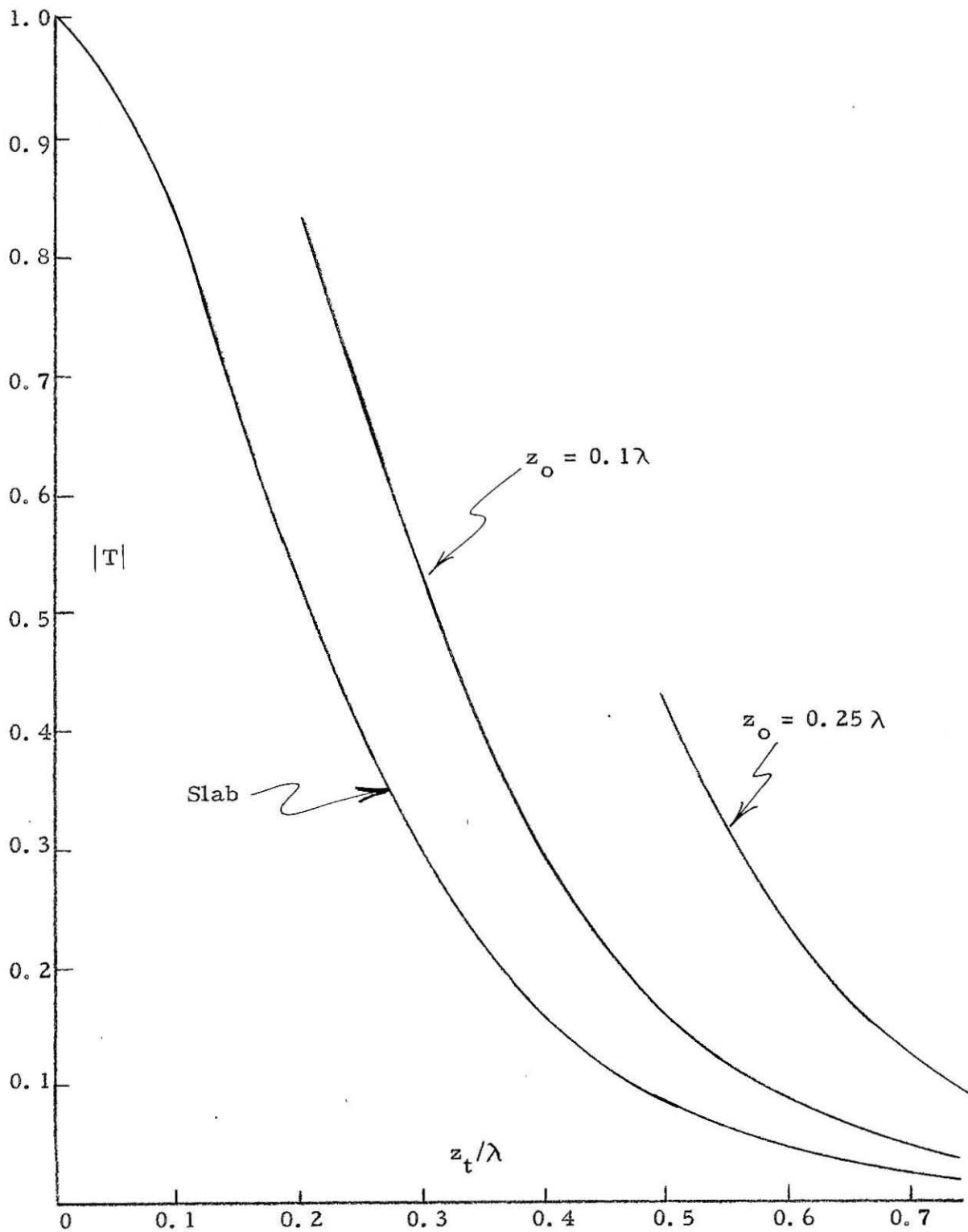


Figure 13.27 Trapezoid, $K = 0 - 1.0i$

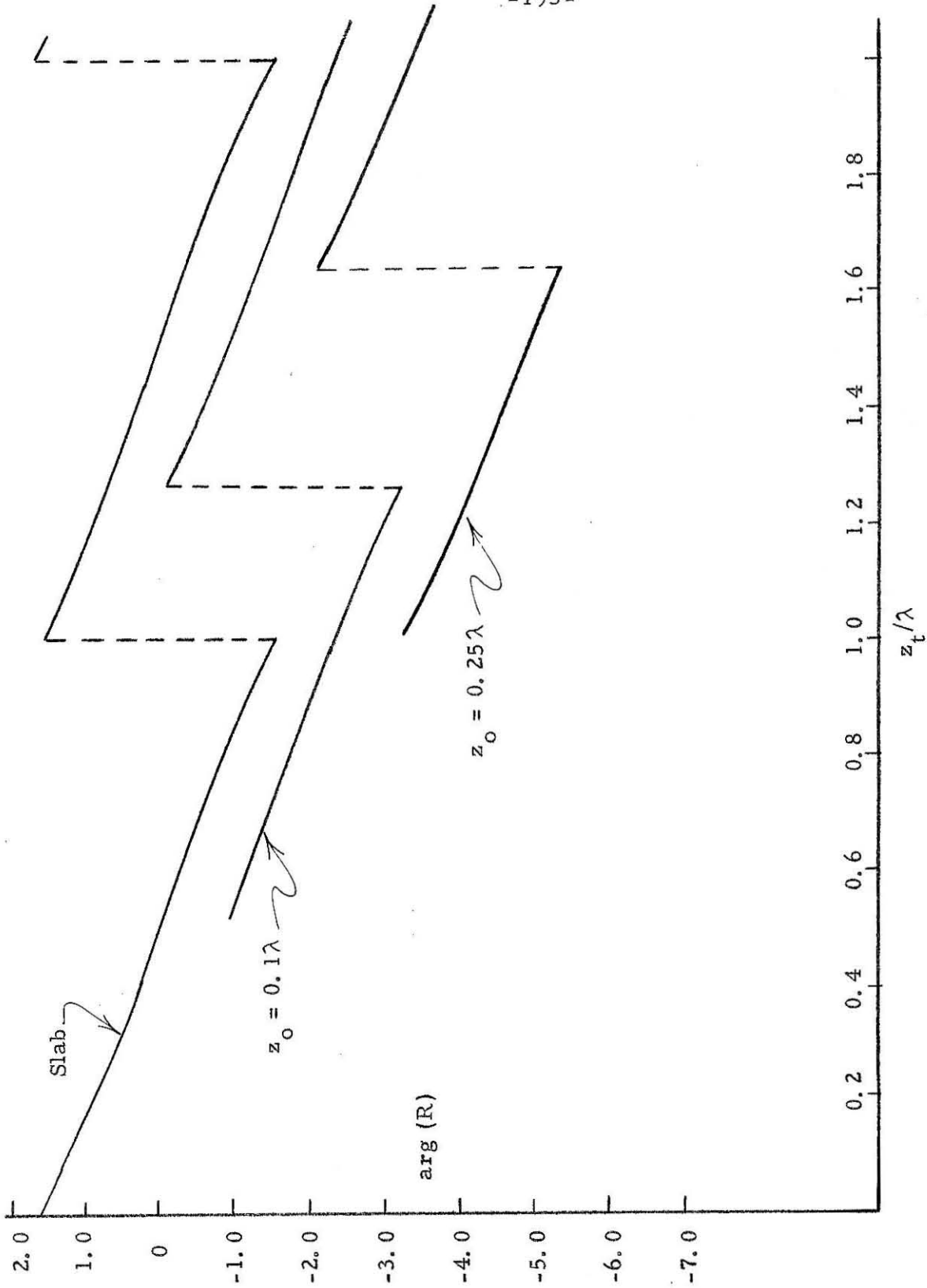


Figure 13.28 Trapezoid, $K = 0.5$

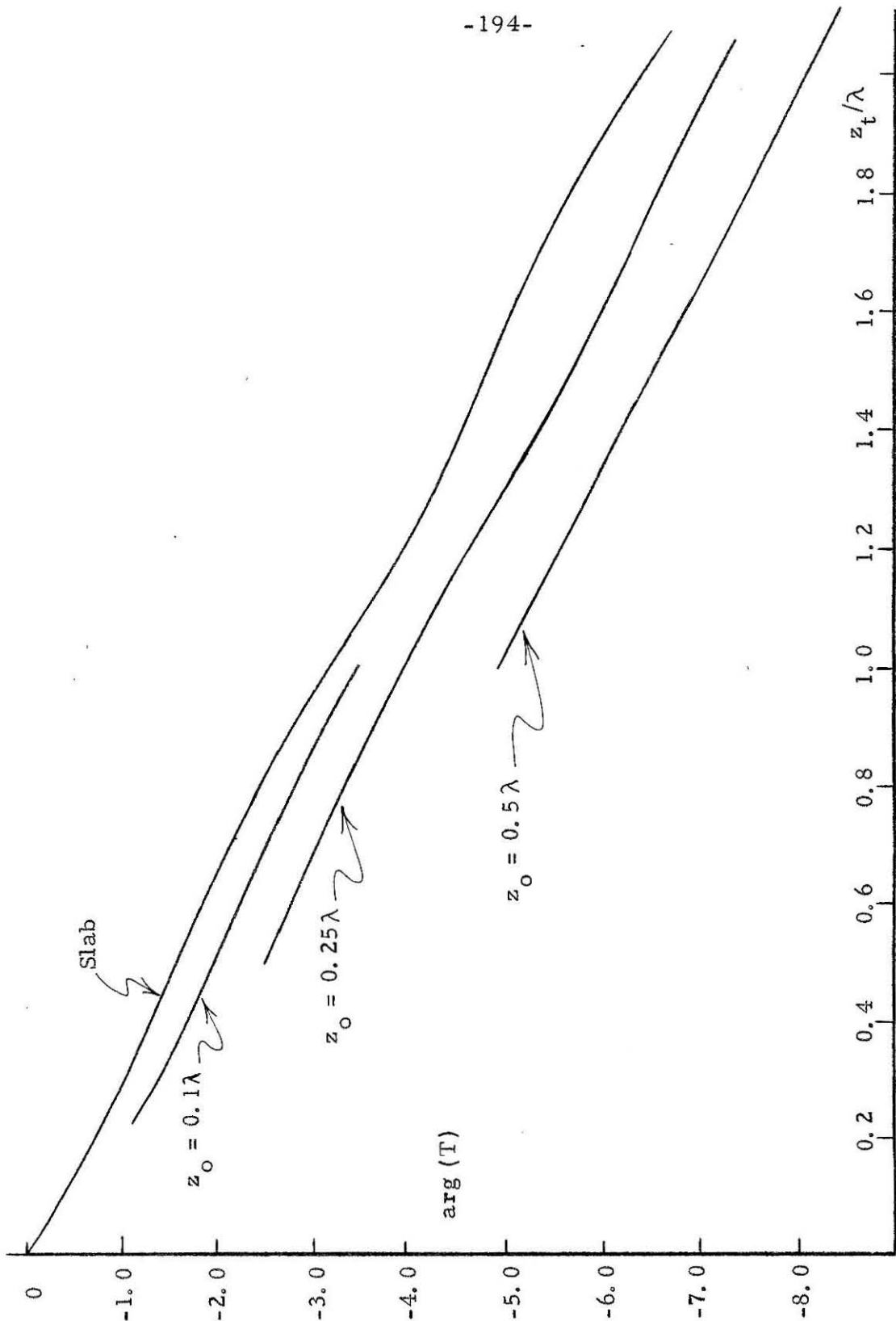


Figure 13.29 Trapezoid, $K = 0.5$

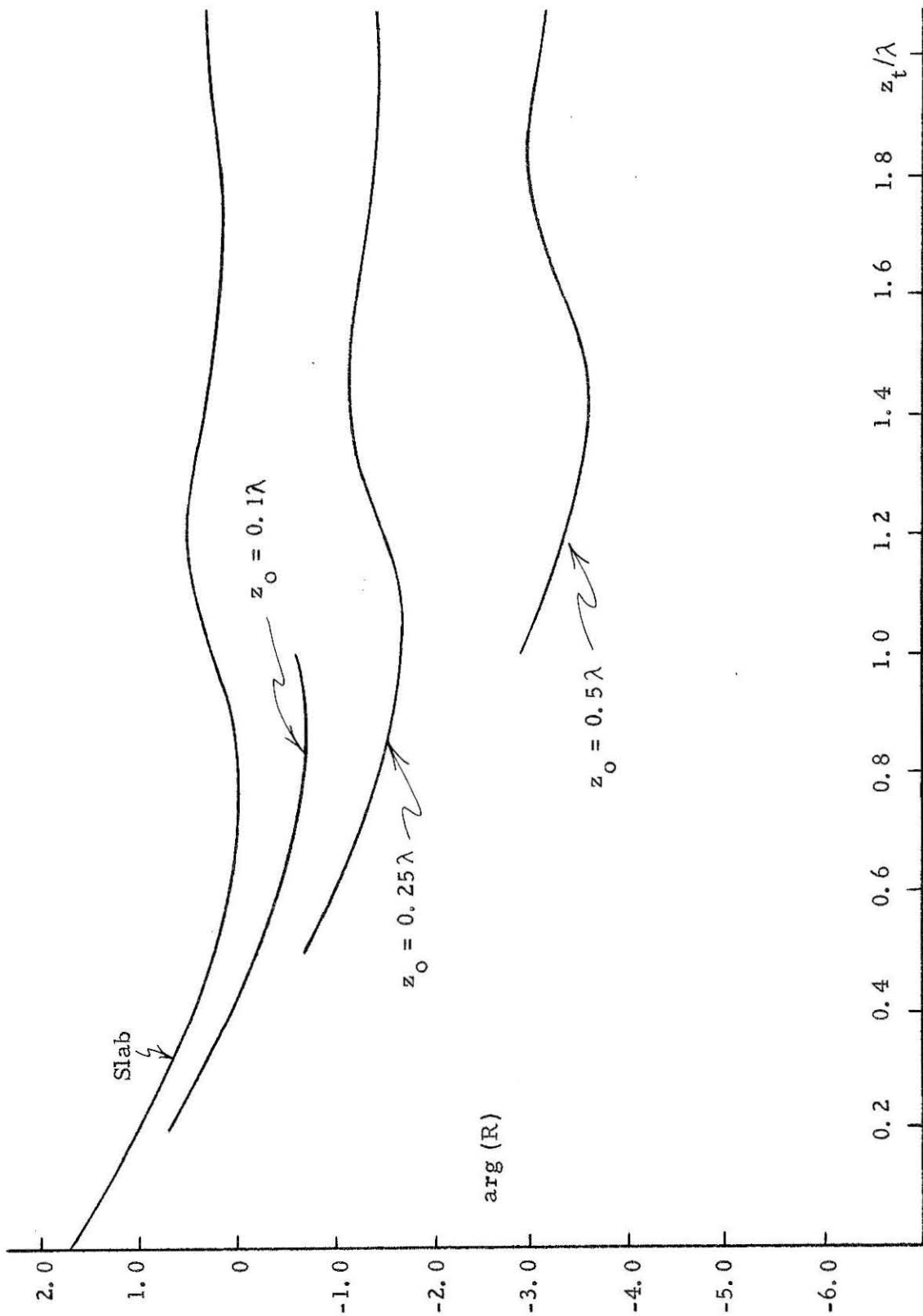


Figure 13.30 Trapezoid, $K = 0.5 - 0.1i$

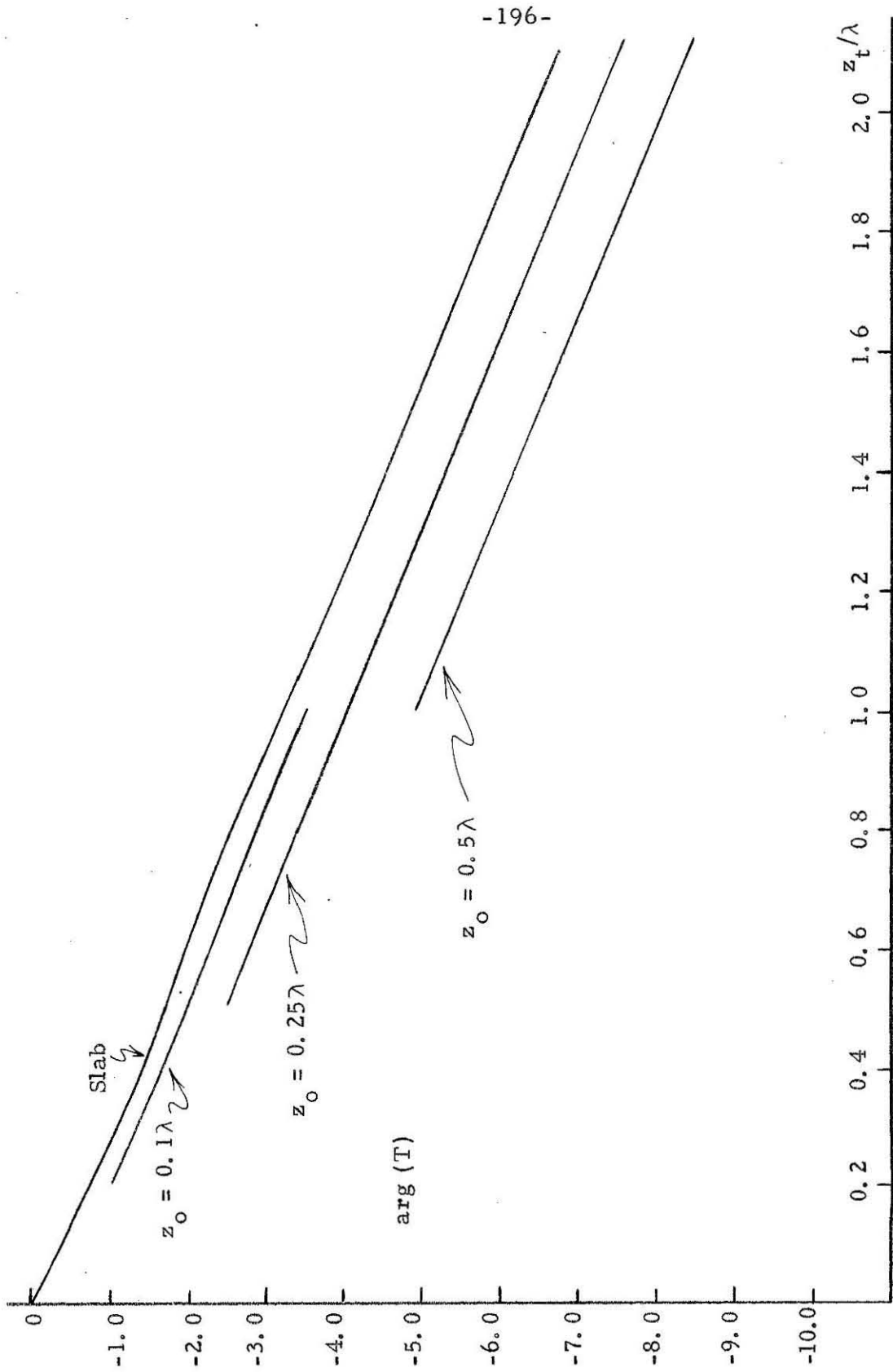


Figure 13.31 Trapezoid, $K = 0.5 - 0.1i$

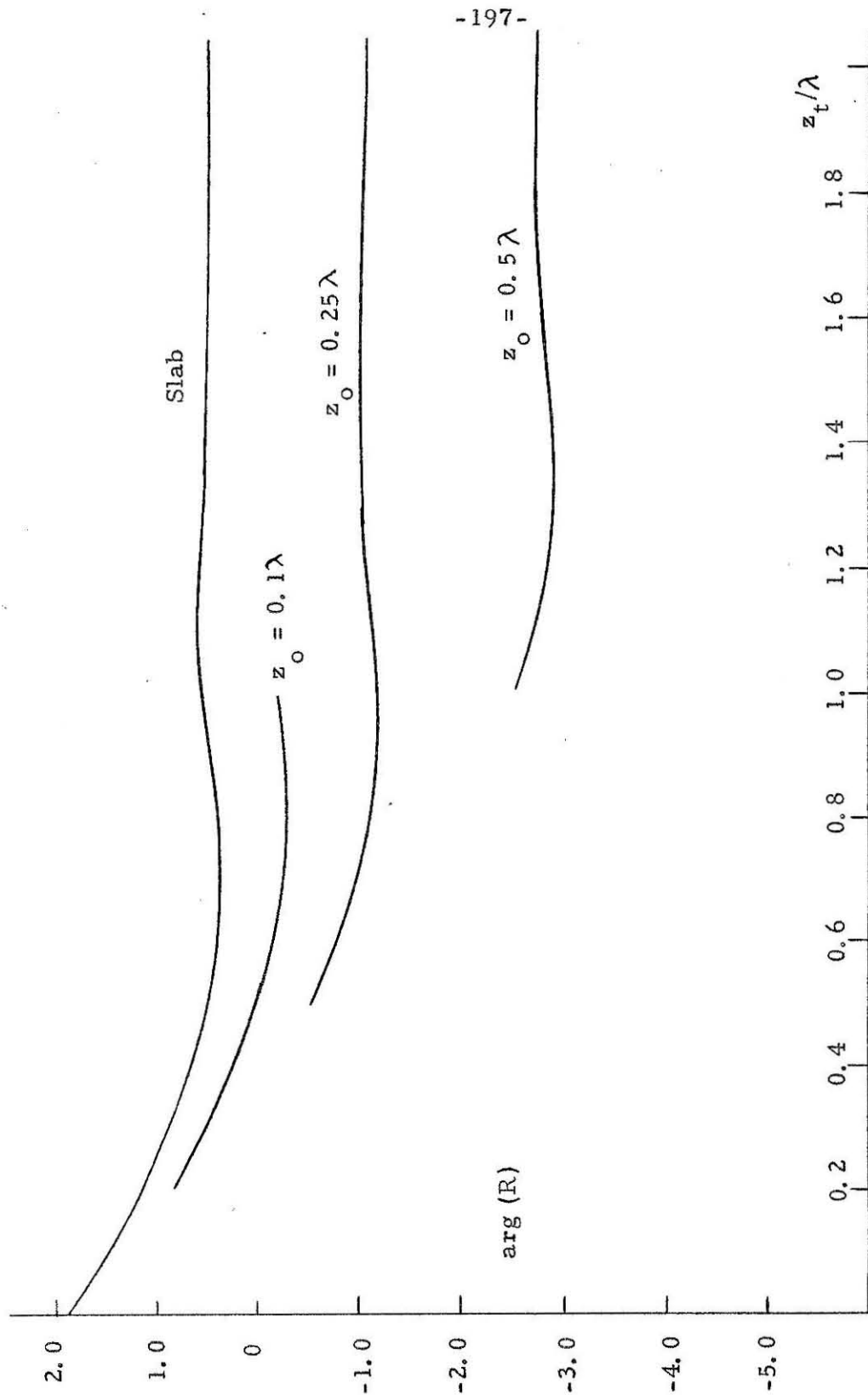


Figure 13.32 Trapezoid, $K = 0.5 - 0.2i$

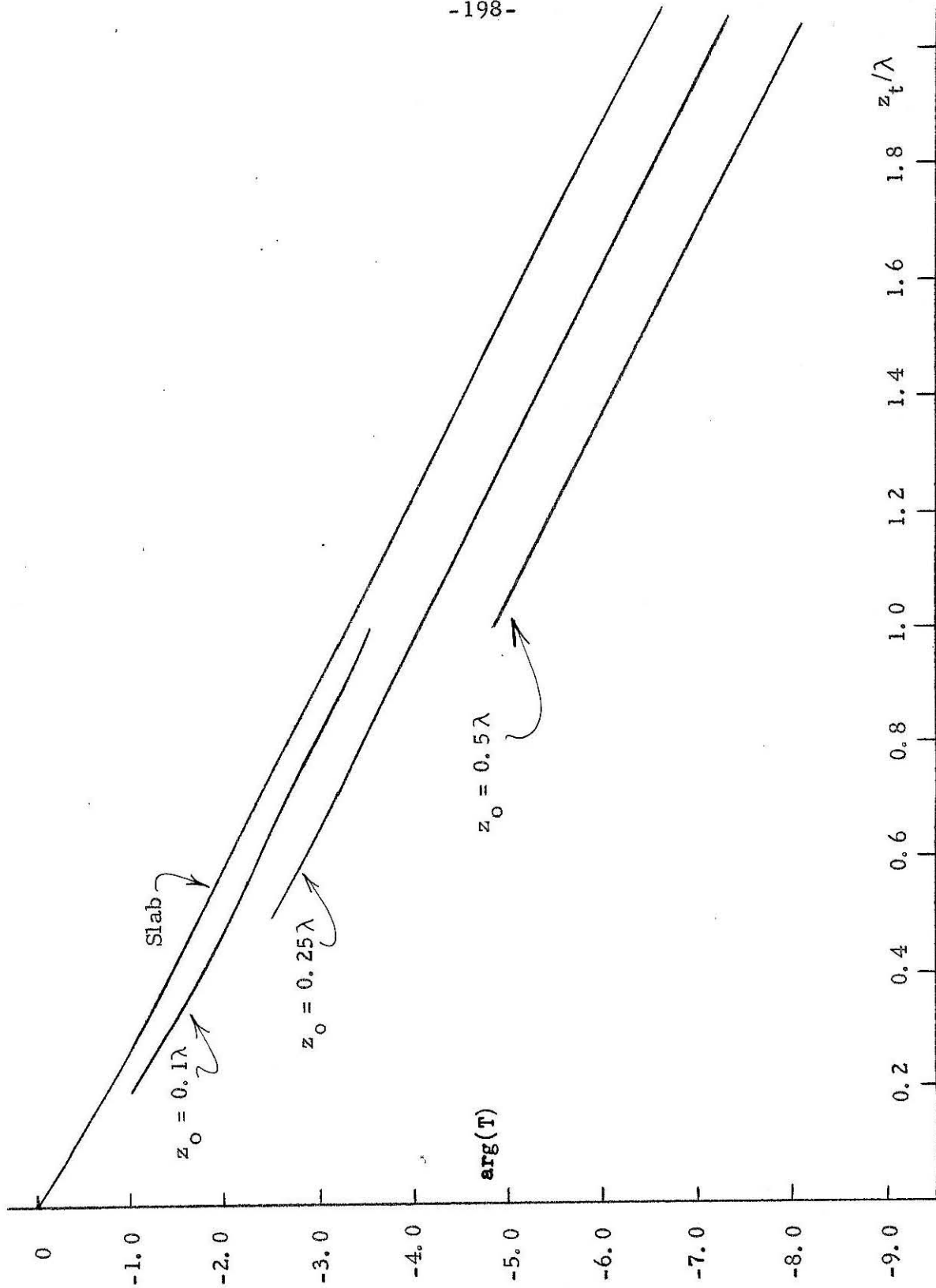


Figure 13.33 Trapezoid, $K = 0.5 - 0.2i$

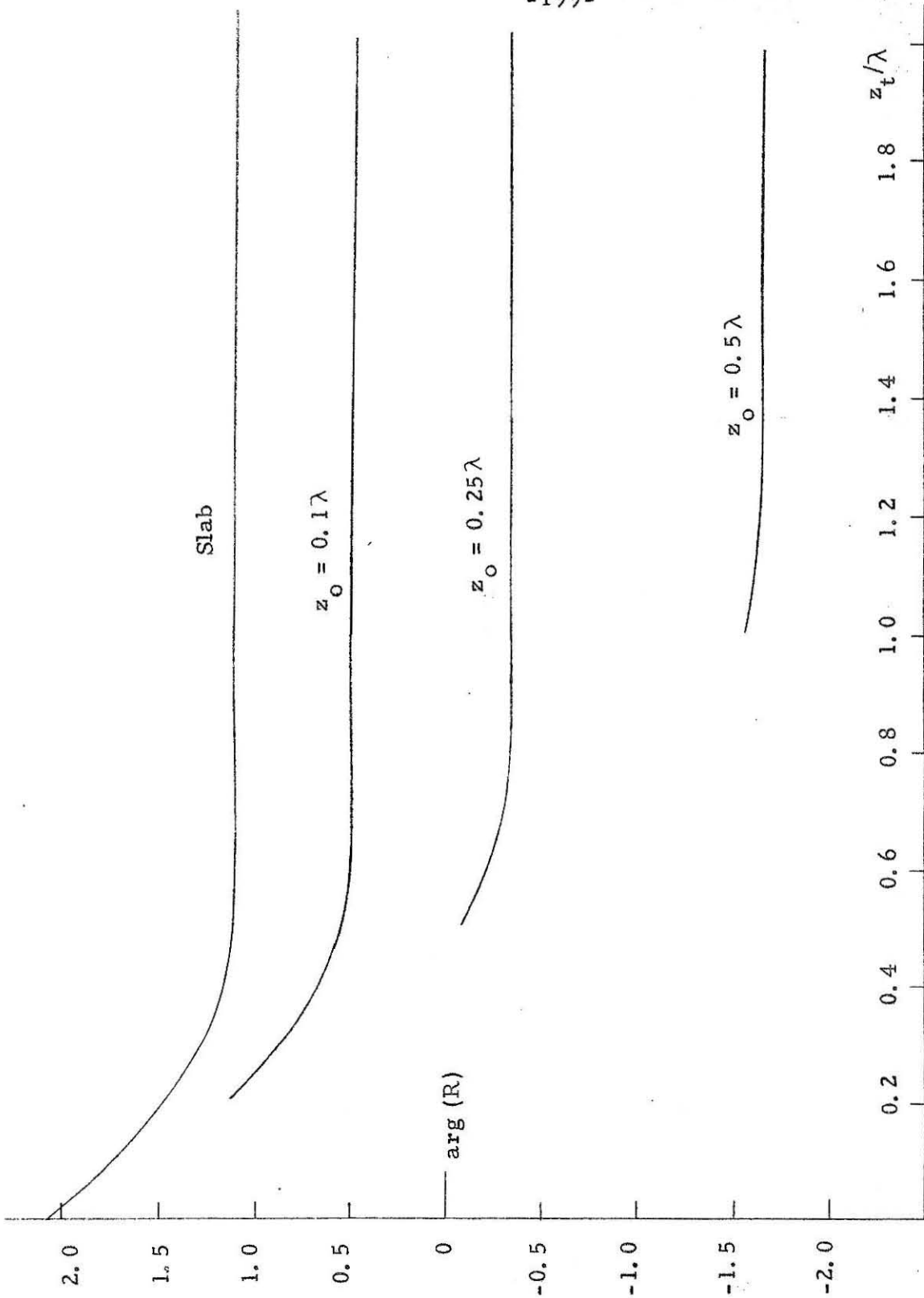


Figure 13.34 Trapezoid, $K = 0.5 - 0.5i$

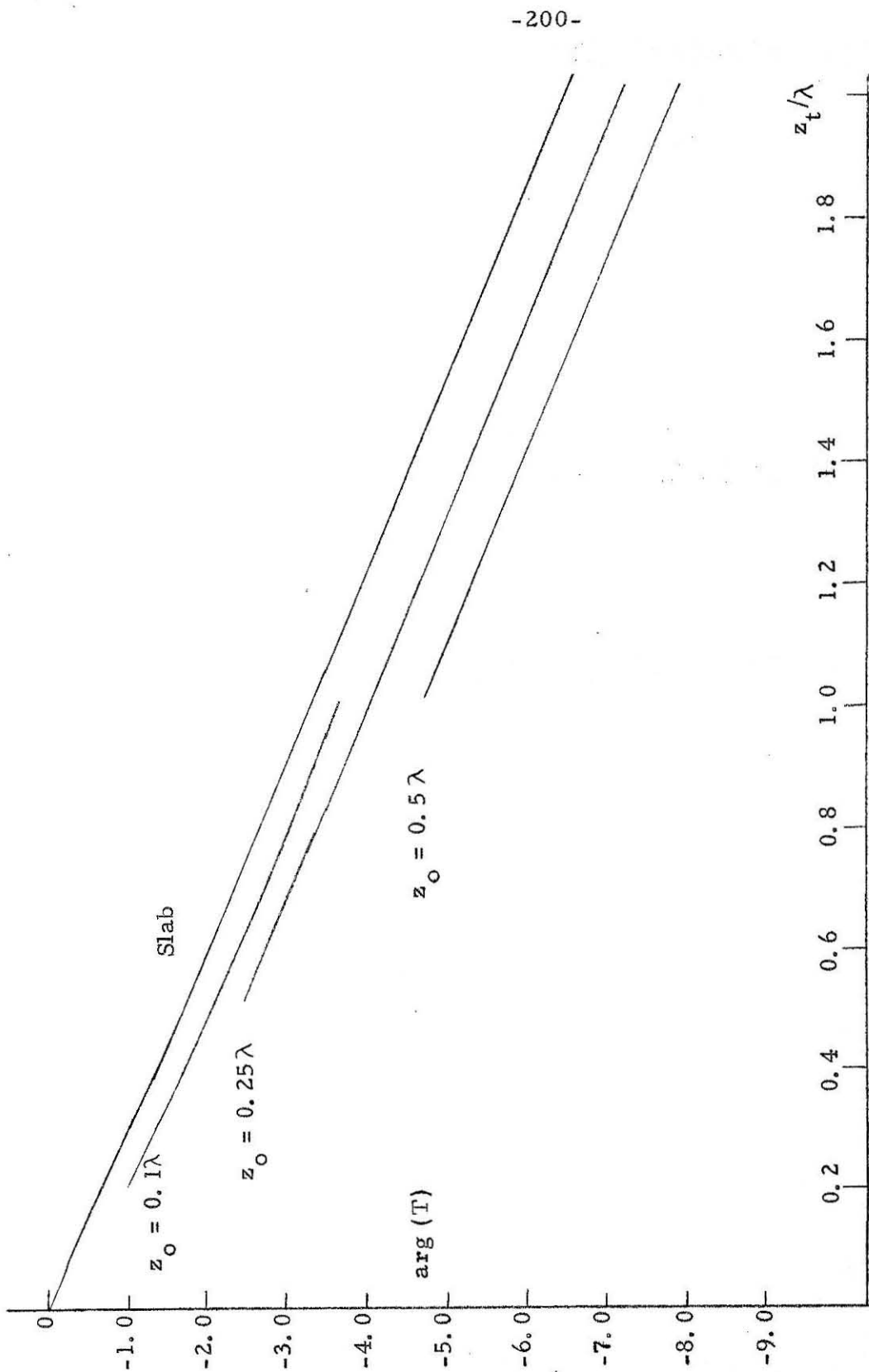


Figure 13.35 Trapezoid, $K = 0.5 - 0.5i$

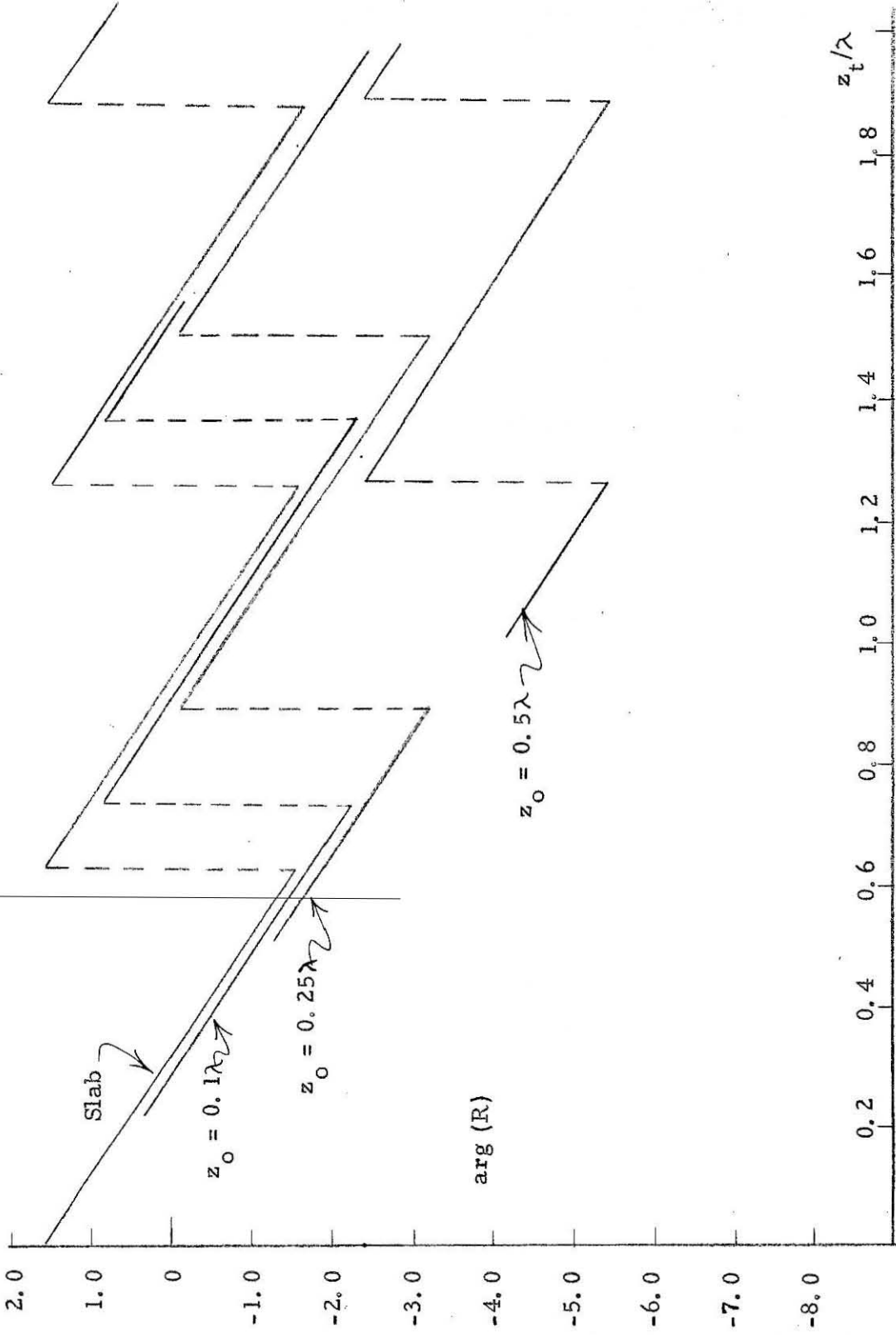


Figure 13.36 Trapezoid, $K = 0.8$

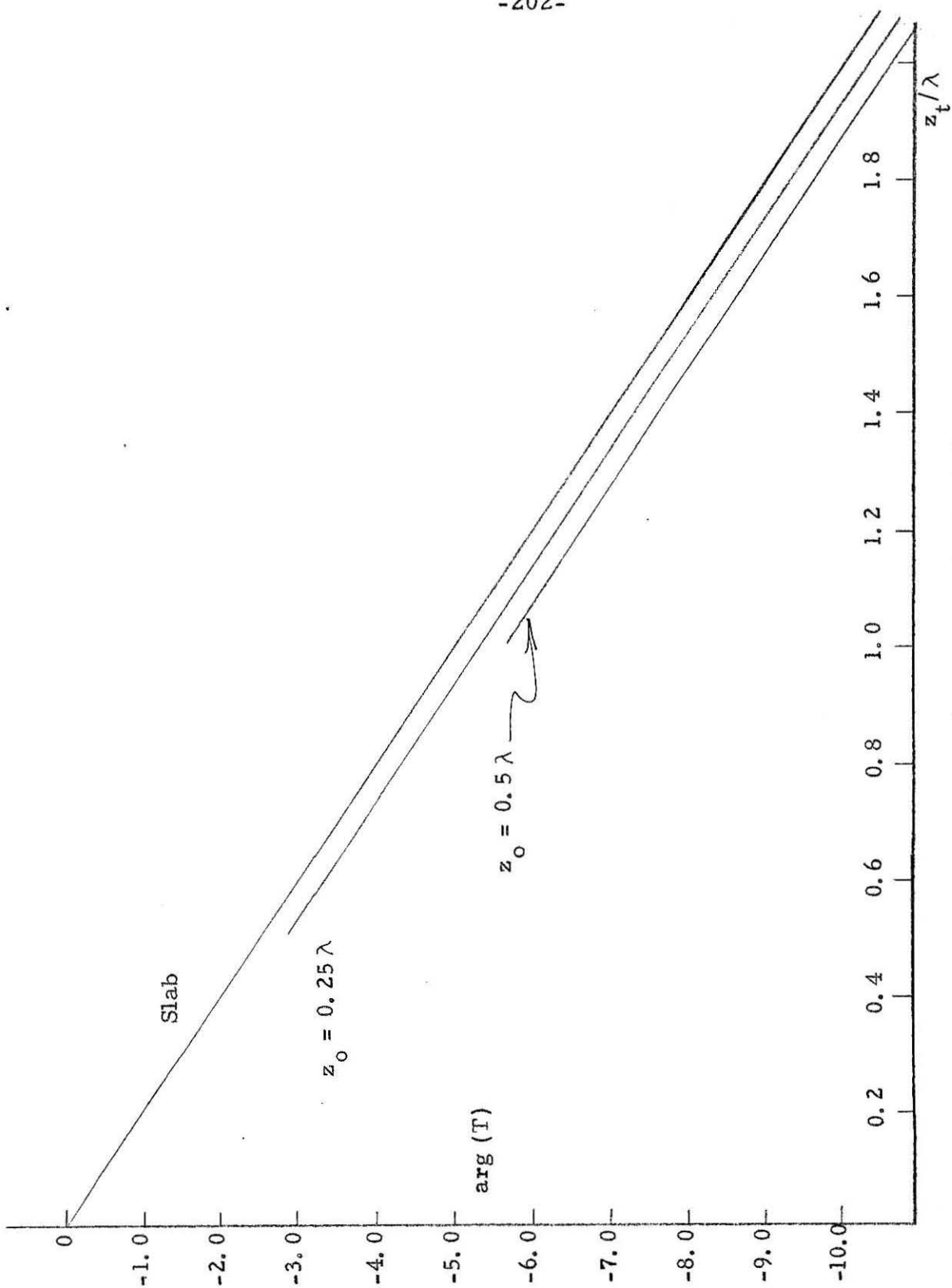


Figure 13.37 Trapezoid, $K = 0.8$

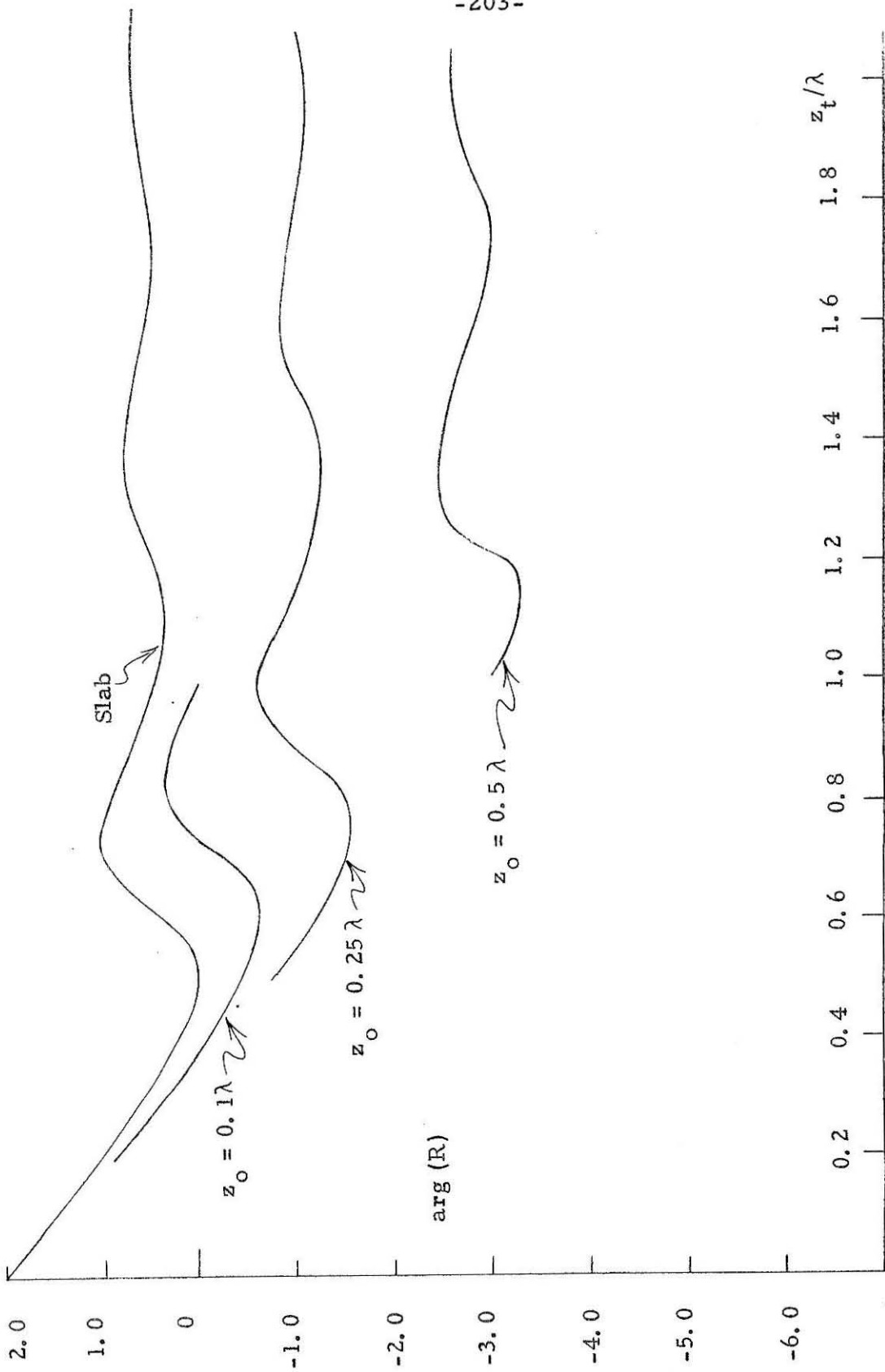


Figure 13.38 Trapezoid, $K = 0.8 - 0.1i$

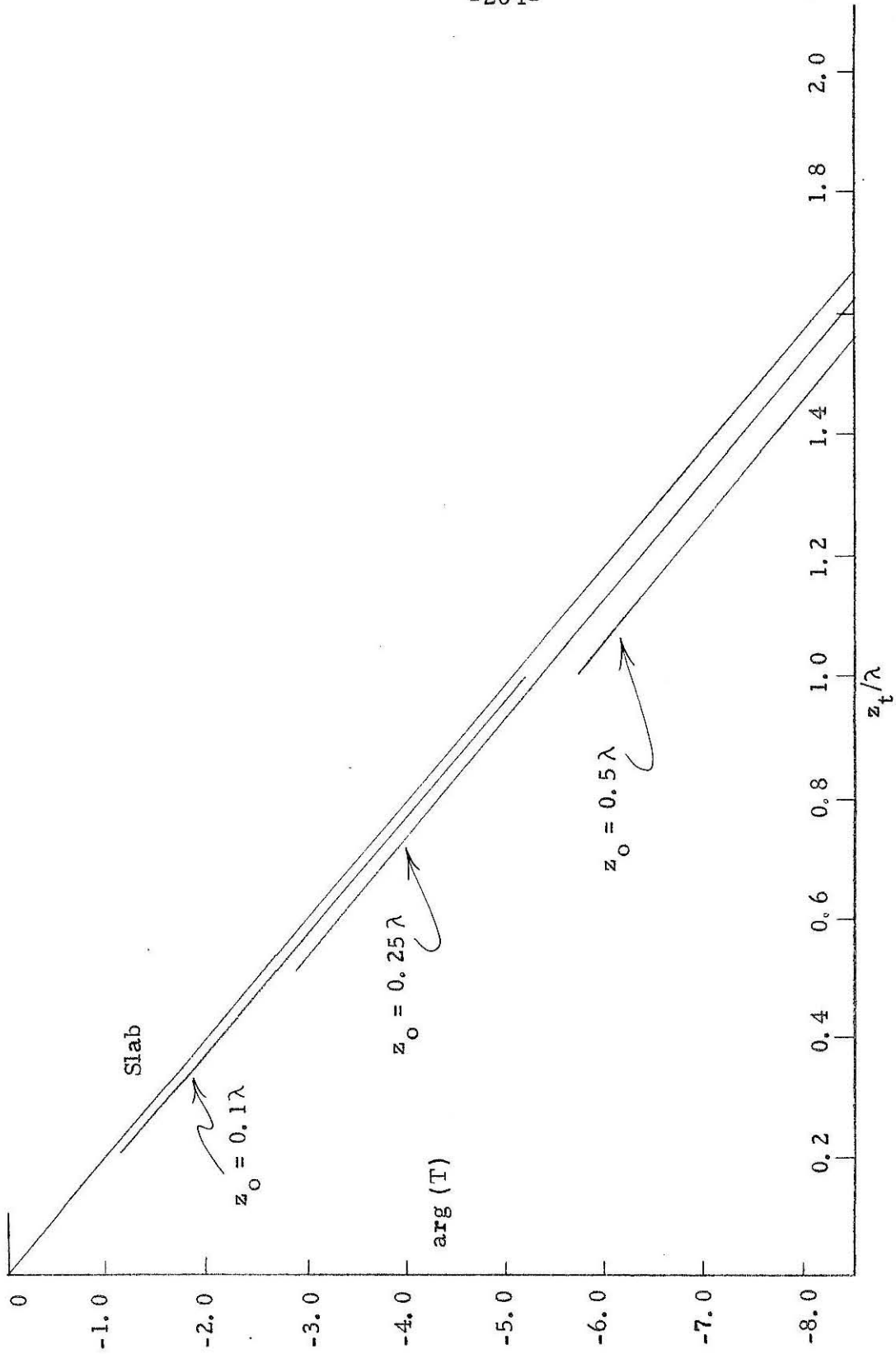


Figure 13.39 Trapezoid, $K = 0.8 - 0.1i$

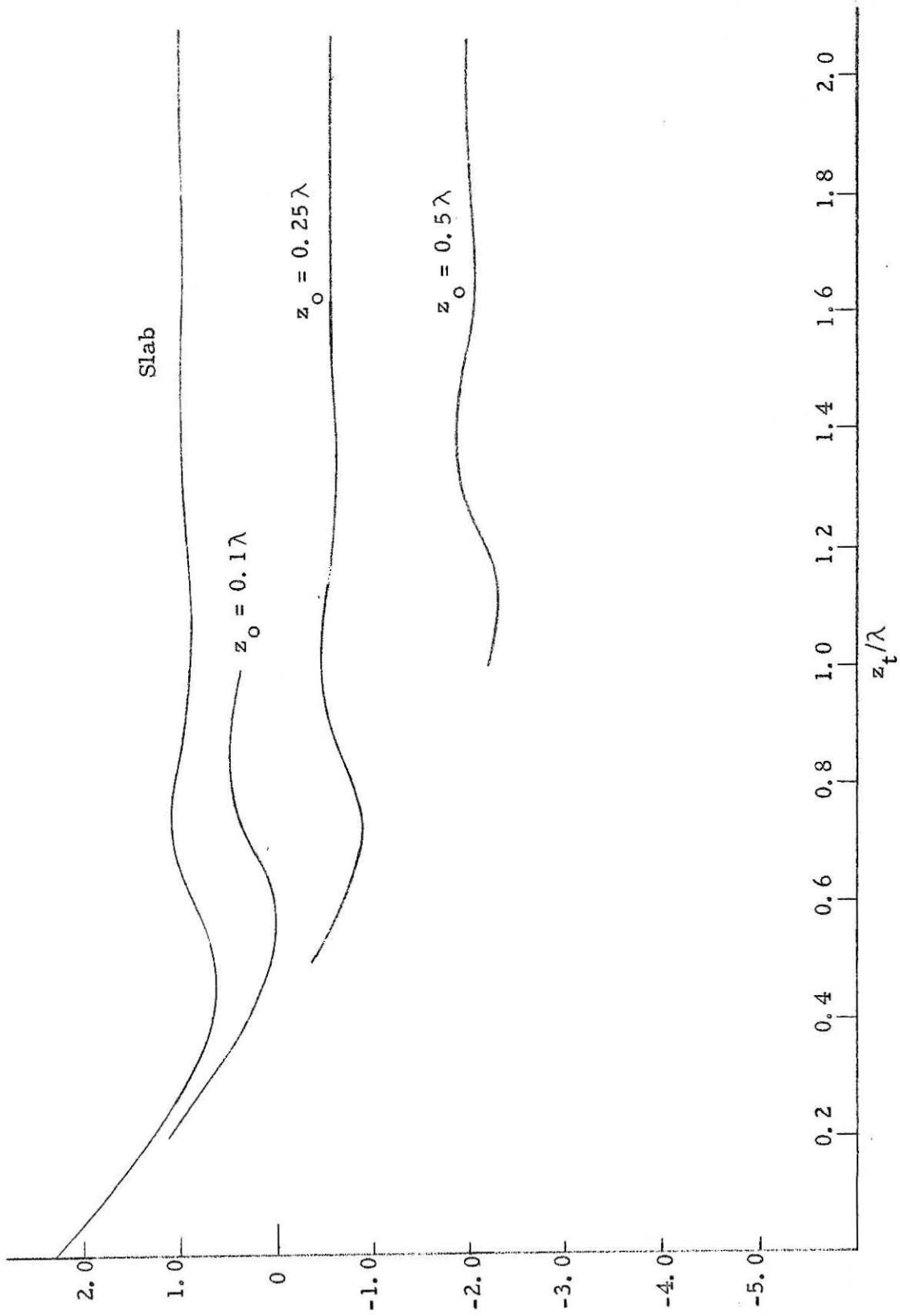


Figure 13.40 Trapezoid, $K = 0.8 - 0.2i$

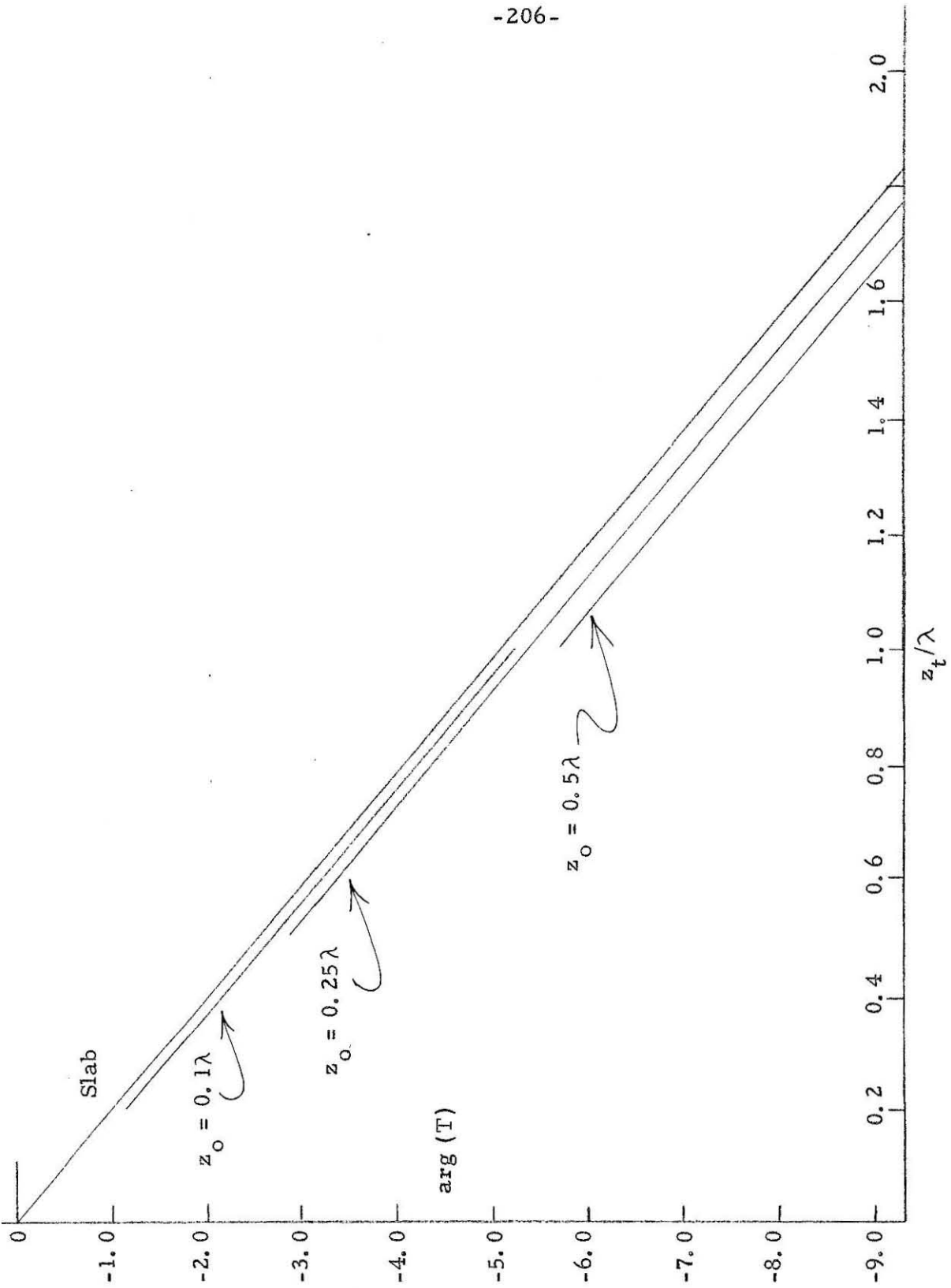


Figure 13.41 Trapezoid, $K = 0.8 - 0.2i$

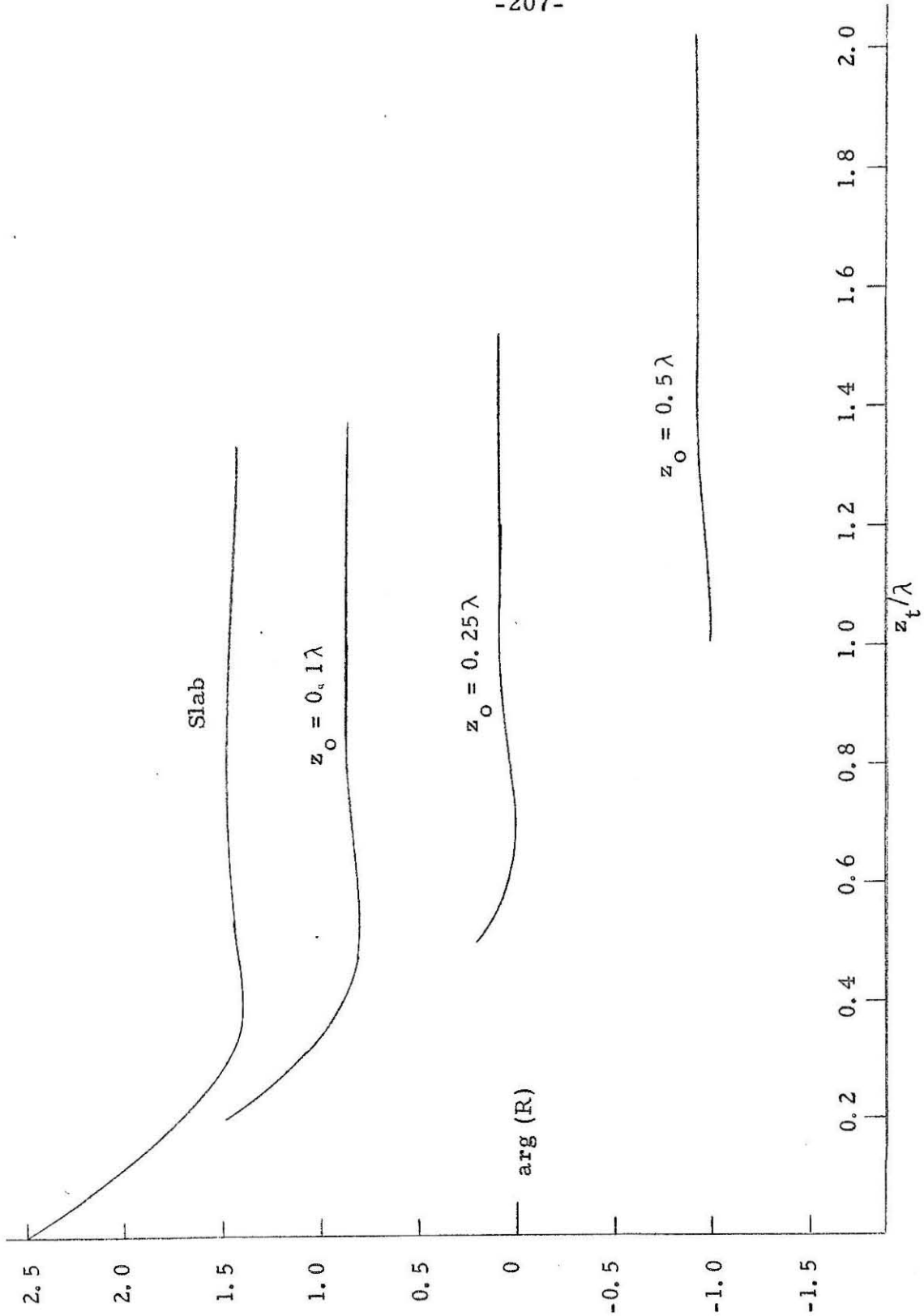


Figure 13.42 Trapezoid, $K = 0.8 - 0.5i$

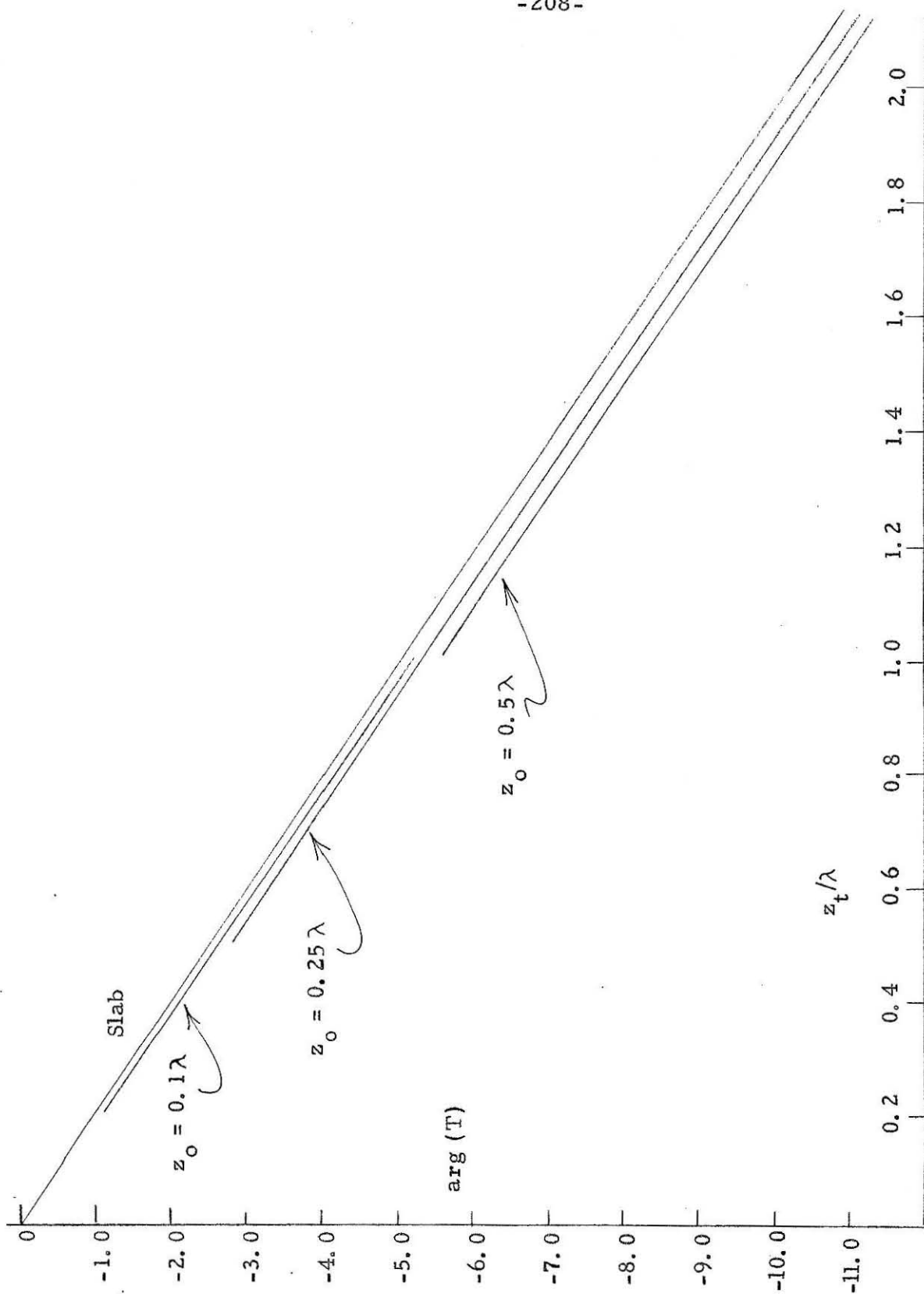


Figure 13.43 Trapezoid, $K = 0.8 - 0.5i$

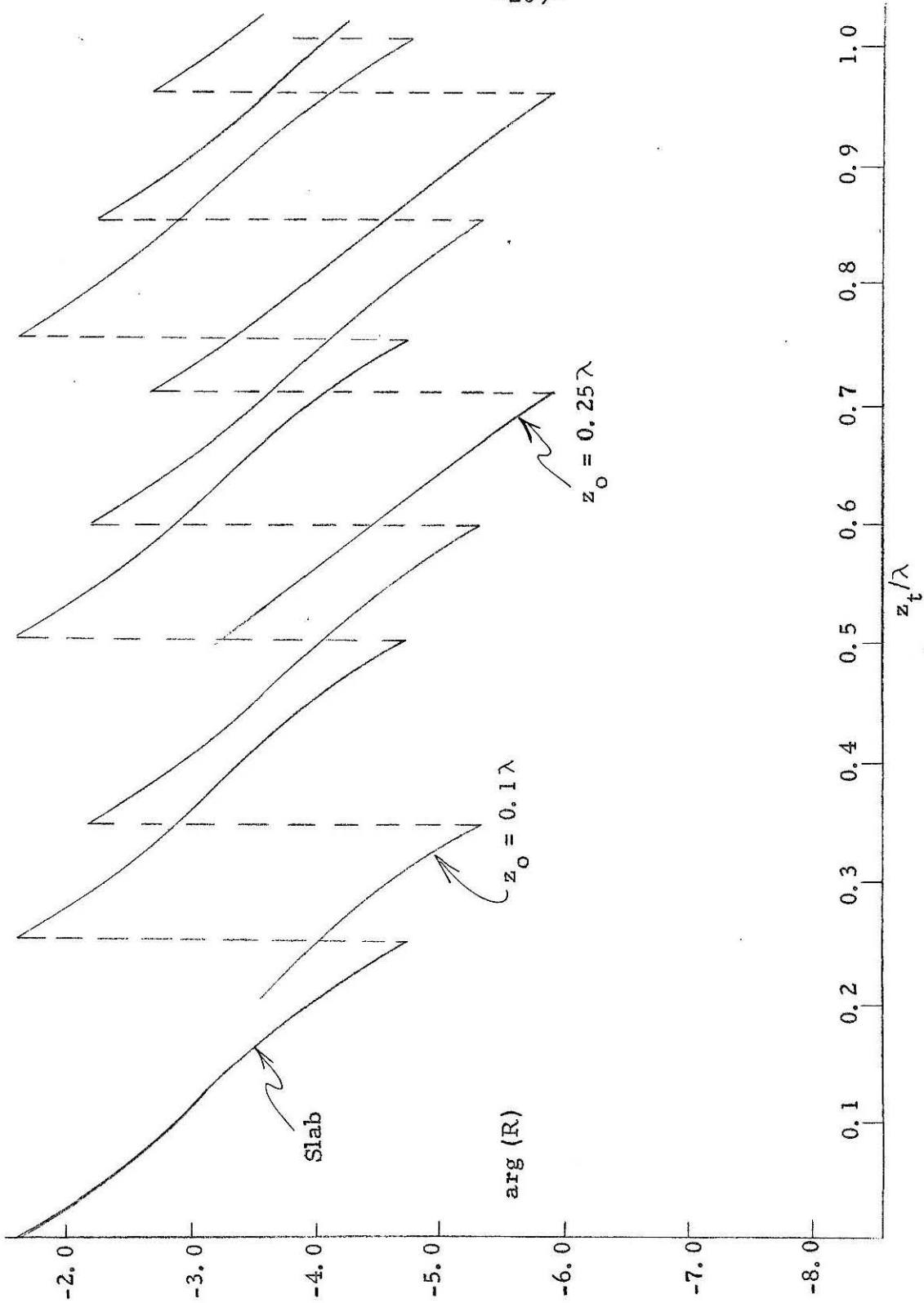


Figure 13.44 Trapezoid, $K = 2.0$

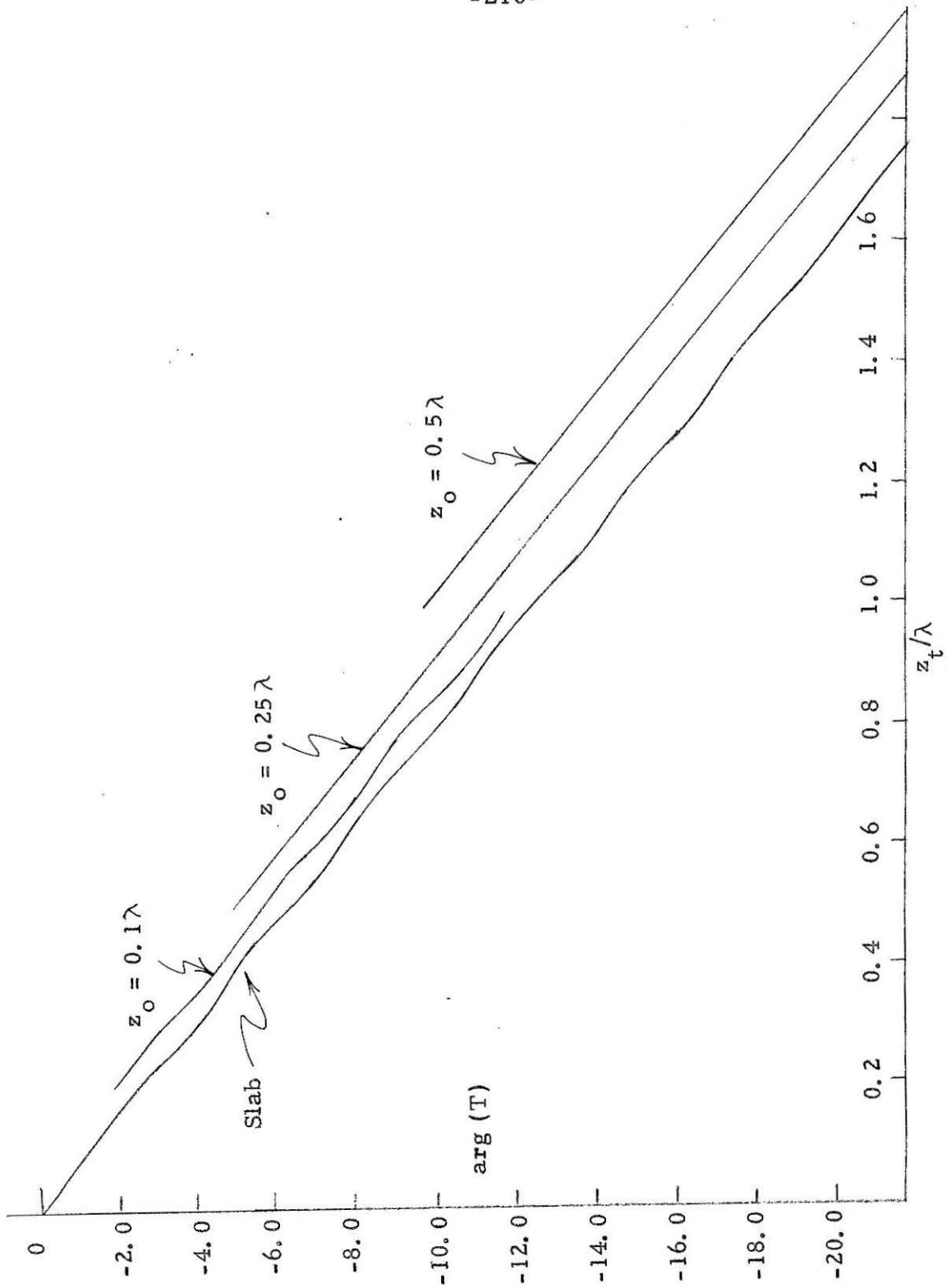


Figure 13.45 Trapezoid, $K = 2.0$

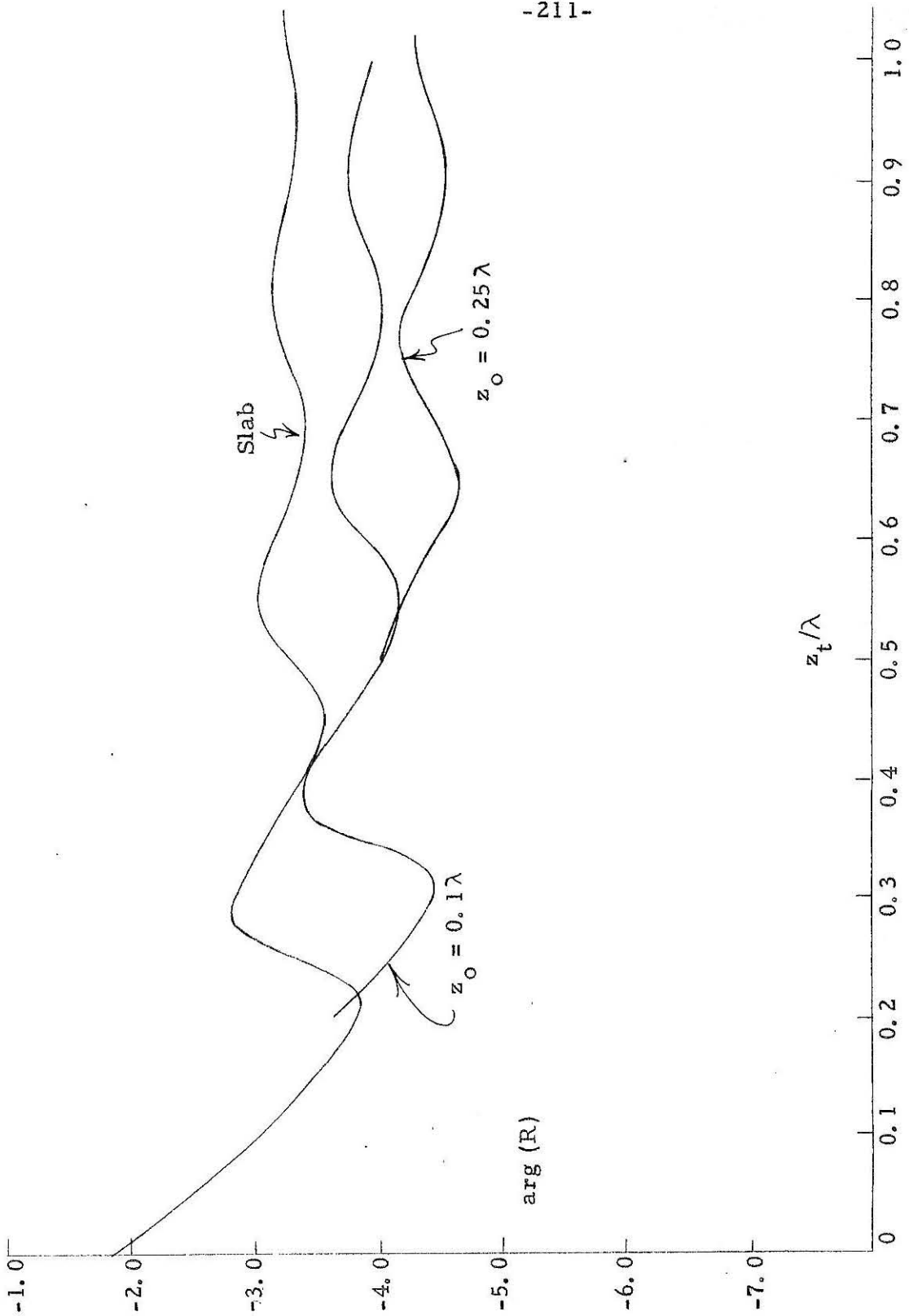


Figure 13.46 Trapezoid, $K = 2.0 - 0.2i$

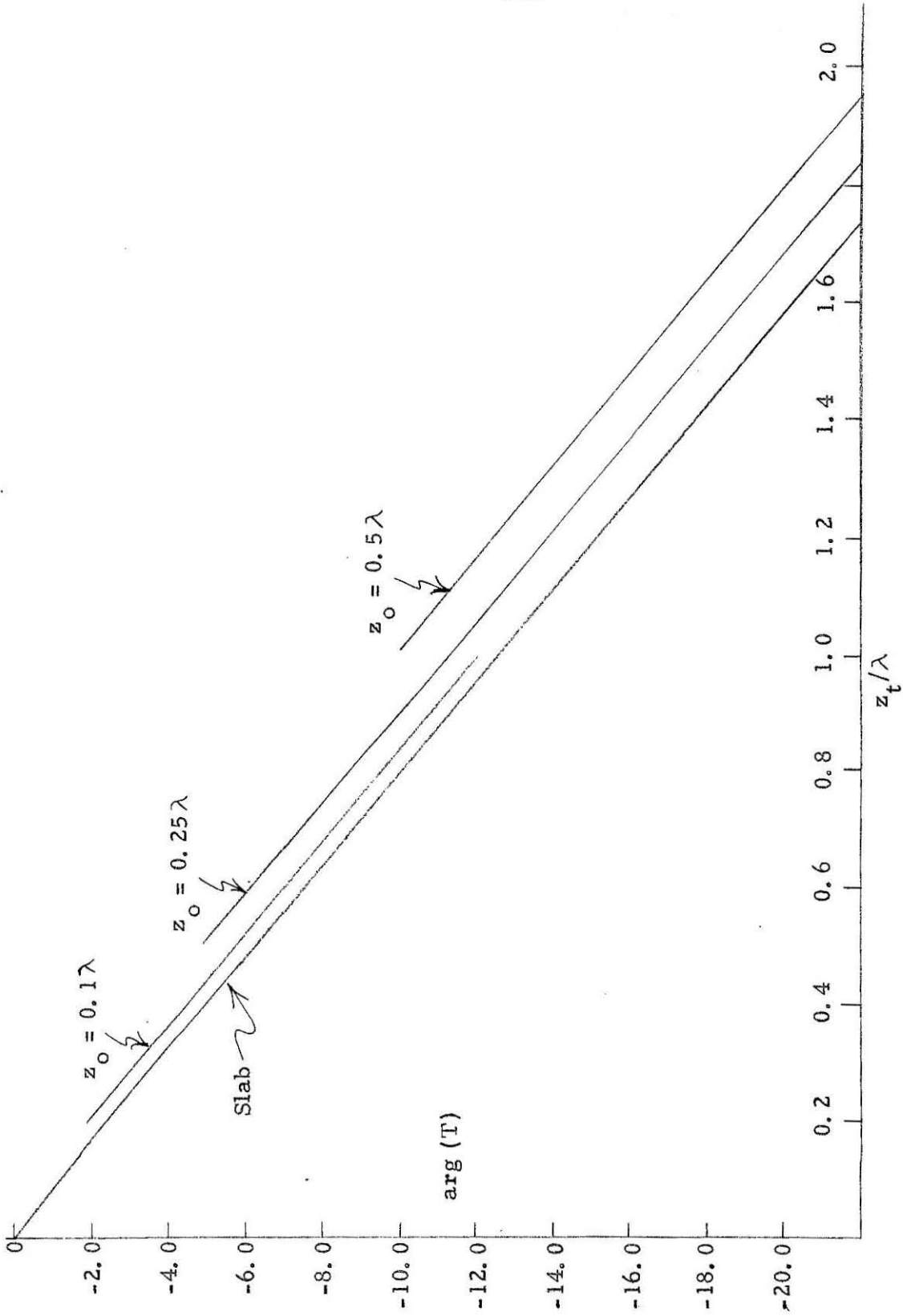


Figure 13.47 Trapezoid, $K = 2.0 - 0.2i$

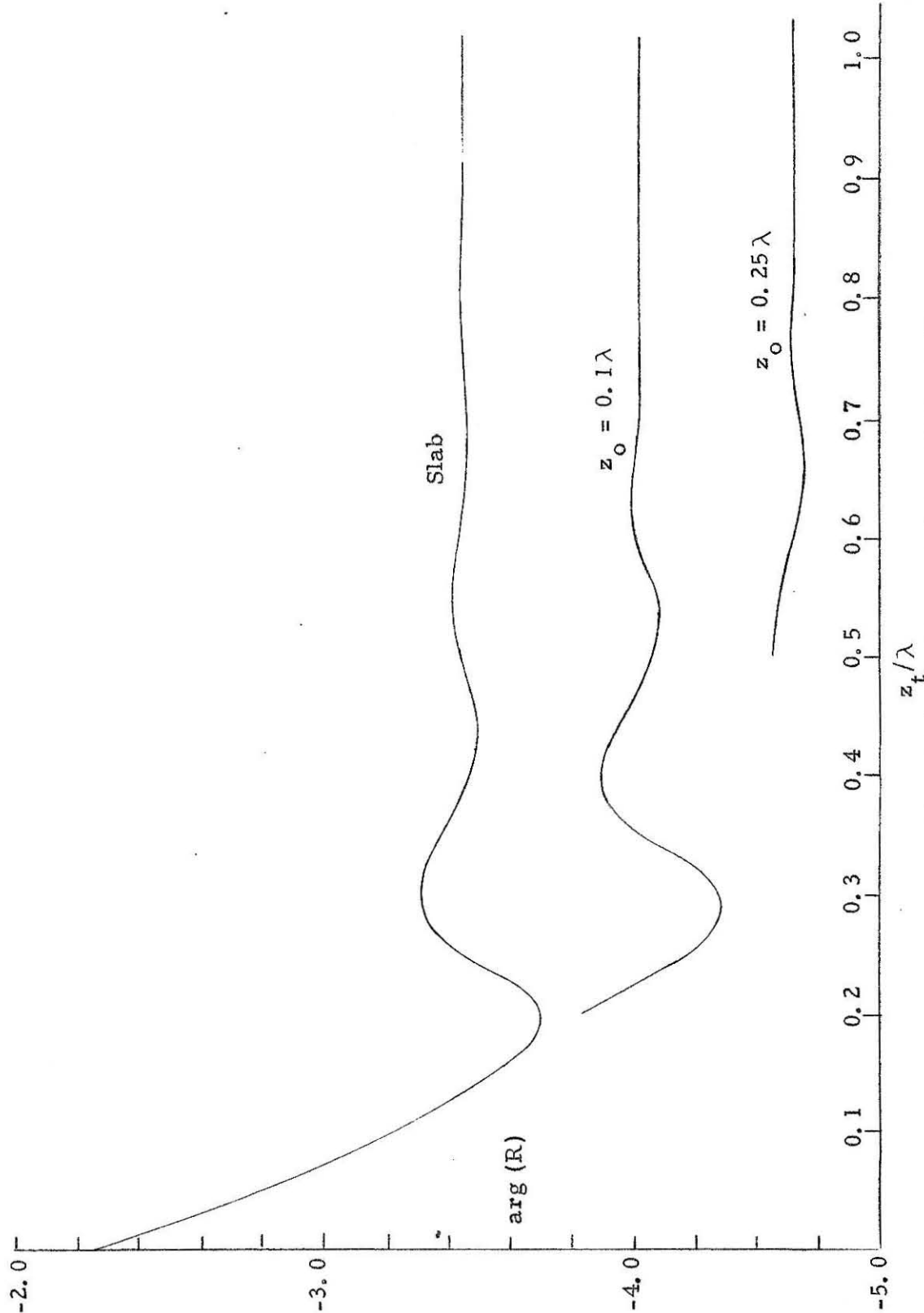


Figure 13.48 Trapezoid, $K = 2.0 - 0.5i$

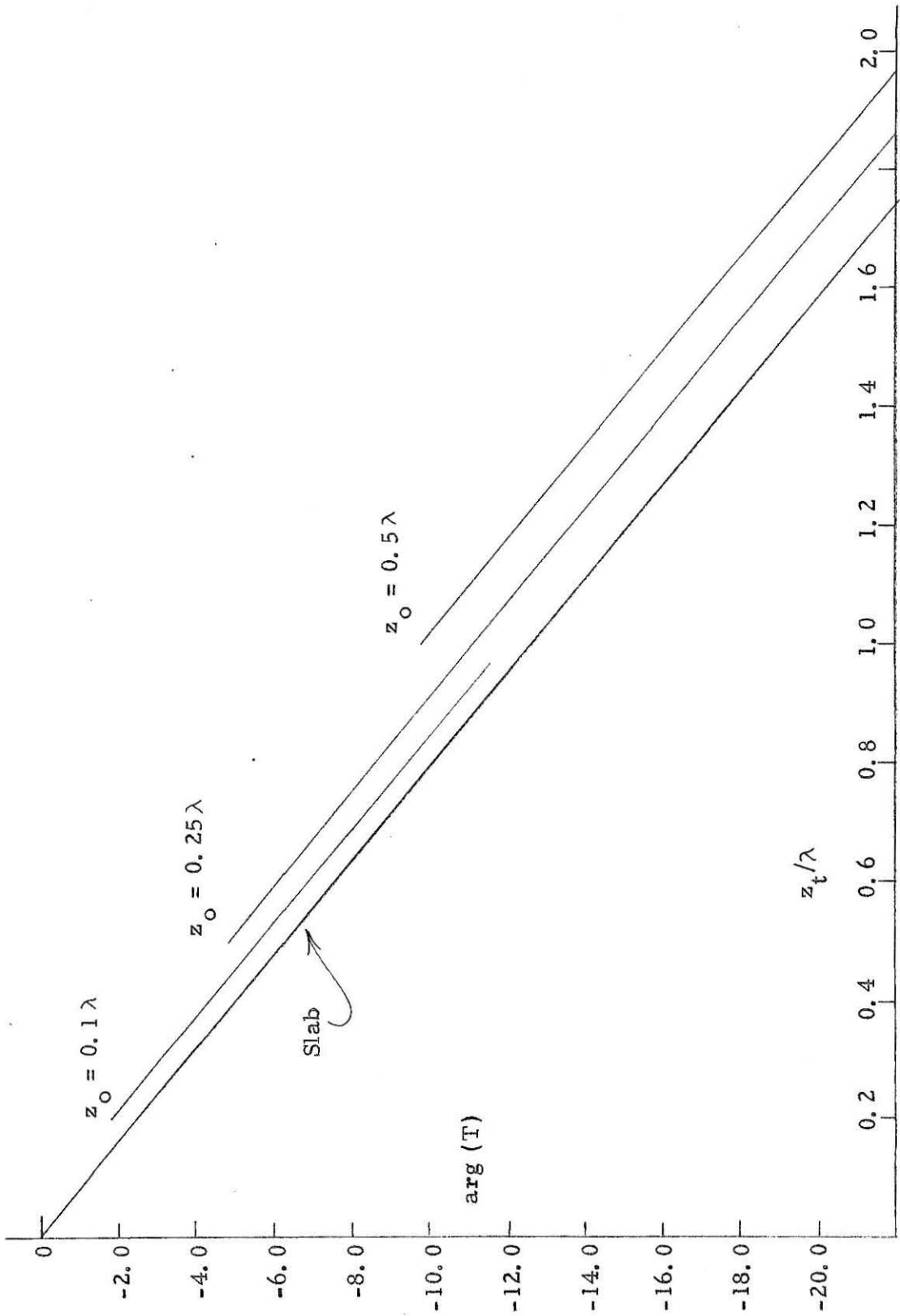


Figure 13.49 Trapezoid, $K = 2.0 - 0.5i$

XIV. SUMMARY

From the analysis of the preceding chapters, and from a study of the numerical results, the following summary of conclusions is drawn:

(1) For the simple half-space problem with a linear transition zone, both reflection and transmission are strong functions of the transition zone thickness, especially over the first one or two wavelengths of thickness.

(2) The values of R and T are less sensitive to the detailed structure of the transition zone, as evidenced by the "kinked ramp" results. For kinked and simple ramps which might serve, respectively, as first and zeroth approximations to some arbitrary smooth profile, the results are more strongly dependent upon zone thickness than upon kink coordinates.

(3) The WKB approximate solution gives fairly accurate results for transition zones thick enough, or propagation exponent changes small enough, that $|k_0 z_0 / (1 - K^2)| \gg 1$.

(4) A truncated power series (polynomial) solution will provide qualitatively correct results for small values of thickness/wavelength, if a sufficient number of terms are kept, but in general the convergence is not rapid, due to the quasi-periodic nature of the solutions. The two approximate methods employed do not overlap well, and the excluded region of zone thickness/wavelength is the most sensitive one.

(5) The reflection from and transmission through a slab with linear transition zones (trapezoid electron distribution) closely approximates the results for the slab with abrupt interfaces, provided the

transition zones are less than, say one tenth wavelength thick. The major effect of the transition zones is the shifting of relative maxima and minima to higher values of slab thickness/wavelength, with corresponding decrease of reflection and increase of transmission.

The above observations, gleaned from the numerical results, are to be understood physically by a consideration of the process of reflection and the alteration of the amplitude and wavelength of the propagating wave. It is clear that the strength of the signal re-radiated by accelerated electrons from any plane of the transition zone is proportional to the field strength and the number density thereat, and the relative phase will be associated with the relative phase of the driving wave. Thus the reflection should tend to decrease as the thickness of the zone increases, since the coherence of the zone's oscillations is thus spoiled. Likewise the transmission should increase due to the relative decrease of "mismatching" established by a finite transition zone. As the zone increases beyond one quarter wavelength thickness, some oscillatory character of transmission and reflection are to be anticipated by virtue of internal interference effects made possible within the thick transition zone. Insensitivity to the exact shape of the profile of electron density is to be expected on the grounds that minor differences in local re-radiated field strength should have only second-order effects on the cumulative field at the transition edge.

At the outset it was implied that a sufficient reason for the presentation of numerical data was the provision of a standard against which to measure the success of approximate procedures. This process has been exemplified in the text and mentioned in the list of obser-

vations above. However, due to the immediate practical importance of problems concerned with transition zones, the numerical data presented herein offer a further utility in making available results for cases which may prove to be of current interest. For example, if the profile of electron density in the shock layer of a hypersonic vehicle were approximated by a linear or piecewise linear distribution, then the signal available to the vehicle's receiving antenna would be approximated by the transmission coefficient for the appropriate parameters, either as plotted in Chapters XI and XII, or as calculable from the expressions therein. The advantage of extensive graphical data is obvious in such a case; the impossibility of presenting sufficient data to cover a multitude of cases is also apparent. Interpolation is, of course, to be employed, so it is hoped that the numerical results herein, rather than merely serving as exemplary material, are not void of engineering value.

The point of view adopted for this analysis has been, of course, that $K(z)$ was well specified, so R and T were derived from it. The demonstrated first order "correction" necessary for transition zones of the order of magnitude of a wavelength in thickness, however, increases greatly the complexity of reversing the procedure to determine $K(z)$ from measured R and T . This is the process, for example, in the application of the microwave probe as a diagnostic tool for determining ionization conditions in a flow device, such as a shock tube, shock tunnel, arc jet, rocket engine, etc. In such applications, time and space resolution requirements impose high frequencies, which engender higher values of transition zone thickness/wavelength. To exemplify the difficulties inherent in the reduction of data to provide ω_p and ν_c from

such measurements, consider the half space reflection problem. A measured value of $|R|$ and $\arg(R)$ would provide a range of possible values of K , depending on z_0/λ (see Chapter XI). If z_0/λ is unknown, then K must go underdetermined. Frequency sweeping is of questionable value, as the medium is highly dispersive, and the complex part of K is likewise a strong function of ν_c/ω . Thus it is seen that the first order effect of transition zone thickness requires that considerable redundancy of measurement be obtained in order to uniquely interpret the data of experiment, even for this half-space problem, which is the simplest of those considered. If a trapezoid electron distribution were involved, the difficulties inherent in the interferometry problem would be superposed on those of the transition zone, and the uncertainty of data reduction would be compounded. So, although it was not the intention at the outset, perhaps the most significant aspect of this effort has been the demonstration of the high degrees of ambiguity to be anticipated in the related practical application.

REFERENCES

1. Margenau, H., Phys. Rev. 508, 69 (1946).
2. Margenau, H., Phys. Rev. 7, 109 (1958).
3. Wu, C. S., On a Generalized Ohm's Law of Plasma, Jet Propulsion Laboratory, California Institute of Technology, Technical Report No. 32-23 (10 May 1960).
4. Vlasov, A. A., J. E. T. P., 291, 8 (1938); J. Phys. USSR, 25, 9, (1945).
5. Stratton, J. A., Electromagnetic Theory, McGraw-Hill, New York (1941).
6. Loeb, L. B., Basic Processes of Gaseous Electronics, University of California Press, Berkeley (1955).
7. Spitzer, L., Physics of Fully Ionized Gases, Interscience Publishers, New York (1956).
8. Bohm, D. and E. P. Gross, Phys. Rev., 1851, 75 (1949).
9. Jeans, Sir James, The Dynamical Theory of Gases, Dover, New York (1954).
10. Lin, S. C., E. L. Resler, and A. Kantrowitz, J. Appl. Phys., 95, 26 (1955).
11. Woodward, A. M. and F. M., Four-Figure Tables of the Airy Functions in the Complex Plane, TNE Report No. T 1800, Telegraph Research Establishment, Malvern, England (UD).
12. Poincelot, P., C. R. Acad. Sci. (Paris), 2031, 244 (1957).
13. Poincelot, P., C. R. Acad. Sci. (Paris), 2298, 244 (1957).
14. Erdelyi, A., Asymptotic Expansions, Dover, New York (1956).
15. Jeffreys, H. and B. S., Methods of Mathematical Physics, Cambridge (1950).
16. Morse, P. M. and H. Feshbach, Methods of Theoretical Physics, Volume II, McGraw-Hill, New York (1953).
17. Hall, J. F., J. Opt. Soc. America, 654, 48 (1958).
18. Wallot, J., Ann. Physik, 734, 60 (1919) -- see also Stratton, ref. 5, Ch. IX, problem 8.

19. Greene, E. and D. Hornig, J. Chem. Phys., 617, 21 (1953).
20. Churchill, R. V., Introduction to Complex Variables and Applications, McGraw-Hill, New York (1948).